

THE SYNTHESIS, SPECTROSCOPIC AND  
ELECTROCHEMICAL CHARACTERISATION OF  
RUTHENIUM(II) AND OSMIUM(II) POLYPYRIDYL  
COMPLEXES CONTAINING ARYL-BRIDGED  
1,2,4-TRIAZOLE LIGANDS.

by

Frances Weldon, B.Sc.

A Thesis presented to Dublin City University for the degree of Doctor of  
Philosophy.

Supervisor Prof. J.G. Vos  
School of Chemical Sciences  
Dublin City University

Sept. 1998.

*To my parents.*

I hereby certify that this material which I now submit for assessment on the programme of study leading to the award of Doctor of Philosophy by research and thesis is entirely my own work and has not been taken from the work of others save and to the extent that such work has been cited and acknowledged within the text of my work.

Signed: Frances Weldon.

Frances Weldon

I.D. No.: 92700233

Date: 16-10-1998.

## Acknowledgements

Firstly I would like to thank my supervisor Prof. J.G. Vos for his help, encouragement and support during my project and in the preparation of this manuscript.

To the members of my research group, past (Helen, Tia, Dave, Margaret, Karen, Miriam, Una, Rachel, Nick and Tim) and present (Christine, Luke, Anthea, Scott, Helen, Benedicte and Stefano), I owe the deepest debt of gratitude- you are the best! A special word of thanks to Tia for doing lifetime measurements and proof-reading, Luke (for keeping me in touch with G.A.A and the use of the study carrel) and Anthea and Christine for your support and friendship over the past years.

Thanks also to all the other postgrads- our neighbours in AG07- Ben, Colm, Bronagh, Davnat, Mairead, Siobhan and Peter, the "lads" in WG30- Paddy, Dominic, Richard, Joe, Conor and Aoife, Deirdre, Karen, Fran, Aogan and Stephen. Thanks to Drs. Paraic James and Josh Howarth for many interesting discussions and always laughing at me when it was a double G&T day!

I would also like to express my sincerest thanks to the technical staff- in particular to Mick Burke for giving so generously of his time in running NMRs and having the odd chat, Maurice, for his help with HPLC equipment and Ambrose and Veronica for delivering and ordering chemicals. Thanks to Vinny and Damien for all the help during my time in SG01.

To the residents of No. 66 Dean Swift- Thanks Sinead, Carol and Mairead for putting up with me over the past few months (especially for not letting me have the "thong" party!). I would also like to thank other housemates from No. 64- Marie and Michaela for all your friendship and support. Thanks also to Catherine D., Collette and Orla.

A huge Thank You to the "Thesis-Busters"- Bronagh, Sinead, Scott, Mairead and Carol for all the photocopying and typing. I promise to return the favour when your turn comes.

Thanks to Sven Rau and Mark Nieuwenhuyzen for Mass Spectra and X-ray data.

And last but by no means least, to my family- Mum and Dad, Thank you for your constant love, encouragement and support- your faith in me was at times the only thing which kept me going and I dedicate this thesis to you. Thanks also my brothers Kieran and Shane and sister-in-law Maria and to Granny and Grandad Weldon for always being there.

## Abstract.

The synthesis, spectroscopic and electrochemical characterisation of ruthenium(II) and osmium(II) polypyridyl mononuclear and dinuclear complexes containing aryl-substituted 5-(2-pyridyl)-1,2,4-triazoles are described. The methods of characterisation include High Performance Liquid Chromatography,  $^1\text{H-NMR}$ , UV/Visible spectroscopy, fluorimetry, electrochemistry and spectroelectrochemistry. The synthesis and characterisation of the bridging ligands used in the metal complexes are described in Chapter 3. The main chapter, Chapter 4, details the synthesis and characterisation of the mononuclear and dinuclear Ru(II) and Os(II) bipyridyl complexes of two of these ligands, 1,3- and 1,4-bis(5-(2-pyridyl)-4*H*-1,2,4-triazol-3-yl)benzene. An examination of the electrochemical absorption and emission data for the mononuclear and dinuclear complexes reveals that the interaction between the metal centres in the dinuclear complexes is in fact very weak. Evidence for this comes from the identical first oxidation and reduction potentials and absorption and emission maxima (within experimental error) for the mononuclear and corresponding dinuclear complexes. Further confirmation of a weak metal-metal interaction comes from the observation that identical absorption spectra are exhibited by the mixed-metal Ru/Os complexes and 1:1 mixtures of their corresponding homometallic dinuclear complexes. However spectroelectrochemical studies indicate the presence of intervalence transitions in some cases for the mixed-valence species. Metal-metal interactions of  $200\text{-}300\text{ cm}^{-1}$  are calculated. Furthermore, luminescence studies on the Ru/Os complexes in both their deprotonated and protonated forms suggest that an intramolecular energy transfer from the Ru-based unit to the osmium component takes place.

Chapter 5 describes the synthesis and characterisation of the Ru(II) and Os(II) complexes of the *N,N*-methylated ligand 1,2-bis(1-methyl-3-(2-pyridyl)-1,2,4-triazol-5-yl)benzene. Two isomers in which the  $\text{M}(\text{bpy})_2$  unit is coordinated via the pyridyl nitrogen and either the N2 or N4 site of the triazole ring are isolated for the mononuclear complexes. In the case of the dinuclear complexes, although two isomers can be distinguished using HPLC, only the N2/N2 coordinated isomers were isolated. Photophysical and electrochemical data for these complexes indicate that the substitution of N1 of the triazole ring results in the ligand having reduced  $\sigma$ -donor capacity and increased  $\pi$ -acceptor capability.

Finally, Chapter 6 describes the preliminary synthesis and characterisation of the ruthenium mononuclear and dinuclear complexes of the hydroquinone-substituted pyridyltriazole ligand, 1,4-dihydroxy-2,5-bis(3-(2-pyridyl)-1,2,4-triazol-1-yl)benzene. The properties of these complexes are complicated by the presence of a redox-active bridge. Nevertheless it appears that the metal-metal interaction found for all the complexes used in this study is quite weak. Therefore it may be concluded that aryl-type spacers are weak mediators of metal-metal interaction.

## Table of Contents

|   | <b>Page</b> |
|---|-------------|
| <b>Chapter 1: Introduction</b>  | <b>1</b>    |
| 1.1 Photosynthesis, Supramolecular Chemistry, and The Design of an Artificial Photochemical Molecular Device                                | 2           |
| 1.2 $[\text{Ru}(\text{bpy})_3]^{2+}$ and the synthetic design and tuning of the MLCT excited state and redox properties of Ru(II) complexes | 8           |
| 1.2.1 Redox properties of Ru(II) polypyridine complexes in the ground state   | 11          |
| 1.3 Dinuclear Metal Complexes   | 14          |
| 1.3.1 The Role of the Bridging Ligand in Dinuclear Complexes  | 16          |
| 1.4 Polynuclear Metal Complexes   | 19          |
| 1.5 Electron Transfer and Spectroelectrochemistry   | 21          |
| 1.5.1 Spectroelectrochemistry   | 29          |
| 1.6 Ruthenium(II) polypyridyl complexes containing pyridyltriazole ligands  | 33          |
| 1.7 Scope of this thesis  | 35          |
| 1.8 References  | 36          |
| <br>  |             |
| <b>Chapter 2: Experimental Procedures</b>   | <b>43</b>   |
| 2.1 Nuclear Magnetic Resonance  | 44          |
| 2.2 Absorption and Emission Measurements  | 44          |
| 2.3 Luminescent Lifetime Measurements   | 46          |
| 2.4 Electrochemistry  | 46          |
| 2.5 Spectroelectrochemistry   | 47          |
| 2.6 High Performance Liquid Chromatography  | 48          |
| 2.7 Elemental Analysis  | 49          |
| 2.8 Mass Spectra  | 49          |
| 2.9 X-Ray Analysis  | 49          |
| 2.10 References   | 50          |

|  |    |
|--|----|
| <b>Chapter 3: Ligand Synthesis and Characterisation</b>  | 51 |
| <b>3.1 Introduction</b>  | 52 |
| <b>3.2 Ligand Synthesis</b>  | 56 |
| 3.2.1 Synthesis of 1,3-bis(5-(2-pyridyl)-4 <i>H</i> -1,2,4-triazol-3-yl)benzene (H <sub>2</sub> L1)  | 56 |
| 3.2.2 Synthesis of 1,4-bis(5-(2-pyridyl)-4 <i>H</i> -1,2,4-triazol-3-yl)benzene (H <sub>2</sub> L2)  | 58 |
| 3.2.3 Attempted Synthesis of 1,2-bis(5-(2-pyridyl)-4 <i>H</i> -1,2,4-triazol-3-yl)benzene  | 60 |
| 3.2.4 Synthesis of 1,4-bis(1-methyl-3-(2-pyridyl)-1,2,4-triazol-5-yl)benzene (L3)  | 61 |
| 3.2.5 Synthesis of 1,4-dihydroxy-2,5-bis(3-(2-pyridyl)-1,2,4-triazol-1-yl)benzene (H <sub>2</sub> L <sub>4</sub> )   | 63 |
| <b>3.3 Discussion</b>  | 65 |
| 3.3.1 Synthesis  | 65 |
| 3.3.2 Electronic Properties  | 73 |
| 3.3.3 Acid-Base Chemistry  | 74 |
| <b>3.4 Conclusions</b>   | 76 |
| <b>3.5 References</b>  | 77 |
| <br>   |    |
| <b>Chapter 4: The Synthesis and Characterisation of Ruthenium and Osmium Complexes Containing 5-(2-Pyridyl)-1,2,4-Triazole Moieties Connected by a Phenyl Spacer</b> | 79 |
| <b>4.1 Introduction</b>  | 80 |
| <b>4.2 Experimental</b>  | 83 |
| 4.2.1 Synthesis of the Metal Complexes   | 83 |
| <b>4.3 Results and Discussion</b>  | 90 |
| 4.3.1 Synthetic Procedure  | 90 |
| 4.3.2 <sup>1</sup> H-NMR Spectroscopy  | 91 |
| 4.3.3 Electronic and Photophysical Properties  | 98 |
| 4.3.3.1 Absorption Spectra   | 98 |

|   |   |     |
|---|---|-----|
| 4.3.3.2   | Emission Properties   | 101 |
| 4.3.3.3   | Emission Properties of the Mixed-Metal RuOs<br>Complexes and the Possibility of Electron/Energy<br>Transfer | 106 |
| 4.3.4   | Acid-Base Properties  | 114 |
| 4.3.5   | Electrochemical Properties  | 119 |
| 4.3.6   | Spectroelectrochemical Measurements   | 125 |
| 4.4   | Concluding Comments   | 140 |
| 4.5   | References  | 141 |
| <br>  |   |     |
| <b>Chapter 5: The Synthesis and Characterisation of Ruthenium and Osmium<br/>Complexes Containing 1-Methyl-3-(2-Pyridyl)-1,2,4-Triazole<br/>Moieties Connected by a Phenyl Spacer</b> |   | 147 |
| 5.1   | Introduction  | 148 |
| 5.2   | Experimental  | 151 |
| 5.2.1   | Synthesis of the Metal Complexes  | 151 |
| 5.2.2   | X-Ray Data Collection and Structure Determination   | 154 |
| 5.3   | Results and Discussion  | 155 |
| 5.3.1   | Synthesis of the Complexes  | 155 |
| 5.3.2   | <sup>1</sup> H-NMR Spectroscopy   | 158 |
| 5.3.3   | X-Ray Data for N <sub>2</sub> -Ru   | 166 |
| 5.3.4   | Electronic and Redox Properties   | 168 |
| 5.3.4.1   | Redox Properties  | 168 |
| 5.3.4.2   | Electronic Properties   | 172 |
| 5.3.4.3   | Spectroelectrochemistry   | 182 |
| 5.4   | Concluding Comments   | 187 |
| 5.5   | References  | 188 |
| <br>  |   |     |
| <b>Chapter 6: Preliminary Studies on Ruthenium Mononuclear and Dinuclear<br/>Complexes Containing Hydroquinone Bridged 3-(2-Pyridyl)-<br/>1,2,4-Triazole Moieties</b>                 |   | 191 |
| 6.1   | Introduction  | 192 |

|                   |  |     |
|-------------------|--|-----|
| <b>6.2</b>        | <b>Synthesis of Complexes</b>                | 199 |
| <b>6.3</b>        | <b>Results and Discussion</b>                | 201 |
| 6.3.1             | Synthesis                                    | 201 |
| 6.3.2             | <sup>1</sup> H-NMR Spectroscopy              | 202 |
| 6.3.3             | Electronic Properties                        | 210 |
| 6.3.4             | Acid-Base Properties                         | 214 |
| 6.3.5             | Electrochemistry and Spectroelectrochemistry | 216 |
| 6.3.6             | Photolysis Studies                           | 222 |
| <b>6.4</b>        | <b>Concluding Comments</b>                   | 229 |
| <b>6.5</b>        | <b>References</b>                            | 230 |
| <br>              |  |     |
| <b>Chapter 7:</b> | <b>Final Remarks and Future Work</b>         | 232 |

## **Appendix 1**

## **Appendix 2**

# **Chapter One**

## **Introduction**

## 1.1 Photosynthesis, Supramolecular Chemistry, and the design of an Artificial Photochemical Molecular Device.

The efficient harvesting of light by plants and photosynthetic bacteria and its conversion into chemically useful forms is a natural phenomenon of the utmost importance to mankind and the basis for a myriad of technological applications. The conversion of light energy into chemical energy in natural photosynthetic systems is based on two types of structures (i) antenna devices, which are made up of hundreds of pigments with the ability to collect solar light and convey the resulting electronic excitation energy to specific sites (ie. the reaction centres) and (ii) reaction centres, where the excitation energy is used to perform a charge-separation process which converts electronic energy into redox chemical energy. The determination of the X-ray structures of the reaction centres of the photosynthetic bacteria *Rhodospseudomonas viridus*<sup>1</sup> and *Rhodobacter sphaeroides*<sup>2</sup> provided an informative insight into the primary events in the photoinduced charge separation process. In the reaction centre of *Rps. viridus* the key molecular components are the bacteriochlorophyll "special pair"(P), a bacteriochlorophyll monomer (BC) and a bacteriopheophytin (BP) (that are present in two structurally equivalent branches), a quinone (Q) and a four-heme c-type cytochrome (Cy). These are held in a fixed geometry by surrounding proteins that span the photosynthetic membrane. Excitation of the special pair is followed by a very fast electron transfer ( $t=3\text{ps}$ ) to the BP "primary" acceptor. The next step is a fast ( $t=200\text{ps}$ ) electron transfer from BP to Q, followed by a slower ( $t=270\text{ns}$ ) reduction of the oxidised special pair by the nearest heme group of Cy. The net result is that transmembrane charge separation has been achieved with a quantum yield approaching unity. However it should be noted that only a fraction of the energy of the photon

initially absorbed is stored as chemical energy since there is a loss of chemical potential along the electron transport chain.

The study of the antenna and charge separation apparatus of natural photosynthesis shows that proper compartmentalisation in the dimensions of space and energy is required to generate vectorial energy or electron migration, and proper organisation in time is required to assure a successful competition of forward over back electron transfer processes<sup>3</sup>. Photochemical functions such as light energy conversion can only be obtained upon the complex manipulation of the absorbed light energy input in the dimensions of space, energy and time, by means of a suitably organised supramolecular system.

In addition, the complexity of natural systems makes any synthetic effort aimed at their exact duplication quite futile. Natural photosynthesis has had, of course, the advantage of approximately 3 billion years of evolutionary development resulting in the assembly of an elegant macromolecular structure composed of many molecules that carry out specific reactions at efficiencies optimum for their survival. Purely synthetic systems, on the other hand, offer the researcher the prospect of much greater flexibility and higher solar efficiencies, together with the possibility of "fine-tuning" the chemistry for the production of specific fuels and chemicals, *e.g.* conversion to electricity, photochemical water splitting and the photoreduction of carbon dioxide. Abiotic systems capable of performing artificial photosynthesis may be designed to operate at higher temperatures than photosynthetic organisms and hence make use of the heat generated by solar radiation to increase efficiencies and/or reaction rates. They may also employ light absorbing materials of higher chemical stability than the natural pigment chlorophyll. It is only necessary to mimic the function, rather than the

structure, of natural systems. Hence the progress of chemical synthesis and the extensive knowledge gained in the fields of molecular photochemistry and reactivity offer the researcher an opportunity to design and construct artificial systems that are at the same time simpler and more efficient than the biological ones. An integral part of this research is the design and synthesis of molecular systems consisting of electron donors and acceptors that mimic the charge separation function of photosynthetic proteins.

Initial research focussed on the development of artificial systems for the photochemical generation of hydrogen and oxygen from water. These systems represented models for photosynthesis and a means of solar energy storage and fuel production. Such systems involved visible light irradiation of aqueous solutions containing, for example, metal complexes such as  $\text{Ru}(\text{bpy})_3\text{SO}_4$ ,  $\text{Co}(\text{NH}_3)_5\text{Cl}\cdot\text{Cl}_2$ , and  $\text{RuO}_2$  as a redox catalyst<sup>4</sup>. In recent years however, there has been a shift in focus from the photochemical splitting of water to the design of molecular components capable of performing the primary acts of photosynthesis, namely electron and energy transfer. This has resulted in an explosive growth in research in the area of supramolecular chemistry. Supramolecular chemistry may be described as “chemistry beyond the molecule” or the “chemistry of the intermolecular bond” and encompasses the structures and functions of organized entities that are formed by the association of two or more chemical species<sup>5</sup>. Molecular devices are structurally organised and functionally integrated chemical systems built into an appropriate supramolecular structure designed to achieve a specific function. Each molecular component performs and/or is involved in one or more single acts, while the entire (supramolecular) device performs one or more complex functions, characteristic of the assembly. Molecular

devices operate chemically, *i.e.* via electronic and/or nuclear arrangements. An appropriate assembly of suitable molecular components capable of performing light-induced functions such as vectorial electron transfer, migration of electronic energy and switch on/off of receptor ability can be called a Photochemical Molecular Device or PMD<sup>6</sup>. Possible applications of such devices range from energy conversion to signal processing, from spectral sensitisation to photocontrolled membrane permeability.

A PMD is generally made up of the following components, each having a specific role: (i) the active components which take part in an elementary act or series of elementary acts such as light absorption/emission, electron or energy acceptance/donation, (ii) the perturbing components used to modify the properties of the active components, such as substituents on the active components or spectator ligands in metal complex assemblies and (iii) the connecting components which, although not taking any active part in the process, must be conducive to electron/energy transfer by providing orbital continuity and having the correct structural orientation.

Figure 1.1 shows an assembly of a PMD for light energy conversion, consisting of a sensitizer species S, possessing suitable redox, ground and excited state properties which is linked to a series of relay species, *i.e.* a series of electron donors and acceptors along a redox gradient. Following sensitization via light absorption an electron is transferred from the excited sensitizer to the relays until charge separation has been achieved via oxidation of the sensitizer and reduction of the final acceptor. The design of a supramolecular assembly which may act as a PMD requires careful choice of the active and connecting components since vectorial electron transfer

requires the correct "downhill" progression of redox potentials to prevent charge recombination. Common requisites for active components are (i) good light absorbing properties (ii) high excited state energy (iii) long lived excited state (iv) stability towards photochemical decomposition and (v) the possibility of being linked, without loss of their useful characteristics, to other components.

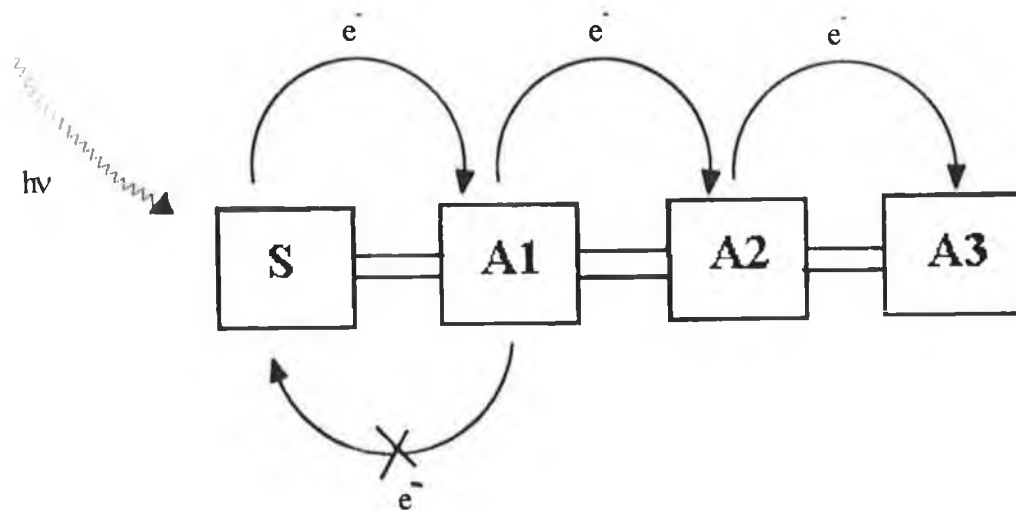


Fig. 1.1. Simplified schematic of a PMD for light energy conversion.

A concept representative of futuristic molecular photochemical devices is that of molecular machines<sup>7</sup> and molecular wires, electronics on the molecular level<sup>8</sup>. In the approach to the design of molecular wires, one of the key steps, photoinduced electron transfer down a rigid link between a donor and acceptor complex, has been extensively studied in recent years<sup>9</sup>. On a molecular scale, transfer of an electron requires overlap of the donor electronic orbitals with those of the acceptor. This overlap is a strong function of separation, since orbitals decay roughly exponentially with distance. Overlap can be extended quite effectively if donor and acceptor orbitals overlap with those of an intervening material. The overall aim is to design nanoconductors that

confer structural rigidity, thereby preventing undesirable spatial arrangements that might lead to molecular short-circuits. Lehn *et al* observed long-range electron delocalization in two ruthenium complexes linked by a conjugated polyene spacer<sup>10</sup>, while Barigelletti and coworkers detected electronic interactions between complexes joined by rod-like polyphenylene moieties<sup>11</sup>. The polyene spacer used by Lehn interconnected two optically and electrochemically active ruthenium moieties separated by 24 Å. The mixed-valence Ru(II)-Ru(III) complex displayed an intervalence absorption band due to an optically promoted transfer of charge between the metal centres. The electronic coupling was calculated to be 140 cm<sup>-1</sup> (0.018 eV), which is consistent with the polyene acting as a conductive wire joining the two complexes. The effect is large in the first excited triplet state of the complex where it appears that an electron is promoted into an extended  $\pi$ -molecular orbital embracing the polyene itself. The conjugated backbone of the polyene acts not only as a molecular wire, but also as a spacer by preventing folding motions that would allow the ruthenium complexes to come into van der Waals contact, thereby resulting in the molecular equivalent of a short circuit.

Grätzel and coworkers have carried out extensive research on the development of a highly efficient molecular photovoltaic system for solar light harvesting and conversion to electricity<sup>12,13,14</sup>. Based on the spectral sensitisation of a nanocrystalline semiconductor film by carboxylated polypyridyl complexes of ruthenium and osmium, a system capable of attaining a conversion efficiency commensurate with that of conventional silicon-based solar cells has been developed. The film comprises nanometre-sized colloidal titanium dioxide particles sintered together to allow for charge carrier transport. This is coated with a monolayer of the ruthenium and

osmium-based sensitisers which show efficiencies exceeding 90% within the wavelength range of their absorption band for the conversion of photons into electric current. The performance of the Ru(II) complex of *cis*-di(thiocyanato)bis(2,2'-bipyridyl-4,4'-dicarboxylate) has so far been found to be unmatched by any other known sensitiser. Using this system, a low-cost photovoltaic cell whose overall light to electric energy conversion is 10% under direct (AM1.5) solar irradiation has been developed. Upon long term illumination this system sustained more than  $5 \times 10^7$  redox cycles without noticeable loss of performance. This corresponds to about 10 years of continuous operation in natural sunlight.

Styring and coworkers have carried out work on the construction of artificial model systems for Photosystem II, involving binuclear ruthenium-manganese complexes<sup>15,16</sup>. In the presence of an external electron acceptor such as methyl viologen ( $MV^{2+}$ ), excitation of the ruthenium-manganese array with visible light leads to an intermolecular electron transfer from the excited state of the Ru(II) moiety to  $MV^{2+}$ , with the formation of Ru(III) and  $MV^{+*}$ . The Ru(III) centre is then reduced back to Ru(II) by an intramolecular electron transfer from the manganese part of the complex.

## **1.2 $[Ru(bpy)_3]^{2+}$ and the synthetic design and tuning of the MLCT excited state and redox properties of Ru(II) complexes.**

Because of their suitable photochemical, photophysical and redox properties, Ru(II) and Os(II) complexes of 2,2'-bipyridyl and related bidentate polypyridine ligands are probably the best photosensitisers for the construction of PMDs<sup>17,18</sup>.  $[Ru(bpy)_3]^{2+}$

first attracted the attention of research workers as a photocatalyst because its photophysical and photochemical properties fulfil the criterion for a light absorption sensitizer quite well.  $[\text{Ru}(\text{bpy})_3]^{2+}$  is a remarkably stable low-spin  $d^6$  complex which can be oxidized (removal of a metal localized electron) yielding  $[\text{Ru}^{\text{III}}(\text{bpy})_3]^{3+}$  or reduced (addition of an electron to a ligand  $\pi^*$  orbital). The absorption spectrum, which exhibits an intense band at 452 nm with a molar extinction coefficient of  $14600 \text{ M}^{-1}\text{cm}^{-1}$  is shown in Figure 1.2<sup>19</sup>.

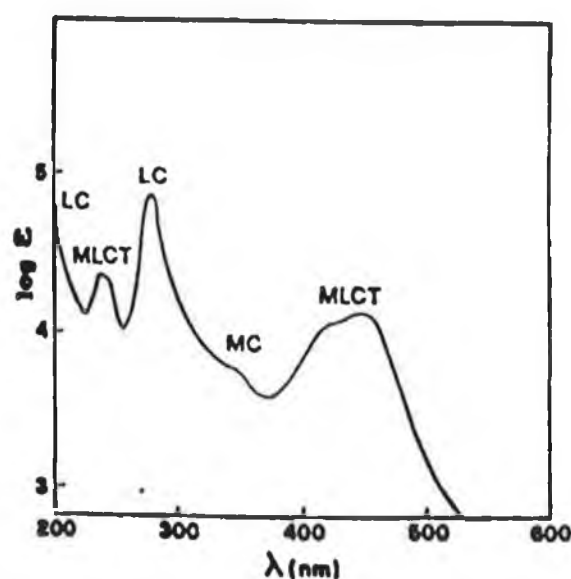


Fig 1.2. Absorption spectrum of  $[\text{Ru}(\text{bpy})_3]^{2+}$ .<sup>19</sup>

This band has been assigned as a Metal-Ligand Charge Transfer (MLCT) transition. Fast intersystem crossing occurs with an efficiency of unity from this singlet MLCT state to 4 closely spaced triplet states. From these emission to the ground state ( $k_r$ ) or radiationless deactivation ( $k_{nr}$ ) to the ground state can occur (Fig. 1.3)<sup>19</sup>. One of the routes for radiationless deactivation is the population of an antibonding triplet metal centred state,  $^3\text{MC}$  ( $e_g^*$ ). This state, (as in all  $d^6$  transition metal complexes) is strongly distorted compared with the ground state nuclear geometry and on population

leads either to rapid radiationless deactivation or more destructively to photodecomposition via cleavage of the Ru-N bond, which in the presence of a coordinating species such as  $\text{Cl}^-$  or  $\text{NCS}^-$  anions results in photosubstitution. This of course is undesirable in any compound to be used as a photocatalyst. Hence, although  $[\text{Ru}(\text{bpy})_3]^{2+}$  has been extensively studied as a sensitizer for solar energy conversion, the fact that it shows photoinstability and only absorbs in a narrow region of the solar spectrum limits its use. Many attempts have therefore been made to improve the photostability of Ru(II) diimine complexes, by eliminating the effect of the  $^3\text{MC}$  excited state and/or modifying their redox and ground state and excited state photophysical properties

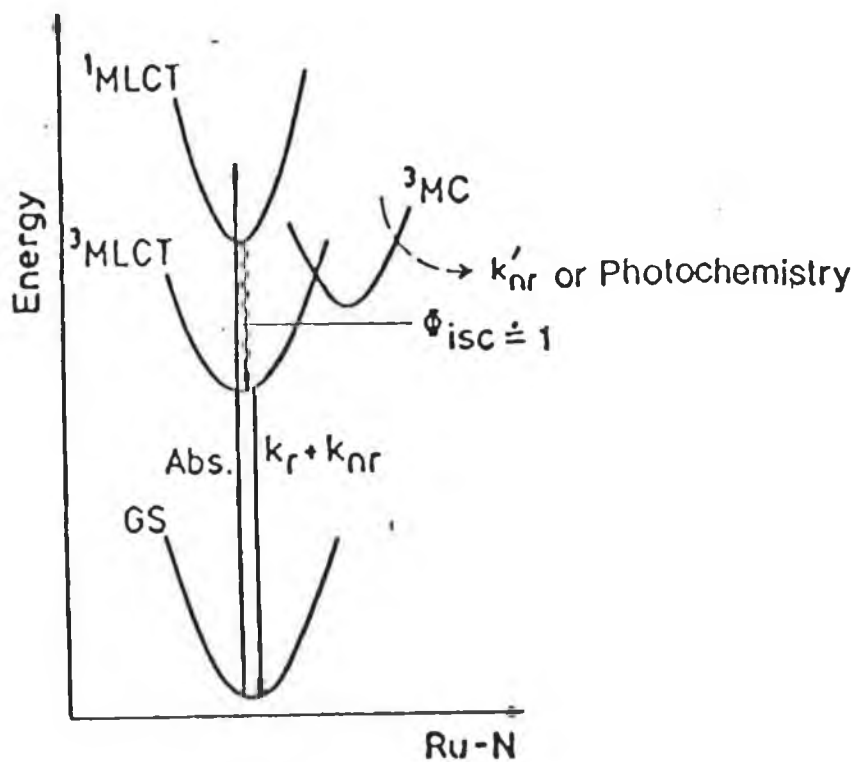


Fig. 1.3 Scheme of photophysical processes of  $[\text{Ru}(\text{bpy})_3]^{2+}$ <sup>19</sup>.

### 1.2.1. Redox properties of Ru(II) polypyridine complexes in the ground state.

A fundamental requirement for the use of complexes of the Ru(II) polypyridine family in PMDs is the stability of the oxidised and/or reduced species. Oxidation of Ru(II) polypyridine complexes generally involves a metal-centred orbital (parent  $\pi_M(t_{2g})$  in octahedral symmetry) with formation of Ru(III) complexes (low spin  $4d^5$  configuration) which are inert to ligand substitution<sup>19</sup>. Substitution of one or more polypyridine ligands can drastically alter the oxidation potential. The substitution of bpy in  $[\text{Ru}(\text{bpy})_3]^{2+}$  with 2  $\text{Cl}^-$  ions to give  $\text{Ru}(\text{bpy})_2\text{Cl}_2$  lowers the potential to 0.35 V (vs S.C.E), whereas the strong  $\pi^*$ -acceptor CO causes an increase to above 1.90 V (vs S.C.E) in  $[\text{Ru}(\text{bpy})_2(\text{CO})_2]^{2+}$ .

Reduction of Ru(II) polypyridine complexes can in principle involve either a metal-centred or a ligand-centred orbital, depending on the relative energy ordering. Reduction is usually found to take place on the  $\pi_L^*$  orbital. The reduced species is quite inert and the reduction process is reversible.

Since population of the  $^3\text{MC}$  state is responsible for instability, this problem may be overcome by increasing the crystal field splitting parameter  $\Delta_o$ . Three main factors influence  $\Delta_o$ :- the electrostatic field generated by the coordinating ligands, L—M  $\sigma$ -bonding (since the energy of the  $e_g$  level depends on this), and L—M  $\pi$ -bonding which affects the energy of the  $t_{2g}$  manifold. Another approach is to alter the energy of the MLCT states. The energy of the  $^3\text{MLCT}$  excited state depends mainly on the reduction potential of the ligand involved in the transition and the oxidation potential of the metal in the complex (which is affected by the electron donor and acceptor properties of all the ligands). Since charge transfer is an optical electron

transfer which ultimately results in short lived charge separation, solvent properties such as polarity and dielectric constant also become important.

Tunability of the excited state properties of Ruthenium polypyridyl complexes can be achieved by one of the following (i) introduction of peripheral substituents on the bipyridyl ligand that are electron-withdrawing or electron-donating (ii) substituting another ligand for bpy. The ligands used generally belong to either of two classes compared to bpy: (i) better  $\pi$ -acceptors but weaker  $\sigma$ -donors (Class I); or (ii) better  $\sigma$ -donors but weaker  $\pi$ -acceptors (Class II). Class I ligands are involved in  $^3\text{MLCT}$  states and are called chromophore ligands. In contrast, Class II ligands, because of their higher  $\pi^*$  energy levels are normally not involved in the  $^3\text{MLCT}$  emitting process, and so are called non-chromophore or spectator ligands. One of the most direct methods to test whether a ligand is involved in the emitting process is Resonance Raman Spectroscopy. It is important to note however that the spectator ligands are by no means irrelevant to the photophysical properties of Ru(II) complexes. Their stronger  $\sigma$ -donating and weaker  $\pi$ -accepting ability can substantially alter the photophysical properties of such complexes, in particular, emission energies, excited state lifetimes and  $^3\text{MC}$  energy levels.

Class II ligands, such as 2-(pyridin-2-yl)-imidazole<sup>20</sup>, 2-(pyridin-2-yl)-pyrazole<sup>21</sup> and 3-(pyridin-2-yl)-1,2,4-triazole<sup>22</sup>, because of their strong  $\sigma$ -donor properties increase the orbital splitting between the  $t_{2g}$  and  $e_g^*$  orbitals. This has consequences for both electrochemical and electronic properties. The oxidation potential of the complex is lowered. If the  $^3\text{MLCT}$  level remains approximately the same, then the  $^3\text{MLCT}$ - $^3\text{MC}$  energy gap will be increased. However a significant increase in the  $\sigma$ -donating ability of the ligands will also destabilise the  $t_{2g}$  level and as

a result, the  $t_{2g}$ - ${}^3\text{MLCT}$  energy gap will decrease which means that the emission energy will exhibit a red shift. A significant decrease in emission energy is not always desired, since it will lead to a decrease in emission yields and excited state lifetimes. Therefore the isolation of the  ${}^3\text{MC}$  states from the emitting states often has to compromise the possible decrease in the emission lifetime, which is crucial for an efficient excited state redox reaction to occur. Class I ligands<sup>23</sup>, such as 2,2'-bipyrazine, 2,2'-bipyrimidine, 2,2'-biquinoline and their derivatives, on the other hand, have strong  $\pi$ -accepting properties and so have a  $\pi^*$  level lower than that of bpy. As a result, the  ${}^3\text{MLCT}$  level is lowered and since the  $\pi^*$  (LUMO) level resides on this ligand, it may partake directly in excited state reactions. Although the  ${}^3\text{MLCT}$  energy can be decreased, the  ${}^3\text{MLCT}$ - ${}^3\text{MC}$  gap will not necessarily increase due to the reduced electrostatic field and low d-d splitting ( $t_{2g}$ - $e_g^*$ ). The most attractive feature of complexes of Class I ligands is that their absorption maxima are red-shifted compared with  $[\text{Ru}(\text{bpy})_3]^{2+}$  thus making the absorbance range more accessible to the solar spectrum. However photochemical stability is a problem in these complexes. Strong  $\pi$ -accepting ligands give rise to a stabilisation of the Ru(II)  $t_{2g}$  levels, caused by the smaller  $\sigma$ -donation of these ligands and  $\pi$ -backbonding with the metal  $d\pi$  orbitals. The net effect is a smaller ligand-field splitting, which makes the  ${}^3\text{MC}$  thermally accessible at ambient temperatures. This is reflected in both temperature dependent studies and the absence of photochemical stability in many of these type of complexes<sup>24</sup>. The problem of photoinstability can however be easily overcome by the introduction of Class II ligands such as triazoles.

Cage type ligands *e.g.* three bidentate diimine ligands linked together, have been used to encapsulate Ru(II), based on the idea that such a rigid matrix might be able to prevent ligand dissociation occurring (from the  ${}^3\text{MC}$  level) while the non-

radiative decay (from the  $^3\text{MLCT}$  level) which occurs by releasing excited state energy via the bipyridyl ring based stretching vibration, might be hindered to a certain extent. Some of these cage type complexes have been synthesised and they do in fact show longer emission lifetimes as well as much higher photochemical stability than  $[\text{Ru}(\text{bpy})_3]^{2+}$ .

Another approach to avoid population of the  $^3\text{MC}$  state by synthetic design is to use Os(II) where the splitting between the  $d_\pi$  and  $d_\sigma^*$  levels is 30 % greater for Os(II) complexes than for Ru(II) when coordinated to the same ligands. The  $d_\pi$ - $d_\sigma^*$  energy gap is so large that the  $^3\text{MC}$  state is inaccessible at room temperature. It can be seen that for a series of complexes of the same metal ion, the energy ordering of the various excited states, and particularly the orbital nature of the lowest excited state, can be controlled by a judicious choice of the ligands. In this way, it is possible to design complexes, having, at least to a certain degree, the desired properties for electron and energy transfer.

### 1.3. Dinuclear Metal Complexes.

The simplest class of supramolecular system suited for the study of photoinduced electron and energy transfer processes fundamental to the design of a PMD are two-component dyads or covalently linked donor acceptor systems, where the active components are transition metal complexes<sup>26</sup>. These systems facilitate the tailoring of excited state energies and ground and excited state redox potentials by the judicious choice of metals and ligands. There has in recent years been an explosive growth in the study of such binuclear metal complexes based on polypyridyl metal

complexes of the  $d\pi^6$  transition metal ions, Ru(II), Os(II), Re(II) etc. with bridging ligands ranging from simple anions such as  $CN^-$  to multichelating aromatic type molecules<sup>6</sup>. These have low-lying MLCT excited states with properties which make them attractive candidates for studies involving intramolecular electron and energy transfer. The excited states are luminescent, relatively photochemically inert and long-lived and are known to undergo excited state electron transfer.

An interesting class of dyads is that of chromophore-luminophore complexes (ie) systems in which the light energy is efficiently absorbed by appropriate molecular components (chromophores) and is then conveyed, by means of intercomponent energy transfer processes, to a specific molecular component, which gives back the energy in the form of light emission (luminophore). An interesting aspect of the behaviour of such chromophore-luminophore complexes is the mimicry of the "antenna effect" of natural systems. From a more practical point of view, chromophore-luminophore complexes are likely to be useful wherever very specific light absorption and emission characteristics are required *e.g* in the design of luminescent labels for biomedical applications. In the rigid rod-like dinuclear Ru(II)/Os(II) terpyridine-type complexes connected by phenylene spacers studied by Barigelletti *et al* it was found that the luminescence of the Ru-based unit was quenched by the connected Os-based moiety with almost unit efficiency<sup>27</sup>. The quenching, which was independent of the number of interposed phenylene spacers was accompanied by quantitative sensitization of the osmium-based luminescence. An extension of this work, involving dinuclear complexes containing Ru- and Os-based bis-terpyridyl chromophoric termini connected by 1,4-phenylenes only, or phenylene and bicyclooctane spacers, showed that phenylene spacers are very efficient in transmitting intermetal electronic

communication<sup>28</sup>. An important role is also played by the spatial localisation of the MLCT excited states involved in the excitation-transfer process. In the homometallic ruthenium and osmium dinuclear compounds containing a 3,5-bis(2-pyridyl)-1,2,4-triazole cyclohexyl-bridged spacer (dpt-cy-dpt) studied by Giuffrida and coworkers, it was found that only a weak interaction, if any, could occur across the dpt-cy-dpt bridge<sup>29</sup>. However an investigation of the heteronuclear dinuclear species  $[(bpy)_2Ru(dpt-cy-dpt)Os(bpy)_2]^{4+}$  revealed that photoinduced intercomponent energy transfer occurs from the highest-lying Ru→bpy charge transfer level to the lower-lying Os→bpy charge transfer excited state<sup>30</sup>. Many systems such as these have been studied in recent years which may prove useful in the design of supramolecular species for performing light-induced functions.

### **1.3.1. The Role of the Bridging Ligand in Dinuclear Complexes.**

In dinuclear complexes the interaction between the donor and acceptor components is strongly dependant on the size, shape, and electronic nature of the bridging ligand. In many cases the bridge is also directly involved in electrochemical reduction and/or light excitation and emission processes. The bridge plays a key role in controlling intercomponent electronic coupling, metal-metal distance and the geometry of the whole system. In addition, with their coordinating sites, bridging ligands play a role (together with the terminal ligands) in determining the spectroscopic and redox properties of the active metal-based units. Therefore it is reasonable to say that the design of a bridging ligand is one of the key steps in realising molecular devices based on polynuclear  $d\pi^6$  ruthenium and osmium transition metal complexes.

Traditionally various *N*-heterocyclic moieties such as pyridine, pyrazine, and pyrimidine have been used to construct bridging ligands. Ligands such as 4,4'-bipyridine, 2,3-bis(2-pyridyl)-pyrazine (dpp) and 2,2'-bipyrimidine can each connect two metal ions, mediating metal-metal electronic interaction through their  $\pi$ -system. In the design of novel bis-bidentate bridging ligands, the selection of the intervening and terminal coordinating fragments is important. The  $\pi$ -donor– $\pi$ -acceptor properties of the bridging ligand and/or the metal-metal distance can be controlled by choosing the appropriate combination of fragments. Currently a number of bridging ligands have been designed where the spacer is made up of a progressive increasing number of rigid units. This facilitates the tuning of metal-metal distance without altering the nature of the active components. It is therefore possible to perform systematic studies on the distance dependence of electron- and/or energy transfer rates.

The role played by the bridge in determining metal-metal electronic coupling has been well documented<sup>31,32</sup>. The superexchange theory of electron transfer provides an approach where the overlap between orbitals of the metal-based fragments is mediated by overlap with the orbitals of the bridging ligand (through-bond interaction). The parameters which govern the extent of interaction are orbital overlap and the energy gap between the relevant metal orbitals and the LUMO/HOMO orbitals of the bridging ligand. Bridging ligands with low energy unoccupied orbitals maximise through-bond intercomponent interactions via electron-transfer pathways, whereas bridges with high energy occupied orbitals maximise through-bond intercomponent interactions via a hole-transfer mechanism. As stated previously, pyridine-, pyrazine-, and pyrimidine-containing ligands have relatively low-lying  $\pi^*$ -orbitals and so act as good acceptors, whereas imidazole-containing ligands such as bis(imidazole) are

poorer  $\pi$ -acceptors and better  $\pi$ -donors. Another interesting feature of imidazole-containing ligands is the ability to control orbital energies by proton transfer. Haga and coworkers have worked extensively on dinuclear complexes containing benzimidazole bridging ligands. The benzimidazole group possesses  $\sigma/\pi$ -donor properties and, more importantly, a dissociative N-H proton. Once the benzimidazole unit is coordinated to the metal ion, the imino N-H proton becomes more acidic and can be easily removed. Deprotonation of benzimidazole moieties of the bridging ligand appears to induce a considerable perturbation on the spectral and redox properties of the dinuclear complex. For the dinuclear complexes  $[M(L)_2(\text{bpbimH}_2)M(L)_2]^{4+}$   $M = \text{Ru, Os, L} = \text{bpy, phen, bpbimH}_2 = 2,2'$ -bis(2-pyridyl)-bibenzimidazole), a study of the mixed-valence compound revealed that the degree of metal-metal interaction in the deprotonated complex was 4-6 times larger than that of their protonated analogues<sup>33</sup>. In contrast, a more recent study of dinuclear Ru complexes containing 2,2'-bis(benzimidazol-2-yl)-4,4'-bipyridine (4,4-bbbpyH<sub>2</sub>) revealed that deprotonation of 4,4-bbbpyH<sub>2</sub> decreased the metal-metal interaction as a result of smaller orbital mixing between the Ru(II)d $\pi$  and bridging ligands  $\pi^*$  orbitals<sup>34</sup>. Similar proton-induced tuning of chemical properties has been reported for the bis(pyridyltriazole) system studied by Haga and coworkers and will be discussed later. Such proton-induced switching of metal-metal interactions in dinuclear ruthenium and osmium complexes opens the way to the possibility of "molecular switching" by proton transfer.

#### 1.4 Polynuclear Metal Complexes.

One of the most commonly used ligands for the construction of polynuclear Ru(II)-polypyridine metal complexes is the bis-chelating ligand 2,3-bis(2-pyridylpyrazine) (2,3-dpp). The typical approach used is the so-called “complexes as metals and complexes as ligands” strategy, where metal complexes replace the metal and/or the ligand in the construction of a compound<sup>35</sup>.



The place of M can be taken by mono- or oligonuclear complexes that possess easily replaceable ligands, while the place of L can be taken by mono- or oligonuclear complexes containing free chelating sites. By an appropriate choice of the reaction partners it is possible to obtain compounds where different metals and ligands can be located in the desired position of the supramolecular structure.

Balzani and coworkers have applied the divergent iterative approach, commonly used in organic synthesis to successively synthesise large dendrimer-shaped polynuclear complexes, containing up to 22 metal centres, using 2,3-dpp and/or 2,5-dpp as the bridging ligand. It was found that the energy of the lowest MLCT excited state of each unit in these complexes depends on metals and ligands in a well-known and predictable way. Hence the synthetic control translates into a high degree of control on the direction of energy flow within these molecules. The decanuclear complex  $[\text{Ru}\{(\mu\text{-}2,3\text{-dpp})\text{Ru}[(\mu\text{-}2,3\text{-dpp})\text{Os}(\text{bpy})_2]_2\}_3]^{20+}$  shown in Figure 1.4 demonstrates the “antenna” effect quite well<sup>36</sup>. The energy absorbed by all the Ru(II) units in the complex flows via efficient intercomponent energy processes from the

centre to the periphery of the complex, where it is re-emitted by the Os(II)-containing units as near-infrared luminescence.

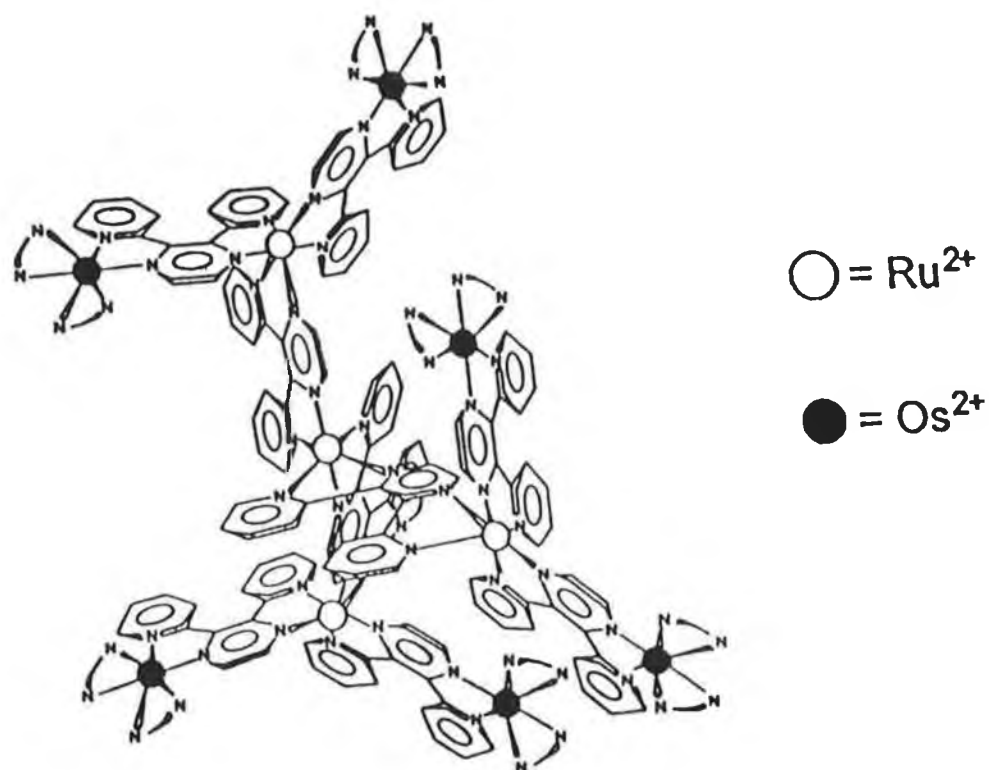
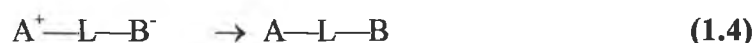
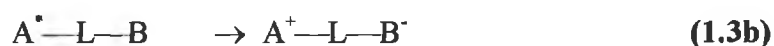


Fig. 1.4 The RuOs decanuclear complex studied by Balzani *et al*<sup>38</sup>.

More recently, the first luminescent and redox active polynuclear Ru(II) compound containing both electron-poor 2,3-dpp and electron-rich 3,5-bis(2-pyridyl)-1,2,4-triazole (Hbpt) bridging ligands has been prepared<sup>37</sup>. While excited states and redox processes are localised on specific sites, perturbations of each component on the redox and excited states of the others, as well as electronic interactions between the metal-based chromophores can be seen. The tetranuclear complex exhibits efficient intercomponent energy transfer in fluid solution at room temperature. However, this process appears to be less efficient at 77 K in rigid matrix.

### 1.5. Electron Transfer and Spectroelectrochemistry.

A very important feature of dinuclear complexes is that in a mixed-valence species containing M(II) and M(III), electron transfer from the M(II) centre to the M(III) centre can occur. Electron transfer is a very simple, weak interaction chemical process in which no bond-breaking or making is involved. In a covalently linked donor acceptor system (CLDA) where a photosensitizer A and a quencher B are covalently linked by a component L, light induced electron transfer processes can include the following:<sup>28</sup>



Suitably produced one electron oxidised or reduced forms can also undergo spontaneous intercomponent electron transfer processes. (1.5 ,1.6)

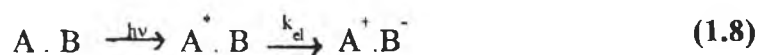
Thermal back electron transfer, or charge recombination is a spontaneous thermodynamically favourable mechanism.



Thermal electron transfer to give  $A^+ \cdot B^-$  is thermodynamically unfavourable but is experimentally accessible, provided that some means is available to generate the thermodynamically unfavoured form, and use it as a reactant. This is obviously

difficult to do by ordinary chemical/electrochemical means, but is feasible under favourable conditions with photochemistry. Absorption of light can lead to the formation of the reactant species  $A^+B^-$  in two ways; (i) following an optical electron transfer process or (ii) following a photoinduced electron transfer. By using pulsed excitation, the back electron transfer reaction can be followed, provided that the generating event is much faster than the electron transfer process to be studied.

Photoinduced electron transfer from a donor to an acceptor is the key step in natural photosynthesis. This process differs from optical electron transfer in that in this case, light absorption populates an excited state localised on a single component, and electron transfer occurs as a subsequent radiationless process



The relationship between this process, optical electron transfer, and charge recombination is shown in terms of potential energy curves in Fig.1.5<sup>38</sup>, where the component localised state  $A^* \cdot B$  is assumed to be essentially undistorted along the reaction coordinate of electron transfer.

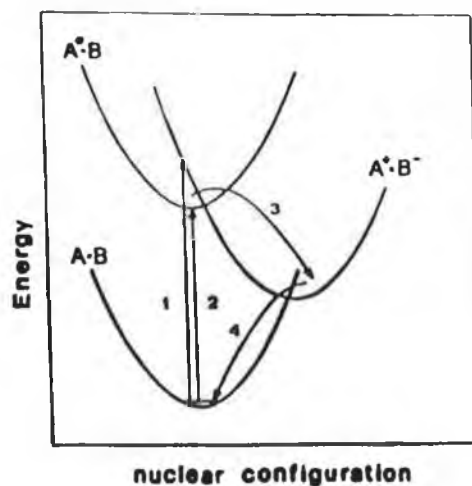


Fig. 1.5. Relationship between optical (1), photoinduced (2 + 3) and thermal (4) electron transfer processes.

Optical electron transfer (1.2) is a radiative process and accounts for new bands which appear in the absorption spectrum of a supermolecule which can differ substantially from the sum of the spectra of the individual molecular components. Optical electron transfers are well known in the fields of mixed-valence compounds where partially oxidised forms show broad structureless bands in the NIR region (7000-10,000  $\text{cm}^{-1}$ ) called Intervalence Transitions or Metal to Metal Charge Transfers (MMCT). The theory of optical electron transfer processes has been dealt with by Hush<sup>39</sup> and the most important conclusions may be summarised as follows:

The energy of an IT band consists of an inner and outer sphere contribution and arises as a direct result of the Franck-Condon principle.

$$\lambda = \lambda_i + \lambda_o \quad (1.9)$$

In the case of a metal complex, configuration changes occurring as a result of electron transfer include changes in vibrations and rotations of solvent dipoles ( $\lambda_o$ ) and also changes in the metal-ligand and intra-ligand bond lengths and angles ( $\lambda_i$ ). The changing nuclear configurations give rise to an activation barrier to electron transfer because nuclear motion occurs on a timescale ( $10^{-11}$ - $10^{-13}$  s) much longer than electronic motion ( $< 10^{-15}$  s). So  $\lambda_i$  an intrinsic property of the binuclear complex, whereas  $\lambda_o$  depends on the reorganisation of the solvent environment according to the Dielectric Continuum Model:

$$\lambda_o = e^2(1/2 a_1 + 1/2 a_2 - 1/d)(1/D_{op}-1/D_s) \quad (1.10)$$

where  $a_1, a_2$  = molecular radii at the redox centres

$d$  = internuclear separation between metal centres

$e$  = unit electron charge

$D_{op} = \eta^2 =$  optical dielectric constant

$D_s =$  static dielectric constant.

A barrier is therefore present between the M(II)-M(III) and M(III)-M(II) species, which can be observed as the IT band. By measuring the IT band in different solvents, the influence of the inner-sphere and outer-sphere energies on the IT band may be calculated.

The extent of electron delocalisation can be calculated from the properties of the intervalence band as shown in Equation 1.11:

$$\alpha^2 = \frac{(4.2 \times 10^{-4}) \epsilon_{\max} \Delta\nu_{1/2}}{d^2 \cdot E_{op}} \quad (1.11)$$

where  $\alpha^2 =$  extent of electron delocalisation,  $\epsilon_{\max} =$  extinction coefficient of the IT band ( $M^{-1}cm^{-1}$ ),  $\Delta\nu_{1/2} =$  peak width at half height of the IT band ( $cm^{-1}$ ),  $d =$  distance between the metal centres (Å) and  $E_{op} =$  energy of the IT band ( $cm^{-1}$ ).

The bandwidth at half height of the IT band can be derived using the equation

$$\Delta\nu_{1/2} = [2310(E_{op} \Delta E)]^{1/2} \quad (1.12)$$

where  $\Delta E$  is the energy difference induced by the asymmetrical environment. This value is found for asymmetric systems such as mixed-metal complexes or homonuclear complexes with an asymmetric bridging ligand. If the measured bandwidth fits with the calculated bandwidth, then the system is most likely valence-trapped (localised). If the band is too narrow, the species is delocalised and the description of the system should be  $M^{2.5} - M^{2.5}$ . The intensity of the intervalence transition depends primarily on

the degree of electronic coupling ( $V_{ab}$ ) between the metal centres which can be calculated using Equation 1.13.

$$V_{ab} = [\alpha^2(E_{op})^2]^{1/2} \quad (1.13)$$

As mentioned previously, the bridging ligand or connector can induce a greater or less degree of electronic coupling between the active components. The value of  $V_{ab}$  depends on the overlap between the electronic wavefunctions of the donor and acceptor groups, which should decrease exponentially with increasing donor-acceptor distance.

The energy, intensity and bandwidth of metal to metal charge transfer (MMCT) or Intervalence charge transfer transitions (IT) provide quantitative information about the nature and extent of electronic communication through the bridge. Adopting the approach of Robin and Day, the situations that arise can be classified as follows<sup>40</sup>:

- Class I.** The electronic coupling between metal centres is very small or totally absent and the properties of the ensemble are essentially a superposition of those of the individual components.
- Class II.** Although most of the properties of the metallic centres are still consistent with their original oxidation states, the electronic coupling between metal centres is appreciable and a number of new properties characteristic of the ensemble *e.g.* IT bands appear in their spectra.
- Class III.** In this class of compounds, the properties of the isolated components are absent and the electronic coupling between the metal centres is strong.

In ligand-bridged complexes, the extent of metal-metal interaction depends on (i) the distance between the metal centres, (ii) the ability of the bridging ligand to delocalise the electronic charge and (iii) the coordination environment of the metal ions.

By definition Class I compounds do not show any stability in the intervalence state and hence do not exhibit any IT bands. The absence of electronic coupling is indicated by a striking similarity in the properties (oxidation, redox potentials, lowest energy CT absorption and emission maxima) of the mononuclear and bi/oligonuclear complexes. An example of such compounds are the mono-, bi- and trinuclear complexes of the tripod in Fig. 1.6 for which Balzani and coworkers have observed nearly identical photophysical and redox properties<sup>41</sup>.

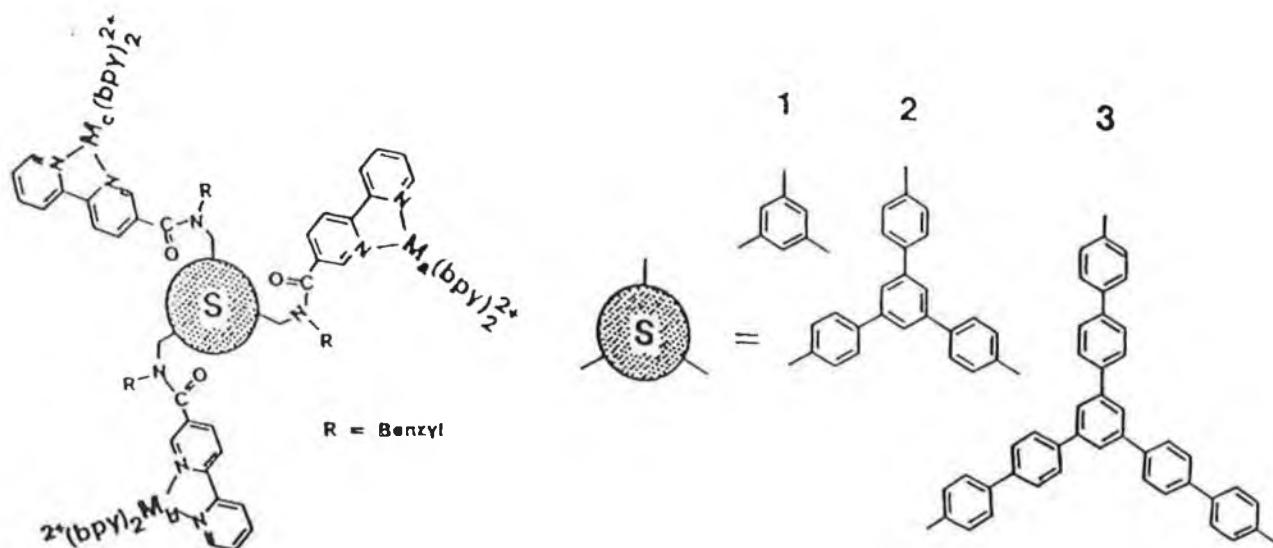


Fig. 1.6 Structure of the trimetallic complexes with spacers S indicated.

Class II compounds show comparatively weaker bands with larger bandwidths ( $\epsilon \leq 5000 \text{ M}^{-1}\text{cm}^{-1}$ ,  $\Delta\nu_{1/2} \geq 2000 \text{ cm}^{-1}$ ). The energy of the IT is solvent dependent and quantitative analysis of this solvent dependence can provide estimates of the matrix coupling element  $V_{ab}$ . Meyer and co-workers have made a systematic study of metal-metal interactions in the complexes  $[(\text{Cl})(\text{bpy})_2\text{Ru}(\text{BL})\text{Ru}(\text{bpy})_2(\text{Cl})]^{2+}$  where BL is a series of bis-monodentate ligands such as 4,4'-bpy, which can be considered as showing very weak interactions ( $\Delta E \leq 100\text{mV}$ ). Weak interactions can also be seen for pyrazine, 2,2'-bipyrimidine ( $\Delta E = 120 \text{ mV}$ ) and for bis(diphenylphosphino)methane ( $\Delta E = 140 \text{ mV}$ )<sup>42</sup>.

Class III compounds show intense IT bands that are fairly narrow ( $\epsilon \geq 5000 \text{ M}^{-1}\text{cm}^{-1}$ ,  $\Delta\nu_{1/2} \leq 2000 \text{ cm}^{-1}$ ). The symmetric binuclear ruthenium complex  $[\{\text{Ru}(\text{tterpy})\}_2(\text{tpbp})]^{2+}$  (tterpy = 4'-p-tolyl-2,2':6,2''-terpyridine, tpbpH<sub>2</sub> = 3,3',5,5'-tetrapyriddylobiphenyl) undergoes two distinct one-electron oxidations with a  $\Delta E_{1/2} = 165 \text{ mV}$ <sup>43,44</sup>. The mixed valence compound shows an intense band in the NIR region with a maximum at 1820 nm ( $\epsilon = 27000 \text{ M}^{-1}\text{cm}^{-1}$ ,  $\nu_{1/2} = 2800 \text{ cm}^{-1}$ ). The intensity of the band and the calculated matrix elements suggest extensive delocalisation of charge. The IT band maximum is also solvent independent (1820 $\pm$ 10 nm in acetonitrile, acetone, DMF and DMSO) as expected for Class III systems.

The work carried out on the Creutz-Taube ion,  $[(\text{NH}_3)_5\text{Ru}(\text{pz})\text{-Ru}(\text{NH}_3)_5]^{5+}$  where pz is pyrazine, a symmetrical, neutral bridging ligand, represents one of the pioneering studies in the area of optical electron transfer transitions<sup>45</sup>. The mixed-valence species shows an intense intervalence band in the NIR region with a maximum at 1570 nm. Using a valence localized description *i.e.* in terms of integral oxidation

states of the metal centres, the overall charge corresponds to a Ru<sup>II</sup>-Ru<sup>III</sup> complex. In a fully delocalized description however, a Ru<sup>II1/2</sup>-Ru<sup>III1/2</sup> complex would result.

The primary objective has been to design donor-acceptor molecules in which the forward electron transfer process is very rapid, while the reverse electron transfer back to the original state is very slow. This reverse reaction is important to the extent that the overall efficiency and quantum yield of any energy-storing process will be reduced. The past few years have seen an explosive growth in the investigations into electron transfer processes in covalently linked donor acceptor systems. The compounds studied have provided a basis from which to study electron transfer mechanisms and the dependence of electron transfer rate constants on various factors in the molecular structure and environment. These include.<sup>46,47</sup>

(1) *Distance between donor and acceptor*: Electron transfer rates have been measured as a function of distance in rigid glasses<sup>48</sup> in molecules where a relatively rigid spacer group holds donor and acceptor apart<sup>49</sup> and also in proteins<sup>50</sup>. Where it has been possible to measure the electron transfer rate dependence on distance, electron transfer rate constants have been found to fit well to an exponential dependence on the edge to edge distance between donor and acceptor.

(2) *Orientation Dependence*: For intramolecular electron transfer in difunctional molecules involving rigid spacers, it has been possible in some cases to measure the effects of the spatial orientation of donor, spacer and acceptor groups on electron transfer rates. Orientation effects are of great theoretical and possibly practical interest, since orientation could become a powerful tool for directing electron transfer processes and discriminating against undesirable electron transfer paths. Such an example of orientation dependence was found by Mc Lendon and coworkers where

electron transfer occurred between two porphyrin molecules held at a series of angles with respect to one another<sup>51</sup>.

(3) *Nature of the linkage*: The molecular structure of the bridging ligand between donor and acceptor has been found to play a very important role in mediating electron transfer. In most cases electron transfer occurs through the bonds of the bridge and not through the surrounding medium. As mentioned previously, electron transfer appears to be mediated by a superexchange mechanism involving the antibonding orbitals of the bridge. Aromatic and unsaturated bridges are therefore in general expected to be more effective than saturated bridges, although there are some exceptions.

(4) *Solvent*: The surrounding solvent changes two parameters that can markedly effect electron transfer rates. Firstly, the exergonicity can be altered through different solvation of the product ion pair,  $D^+ - A^-$ . Secondly, from Equation 1.10, the external contribution to the reorganisation energy,  $\lambda_o$ , can be altered by changes in the optical and static dielectric constants for the solvent.

(5) *Temperature*: As with any rate constant, electron transfer rate constants usually exhibit an Arrhenius dependence behaviour, but the activation energies are usually small<sup>52</sup>.

### 1.5.1. Spectroelectrochemistry.

Spectroelectrochemistry involves the combination of an electrochemical technique with a spectroscopic one so that the two measurements may be performed

simultaneously. In general, the electrochemical technique serves as the system excitation signal and the system response is measured spectroscopically. Optical spectroelectrochemistry is a formidable technique, since it can guarantee the integrity of one-electron transfer as a chemically and electrochemically reversible step, and it can fingerprint the product. In addition, the resultant spectrum will generally provide valuable information as to the constitution of the product<sup>53</sup>. Other advantages of the method include (i) species are studied near their ground state, thus avoiding large perturbations like in photochemically triggered reactions (ii) the measurement, being static, is relatively simple and easy to perform (iii) interferences from intermolecular effects are absent/negligible. The technique is routinely used to monitor changes in the spectrum of transition metal complexes upon oxidation and/or reduction *viz.* bleaching of MLCT bands, formation of intervalence and LMCT bands. The sample may also be chemically oxidized or reduced using Ce(IV) and Eu<sup>2+</sup>, respectively.

Spectroelectrochemistry is most commonly used in the analysis of mixed-valence dinuclear complexes to probe the extent of metal-metal interaction and electronic coupling between the M(II) and M(III) centres. The bandwidth and intensity of intervalence transitions, if observable, can give a good indication of the electronic communication between metal centres. Studies show that complexes with bridging ligands which are electron-rich such as 3,5-bis(2-pyridyl)-1,2,4-triazole (Hbpt)<sup>54</sup>, bibenzimidazole and cyanide<sup>55</sup> show moderately intense IT bands.

Intervalence transitions have also been observed for complexes with highly conjugated bridging ligands. Using spectral deconvolution techniques Ribou and coworkers found IT bands in the region 10080-11000 cm<sup>-1</sup> with extinction coefficients between 410 and 740 M<sup>-1</sup>cm<sup>-1</sup> for pentaammine ruthenium(II) and -ruthenium(III)

moieties linked by dipyridylpolyenes, dipyridylthiophenes, and dipyridylfuran<sup>56</sup>. In a similar study by Woitellier *et al.*, binuclear pentaammineruthenium complexes of  $\alpha,\omega$ -dipyridylpolyenes, where the metal-metal distance ranged from 15.8-20.6 Å, were studied<sup>57</sup>. As expected the intervalence transition moved to higher energies with increasing length of the bridge. In a recent interesting study by Meyer and coworkers the solvent dependence of the intervalence properties of the mixed-valence complexes  $[(bpy)_2ClOs(L)Ru(NH_3)_5]^{4+}$  (L = 4,4'-bpy, pyrazine) were examined<sup>58</sup>. For L = 4,4'-bpy it was found that oxidation states were  $Os^{III}-Ru^{II}$  in solvents of D.N. < 14, whereas in solvents of higher donor number, they were  $Os^{II}-Ru^{III}$ . Both isomers displayed broad, solvent dependent IT bands in the NIR. Similarly for the pyrazine-bridged species two isomers were distinguished. The  $Os^{III}-Ru^{II}$  isomer, dominant in solvents of D.N. < 22, exhibited a narrow structured IT band at  $8100\text{ cm}^{-1}$ , which is almost solvent independent in solvents of D.N.  $\geq 11.9$ . The second  $Os^{II}-Ru^{III}$  isomer, dominant at D.N. > 24 showed broad solvent dependent IT bands. These compounds therefore display properties at the Class II-Class III interface in the Robin and Day classification scheme.

Dinuclear homometallic rod-like complexes are very suitable for investigations concerning intervalence transitions. Oxidation of the ruthenium bis(4'-tolyl-2,2',6',2''-terpyridine) (ttpy) complexes containing 2,3,5,6-tetrapyridylpyrazine leads to the appearance of an IT band at  $6330\text{ cm}^{-1}$ , while for the phenyl-separated species,  $[(ttpy)Ru(tpy-(ph)_n-tpy)Ru(ttpy)]^{4+}$  (tpy = terpyridyl,  $n = 1-2$ ), IT bands in the region  $8000\text{ cm}^{-1}$  are observed<sup>59</sup>. The interaction energy decreases with increasing number of phenyl spacers. Comparison of the results obtained for dinuclear Ru complexes separated by polyene bridges indicate that the decreasing effect on the interaction

energy caused by a phenyl ring is equal to that caused by two double bonds. Hence polyphenylated bridges can replace the synthetically less accessible and chemically more fragile polyene systems in a variety of photochemical molecular devices.

Spectroelectrochemistry has also been successfully applied in detecting redox orbital localisation in  $d^6$  metal tris-(diimines)<sup>60</sup>. The ruthenium(II) mixed-ligand complexes *cis*-[Ru(bpy)<sub>2</sub>(NCS)<sub>2</sub>] (**1**), [Ru(bpy)<sub>2</sub>(pn)]<sup>2+</sup> (**2**) (pn=1,2-diaminopropane) and [Ru(bpy)<sub>2</sub>(phen)]<sup>2+</sup> (**3**) were subjected to two (for **1** and **2**) and three (for **3**) step-wise one-electron reductions and one-electron oxidations (all fully reversible). The products were studied *in situ* by solution UV/VIS/NIR spectroscopy and it was found that in all cases reductions took place on separate bpy ligands, while the third reduction of **3** took place on phen. Bands of the reduced species in the VIS/NIR region were observed and assigned to radical anion ligands. Upon oxidation of the complexes, LMCT bands appeared in the regions 575 nm and 720 nm.

While much work has been carried out in the investigation of intervalence transitions in ruthenium and osmium complexes, much less work has been done on LMCT states, probably due to their weak intensities ( $\epsilon \leq 500 \text{ cm}^{-1}$ ) and non-emissive nature. The visible absorption spectrum of [Ru(bpy)<sub>3</sub>]<sup>3+</sup> has two bands with maxima at 670 nm and 415 nm. In general low-energy LMCT transitions are favourable when the metal is oxidising and the ligand reducing. Hence, reasonably intense LMCT bands are to be expected with Ru(III) and Os(III) complexes with substituted bpy ligands. In a study carried out by Kalyanasundaram and coworkers, the properties of LMCT bands were examined by a systematic tuning of the donor strength of the bpy ligand using different substituents (Me, OMe, NH<sub>2</sub>, NMe<sub>2</sub>) on the 4,4'-position<sup>61</sup>. They found that the intensity of the LMCT transition increased with decreasing values of the redox

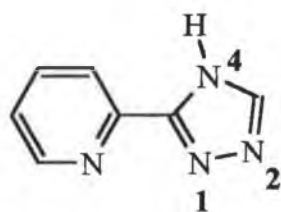
potential  $E(\text{Ru}^{\text{III}}/\text{Ru}^{\text{II}})$ . Also in the mixed-ligand complexes, replacement of a donor ligand by a poorer donor/acceptor ligand caused a red-shift in the observed LMCT transition. This report appears to be the most elaborate study carried out on the nature of the Ru(III) species to date.

#### 1.6. Ruthenium (II) polypyridyl complexes containing pyridyltriazole ligands.

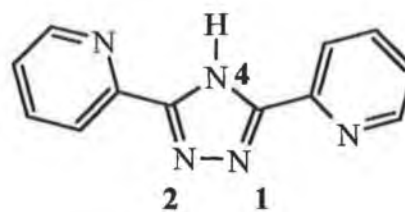
Much of the work done concerning the tuning of the excited state of Ru(II) polypyridyl complexes has focussed on the use of Class 1 ligands such as the biquinolines<sup>62</sup>. Triazoles are Class II ligands *i.e.* strong  $\sigma$ -donors and weak  $\pi$ -acceptors and contain two different coordination sites N1 and N4, which have been shown to have quite different  $\sigma$ -donor properties<sup>63</sup>. The first report of Ru(II) complexes containing 1,2,4-triazole was by Vos and coworkers, in which two 1,2,4-triazoles were bound to the  $\text{Ru}(\text{bpy})_2^{2+}$  unit in a monodentate fashion<sup>64</sup>. This work led to the synthesis of a number of 5-(2-pyridyl)-1,2,4-triazole ligands and their ruthenium complexes, the investigation of which showed these ligands to be novel and indeed unique in some of their characteristics<sup>65</sup>.

Pyridyltriazoles possess an acid-base chemistry which may be utilised to control the properties of the complex, since protonation reduces the  $\sigma$ -donor capacity of the ligand which in turn has marked effects on the ground and excited state properties of the complex. In general, pyridyltriazole complexes in the deprotonated form are photostable, whereas when protonated, as a result of their decreased  $\sigma$ -donor ability, they exhibit photochemical reactivity. This pH dependant photoreactivity was demonstrated for a series of pyridyltriazole complexes by using temperature dependent

luminescence lifetime data and photolysis studies. It was shown that for the Ru(II) complex of 5-(2-pyridyl)-1,2,4-triazole (Fig. 1.7) for example, photolysis in the presence of anions such as  $\text{Cl}^-$  lead to substitution of the pyridyltriazole, whereas in their absence, photolysis resulted in photoisomerisation (from coordination at N1 to N4). Perhaps the most extensively investigated complexes of this type are those containing the bridging ligand 3,5-bis(2-pyridyl)-1,2,4-triazole (Hbpt) (Fig. 1.7)<sup>66,67</sup>. Dinuclear complexes of this ligand, of which there are two geometrical isomers, have been found to exhibit strong interaction between the two metal centres in the mixed-valence state. The negative charge on the bridging triazole facilitates electronic communication between the metal centres. For this system and its methyl analogue it has been shown that the mixed-valence species of the complexes  $[(\text{Ru}(\text{bpy})_2)_2\text{bpt}]^{3+}$  and  $[(\text{Ru}(\text{bpy})_2)_2\text{mbpt}]^{3+}$  (Hmbpt=3-(6-methyl-2-pyridyl)-5-(2-pyridyl)-1,2,4-triazole) exhibit intervalence bands at  $5556\text{ cm}^{-1}$  and  $5400\text{ cm}^{-1}$ , respectively<sup>68</sup>. The extent of electron delocalisation is quite high in both cases ( $\alpha^2 = 0.016$  and  $0.020$ , respectively) suggesting a fairly strong metal-metal interaction. This relatively high degree of electronic delocalisation is thought most likely to be induced by enhanced hole transfer via the deprotonated triazolate bridge.



5-(2-pyridyl)-1,2,4-triazole (Hpтр)



3,5-bis(2-pyridyl)-1,2,4-triazole (Hbpt)

Figure 1.7 Structures of the ligands Hpтр and Hbpt.

## 1.7. Scope of this thesis.

This thesis describes the synthesis and characterisation of mononuclear and dinuclear ruthenium and osmium bis(bipyridyl) and ruthenium-osmium mixed-metal complexes containing different pyridyltriazole ligands.

In Chapter 2 the experimental methodology used to characterise the complexes synthesised in the course of this work will be described. Chapter 3 will describe in detail the synthesis and characterisation of the bridging ligands 1,3- and 1,4-bis(5-(2-pyridyl)-4*H*-1,2,4-triazol-3-yl)benzene ( $H_2L1$  and  $H_2L2$ ), the related ligand 1,4-bis(1-methyl-3-(2-pyridyl)-1,2,4-triazol-5-yl)benzene ( $L3$ ) and the ligand 1,4-dihydroxy-2,5-bis(3-(2-pyridyl)-1,2,4-triazol-1-yl)benzene ( $H_2L4$ ). In Chapter 4 the synthesis and characterisation of the ruthenium and osmium mononuclear and dinuclear complexes and the RuOs dinuclear complexes of the ligands  $H_2L1$  and  $H_2L2$  will be discussed. Particular attention will be paid to the spectroelectrochemistry of these compounds. Similarly, in Chapter 5 the properties of the ruthenium and osmium mononuclear, homodinuclear and heterodinuclear complexes of  $L3$  will be described. Chapter 6 involves the preliminary characterisation of the ruthenium mononuclear and dinuclear complexes  $H_2L4$ .

Finally two appendices are supplemented to this thesis. The first consists of X-Ray crystal data for the N2-coordinated Ru mononuclear complex of the ligand  $L3$ . The second relates to poster presentations and contributions made to publications during the course of my research.

## 1.8 References.

---

1. J. Deisenhofer and H. Michel, *Angew. Chem. Int. Ed. Engl.*, 1989, 28, 829.
2. G. Feher, J.P. Allen, M.Y. Okamura and D.C. Rees, *Nature.*, 1989, 111.
3. J.P. Sauvage, J.P. Collin, J.C. Chambron, S. Guillerez and C. Coudret, *Chem. Rev.*, 1994, 94, 993.
4. J.M. Lehn, J.P. Sauvage and R. Ziessel, *Nouveau Journal de Chimie.*, 1979, 3, 423.
5. J.M. Lehn, *Angew. Chem. Int. Ed. Engl.*, 1988, 27, 29.
6. V. Balzani, L. Moggi and F. Scandola, In *Supramolecular Photochemistry*: Balzani, V., Ed.; Dordrecht, The Netherlands, 1987, p1
7. V. Balzani, M. Gomez-Lopez and J.F. Stoddart, *Acc. Chem. Res.*, 1998, 31, 405.
8. D. Gust, *Nature.*, 1994, 32, 133.
9. M.D. Ward, *Chem. Soc. Rev.*, 1997, 26, 365.
10. A.C. Benniston, V. Goulle, A. Harriman and J.M. Lehn, *J. Phys. Chem.*, 1994, 98, 7798
11. F. Barigelletti, L. Flamigni, V. Balzani, J.P. Collin, J.P. Sauvage, A. Sour, E.C. Constable and A.M. Cargill Thompson, *J. Am. Chem. Soc.*, 1994, 116, 7692.
12. M. Graetzel, *Platinum Metals Rev.*, 1994, 38, 151.

- 
- 13 Md. K. Nazeeruddin, R. Humphry-Baker, M. Graetzel and B.A. Murrer, *J. Chem. Soc., Chem. Commun.*, 1998, 719.
  - 14 N. Papageorgiou, Y. Athanassov, P. Bonhote, H. Petersson, A. Azam and M. Graetzel, *J. Chem. Soc., Chem. Commun.*, 1995, 65.
  - 15 L. Sun, L. Hammarstrom, T. Norrby, H. Berglund, R. Davydov, M. Andersson, A. Borje, P. Korall, C. Philouze, M. Almgren, S. Styring and B. Akermark, *J. Chem. Soc., Chem. Commun.*, 1997, 607.
  - 16 L. Sun, H. Berglund, R. Davydov, T. Norrby, L. Hammarstrom, P. Korall, A. Borje, C. Philouze, K. Berg, A. Tran, M. Andersson, G. Stenhagen, J. Martensson, M. Almgren, S. Styring and B. Akermark, *J. Am. Chem. Soc.*, 1997, 119, 6996.
  - 17 V. Balzani, F. Bolletta, M.T. Gandolfi and M. Maestri, *Top. Curr. Chem.*, 1978, 75, 1.
  - 18 K. Kalyanasundaram, *Photochemistry of Polypyridine and Porphyrin Complexes*; Academic Press; New York, 1992.
  19. A. Juris, V. Balzani, F. Barigelletti, S. Campagna, P. Belser and A. von Zelewsky, *Coord. Chem. Rev.*, 1988, 84, 85.
  - 20 M. Haga, T. Matsumura-Inoue, K. Shimizu, and G.P. Sato, *J. Chem. Soc., Dalton Trans.*, 1989, 371.
  - 21 P.J. Steel and E.C. Constable, *J. Chem. Soc., Dalton Trans.*, 1990, 1389.

- 
- 22 R. Hage, A.H.J. Dijkhuis, J.G. Haasnoot, R. Prins, J. Reedijk, B.E. Buchanan and J.G. Vos, *Inorg. Chem.*, 1988, 27, 2185.
- 23 D.P. Rillema, G. Allen, T.J. Meyer and D. Conrad, *Inorg. Chem.*, 1983, 22, 1617.
- 24 R. Wang, J.G. Vos, R. Schmehl and R. Hage, *J. Am. Chem. Soc.*, 1992, 114, 1964.
- 25 V. Balzani, *J. Photochem. Photobiol. A: Chemistry*, 1990, 51, 55.
- 26 V. Balzani and F. Scandola, *Supramolecular Photochemistry*; Horwood: Chichester, U.K 1991.
- 27 M. Beley, S. Chodorowski, J.P. Collin, J.P. Sauvage, L. Flamigni and F. Barigelletti, *Inorg. Chem.*, 1994, 33, 2543.
- 28 F. Barigelletti, L. Flamigni, J.P. Collin and J.P. Sauvage, *J. Chem. Soc. Chem. Commun.*, 1997, 333.
- 29 G. Giuffrida, G. Calogero, G. Guglielmo, V. Ricevuto, M. Ciano and S. Campagna, *Inorg. Chem.*, 1993, 32, 1179.
- 30 G. Giuffrida, G. Calogero, V. Ricevuto and S. Campagna, *Inorg. Chem.*, 1995, 34, 1957.
- 31 V. Balzani, A. Juris, M. Venturi, S. Campagna and S. Serroni, *Chem. Rev.*, 1996, 96, 759.
- 32 G. Giuffrida and S. Campagna, *Coord. Chem. Rev.*, 1994, 135/136, 517.
- 33 M. Haga, T. Ano, K. Kano and S. Yamambe, *Inorg. Chem.*, 1991, 30, 3843.

- 
34. M. Haga, Md. M. Ali, S. Koseki, K. Fujimoto, A. Yoshimura, K. Nozaki, T. Ohno, K. Nakajima and D. Stufkens, *Inorg. Chem.*, 1996, 35, 3335.
35. G. Denti, S. Serroni, S. Campagna, A. Juris, M. Ciano and V. Balzani, In *Perspectives in Coordination Chemistry*: Williams, A.E. Merbach Eds.; VCH: Basel, Switzerland, 1992, 153.
36. G. Denti, S. Campagna, S. Serroni, M. Ciano and V. Balzani, *J. Am. Chem. Soc.*, 1992, 114, 2944.
37. S. Serroni, S. Campagna, G. Denti, T.E. Keyes and J.G. Vos, *Inorg. Chem.*, 1996, 35, 4513.
38. F. Scandola and V. Balzani, *Topics in Current Chemistry.*, 1991, 158, 83.
39. N.S. Hush, *Prog. Inorg. Chem.* 1967, 8, 391.
40. M.B. Robin, P. Day, *Adv. Inorg. Chem. Radiochem.*, 1967, 10, 247.
41. P. Belser, A. von Zelewsky, M. Frank, C. Seel, F. Voegtle, L. De Cola, F. Barigelletti and V. Balzani, *J. Am. Chem. Soc.*, 1993, 115, 4076.
42. K. Kalyanasundaram and Md. K. Nazeeruddin, *Inorg. Chim. Acta.*, 1994, 226, 213.
43. M. Beley, J.P. Collin and J.P. Sauvage, *Inorg. Chem.*, 1993, 32, 4359.
44. M. Beley, J.P. Collin, R. Louis, B. Metz and J.P. Sauvage, *J. Am. Chem. Soc.*, 1991, 113, 8521.
45. C. Creutz and H. Taube, *J. Am. Chem. Soc.*, 1969, 91, 3988; *ibid.*, 1973, 95, 1086.

- 
46. J.R. Bolton, J.A. Schmidt, T.F. Ho, J. Liu, K.L. Roach, A.C. Weedon, M.D. Archer, J.H. Wilford and V.P. Gadzekpo, *Adv. Chem. Series.*, 1993, 228, 117.
47. J.R. Miller, *Adv. Chem. Series.* 1993, 228, 430.
48. J.P. Miller, J.V. Beitz and R.K. Huddleston, *J. Am. Chem. Soc.*, 1984, 106, 5057.
49. L. De Cola, V. Balzani, F. Barigelletti, L. Flamigni, P. Belser, A. von Zelewsky, M. Frank and F. Voegtle, *Inorg. Chem.* 1993, 32, 5228.
50. S.L. Mecklenburg, D.G. McCafferty, J.R. Schoonover, B.M. Peek, B.W. Erickson and T.J. Meyer, *Inorg. Chem.*, 1994, 33, 2974.
51. D. Heiler, G. McLendon and P. Rogalsky, *J. Am. Chem. Soc.*, 1978, 109, 604.
52. J.T. Hupp, G.A. Neyhart, T.J. Meyer and E.M. Kober, *J. Phys. Chem.*, 1992, 96, 10820.
53. G.A. Heath, In *Molecular Electrochemistry of Inorganic, Bioinorganic and Organometallic Compounds*. A.J.L. Pombeiro and J.A. McCleverty Eds., Kluwer, The Netherlands. p 533.
54. R. Hage, J.G. Haasnoot, H.A. Niewenhuis, J. Reedijk, D.H. de Ridder, J.G. Vos and R. Wang, *J. Am. Chem. Soc.*, 1990, 112, 9245.
55. C.A. Bigozzi, S. Roffia, C. Chiorboli, J. Davila, M.T. Indelli, and F. Scandola *Inorg. Chem.*, 1989, 28, 4350.

- 
56. A.C. Ribou, J.P. Launay, K. Takahashi, T. Nihira, S. Taruntani and C.W. Spangler, *Inorg. Chem.*, 1994, 33, 1325.
57. S. Woitellier, J.P. Launay and C.W. Spangler, *Inorg. Chem.*, 1989, 28, 758.
58. G.A. Neyhard, C.J. Timpson, W. Douglas Bates and T.J. Meyer, *J. Am. Chem. Soc.*, 1996, 118, 3730.
59. J.P. Collin, P. Laine, J.P. Launay, J.P. Sauvage and A. Sour, *J. Chem. Soc., Chem. Commun.*, 1993, 434.
60. P.S. Braterman, J. Song and R.D. Peacock, *Spectrochim. Acta.*, 1992, 48A, 899.
61. M.K. Nazeeruddin, S.M. Zakeeruddin and K. Kalyanasundaram, *J. Phys. Chem.*, 1993, 97, 9607.
62. R.P. Thummel, F. Lefoulon and S. Chirayil, *Inorg. Chem.*, 1987, 26, 3072.
63. B.E. Buchanan, J.G. Vos, M. Kaneko, W.J.M. van der Putten, J.M. Kelly, R. Hage, R.A.G. de Graaff, R. Prins, J.G. Haasnoot and J. Reedijk, *J. Chem. Soc., Dalton Trans.*; 1990, 2425.
64. J.G. Vos, J.G. Haasnoot and G. Vos, *Inorg. Chim. Acta.*, 1983, 162, 155.
65. R. Hage, J.G. Haasnoot, J. Reedijk, J.G. Vos and R. Wang, *J. Chem. Soc., Dalton Trans.*, 1987, 1389.
66. R. Hage, J.G. Haasnoot, H.A. Niewenhuis, J. Reedijk, D.H. de Ridder, J.G. Vos and R. Wang, *J. Am. Chem. Soc.*, 1990, 112, 9245.
67. R. Hage, Ph.D Thesis 1991, Leiden University.

- 
68. R. Hage, J.G. Haasnoot, J. Reedijk, R. Wang and J.G. Vos, *Inorg. Chem.*, 1991, 30, 3263.

## **Chapter Two**

### **Experimental Procedures**

All synthetic reagents were of commercial grade and no other purification was employed, unless otherwise stated. All solvents employed in spectroscopic measurements, with the exception of ethanol, were HPLC grade.

## **2.1 Nuclear Magnetic Resonance Spectroscopy.**

<sup>1</sup>H-NMR spectra were recorded on a Bruker AC400 (400MHz) instrument. The solvents used were deuterated dimethyl sulphoxide and deuterated acetonitrile or acetone for ligands and complexes, respectively. The chemical shifts were recorded relative to TMS. The spectra were converted from their Free Induction Decay (FID) profiles using a Bruker WINNMR software package.

The 2-D COSY (correlated spectroscopy) experiments involved the accumulation of 128 FIDs of 16 scans. Digital filtering was sine-bell squared and the FID was zero filled in the F1 dimension. Acquisition parameters were F1 = ± 500 Hz, F2 = 1000 Hz and  $t_{1/2}$  = 0.001 s. The cycle time delay was 2 s.

## **2.2 Absorption and Emission Measurements.**

UV/Visible spectra were obtained using a Shimadzu UV3100 UV-Vis-NIR spectrophotometer interfaced to an Elonex PC433 personal computer. Unless otherwise stated, the solvent used was acetonitrile. Extinction coefficients are accurate up to 5 %.

Emission spectra were obtained on a Perkin-Elmer LS50B luminescence spectrometer equipped with a red sensitive Hamamatsu R928 detector, interfaced with an Elonex PC466 personal computer employing Perkin-Elmer FL WinLab custom built software. At room temperature, unless otherwise indicated, acetonitrile was the

solvent used, and excitation and emission slit widths of 10 nm, respectively were employed. At 77 K measurements were carried out in ethanol/methanol (4:1 v/v) using excitation and emission slit widths of 5 nm. The spectra were not corrected for the photomultiplier response.

To ensure protonation/deprotonation, a few drops of perchloric acid or  $\text{NH}_3$ /diethyl amine solution were added to the sample.

Quantum yields of emission,  $\Phi_{\text{em}}$ , were carried out according to the method of optically dilute measurements described by Demas and Crosby<sup>1</sup>. The standard used was  $[\text{Ru}(\text{bpy})_3]^{2+}$ , known to have a quantum yield of 0.028 in aqueous, air equilibrated solution<sup>2</sup> or  $[\text{Os}(\text{bpy})_3]^{2+}$ , which has a quantum yield of 0.005 in deaerated acetonitrile<sup>3</sup>. Normalisation of absorbance intensity was carried out prior to emission measurement and  $\Phi_{\text{em}}$  was determined using Equation 2.1:

$$\Phi_{\text{em}} = 0.028 (A_s/A_{\text{ref}}) (n_s/n_{\text{ref}})^2 \quad (2.1)$$

where  $\Phi_{\text{em}}$  is the emission quantum yield,  $A_s$  and  $A_{\text{ref}}$  are the integrated areas of the emission band of the sample and reference, respectively, and  $n_s$  and  $n_{\text{ref}}$  the solvent refractive indices of the sample and reference solutions.

The ground state  $\text{pK}_a$  was measured by monitoring the UV/Vis absorption intensity as a function of pH. The excited state acid-base equilibria were measured by monitoring the emission intensity as a function of pH. The excitation wavelength for the emission titration was chosen from a suitable isobestic point determined from the absorption titration spectra. The samples were dissolved in a few drops of HPLC grade acetonitrile and then added to 100  $\text{cm}^3$  of Britton-Robinson buffer (0.04 M boric acid, 0.04 M acetic acid, 0.04 M phosphoric acid). The pH was adjusted by adding conc. NaOH or conc.  $\text{H}_2\text{SO}_4$  and was measured using a Corning 240 digital pH

meter Ground state pKa's were determined from the point of inflection of a plot of percentage change in absorbance versus pH.

### **2.3 Luminescent lifetime measurements.**

Luminescent lifetimes were measured using the third harmonic (355 nm) of a Spectron Q-switched Nd-YAG spectrum laser system. Emission was detected in a right angled configuration to the laser using an Oriel model IS520 gated intensified CCD coupled to an Oriel model MS125 spectrograph. Room temperature lifetimes were carried out in acetonitrile, unless otherwise stated. The samples used were all of low concentration ( $10^{-4}$ - $10^{-5}$  M) and degassing was carried out by bubbling nitrogen through the sample for at least 20 minutes. Lifetimes conforming to single exponential decays were analysed using Microsoft Excel. The lifetime errors are estimated to be less than 8 %.

### **2.4 Electrochemistry.**

For electrochemical measurements the organic solvents employed were HPLC grade, dried over molecular sieve. The electrolyte used was home-made tetraethylammoniumperchlorate (TEAP). This was prepared by dissolving tetraethylammoniumbromide (1 M) in water. Perchloric acid (1 M) was added dropwise until precipitation of the white perchlorate salt ceased. The product was collected by filtration and redissolved in hot water, neutralised and then recrystallised five times from hot water.

The electrochemical cell used was a conventional three-compartment cell with glass frits. The reference electrode used was a saturated calomel electrode. The working electrode was a 3 mm diameter teflon shrouded glassy carbon electrode and a platinum gauze was used as the counter electrode. Prior to reduction measurements the solutions were degassed for 15 min. with nitrogen. The pH was adjusted using perchloric acid or ammonium hydroxide. Cyclic voltammetry was carried out using a CH instruments Model 660 electrochemical workstation interfaced to an Elonex 486 PC. A scan rate of  $10 \text{ mVs}^{-1}$  was used.

## 2.5 Spectroelectrochemistry.

Spectroelectrochemistry was carried out as shown in Figure 2.1<sup>4</sup> using a home-made Pyrex glass thin layer cell (1 mm), a platinum gauze as working electrode, a Ag/AgCl quasi-reference electrode and a platinum wire as counter electrode. The electrolyte used was 0.1 M TEAP in acetonitrile and the UV/Visible/NIR spectra were recorded using the Shimadzu 3100 UV/NIR spectrometer interfaced to an Elonex PC433 personal computer. The working electrode was held at the required potential during the spectral scan using an EG&G PAR Model 362 scanning potentiostat. Since all measurements were carried out at anodic potentials no degassing of samples was carried out.

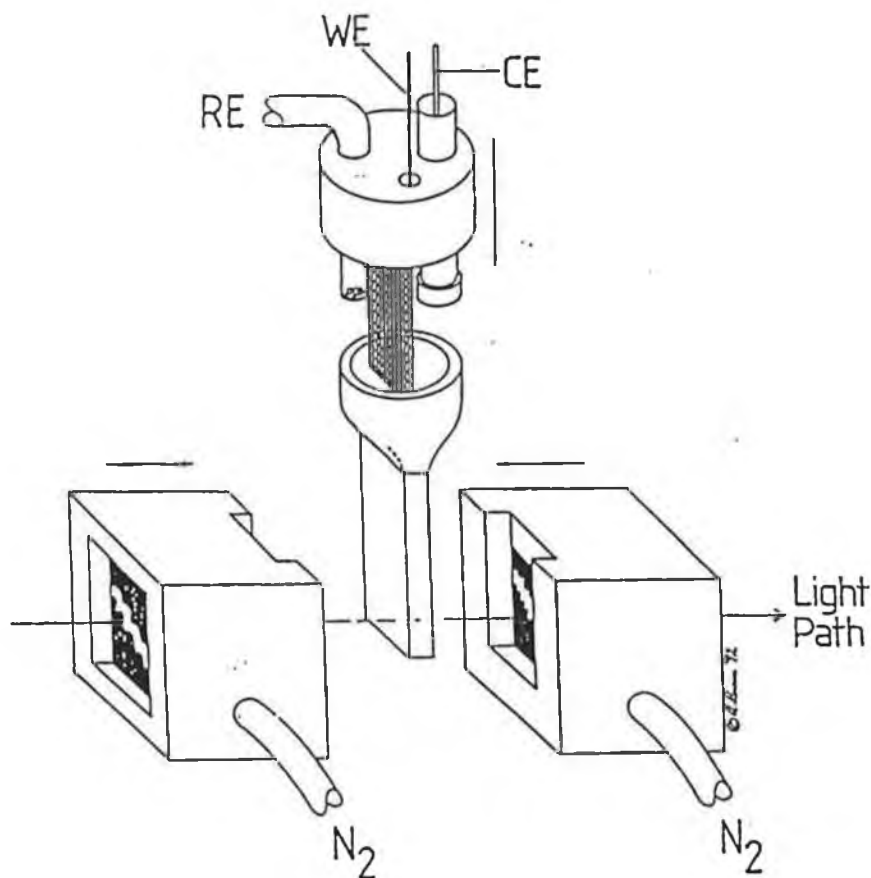


Figure 2.1. Representation of the OTTLE cell employed for spectroelectrochemistry.

## 2.6 High Performance Liquid Chromatography.

Analytical HPLC experiments were carried out using a Waters HPLC system, consisting of a model 501 pump, a 20 $\mu$ l injector loop, a Partisil SCX radial PAK cartridge mounted in a radial compression Z module and a 990 photodiode array detector. The system was controlled by a NEC APCIII computer. The detection wavelength used was 280 nm which corresponds to the most intense band in the absorption spectrum ( $\pi$ - $\pi^*$ ) for all the ruthenium complexes studied in this work. The mobile phase used was 80:20 CH<sub>3</sub>CN:H<sub>2</sub>O containing 0.1 M LiClO<sub>4</sub>. The flow rate used was 2.0 ml/min.

Semi-preparative HPLC was carried out using an ACS pump, a 1 ml injection loop and a Waters Partisil SCX 10  $\mu$ m cation exchange column (25 x 100 mm).

The mobile phase used was 80:20 CH<sub>3</sub>CN:H<sub>2</sub>O containing KNO<sub>3</sub> (0.12-0.20 M). The flow rate used varied between 1.50-2.0 ml/min.

### **2.7 Elemental analysis.**

Elemental analyses were carried out by the Microanalytical laboratories at University College Dublin.

### **2.8 Mass Spectra.**

The Mass Spectra data were obtained from the University of Jena, Germany by Sven Rau. DEI and CI ionization methods were used.

### **2.9 X-Ray Analysis.**

X-Ray data collection and analysis were carried out by Mark Nieuwenhuyzen in the Chemistry Department, The Queen's University of Belfast.

## 2.10 References.

---

1. J.N. Demas and G.A. Crosby, *J. Phys. Chem.*, 1971, 75, 8, 991.
2. K. Nakamura, *Bull. Chem. Soc. Jpn.*, 1982, 55, 2697.
3. J.V. Caspar, R.S. Lumpkin and T.J. Meyer, *J. Phys. Chem.*, 1986, 90, 3722.
4. S.A. Macgregor, E. McInnes, R.J. Sorbie and L.J. Yellowlees in *Molecular Electrochemistry of Inorganic, Bioinorganic and Organometallic Compounds*, A.J.L. Pombeiro and J.A. Mc Cleverty Eds., Kluwer, The Netherlands, 1991, p. 505.

## **Chapter Three**

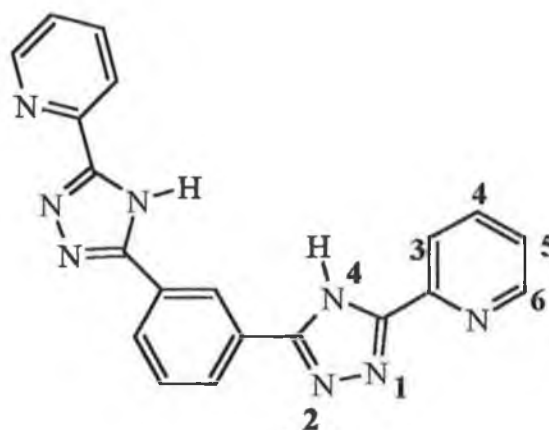
### **Ligand Synthesis and Characterisation**

### 3.1 Introduction.

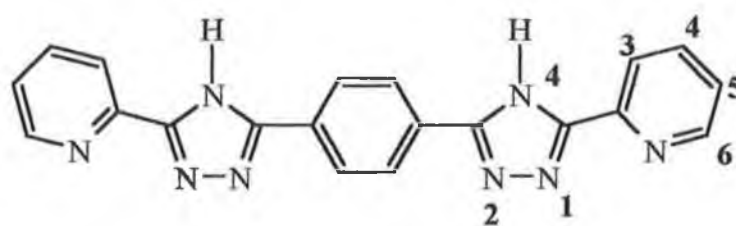
In this chapter the syntheses of the pyridyltriazole-based ligands prepared in the course of this work are described. The structures, names and abbreviations of these ligands are presented in Figure 3.1. Since the first report on ruthenium complexes of 1,2,4-triazoles in 1983<sup>1</sup>, a number of triazole-containing ligands have been synthesised by Hage and coworkers<sup>2,3,4</sup>. Those chosen here form part of a family of pyridyltriazole-based systems, which based on the interesting properties found for the ligand 3,5-bis(2-pyridyl)-1,2,4-triazole (Hbpt)<sup>5</sup>, merit attention. In the complexes containing Hbpt, the bridging triazolite ligand directly coordinates two M(bpy)<sub>2</sub> units yielding complexes with a relatively short distance between metal centres and a rather strong metal-metal interaction<sup>6</sup>. It was of interest to design a bridging ligand containing two pyridyltriazole units linked by a spacer and to investigate the effect this would have on the properties of its dinuclear complexes. With this in mind it was decided to synthesise ligands consisting of a central benzene ring with two pyridyltriazole moieties bound at the 1,4-, 1,3-, and 1,2-positions.

The syntheses are based mainly on the work of Hergenrother, who in the course of investigating the use of diamidrazones in polymer synthesis, prepared 1,2,4-triazoles and 1,2,4-oxadiazoles from *N*-acylamidrazones<sup>7</sup>. These *N*-acylamidrazones were prepared in essentially quantitative yields by low temperature solution condensation of 2-pyridylamidrazone and an acid chloride in polar solvents such as *N,N*-dimethylacetamide and hexamethylphosphoramide, and/or by an interfacial method. The corresponding 1,2,4-triazoles were then obtained by refluxing the *N*-acylamidrazones under an inert atmosphere at elevated temperature (250-300 °C) in solvents such as *N*-methylpyrrolidone, *m*-cresol or hexamethylphosphoramide.

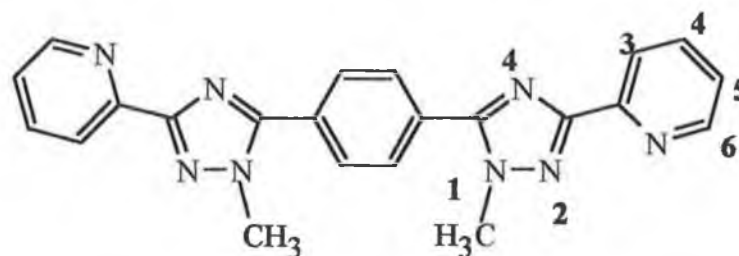
The ligand H<sub>2</sub>L4 was prepared as a result of work carried out by T. Keyes on pyridyltriazole ligands containing quinone/hydroquinone moieties and 1,4-dihydroxy-bis(pyrazol-1-yl)benzenes (Fig. 3.2)<sup>8</sup>. The former had been previously investigated by Catalan and coworkers as photostabilizers to protect polymers and other light sensitive materials from degradation caused by the ultraviolet component of sunlight and various kinds of artificial light<sup>9</sup>. In the metal complexes studied by Keyes *et al* coordination of the M(bpy)<sub>2</sub> centre occurs via N2 of the pyrazole ring and the oxygen of the hydroquinone moiety. The mononuclear compounds are photostable and exhibit intense, broad range visible absorbances with  $\lambda_{\text{max}}$  tailing to 800 nm. The first redox process is hydroquinone-based and the lowest energy absorption is assigned to a hydroquinone — 2,2'-bipyridyl interligand transition<sup>10</sup>. The dinuclear O,N-coordinated complexes likewise exhibit strong absorbances over a broad visible spectrum. Furthermore they give rise to stable mixed-valence species, which exhibit interaction between the metal centres. The metal-metal interaction is particularly strong for the dinuclear complex of the ligand 1,4-dihydroxy-2,5-bis(pyrazol-1-yl)benzene, where the metals are bound via anionic hydroxyls through a bridging hydroquinone moiety<sup>11</sup>. Furthermore in the hydroquinone-substituted pyridyltriazole ligand 3-(2,5-dihydroxyphenyl)-5-(2-pyridyl)-1,2,4-triazole (Fig. 3.2), there was strong evidence to suggest that a reversible intramolecular proton transfer occurred via hydrogen-bridge formation between the hydroquinone and the triazole upon oxidation of the hydroquinone. In order to investigate the role played by the negative triazole bridge in this process, it was of interest to synthesise an analogous ligand containing a neutral triazole ring. The ligand H<sub>2</sub>L4 meets these requirements.



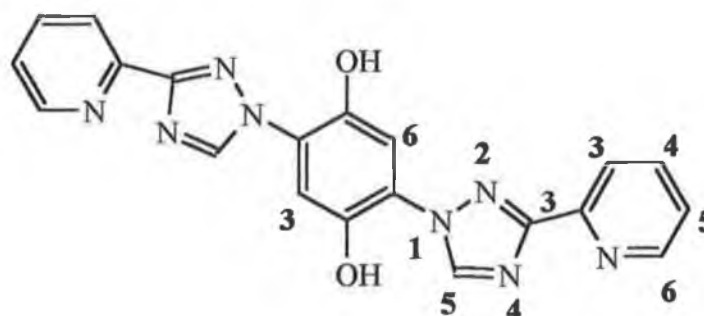
1,3-bis(5-(2-pyridyl)-4H-1,2,4,-triazol-3-yl)benzene (H<sub>2</sub>L1)



1,4-bis(5-(2-pyridyl)-4H-1,2,4,-triazol-3-yl)benzene (H<sub>2</sub>L2)

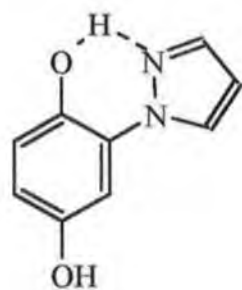


1,4-bis(1-methyl-3-(2-pyridyl)-1,2,4,-triazol-5-yl)benzene (L3)

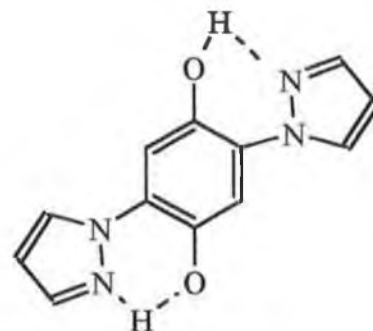


1,4-dihydroxy-2,5-bis(3-(2-pyridyl)-1,2,4-triazol-1-yl)benzene (H<sub>2</sub>L4)

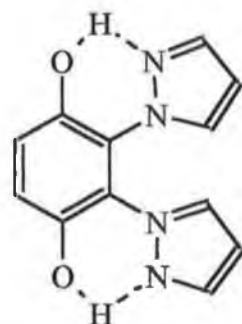
Figure 3.1. Structures of the ligands discussed in this chapter.



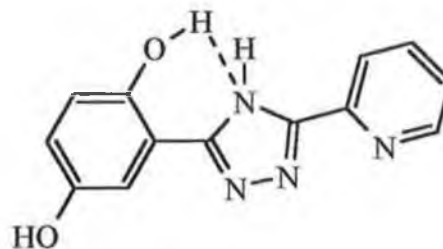
1,4-dihydroxy-2-(pyrazol-1-yl)benzene



1,4-dihydroxy-2,5-bis(pyrazol-1-yl)benzene



1,4-dihydroxy-2,3-bis(pyrazol-1-yl)benzene



3-(2,5-dihydroxyphenyl)-5-(2-pyridyl)-1,2,4-triazole

Figure 3.2. Structures of some of the ligands studied by T. Keyes<sup>8</sup>.

## 3.2 Ligand Synthesis.

### 3.2.1 Synthesis of 1,3-bis(5-(2-pyridyl)-4H-1,2,4-triazol-3-yl)benzene (H<sub>2</sub>L1).

This synthesis involved three steps:

#### 3.2.1.1. Synthesis of 2-pyridylamidrazone.

2-cyanopyridine (22g, 0.21 mol) and excess hydrazine hydrate (15 g, 0.3 mol) were mixed in a minimum amount of ethanol and allowed to stir overnight. The pale yellow needle-like crystals were filtered, washed with diethyl ether and air dried.

Yield = 26.8g (94%). M.P. = 96-98 °C (lit. 95-96 °C)<sup>12</sup>

<sup>1</sup>H-NMR [CDCl<sub>3</sub>]: δ (ppm): 7.24 (1H, dd, pyridyl H<sub>5</sub>, J = 6Hz), 7.67 (1H, dd, pyridyl H<sub>4</sub>, J = 7.8Hz), 8.00 (1H, d, pyridyl H<sub>3</sub>, J = 7.8Hz), 8.50 (1H, d, pyridyl H<sub>6</sub>, J = 6Hz), 4.63 (2H, s, broad H<sub>NH</sub>), 5.42 (2H, s, H<sub>NH2</sub>).

<sup>13</sup>C-NMR [CDCl<sub>3</sub>]: δ(ppm): 119.90, 123.90, 136.50, 148.10, 148.80, 150.97.

#### 3.2.1.2 Preparation of Isophthaloyl dichloride.

To a solution of isophthalic acid (16.61 g, 0.1 mol) and DMF (1 cm<sup>3</sup>), thionyl chloride (30 cm<sup>3</sup>, 0.4 mol) was added under a nitrogen atmosphere. The reaction mixture was then heated to reflux temperature for 30 min, by which time a deep yellow solution had formed. After cooling, any excess thionyl chloride was removed by distillation, and upon cooling of the remaining solution, white crystals formed. These were collected under vacuum and washed with hexane.

Yield = 9.2g (50%). M.P. = 40-42 °C (lit. 43-44 °C)<sup>13</sup>

<sup>1</sup>H-NMR [CDCl<sub>3</sub>]: δ (ppm): 8.86 (1H, s, phenyl H<sub>2</sub>), 8.43 (2H, d, phenyl H<sub>4</sub>, H<sub>6</sub>, J = 7.9Hz), 7.74 (1H, t, phenyl H<sub>5</sub>, J = 7.9Hz)

$^{13}\text{C-NMR}$  [ $\text{CDCl}_3$ ]:  $\delta$  (ppm): 130.23, 134.08, 134.70, 137.30, 167.56.

### 3.2.1.3 Preparation of *N,N'*-Isophthaloyl-bis((2-pyridyl)hydrazidine).

2-Pyridylamidrazone (6.8 g, 0.05 mol) was dissolved in a minimum amount of dry THF and 10 cm<sup>3</sup> triethylamine under a nitrogen atmosphere. To this was added dropwise, under  $\text{N}_2$ , with constant stirring, a solution of isophthaloyl dichloride (5.08 g, 0.025 mol) in THF, while maintaining the reaction mixture at 0°C. The reaction mixture was then reduced to approx. 25 cm<sup>3</sup> volume and an equivolume of water added. The yellow product was filtered, washed with water, hot methanol and diethyl ether and dried under vacuum and in the oven at 60 °C.

Yield = 7.2g (72%) M.P= 268-270 °C (lit. 278-279 °C dec.)

$^1\text{H-NMR}$  [ $(\text{CD}_3)_2\text{SO}$ ]:  $\delta$  (ppm): 8.42 (1H, s, phenyl  $\text{H}_2$ ), 8.20 (2H, d, pyridyl  $\text{H}_3$ ,  $J = 7.9\text{Hz}$ ), 7.60 (1H, t, phenyl  $\text{H}_5$ ,  $J = 7.4\text{Hz}$ ), 8.02 (1H, d, phenyl  $\text{H}_4, \text{H}_6$ ,  $J = 7.4\text{Hz}$ ), 7.91 (1H, dd, pyridyl  $\text{H}_4$ ,  $J = 7.9\text{Hz}$ ), 7.49 (1H, dd, pyridyl  $\text{H}_5$ ,  $J = 5\text{Hz}$ ), 8.60 (1H, d, pyridyl  $\text{H}_6$ ,  $J = 5\text{Hz}$ ), 7.02 (3H, s,  $\text{H}_{\text{NH}}$ ), 10.30 (1H, s,  $\text{H}_{\text{NH}}$ ).

$^{13}\text{C-NMR}$  [ $\text{CDCl}_3$ ]:  $\delta$  (ppm): 120.85, 124.87, 126.85, 128.28, 130.27, 134.45, 136.99, 147.94, 148.16, 150.60, 162.78.

### 3.2.1.4 Cyclization of *N,N'*-Isophthaloyl-bis((2-pyridyl)hydrazidine) to form *H<sub>2</sub>L1*.

*N,N'*-Isophthaloyl-bis((2-pyridyl)hydrazidine) (7.00 g, 0.017 mol) was suspended in a minimum volume (~ 30 cm<sup>3</sup>) of ethylene glycol and heated under reflux

temperature for 2 hours. A white crystalline precipitate was obtained upon cooling of the solution. Further precipitation of the product was induced by the addition of a small amount of water to the mother liquor. The ligand was titrated with boiling methanol, filtered and dried in the oven overnight. Completion of cyclisation was confirmed by the disappearance of the C=O stretch at  $1630\text{ cm}^{-1}$  in the IR spectrum.

Yield = 2.8g (44%) M.P =  $320\text{-}322\text{ }^{\circ}\text{C}$  (Lit.  $326.5\text{-}327.5\text{ }^{\circ}\text{C}$ )<sup>6</sup>

$^1\text{H-NMR}$  [(CD<sub>3</sub>)<sub>2</sub>SO]:  $\delta$  (ppm): 8.88 (1H, s, phenyl H<sub>2</sub>), 8.16 (2H,d, phenyl H<sub>4</sub>,H<sub>6</sub>, J = 7.9Hz), 7.65 (1H,t, phenyl H<sub>5</sub>, J = 7.9Hz), 8.23 (1H, d, pyridyl H<sub>3</sub>, J = 7.9Hz), 8.02 (1H, dd, pyridyl H<sub>4</sub>, J = 7.9Hz), 7.55ppm (1H, dd, pyridyl H<sub>5</sub>, J = 6Hz), 8.72 (1H, d, pyridyl H<sub>6</sub>, J = 5Hz), 14.90 (1H, s (broad), H<sub>NH</sub>).

$^{13}\text{C-NMR}$  [(CD<sub>3</sub>)<sub>2</sub>SO]:  $\delta$  (ppm): 121.53, 123.38, 123.62, 125.06, 126.58, 129.41, 131.40, 137.80, 146.31, 149.52, 149.72.

Mass Spectrum: m/z 367 (M+1).

Calcd. for C<sub>20</sub>H<sub>14</sub>N<sub>8</sub> = C: 65.56; H: 3.85; N: 30.59 %. Anal. found: C: 65.39; H: 3.76; N: 30.57 %.

### **3.2.2 Synthesis of 1,4-bis(5-(2-pyridyl)-4H-1,2,4-triazol-3-yl)benzene (H<sub>2</sub>L<sub>2</sub>).**

#### **3.2.2.1. Preparation of *N,N'*-Terephthaloyl-bis((2-pyridyl)hydrazidine).**

This intermediate was prepared using two methods:

- As for the *N,N'*-isophthaloyl-intermediate except that a solution of terephthaloyl dichloride (5.08 g, 0.025 mol) was added to the 2-pyridylamidrazone solution (6.8 g, 0.05 mol). Yield = 6.00g (60%).

M.P. >  $300\text{ }^{\circ}\text{C}$ .

b) By an Interfacial Method:

A solution of terephthaloyl dichloride (2.03 g, 0.01 mol) in 100 cm<sup>3</sup> of dichloromethane was added rapidly to a vigorously stirred solution of 2-pyridylamidrazone (2.72 g, 0.02 mol) in an equivolume of water, whereupon a yellow precipitate was immediately formed. The reaction mixture was then stirred for a further 10 min. Following evaporation of the dichloromethane, the yellow precipitate was filtered, washed with water, methanol, diethyl ether and dried in the oven overnight at 80 °C. Yield = 2.75 g (68%).

M.P. > 300 °C.

<sup>1</sup>H-NMR [(CD<sub>3</sub>)<sub>2</sub>SO]: δ (ppm): 8.00 (2H, s, phenyl H), 8.19 (1H, d, pyridyl H<sub>3</sub>, J = 7.9Hz), 7.72 (1H, dd, pyridyl H<sub>4</sub>, J = 7.9Hz), 7.51 (1H, dd, pyridyl H<sub>5</sub>, J = 4.9Hz), 8.62 (1H, d, pyridyl H<sub>6</sub>, J = 4.4Hz), 7.03 (2H, s, H<sub>NH</sub>), 10.30 (1H, s (broad), H<sub>NH</sub>).

<sup>13</sup>C-NMR [(CD<sub>3</sub>)<sub>2</sub>SO]: δ (ppm): 120.89, 125.01, 127.57, 127.96, 137.09, 148.24, 148.44, 150.30, 161.72.

**3.2.2.2.**      Cyclization of *N,N'*-Terephthaloyl-bis((2-pyridyl)hydrazidine) to form H<sub>2</sub>L<sub>2</sub>.

This was carried out as previously described for H<sub>2</sub>L<sub>1</sub>.

Yield = 1.40 g ( 57%) M.P. > 300 °C

<sup>1</sup>H-NMR [(CD<sub>3</sub>)<sub>2</sub>SO]: δ (ppm): 8.23 (2H, s, phenyl H), 8.19 (1H, d, pyridyl H<sub>3</sub>, J = 7.9Hz), 8.02(1H, dd, pyridyl H<sub>4</sub>, J = 7.9Hz), 7.54 (1H, dd, pyridyl H<sub>5</sub>, J = 6Hz), 8.72 (1H, d, pyridyl H<sub>6</sub>, J = 5Hz), 14.50 (1H, s (broad), H<sub>NH</sub>) .

$^{13}\text{C-NMR}$  [ $(\text{CD}_3)_2\text{SO}$ ]:  $\delta$  (ppm): 121.52, 123.21, 125.11, 126.40, 126.81, 127.45, 137.88, 149.69, 150.41.

Mass Spectrum:  $m/z$  367 (M+1).

Calcd. for  $\text{C}_{20}\text{H}_{14}\text{N}_8$  = C: 65.56; H: 3.85; N: 30.59 %. Anal. found: C: 65.83; H: 3.94; N: 30.28 %.

### **3.2.3 Attempted synthesis of 1,2-bis(5-(2-pyridyl)-4H-1,2,4-triazol-3-yl)benzene.**

#### **3.2.3.1. Preparation of *N,N'*-Phthaloyl-bis((2-pyridyl)hydrazidine).**

2-Pyridylamidrazone (6.8 g, 0.05 mol) was dissolved in a minimum amount of dry THF and 10 cm<sup>3</sup> triethylamine under a nitrogen atmosphere. To this was added dropwise, under  $\text{N}_2$ , with constant stirring, a solution of phthaloyl dichloride (3.6 cm<sup>3</sup>, 0.025 mol) in THF, while maintaining the reaction mixture at 0°C. The reaction mixture was then reduced to approx. 25 cm<sup>3</sup> volume and an equivolume of water added. The product was filtered and recrystallised from methanol. However NMR analysis revealed that the yellow product obtained was not the desired one, but rather was indicative of the phthalimide structure shown in Fig. 3.3. This was supported by mass spectral data and microanalysis.

Yield = 3 g (45 %) M.P = 196-198 °C

$^1\text{H-NMR}$  [ $(\text{CD}_3)_2\text{SO}$ ]:  $\delta$  (ppm): 8.86 (1H, d, pyridyl H<sub>6</sub>, J = 4Hz), 8.24 (1H, d, pyridyl H<sub>3</sub>, J = 7.9Hz), 7.98 (1H, dd, pyridyl H<sub>4</sub>, J = 7.9Hz), 7.81 (4H, m, H<sub>phenyl</sub>, J = 4.4Hz), 7.70 (1H, s (broad), H<sub>NH</sub>), 7.61 (1H, dd, pyridyl H<sub>5</sub>, J = 4Hz), 7.53 (1H, s (broad), H<sub>NH</sub>).

$^{13}\text{C-NMR}$   $[(\text{CD}_3)_2\text{SO}]$ :  $\delta$  (ppm): 121.93, 122.44, 126.22, 131.66, 133.71, 137.41, 148.46, 149.01, 160.54, 165.25.

DEI Mass Spectrum:  $m/z$  266 ( $\text{M}^+$ ).

Calcd. for  $\text{C}_{14}\text{H}_{10}\text{N}_4\text{O}_2$  = C: 63.15; H: 3.79; N: 21.04 %. Anal. found: C: 63.12; H: 3.85; N: 20.91 %.

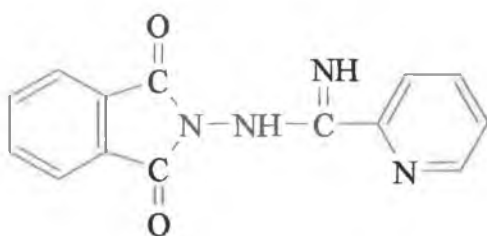


Figure 3.3 Proposed phthalimide structure for product formed in 3.2.3.1.

### 3.2.4 Synthesis of 1,4-bis(1-methyl-3-(2-pyridyl)-1,2,4-triazol-5-yl)benzene (L3).

#### 3.2.4.1. Synthesis of $N^2$ -methyl-2-pyridylamidrazone.

2-cyanopyridine (36 g, 0.35 mol) and excess methylhydrazine (18.43 g, 0.40 mol) were mixed in a minimum amount of ethanol and allowed to stir overnight. The pale yellow crystalline product was filtered, washed with diethyl ether and air dried.

Yield = 26.7 g (50%). M.P. = 108-110 °C (lit. 109-110 °C)<sup>14</sup>

$^1\text{H-NMR}$   $[\text{CDCl}_3]$ :  $\delta$  (ppm): 7.24 (1H, dd, pyridyl  $\text{H}_5$ ,  $J = 5.9\text{Hz}$ ), 7.67 (1H, dd, pyridyl  $\text{H}_4$ ,  $J = 7.9\text{Hz}$ ), 8.08 (1H, d, pyridyl  $\text{H}_3$ ,  $J = 7.9\text{Hz}$ ), 8.50 (1H, d, pyridyl  $\text{H}_6$ ,  $J = 5.9\text{Hz}$ ), 5.24 (2H, s, (broad)  $\text{H}_{\text{NH}}$ ), 2.98 (3H, s,  $\text{H}_{\text{CH}_3}$ ).

<sup>13</sup>C-NMR [CDCl<sub>3</sub>]: δ (ppm): 38.48, 119.60, 123.32, 136.02, 146.41, 147.77, 150.72.

**3.2.4.2.**      Preparation of *N,N'*-Terephthaloyl-bis(*N*<sup>2</sup>-methyl-2-pyridyl)hydrazidine) intermediate.

The intermediate was prepared as for the ligand H<sub>2</sub>L2 by the dropwise addition of a THF solution of terephthaloyl dichloride (5.08 g, 0.025 mol) to a solution of *N*<sup>2</sup>-methyl-2-pyridylamidrazone (7.50 g, 0.05 mol) and triethylamine in THF.

Yield = 7.00 g (65%)                      M.P. = 178-180 °C

<sup>1</sup>H-NMR [CDCl<sub>3</sub>]: δ (ppm): 8.15 (2H, s, phenyl H), 8.10 (1H, d, pyridyl H<sub>3</sub>, J = 7.9Hz), 7.65 (1H, dd, pyridyl H<sub>4</sub>, J = 7.9Hz), 7.43 (1H, dd, pyridyl H<sub>5</sub>, J = 5.9Hz), 8.60 (1H, d, pyridyl H<sub>6</sub>, J = 5.9Hz), 10.30 (1H, s, (broad) H<sub>NH</sub>), 4.11 (3H, s, H<sub>CH3</sub>).

<sup>13</sup>C-NMR [CDCl<sub>3</sub>]: δ (ppm): 38.50, 120.82, 124.67, 128.85, 129.10, 136.89, 148.24, 150.26, 153.79, 161.2.

**3.2.4.3.**      Cyclization of *N,N'*-Terephthaloyl-bis(*N*<sup>2</sup>-methyl-2-pyridyl)hydrazidine) intermediate to form L3.

Cyclization was carried out in ethylene glycol as described for H<sub>2</sub>L1 and H<sub>2</sub>L2. The white product was recrystallised from methanol.

Yield = 4.20 g (66%)                      M.P. = 278-280 °C

<sup>1</sup>H-NMR [CDCl<sub>3</sub>]: δ (ppm): 8.07 (2H, s, phenyl H), 8.10 (1H, d, pyridyl H<sub>3</sub>, J = 7.9Hz), 7.92 (1H, dd, pyridyl H<sub>4</sub>, J = 7.9Hz), 7.45 (1H, dd, pyridyl H<sub>5</sub>, J = 5Hz), 8.67 (1H, d, pyridyl H<sub>6</sub>, J = 5Hz), 4.12 (3H, s, H<sub>CH3</sub>).

<sup>13</sup>C-NMR [CDCl<sub>3</sub>]: δ (ppm): 37.65, 121.58, 124.15, 129.00, 129.13, 137.16, 149.45, 149.71, 154.26, 159.88.

Mass Spectrum:  $m/z$  395 (M+1).

Calcd. for  $C_{22}H_{18}N_8$  = C: 66.98; H: 4.60; N: 28.41 %. Anal. found: C: 66.69; H: 4.61; N: 27.88 %.

### 3.2.5 Synthesis of 1,4-dihydroxy-2,5-bis(3-(2-pyridyl)-1,2,4-triazol-1-yl)benzene (H<sub>2</sub>L4)

5-(2-pyridyl)-1,2,4-triazole (Hptr) was prepared as described by Hage<sup>15</sup>.

1,4-benzoquinone (3.0 g, 27.7 mmol) was dissolved in dry 1,4-dioxane. To this was added in 2 g quantities at 30 min intervals 5-(2-pyridyl)-1,2,4-triazole (8.1 g, 55.81 mmol). The reaction mixture was heated at reflux after each addition and was allowed to reflux for a further 2 hours after all the 5-(2-pyridyl)-1,2,4-triazole had been added. The reaction was followed using TLC on silica (ethyl acetate:methanol 4:1). The solution was allowed to cool and upon addition of methanol it was possible to obtain a precipitate containing mostly the desired product. Subsequent recrystallisation from methanol and acetone yielded a white powder.

Yield = 1.4 g (13 %)

M.P. = 260 °C dec.

<sup>1</sup>H-NMR [CDCl<sub>3</sub>]:  $\delta$  (ppm): 7.17 (1H, s, phenyl H), 7.35 (1H, dd, pyridyl H<sub>5</sub>, J = 4.9Hz), 7.79 (2H, m, pyridyl H<sub>3</sub>,H<sub>4</sub>, J = 7.9Hz), 8.55 (1H, d, pyridyl H<sub>6</sub>, J = 4.4Hz), 8.76 (1H, s, triazole H<sub>CH</sub>), 10.15 (1H, s, hydroxyl H).

<sup>13</sup>C-NMR [CDCl<sub>3</sub>]:  $\delta$  (ppm): 118.82, 121.44, 121.67, 124.17, 137.01, 145.72, 148.25, 149.16, 149.62, 161.20.

Mass Spectrum:  $m/z$  398 (M+1).

Calcd. for  $C_{20}H_{14}N_8O_2 \cdot CH_3OH \cdot 3/2H_2O$  = C: 55.13; H: 4.62; N: 24.50 %. Anal.

found: C: 55.25; H: 4.35; N: 24.83 %.

### **3.3 Discussion**

#### **3.3.1 Synthesis.**

The synthetic route used for the syntheses of the ligands H<sub>2</sub>L1-L3 is outlined in Figure 3.4. As stated in the introduction, the procedures were based on the work of Hergenrother<sup>7</sup> and feature nucleophilic substitution at the carbonyl group of the acid chlorides. Both low temperature condensation and interfacial methods for preparation of the intermediate acylamidrazones were equally effective in terms of yield and purity of product formed. The increased stability of these intermediates with larger substituents is noteworthy, as reflected by their high melting points and the high temperatures required to ensure ring closure and formation of the desired triazole system. Problems with solubility were encountered for both the ligands and their intermediates, in particular for H<sub>2</sub>L2. Aprotic amphoteric solvents such as DMSO and DMF were found to have the greatest solubilising properties.

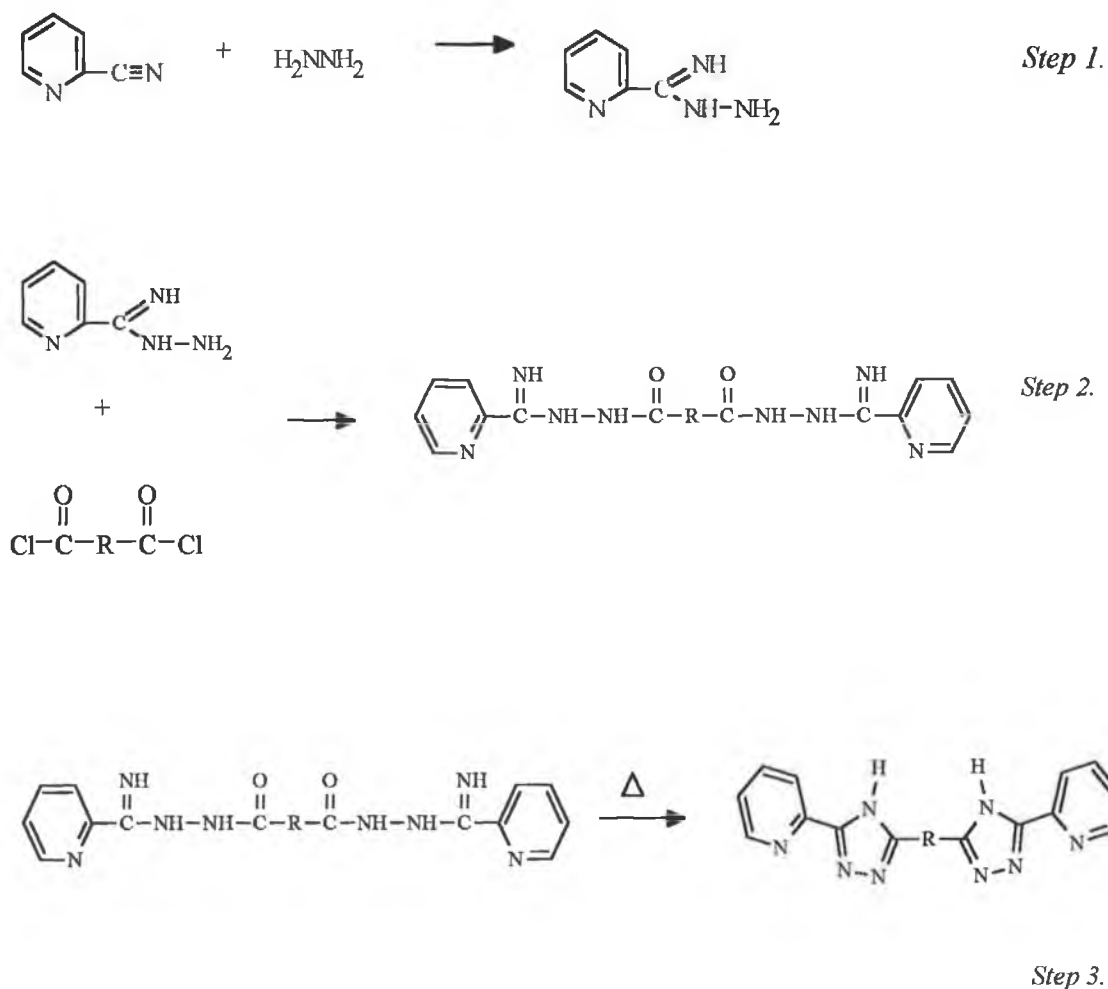


Figure 3.4. Synthetic route for formation of ligands  $H_2L1$ ,  $H_2L2$  and  $L3$ .

Many attempts to synthesise the ligand 1,2-bis(5-(2-pyridyl)-4*H*-1,2,4-triazol-3-yl)benzene were made, but in each case a phthalimide product was obtained. This appears to be due mainly to steric reasons, outlined in the mechanism shown below (Fig. 3.5). The close proximity of the NH to the carbonyl group in the intermediate facilitates internal nucleophilic attack and subsequent ring closure to form a phthalimide ring system. This structural assignment was supported by NMR (Fig. 3.6), the mass spectral data and microanalysis, together with IR and UV spectral analysis of the product and comparison with known phthalimide ring systems. The UV spectrum

shows intense absorption bands at 228 nm, 213 nm and a shoulder at 320 nm. A strong phosphorescence at 337 nm is also observed. The IR spectrum shows carbonyl stretches at  $1701\text{ cm}^{-1}$  and characteristic NH stretches at  $3427$  and  $3303\text{ cm}^{-1}$ .

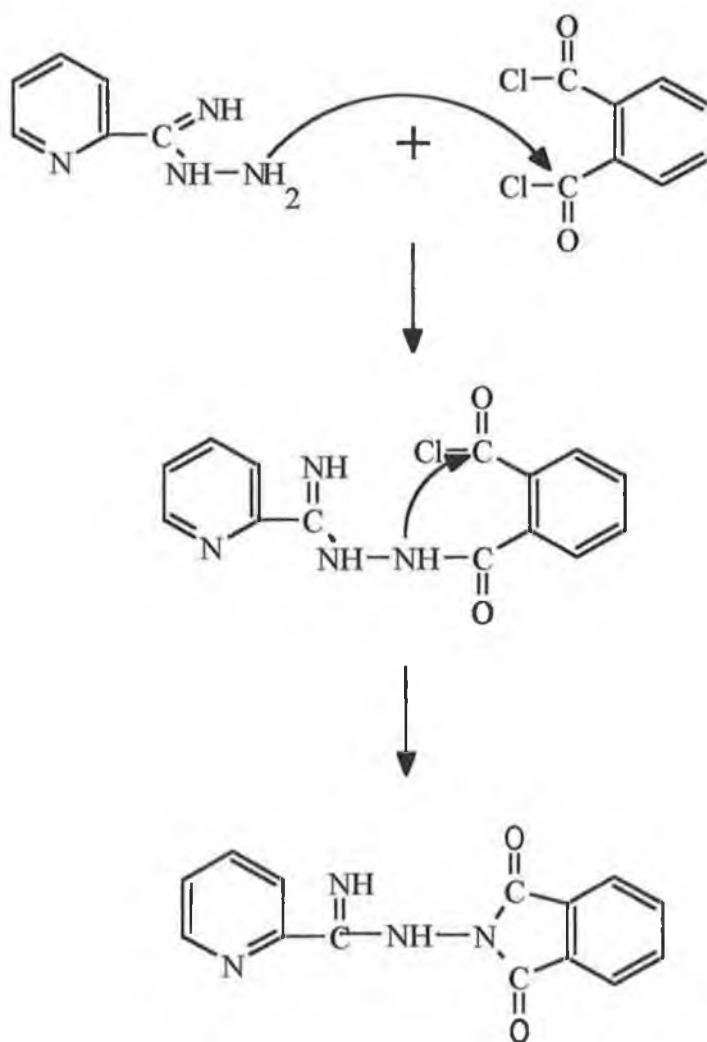


Figure 3.5. Proposed mechanism for the formation of Phthalimide structure.

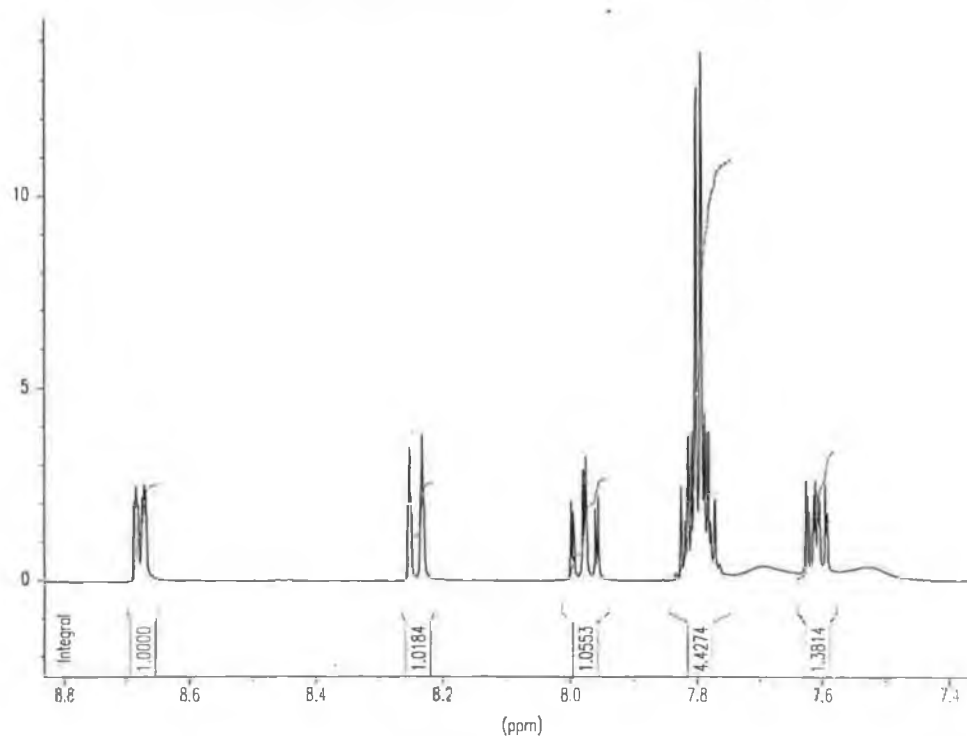


Figure 3.6  $^1\text{H-NMR}$  spectrum of phthalimide product obtained in  $d_6\text{-DMSO}$ .

Attempts to synthesise an unsymmetric analogue of  $\text{H}_2\text{L}_2$ , containing only one  $N$ -methyl group proved unsuccessful. The afore-mentioned ligand  $\text{Hbpt}$  possesses an inherent asymmetry due to the different  $\sigma$ -donor capacities of  $\text{N}1$  and  $\text{N}4$ . The resulting asymmetric coordination geometry of the metal centres in the dinuclear complexes induces differences in the oxidation potentials of each metal centre, thereby facilitating the study of intervalence transitions and the extent of metal-metal communication in the mixed-valence species. The introduction of an  $N$ -methyl substituent on one triazole ring of the ligand  $\text{H}_2\text{L}_2$  would give rise to an asymmetric bridging ligand with two distinct coordination sites. Dinuclear complexes of such a ligand would be expected to demonstrate interesting electron and energy transfer properties. The methods employed to synthesise this target ligand involved direct alkylation of the ligand  $\text{H}_2\text{L}_2$  using  $\text{CH}_3\text{I}/\text{NaH}$  and  $\text{CH}_3\text{I}/\text{NaOH}$  and also introduction of the methyl group using methyl hydrazine in the hydrazidine formation step. The

latter resulted in formation of the *N,N*-dimethyl ligand L3, while the former gave rise to a mixture of products which could not be separated by conventional TLC or column chromatography.

The ligand H<sub>2</sub>L4 was prepared by a synthetic method based on the nucleophilic addition of *N*-substituted pyrazoles to *p*-benzoquinone. In the case of pyrazole addition three products, 2-(pyrazol-1-yl)-, 2,3-bis(pyrazol-1-yl)- and 2,5-bis(pyrazol-1-yl)-1,4-dihydroxybenzene, in a ratio of approximately 60:30:10 were formed. An investigation of this reaction with regard to the influence of the substituent on the pyrazole ring by Ballesteros and coworkers<sup>16</sup> revealed that the nucleophilic character and basicity of the pyrazoles were important factors in determining the products of the reaction. In general the preferred formation of 2,3-bis adducts was observed. In the addition of 5-(2-pyridyl)-1,2,4-triazole to 1,4-benzoquinone however, only one product, the 2,5-bis adduct, was formed. This is most likely due to steric hindrance by the bulky pyridyltriazole moiety, thereby inhibiting formation of a 2,3-bis adduct. The ligands studied by both Keyes<sup>8</sup> and Catalan<sup>9</sup> were found to show extensive intramolecular hydrogen-bonding between the hydroxyl groups and the adjacent nitrogens. The <sup>1</sup>H-NMR spectrum of H<sub>2</sub>L4 has a phenolic proton resonance at low field, which suggests H-bridging between the phenol and the triazole N2 (Fig. 3.7).

All the ligands described have been modelled using Hyperchem. They all possess a two-fold symmetry and have  $\pi$ -electronic systems which are extended and uninterrupted across the molecule (Figure 3.8 (a), (b)). The symmetric nature of the ligands is reflected in the simplicity of their <sup>1</sup>H-NMR spectra which were readily assigned using splitting patterns and coupling constants.

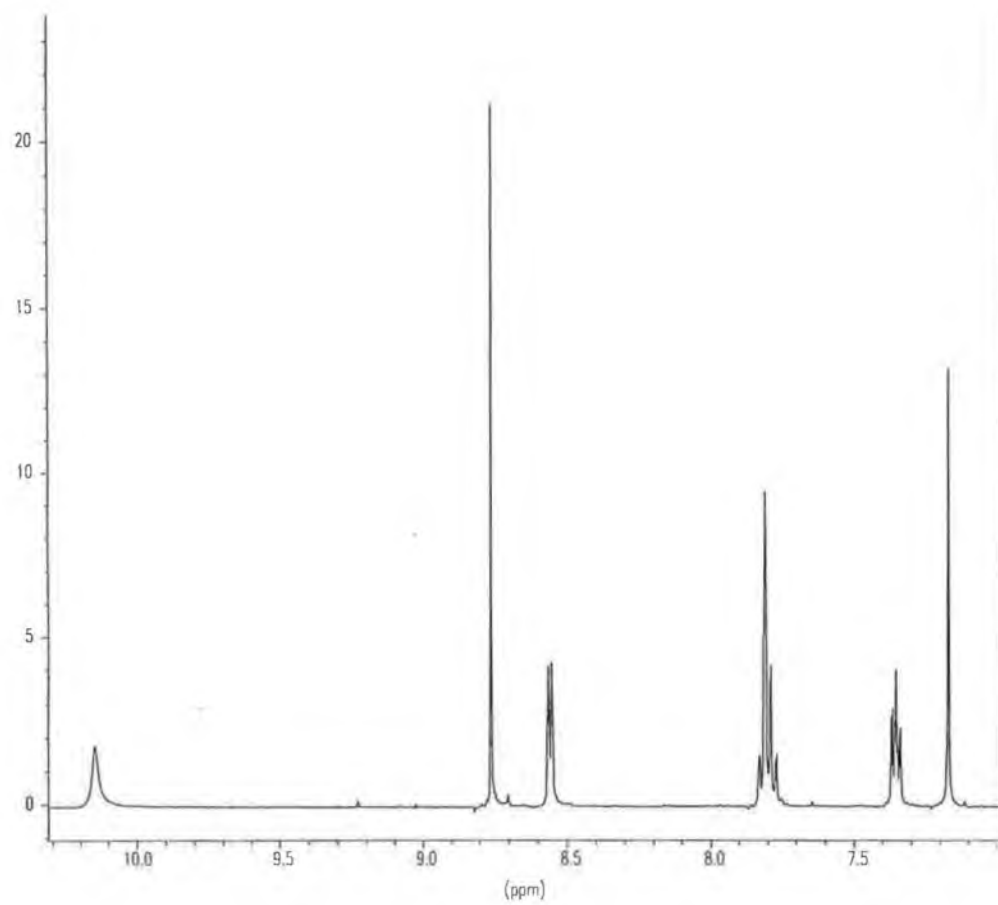
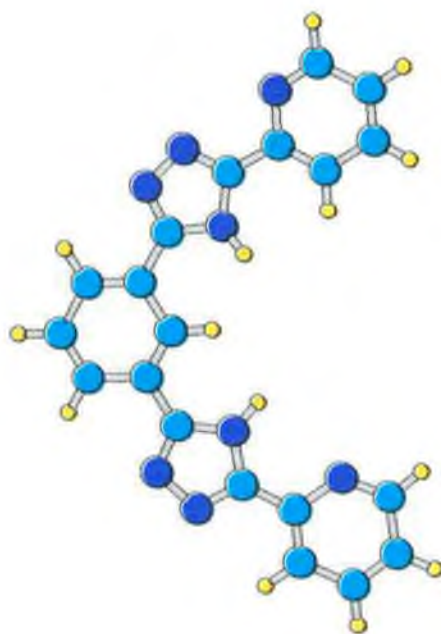
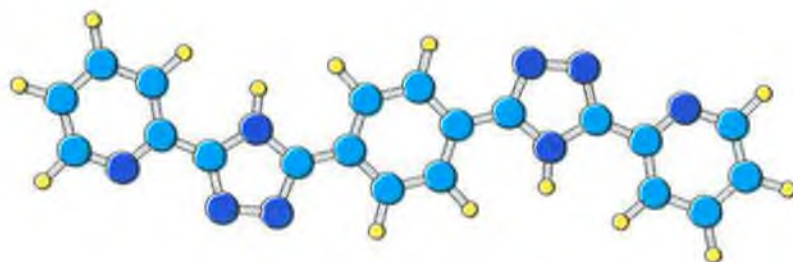


Figure 3.7.  $^1\text{H-NMR}$  spectrum of  $\text{H}_2\text{L4}$  in  $d_6$ -dimethyl sulphoxide.

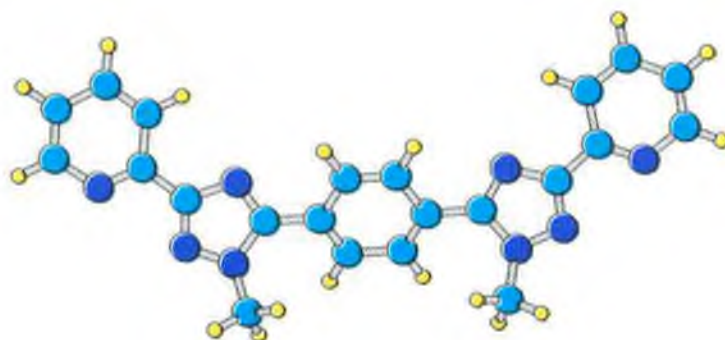


1,3-bis(5-(2-pyridyl)-4H-1,2,4-triazol-3-yl)benzene (H<sub>2</sub>L1)

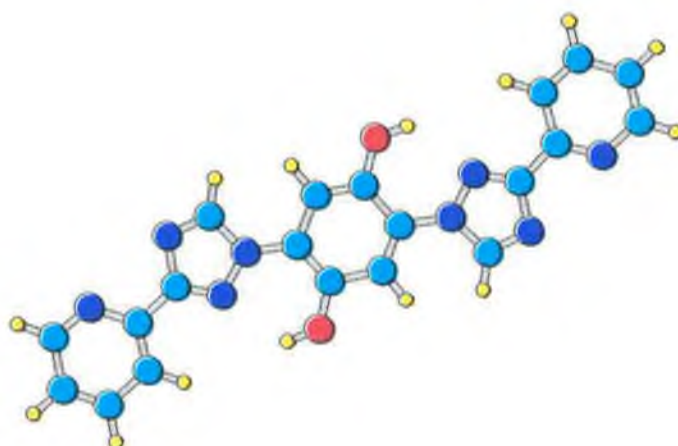


1,4-bis(5-(2-pyridyl)-4H-1,2,4-triazol-3-yl)benzene (H<sub>2</sub>L2)

*Figure 3.8 (a) Hyperchem models of the ligands discussed in this chapter.  
Turquoise = Carbon, Blue = Nitrogen, Yellow = Hydrogen.*



1,4-bis(1-methyl-3-(2-pyridyl)-1,2,4-triazol-5-yl)benzene (L3)



1,4-dihydroxy-2,5-bis(3-(2-pyridyl)-1,2,4-triazol-1-yl)benzene (H<sub>2</sub>L4)

*Figure 3.8 (b) Hyperchem models of the ligands discussed in this chapter.  
Turquoise = Carbon, Blue = Nitrogen, Yellow = Hydrogen, Red = Oxygen.*

### 3.3.2 Electronic properties.

The UV absorption and emission data for the ligands are presented in Table 3.1

**Table 3.1** Absorption and Emission data of the ligands\*.

| Ligand            | Absorbance $\lambda_{\max}/\text{nm}$ ,<br>(log $\epsilon$ ) | Emission (nm)<br>300 K |
|-------------------|--|------------------------|
| H <sub>2</sub> L1 | 280 (4.40), 234 (4.28)                                       | 378                    |
| L1 <sup>2-</sup>  | 282  | 417                    |
| H <sub>2</sub> L2 | 284 (4.30)   | 366                    |
| L2 <sup>2-</sup>  | 300  | 434                    |
| L3                | 279 (4.77), 234  | 350                    |
| H <sub>2</sub> L4 | 310 (4.00), 275 (4.23)                                       | 368                    |
| L4 <sup>2-</sup>  | 324  | 379                    |

\* all measurements in acetonitrile, ligands were deprotonated using diethylamine

As expected, all the compounds show high intensity bands typical of  $\pi-\pi^*$  and  $n-\pi^*$  transitions. For ligands H<sub>2</sub>L1 and H<sub>2</sub>L2 these shift to lower energy upon deprotonation, which is consistent with expectations as the degree of  $\pi$ -delocalisation increases. Similarly, upon deprotonation of the hydroquinone-containing ligand, H<sub>2</sub>L4, the solution turns yellow with a resultant bathochromic shift in absorbance. Deprotonation of the hydroxyl group to produce its associated anion causes a red shift in the absorbance as a result of delocalisation of the excess charge around the molecule. Furthermore the anionic phenol quenches the excited state of L4<sup>2-</sup> when deprotonated as reflected in the significant decrease in emission intensity. It is also possible that semiquinone and quinone products are produced in solution upon deprotonation<sup>17</sup>. In general the ligands are very fluorescent at ambient temperature in

acetonitrile, emitting in the near-UV region. As for H<sub>2</sub>L4, quenching of the emission intensity upon deprotonation is observed for H<sub>2</sub>L1 and H<sub>2</sub>L2.

### 3.3.3 Acid-Base Chemistry.

Triazoles exhibit amphoteric properties, dissolving in both alkaline and acidic media due to the acidic NH group and basic properties of other nitrogen atoms, respectively. The spectroscopic changes observed during the pH titration are associated with protonation of the neutral ligands at low pH and deprotonation at higher pH. With the exception of L3, which exhibits only one acid-base equilibrium associated with the pyridyl moiety, the ligands exhibit two stepwise acid-base equilibria corresponding to the pyridyl and triazole moieties (H<sub>2</sub>L1, H<sub>2</sub>L2) and pyridyl and hydroquinone moieties (H<sub>2</sub>L4), respectively. The UV spectra obtained during the pK<sub>a</sub> titration of L3 is shown in Figure 3.9.

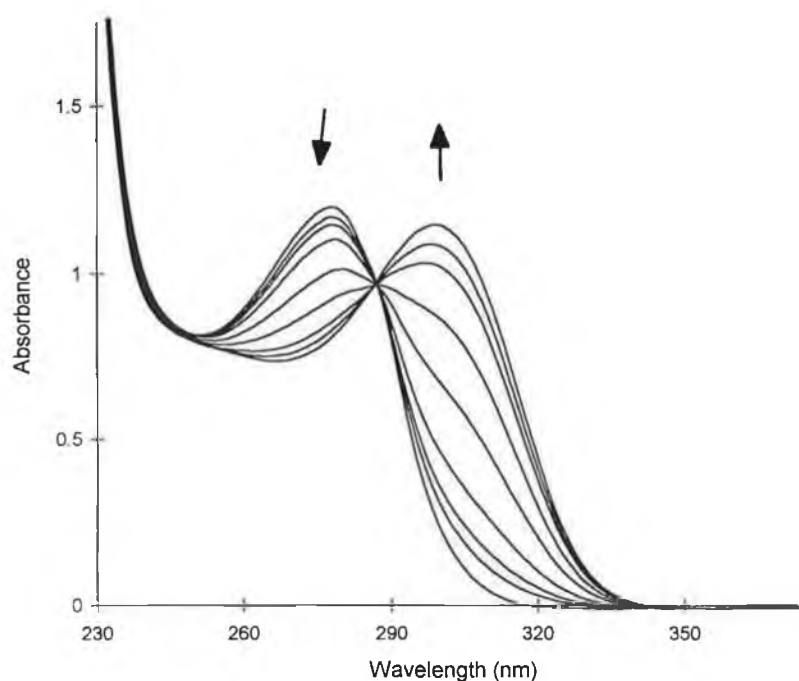


*Figure 3.9. pH dependence of the absorption spectra of L3 in Britton-Robinson buffer. pH values = 1.70, 2.10, 2.36, 2.79, 3.17, 3.63, 3.98, 4.2, 6.19.*

This ligand shows a well-defined acid-base equilibrium with an isobestic point at 287 nm. Although isobestic points were observed over some pH ranges for the other ligands during the pH titrations, the attainment of clean spectra proved difficult. This was particularly the case for the ligand H<sub>2</sub>L<sub>4</sub>, where at alkaline pH values the formation of semiquinone radical intermediates occurs<sup>17</sup>. The situation is aggravated in aqueous solution, where, in the presence of available protons, the intermediates can undergo further reactions such as disproportionation.

From an investigation of the acid-base properties of the ligands the pK<sub>a</sub> values for the ligands were determined as shown below (Table 3.2). The values obtained fall within the ranges expected.

**Table 3.2** Acid-base properties of the ligands, measured in Britton-Robinson buffer.

| <b>Ligand</b>                 | <b>Pyridyl (pK<sub>a1</sub>)</b><br>± 0.30 | <b>Triazole (pK<sub>a2</sub>)</b><br>± 0.30 | <b>Hydroxyl (pK<sub>a2'</sub>)</b><br>± 0.30 |
|-------------------------------|--|---|--|
| H <sub>2</sub> L <sub>1</sub> | 2.22                                       | 9.52  | ---  |
| H <sub>2</sub> L <sub>2</sub> | 2.55                                       | 10.36                                       | ---  |
| L <sub>3</sub>                | 3.17                                       | ---   | ---  |
| H <sub>2</sub> L <sub>4</sub> | 3.03                                       | ---   | 9.50   |

### 3.4 Conclusions.

A series of symmetric bis(pyridyltriazole) ligands in which two pyridyltriazole moieties are linked by a phenyl ring and a hydroquinone ring, respectively, have been prepared and characterised. The synthetic strategies used were based on methods previously employed for analogous compounds. Attempts to synthesise an asymmetric ligand containing a methyl substituent on N1 of one triazole ring proved unsuccessful. Furthermore in the course of trying to synthesise 1,2-bis(5-(2-pyridyl)-4*H*-1,2,4-triazol-3-yl)benzene a *N*-substituted phthalimide was formed instead.

The symmetric nature of the ligands is reflected in the simplicity of their <sup>1</sup>H-NMR spectra. The ligands all exhibit high energy, high intensity absorption bands in the UV region and are highly fluorescent. In addition, they possess acid-base properties which may be exploited to induce perturbations in the spectral and redox characteristics of their metal complexes.

### 3.4 References.

- 1 J.G. Vos, J.G. Haasnoot and G. Vos, *Inorg. Chim. Acta.*, 1983, 162, 155.
- 2 H.A. Nieuwenhuis, J.G. Haasnoot, R. Hage, J. Reedijk, T.L. Snoeck, D.J. Stufkens and J.G. Vos, *Inorg. Chem.*, 1991, 30, 48.
- 3 R. Hage, R. Prins, J.G. Haasnoot, J. Reedijk and J.G. Vos, *J. Chem. Soc. Dalton Trans.*, 1987, 1389.
- 4 B.D.J. Fennema, R. Hage, J.G. Haasnoot, J. Reedijk and J.G. Vos, *Inorg. Chim. Acta*, 1990, 171, 223.
- 5 J.F. Geldard and F. Lions, *J. Org. Chem.*, 1965, 30, 318.
- 6 R. Hage, J.G. Haasnoot, H.A. Nieuwenhuis, J. Reedijk, D.J.A. de Ridder and J.G. Vos, *J. Am. Chem. Soc.*, 1990, 112, 9245.
- 7 P.M. Hergenrother, *J. Heterocyclic Chem.*, 1969, 6, 965.
- 8 T.E. Keyes, Ph.D. Thesis, Dublin City University, 1995.
- 9 J. Catalan, F. Fabero, M.S. Guijarro, R.M. Claramunt, M.D. Santa-Maria, M.D. Foces-Foces, F.H. Cano, J. Elguero and R. Sastre, *J. Am. Chem. Soc.*, 1990, 112, 747; 1991, 113, 4046.
- 10 T.E. Keyes, P.M. Jayaweera, J.J. Mc Garvey and J.G. Vos, *J. Chem. Soc. Dalton Trans.*, 1997, 1627.
- 11 T.E. Keyes, R.J. Forster, C. Coates, P.M. Jayaweera, J.J. Mc Garvey and J.G. Vos, *Inorg. Chem.*, in press.
- 12 F.H. Case, *J. Org. Chem.*, 1965, 30, 931.
- 13 Aldrich Catalogue Handbook of Fine Chemicals 1992-1993.
- 14 S. Kubota, M. Uda and T. Nakagawa, *J. Heterocyclic Chem.*, 1975, 12, 855.
- 15 R. Hage, Ph.D Thesis 1991, Leiden University.

- 
- 16 P. Ballesteros, R.M. Claramunt, C. Escolastico and M.D. Santa Maria, *J. Org. Chem.*, 1992, 57, 1873.
- 17 D. Plancherel, J.G. Vos, A. von Zelewsky, *J. Photochem.*, 1987, 36, 267.

## **Chapter Four**

### **The Synthesis and Characterisation of Ruthenium and Osmium Complexes Containing 5-(2-pyridyl)- 1,2,4-Triazole Moieties Connected by a Phenyl Spacer**

## 4.1 Introduction.

The design and synthesis of polynuclear metal complexes containing electroactive and photoactive units are topics of great interest, not only for theoretical reasons, but also because of the potential of multicomponent systems to serve as building blocks for supramolecular assemblies and molecular devices. Many reports have appeared on the subject in recent years with a view to designing metal-based supramolecular systems featuring made-to-order energy migration and redox patterns which could play a role in performing such functions as solar energy conversion and multielectron catalysis<sup>1,2,3</sup>.

Ruthenium(II) and Osmium(II) polypyridyl complexes, because of their suitable photophysical and redox properties, have received a great deal of attention as building blocks to synthesise redox-active and luminescent polynuclear metal complexes where electron and/or energy transfer processes can be induced by light<sup>4,5</sup>. Particular attention has been paid to metal-metal interactions in dinuclear and polynuclear metal complexes. Metal-metal interactions affect the electrochemical and photophysical properties of dinuclear species and the rate of energy and electron transfer between metal units. The degree of metal-metal interaction also creates a distinction between supramolecular polynuclear species (made of weakly interacting components which maintain most of their specific properties in the polynuclear species) and polynuclear macromolecules (made of strongly interacting components which lose their specific properties in the assembly).

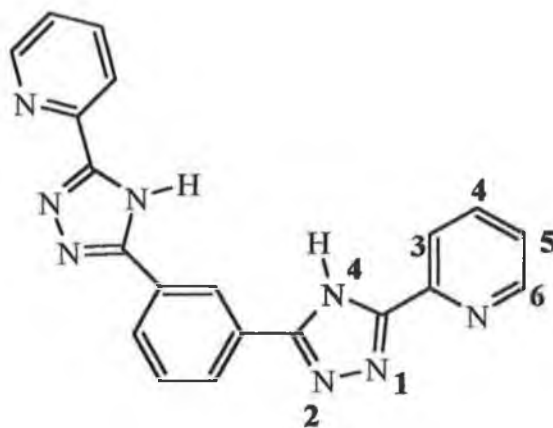
The important role played by the bridging ligand in determining the metal-metal interaction is well recognized. The bridging ligand or spacer separating the metal units has a two-fold function within a supramolecular structure; (i) a structural role in

controlling intercomponent distances and angles (ii) control of the electronic communication between components. From a structural point of view, rigid spacers such as those based on aromatic rings<sup>6,7</sup> and bicyclo aliphatic species<sup>8,9</sup> are preferred to flexible spacers such as aliphatic chains, while from an electronic viewpoint, aromatic spacers allow better communication than aliphatic ones.

As already mentioned in Chapter 1, the anion of 3,5-bis(2-pyridyl)-1,2,4-triazole,  $bpt^-$ , is particularly interesting as a bridging ligand and the photochemical and photophysical properties of its ruthenium and osmium homo- and heterometallic complexes have been extensively studied<sup>10,11</sup>. The interaction between metal centres in the dinuclear complexes is very efficient, thereby supporting the conclusion that this ligand is a convenient bridge for polynuclear complexes which can exhibit photoinduced electron or energy transfer. As a consequence, research has been carried out on complexes containing higher members of the Hbpt template and some of these will be the subject of this chapter.

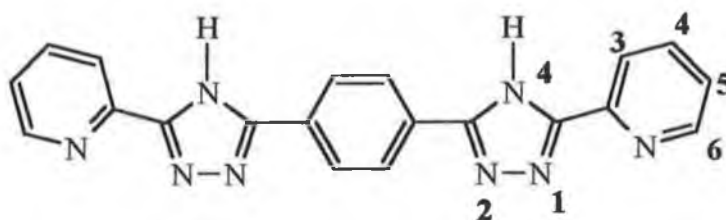
The synthesis and characterisation of a series of mononuclear and dinuclear ruthenium and osmium complexes containing the ligands  $H_2L1$  and  $H_2L2$  (Figure 4.1) are described. In addition to the homodinuclear complexes, the mixed metal Ru/Os complexes of each ligand are also studied. Preliminary studies carried out on the dinuclear complexes of  $H_2L2$  suggested that a metal-metal interaction existed<sup>12</sup> as intervalence absorption bands were obtained for the mixed-valence species. This chapter reports a detailed analysis of the photophysical, electrochemical and spectroelectrochemical properties of the mononuclear and dinuclear complexes. The extent of ground and excited state metal-metal interaction in the dinuclear complexes is

investigated. Furthermore, the effect of protonation on the properties of the complexes is studied.



1,3-bis(5-(2-pyridyl)-4H-1,2,4-triazol-3-yl)benzene

(H<sub>2</sub>L1)



1,4-bis(5-(2-pyridyl)-4H-1,2,4-triazol-3-yl)benzene

(H<sub>2</sub>L2)

Figure 4.1 Structures of the ligands H<sub>2</sub>L1 and H<sub>2</sub>L2.

## 4.2 Experimental

### 4.2.1 Synthesis of the Metal Complexes.

In this section the synthesis of the mononuclear and dinuclear Ru(bpy)<sub>2</sub>- and Os(bpy)<sub>2</sub>-complexes of the ligands H<sub>2</sub>L1 and H<sub>2</sub>L2, the preparation of which has been described in Chapter 3, will be discussed.

#### Cis-[Ru(bpy)<sub>2</sub>Cl<sub>2</sub>].2H<sub>2</sub>O

The method employed was based on that used by Sullivan<sup>13</sup>. RuCl<sub>3</sub>.xH<sub>2</sub>O (7.80 g, 30 mmol) and LiCl.H<sub>2</sub>O (1.00 g, 16.55 mmol) were heated at reflux in 50 cm<sup>3</sup> DMF under N<sub>2</sub>. To this solution 2,2'-bipyridyl (9.40 g, 60 mmol) was added slowly and the mixture allowed to reflux for a further 8 hours. After cooling, 250 cm<sup>3</sup> acetone was added to the purple solution, which was then left at 0 °C overnight. The dark-purple crystalline product was isolated, washed firstly with a minimum amount of ice-cold water to remove any Ru-CO complex formed by degradation of DMF<sup>14</sup>, then with diethyl ether and allowed to air-dry. Yield = 12.10 g (78 %).

#### Cis-[Os(bpy)<sub>2</sub>Cl<sub>2</sub>].2H<sub>2</sub>O

This synthesis was based on the method used by Buckingham and coworkers<sup>15</sup>. Potassium hexachloroosmate (1.90 g, 3.95 mmol) was dissolved in 30 cm<sup>3</sup> DMF and heated to 120 °C. To this was slowly added dropwise a solution of 2,2'-bipyridyl (1.30 g, 8.30 mmol) in 10 cm<sup>3</sup> DMF with heating at reflux temperature between additions. The mixture was then allowed to reflux for 1 hour. The product [Os(bpy)<sub>2</sub>Cl]Cl<sub>2</sub> was isolated by the dropwise addition of the reaction solution to diethyl ether with vigorous stirring. When the precipitate had formed it was filtered

and washed repeatedly with diethyl ether. The bis-bipyridyl-dichlororoosmium(III) chloride (2.00 g, 3.10 mmol) was dissolved in a mixture of DMF and methanol (2:1 v/v). To this was added with stirring over a period of 40 mins a solution of sodium dithionate (4.40 g in 200 cm<sup>3</sup> H<sub>2</sub>O), while keeping both solutions in an ice-bath. The solution containing the dark purple suspension of the product was stored overnight at 4 °C and the precipitate formed collected by filtration, washed with water and diethyl ether and air-dried. Yield = 1.50g (68 %).

**[Ru(bpy)<sub>2</sub>HL1]PF<sub>6</sub>·H<sub>2</sub>O (mRu)**

H<sub>2</sub>L1 (0.732 g, 2 mmol) was dissolved in DMF/H<sub>2</sub>O (2:1 v/v). To the solution was added cis-[Ru(bpy)<sub>2</sub>Cl<sub>2</sub>].2H<sub>2</sub>O (0.39 g, 0.75 mmol) which was then heated at reflux for 8 hours. Upon cooling, the solution was filtered to remove unreacted ligand starting material. A few drops of an aqueous NH<sub>4</sub>PF<sub>6</sub> solution were then added and the DMF/H<sub>2</sub>O removed by evaporation under reduced pressure. The resulting solid was dissolved in acetone/water (2:1 v/v) and allowed to recrystallise. The crude product, which contained some dinuclear complex, was purified by column chromatography on neutral alumina. The dinuclear complex was first eluted using acetonitrile and the desired mononuclear complex eluted using acetonitrile/methanol (1:1 v/v). It was isolated as the hexafluorophosphate salt and recrystallised from acetone/water (2:1 v/v) to which a few drops of aqueous NH<sub>3</sub> were added. Yield = 0.32 g (45 %).

Calcd. for Ru<sub>1</sub>C<sub>40</sub>H<sub>31</sub>N<sub>12</sub>OP<sub>1</sub>F<sub>6</sub> = C: 50.98; H: 3.26; N: 17.84 %. Anal. Found: C: 50.62; H: 3.60; N: 17.54 %.

[(Ru(bpy)<sub>2</sub>)<sub>2</sub>L1](PF<sub>6</sub>)<sub>2</sub>·5H<sub>2</sub>O (mRuRu)

cis-[Ru(bpy)<sub>2</sub>Cl<sub>2</sub>].2H<sub>2</sub>O (0.52 g, 1 mmol) and H<sub>2</sub>L1 (0.146 g, 0.4 mmol) were dissolved in DMF/H<sub>2</sub>O (2:1 v/v) and the mixture was heated at reflux for 4 hours. Following the addition of a few drops of aqueous NH<sub>4</sub>PF<sub>6</sub>, the reaction mixture was evaporated to dryness under reduced pressure. The resulting solid was obtained in its pure form by recrystallisation from acetone/water (2:1 v/v). Yield = 0.515 g (87 %).

Calcd. for Ru<sub>2</sub>C<sub>60</sub>H<sub>54</sub>N<sub>16</sub>O<sub>5</sub>P<sub>2</sub>F<sub>12</sub> = C: 45.82; H: 3.46; N: 14.25 %. Anal. Found: C: 46.09; H: 3.43; N: 14.08 %.

[Os(bpy)<sub>2</sub>HL1]PF<sub>6</sub>·H<sub>2</sub>O (mOs)

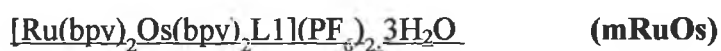
H<sub>2</sub>L1 (0.30 g, 0.82 mmol) and cis-[Os(bpy)<sub>2</sub>Cl<sub>2</sub>].2H<sub>2</sub>O (0.183 g, 0.30 mmol) were dissolved in hot DMF/H<sub>2</sub>O (4:1 v/v). A small amount of zinc metal was added to reduce any [Os(bpy)<sub>2</sub>Cl]Cl<sub>2</sub> present in the cis-[Os(bpy)<sub>2</sub>Cl<sub>2</sub>].2H<sub>2</sub>O starting material and the reaction mixture was allowed to reflux for 8 hours. The solution was cooled and filtered to remove unreacted ligand and the zinc metal. Following evaporation of the solvent, the crude product was dissolved in dichloromethane and any residual [Os(bpy)<sub>2</sub>Cl]Cl<sub>2</sub> present removed by filtration. As before, purification on neutral alumina gave the desired mononuclear complex using acetonitrile/methanol (1:1 v/v) as eluent. Yield = 0.12 g (40 %). Calcd. for Os<sub>1</sub>C<sub>40</sub>H<sub>31</sub>N<sub>12</sub>OP<sub>1</sub>F<sub>6</sub> = C: 46.60; H: 3.03; N: 16.30 %. Anal. Found: C: 46.42; H: 3.14; N: 16.09 %.

[(Os(bpy)<sub>2</sub>)<sub>2</sub>L1](PF<sub>6</sub>)<sub>2</sub>·4H<sub>2</sub>O (mOsOs)

This complex was prepared in a similar manner to mOs except that H<sub>2</sub>L1 (0.732 g, 0.20 mmol) and cis-[Os(bpy)<sub>2</sub>Cl<sub>2</sub>].2H<sub>2</sub>O (0.244 g, 0.40 mmol) were heated at reflux in

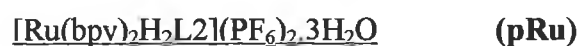
DMF/H<sub>2</sub>O (2:1 v/v). Following removal of unreacted [Os(bpy)<sub>2</sub>Cl]Cl<sub>2</sub> from a dichloromethane solution of the crude product, purification by column chromatography using acetonitrile as eluent gave the desired dinuclear complex.

Yield = 0.12 g (36 %). Calcd. for Os<sub>2</sub>C<sub>60</sub>H<sub>52</sub>N<sub>16</sub>O<sub>4</sub>P<sub>2</sub>F<sub>12</sub> = C: 41.62; H: 3.03; N: 12.94 %. Anal. Found: C: 41.72; H: 3.08; N: 12.81 %.



[Ru(bpy)<sub>2</sub>HL1]PF<sub>6</sub> (0.10 g, 0.11 mmol), cis-[Os(bpy)<sub>2</sub>Cl<sub>2</sub>].2H<sub>2</sub>O (0.067 g, 0.12 mmol) and a small amount of zinc metal were dissolved in 50 cm<sup>3</sup> Methanol/Ethanol/water (2:1:1 v/v). The mixture was heated at reflux temperature for 8 hr. The progress of the reaction was monitored using the analytical HPLC system. When all the Os(bpy)<sub>2</sub>Cl<sub>2</sub>.2H<sub>2</sub>O had reacted, the solution was filtered to remove the zinc metal and then concentrated to ~15 cm<sup>3</sup>. A few drops of aqueous conc. NH<sub>4</sub>PF<sub>6</sub> solution added to precipitate the PF<sub>6</sub> salt. The product was collected by filtration and recrystallised from acetone/water (1:1 v/v). Purification of the product was achieved by column chromatography on neutral alumina using acetonitrile as eluent.

Yield = 70 mg (41 %). Calcd. for Ru<sub>1</sub>Os<sub>1</sub>C<sub>60</sub>H<sub>50</sub>N<sub>16</sub>O<sub>3</sub>P<sub>2</sub>F<sub>12</sub> = C: 44.34; H: 3.10; N: 13.79 %. Anal. Found: C: 44.15; H: 2.93; N: 13.46 %.



This complex was prepared by two methods:

(a) H<sub>2</sub>L2 (0.732 g, 2 mmol) was dissolved in 150 cm<sup>3</sup> H<sub>2</sub>O acidified by addition of 2 M sulphuric acid and to this was slowly added cis-[Ru(bpy)<sub>2</sub>Cl<sub>2</sub>].2H<sub>2</sub>O (0.416 g, 0.8 mmol). The solution was heated at reflux temperature for 8 hours. After this period,

the orange solution was neutralised by addition of conc. NaOH, and the volume reduced to 50 cm<sup>3</sup>. The Na<sub>2</sub>SO<sub>4</sub> salt was removed by filtration and a few drops of aqueous concentrated NH<sub>4</sub>PF<sub>6</sub> solution was added to form the PF<sub>6</sub> salt. This product was collected by filtration and recrystallised from acetone/water (1:1 v/v). Purification of the product was carried out by semi-preparative HPLC using 80:20 CH<sub>3</sub>CN/H<sub>2</sub>O containing 0.12 M KNO<sub>3</sub> as mobile phase. Yield = 0.295 g (40 %).

(b) As for the complex **mRu** except that H<sub>2</sub>L2 (0.732 g, 2 mmol) and cis-[Ru(bpy)<sub>2</sub>Cl<sub>2</sub>].2H<sub>2</sub>O (0.39 g, 0.75 mmol) were used. The crude product was purified by column chromatography using neutral alumina and acetonitrile/methanol as eluent. Yield = 0.22 g (32 %). Calcd. for Ru<sub>1</sub> C<sub>40</sub>H<sub>36</sub>N<sub>12</sub>O<sub>3</sub>P<sub>2</sub>F<sub>12</sub> = C: 42.74; H: 3.20; N: 14.95 %. Anal. Found: C: 42.78; H: 3.06; N: 14.96 %.

[(Ru(bpy)<sub>2</sub>)<sub>2</sub>L2](PF<sub>6</sub>)<sub>2</sub>.3H<sub>2</sub>O            (**pRuRu**)

This complex was also prepared by two methods.

(a) [Ru(bpy)<sub>2</sub>HL2]PF<sub>6</sub> (0.30 g, 0.32 mmol) and cis-[Ru(bpy)<sub>2</sub>Cl<sub>2</sub>].2H<sub>2</sub>O (0.166 g, 0.32 mmol) were dissolved in a methanol/ethanol/water (2:1:1 v/v/v) mixture and the solution heated at reflux for 5 hours. The reaction mixture was concentrated to 15 cm<sup>3</sup> and a few drops of aqueous NH<sub>4</sub>PF<sub>6</sub> were added. The resulting precipitate was filtered off and recrystallised from acetone/water (2:1 v/v). The complex was purified using column chromatography on neutral alumina using acetonitrile as eluent.

Yield = 0.22 g (45 %)

(b) As described for **mRuRu** using cis-[Ru(bpy)<sub>2</sub>Cl<sub>2</sub>].2H<sub>2</sub>O (0.32 g, 0.6 mmol) and H<sub>2</sub>L2 (0.07 g, 0.20 mmol) and heating at reflux for 6 hours. The crude product,

isolated as the PF<sub>6</sub> salt, was purified by column chromatography on neutral alumina using acetonitrile as eluent. Yield = 0.37 g (40 %). Calcd. for Ru<sub>2</sub>C<sub>60</sub>H<sub>50</sub>N<sub>16</sub>O<sub>3</sub>P<sub>2</sub>F<sub>12</sub> = C: 46.90; H: 3.28; N: 14.59 %. Anal. Found: C: 47.07; H: 3.34; N: 14.48 %.

[Os(bpy)<sub>2</sub>HL2]PF<sub>6</sub>·3H<sub>2</sub>O (pOs)

This complex was prepared as described for mOs except that H<sub>2</sub>L2 (0.55 g, 1.50 mmol) and cis-[Os(bpy)<sub>2</sub>Cl<sub>2</sub>].2H<sub>2</sub>O (0.30 g, 0.50 mmol) were heated at reflux in DMF/H<sub>2</sub>O for 5 hours. The product obtained was purified using column chromatography on neutral alumina. Elution with acetonitrile removed the dinuclear complex and residual Os(III) species, and the desired mononuclear complex was obtained by elution with methanol. Yield = 0.20 g (40 %). Calcd. for Os<sub>1</sub>C<sub>40</sub>H<sub>35</sub>N<sub>12</sub>O<sub>3</sub>P<sub>1</sub>F<sub>6</sub> = C: 45.04; H: 3.28; N: 15.75 %. Anal. Found: C: 45.00; H: 3.02; N: 15.56 %.

[(Os(bpy)<sub>2</sub>)<sub>2</sub>L2](PF<sub>6</sub>)<sub>2</sub>·4H<sub>2</sub>O (pOsOs)

This complex was prepared in a similar manner to mOsOs except that H<sub>2</sub>L2 (0.084 g, 0.23 mmol) and cis-[Os(bpy)<sub>2</sub>Cl<sub>2</sub>].2H<sub>2</sub>O (0.304 g, 0.50 mmol) were heated at reflux in DMF/H<sub>2</sub>O (2:1 v/v). Following removal of unreacted [Os(bpy)<sub>2</sub>Cl]Cl<sub>2</sub> from a dichloromethane solution of the crude product, purification by column chromatography using neutral alumina and acetonitrile as eluent gave the desired dinuclear complex. Yield = 0.16 g (44 %).

Calcd. for Os<sub>2</sub>C<sub>60</sub>H<sub>52</sub>N<sub>16</sub>O<sub>4</sub>P<sub>2</sub>F<sub>12</sub> = C: 41.62; H: 3.03; N: 12.94 %. Anal. Found: C: 41.62; H: 3.06; N: 12.62 %.



This complex was prepared in a similar manner to **mRuOs** using [Ru(bpy)<sub>2</sub>HL2]PF<sub>6</sub> (0.10 g, 0.13 mmol) and cis-[Os(bpy)<sub>2</sub>Cl<sub>2</sub>].2H<sub>2</sub>O (0.08 g, 0.13 mmol). The desired complex was purified by column chromatography on neutral alumina using acetonitrile as eluent. Yield = 0.10 g (50 %). Calcd. for Ru<sub>1</sub>Os<sub>1</sub>C<sub>60</sub>H<sub>50</sub>N<sub>16</sub>O<sub>3</sub>P<sub>2</sub>F<sub>12</sub> = C: 44.35; H: 3.10; N: 13.79 %. Anal. Found: C: 44.51; H: 3.03; N: 13.70 %.

### 4.3. Results and Discussion.

#### 4.3.1. Synthetic Procedure.

The synthetic methods used for the synthesis of the mononuclear and dinuclear complexes were quite straightforward. Any problems encountered involved solubility of the ligand, in particular H<sub>2</sub>L2. In the course of preparing the mononuclear complexes of this ligand, two solvent schemes were used- acidified aqueous solution and a DMF/water mixture. Both were found to give the desired complex in satisfactory quantities. However, the latter was the preferred method in terms of ease of work up of the reaction. It is important when synthesising mononuclear complexes to ensure complete dissolution of the ligand before adding M(bpy)<sub>2</sub>Cl<sub>2</sub>.2H<sub>2</sub>O so as to minimise the amount of dinuclear complex formed.

The dinuclear complexes have been prepared directly using a ligand : M(bpy)<sub>2</sub>Cl<sub>2</sub>.2H<sub>2</sub>O ratio of 1:2, or alternatively by an indirect route from the corresponding mononuclear complexes. The indirect route, which represents a simplified version of the “complexes as ligands” strategy developed by Barigelletti and coworkers<sup>16,17</sup>, was found to produce less side-products than the use of a 2:1 metal/ligand ratio. This method is especially useful for the synthesis of the RuOs heterodinuclear complexes, and care was taken to ensure that no RuRu dinuclear complex was present as an impurity in the Ru mononuclear starting material, since this could interfere with the photophysical and electrochemical properties.

As has been observed for other pyridyltriazole complexes, the ligands H<sub>2</sub>L1 and H<sub>2</sub>L2 deprotonate upon coordination of the metal centre<sup>18</sup>. However the added precaution of recrystallising the complexes in acetone/water containing a few drops of ammonia was taken to ensure that in all cases the deprotonated complexes were

isolated. With the exception of **pRu** (isolated as the dication), the free pyridyltriazole arm was protonated in the mononuclear complexes, thereby yielding complexes with an overall +1 charge. The complexes were purified mostly by column chromatography on neutral alumina, although in some cases semi-preparative HPLC was also used. The mononuclear compounds contained dinuclear complex as the main impurity and vice versa. Purification by chromatography on neutral  $\text{Al}_2\text{O}_3$  gave an excellent separation of bands associated with the mononuclear and dinuclear species, respectively. The dinuclear complexes were eluted using acetonitrile, while the mononuclear complexes, which remained at the top of the column, were eluted by the addition of methanol (50-100 %) to the mobile phase. Silica columns were also investigated for their use in purifying the complexes. Using a mobile phase of 80:20  $\text{CH}_3\text{CN}/\text{H}_2\text{O}$  containing  $\text{KNO}_3$  it was possible to achieve a gradient elution of monomeric and dimeric species with increasing concentrations of potassium nitrate. However given that this method of chromatography did not result in as good a separation of monomer and dimer and involved the evaporation of solvent containing high concentrations of nitrate salt (known to be potentially explosive when heated), it was not pursued further for the purpose of purification.

#### 4.3.2. $^1\text{H}$ -NMR Spectroscopy.

Representative  $^1\text{H}$ -NMR spectra of the complexes are shown in Figures 4.2-4.5. Tables 4.1 and 4.2 present the  $^1\text{H}$ -NMR data for the **m**- and **p**-complexes, respectively. Where spectra of the complexes have been obtained in  $d_6$ -DMSO, coordination induced shifts for the bridging ligand resonances (presented in Section

3.2) are also given. It has only been possible to assign ranges of proton resonances for the bpy ligands due to their coincidental chemical shifts. These fall within the ranges normally observed for analogous complexes.

Assignment of the bridging ligand resonances has been made using splitting patterns, coupling constants and by finding cross-peaks in the 2D COSY spectra. For the bridging ligands H<sub>2</sub>L1 and H<sub>2</sub>L2, H3 and H6 are observed as doublets and H4 and H5 as doublets of doublets, with coupling constants of approximately 7.8 Hz for H3 and H4 and 5 Hz for H5 and H6.

The relative simplicity of the NMR spectra obtained for the homodinuclear complexes reflects the symmetric environment of the metal centres. For the mononuclear complexes, however, the spectra are more complicated because of the presence of resonances for the free and bound pyridyltriazole arms and the bipyridine rings. Coordination of the M(bpy)<sub>2</sub> unit induces a shift in the resonances associated with the bound pyridyltriazole arm, the greatest change occurring for the pyridyl H6 proton, which is shifted over 1 ppm upfield. This behaviour is typical for coordinated pyridine rings and is due to the diamagnetic anisotropic interaction of the H6 proton with an adjacent bpy ligand<sup>19,20</sup>. Once this H6 has been identified, the other protons of the ring can be identified by their coupling constants and by using 2D COSY techniques. Due to the negative charge on the triazole ring, the other protons of the coordinated pyridyltriazole arm are all generally shifted upfield, although to a much lesser extent.

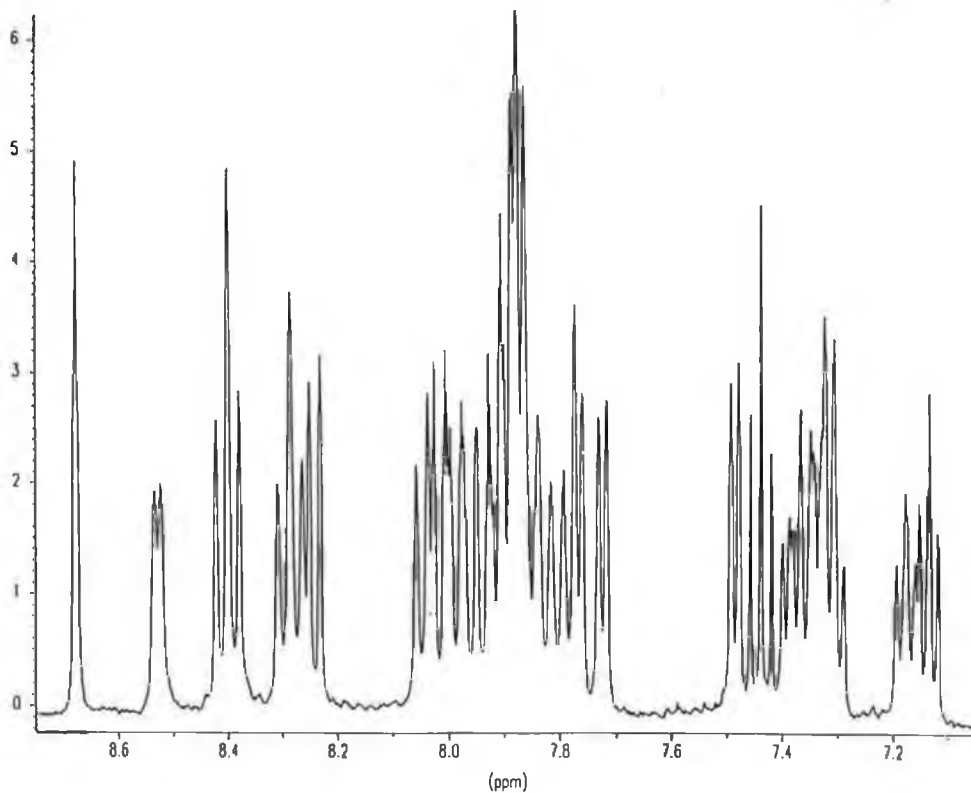


Figure 4.2  $^1\text{H-NMR}$  spectrum of **mRu** in  $d_3$ -acetonitrile.

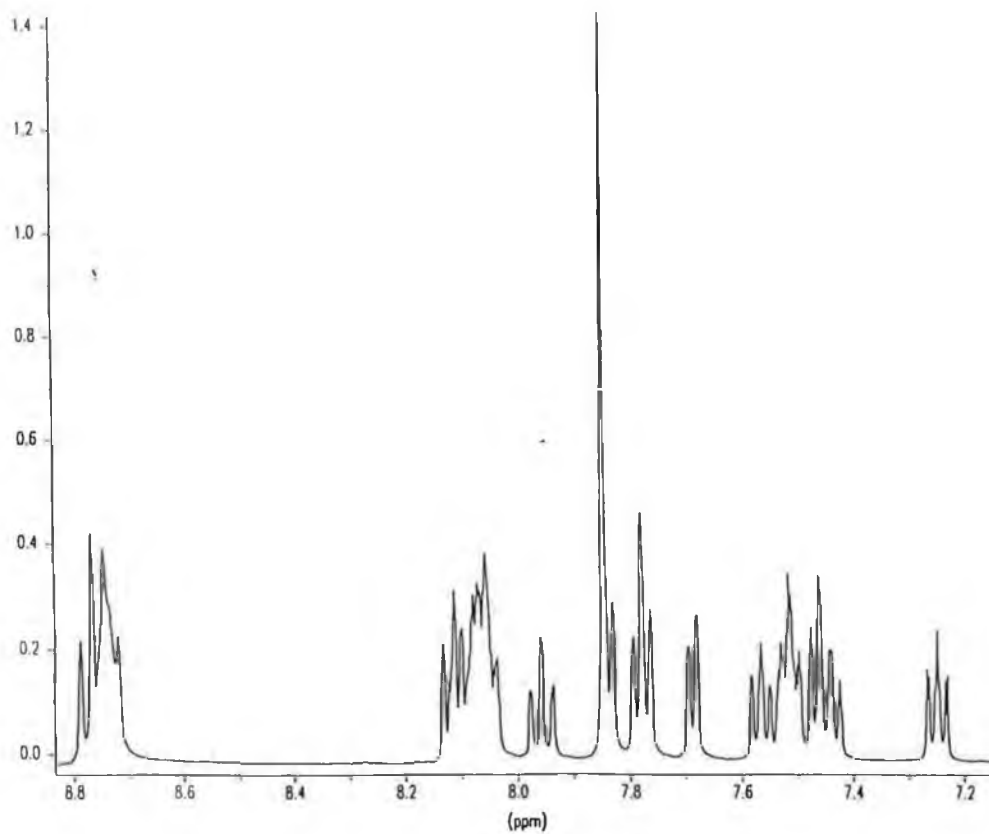


Figure 4.3  $^1\text{H-NMR}$  spectrum of **pRuRu** in  $d_6$ -dimethyl sulphoxide.

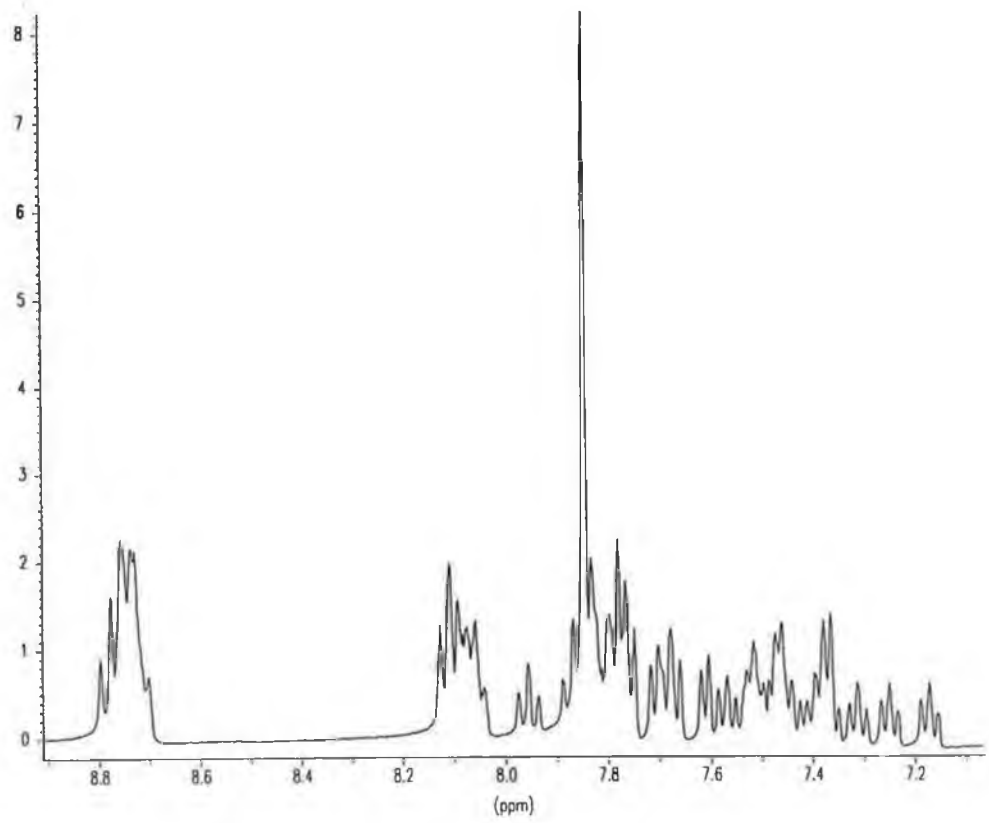


Figure 4.4  $^1\text{H-NMR}$  spectrum of **pRuOs** in  $d_6$ -dimethyl sulphoxide.

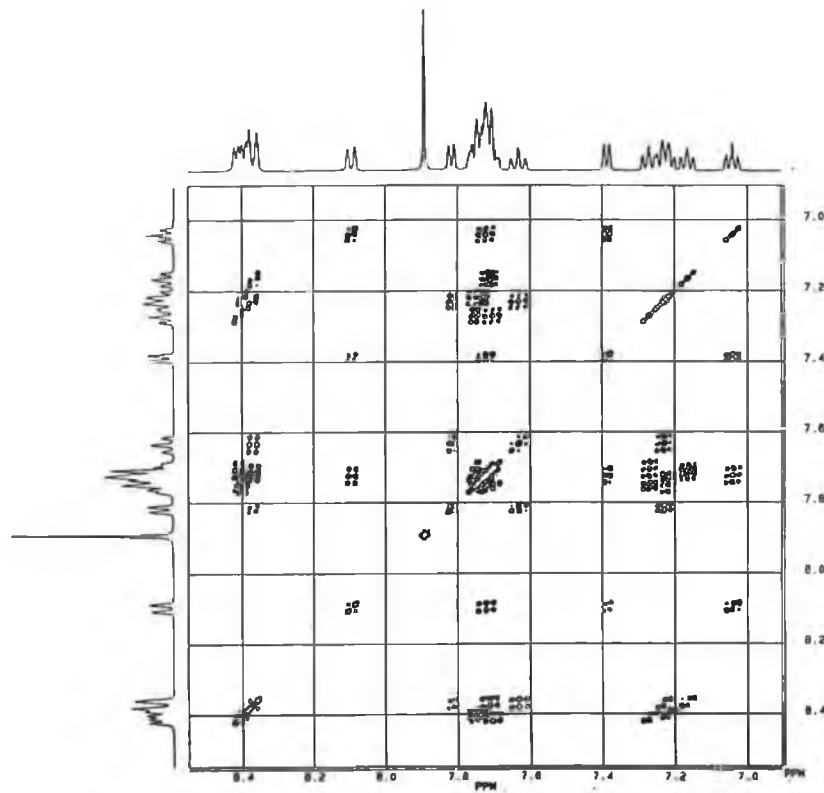


Figure 4.5 COSY NMR spectrum of **pOsOs** in  $d_3$ -acetonitrile.

**Table 4.1**  $^1\text{H-NMR}$  data for the **m**-complexes with  $\text{H}_2\text{L1}$ , as measured in  $\text{CD}_3\text{CN}$ , unless otherwise indicated. The values in parentheses are the changes in chemical shift compared to the free ligand. (f) and (b) refer to the free and bound pyridyltriazole arms, respectively.

| Complex                     | $\text{H}_2\text{L1}$ Resonances |                   |                   |                   |                     |
|-----------------------------|----------------------------------|-------------------|-------------------|-------------------|---------------------|
|                             | H3                               | H4                | H5                | H6                | Phenyl              |
| <b>mRu</b> (f)              | 8.24                             | 7.78              | 7.18              | 8.53              | 8.68 (s), 7.44 (t), |
| (b)                         | 8.05                             | 7.90              | 7.12              | 7.49              | 7.88 (d)            |
| <b>mOs</b> <sup>a</sup> (f) | 8.19                             | 8.00              | 7.48              | 8.74              | 8.65 (s), 7.55 (t), |
| (b)                         | 8.05 (-0.18)                     | 7.86 (-0.16)      | 7.19 (-0.30)      | 7.65 (-1.07)      | 8.14 (d)            |
| <b>mRuRu</b>                | 8.09                             | 7.88              | 7.12              | 7.48              | 8.37 (s), 7.29 (t), |
|                             |                                  |                   |                   |                   | 7.85 (d)            |
| <b>mRuRu</b> <sup>a</sup>   | 8.17 (-0.06)                     | 7.96 (-0.06)      | 7.25 (-0.25)      | 7.77 (-0.95)      | 8.35 (s), 7.34 (t), |
|                             |                                  |                   |                   |                   | 7.83 (d)            |
| <b>mOsOs</b>                | 8.10                             | 7.72              | 7.03              | 7.37              | 8.41 (s), 7.32 (t), |
|                             |                                  |                   |                   |                   | 7.86 (d)            |
| <b>mRuOs</b>                | 8.01 <sup>b</sup>                | 7.88 <sup>b</sup> | 7.14 <sup>b</sup> | 7.49 <sup>b</sup> | 8.38 (s), 7.64 (t), |
|                             | 7.95 <sup>c</sup>                | 7.74 <sup>c</sup> | 7.06 <sup>c</sup> | 7.39 <sup>c</sup> | 7.88 (d)            |
| bpy rings                   | 8.31-8.45                        | 7.62-8.00         | 7.15-7.40         | 7.70-7.85         |                     |

<sup>a</sup> Measured in  $(\text{CD}_3)_2\text{SO}$ , <sup>b</sup> Ruthenium bound to pyridyltriazole arm,

<sup>c</sup> Osmium bound to pyridyltriazole arm

**Table 4.2**  $^1\text{H-NMR}$  data for the **p**-complexes with  $\text{H}_2\text{L}_2$ , as measured in  $\text{CD}_3\text{CN}$ , unless otherwise indicated. The values in parentheses are the changes in chemical shift compared to the free ligand. (f) and (b) refer to the free and bound pyridyltriazole arms, respectively.

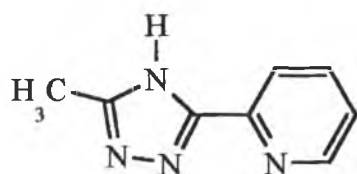
| Complex                   | $\text{H}_2\text{L}_2$ Resonances |                   |                   |                   |              |
|---------------------------|-----------------------------------|-------------------|-------------------|-------------------|--------------|
|                           | H3                                | H4                | H5                | H6                | Phenyl       |
| <b>pRu</b> (f)            | 8.16                              | 8.10              | 7.47              | 8.63              | 7.95         |
| (b)                       | 8.32                              | 7.97              | 7.25              | 7.58              |              |
| <b>pOs</b> (f)            | 8.18                              | 7.95              | 7.48              | 8.68              | 7.76-7.77    |
| (b)                       | 8.04                              | 7.75              | 7.06              | 7.41              |              |
| <b>pRuRu</b>              | 8.11                              | 7.82              | 7.11              | 7.48              | 7.90         |
| <b>pRuRu</b> <sup>a</sup> | 8.12 (-0.07)                      | 7.96 (-0.06)      | 7.25 (-0.29)      | 7.69 (-1.03)      | 7.85 (-0.38) |
| <b>pOsOs</b>              | 8.10                              | 7.72              | 7.05              | 7.39              | 7.90         |
| <b>pRuOs</b>              | 8.13 <sup>b</sup>                 | 7.83 <sup>b</sup> | 7.13 <sup>b</sup> | 7.50 <sup>b</sup> | 7.90         |
|                           | 8.11 <sup>c</sup>                 | 7.75 <sup>c</sup> | 7.05 <sup>c</sup> | 7.39 <sup>c</sup> |              |
| bpy rings                 | 8.31-8.45                         | 7.62-8.00         | 7.15-7.40         | 7.70-7.85         |              |

<sup>a</sup> Measured in  $(\text{CD}_3)_2\text{SO}$ , <sup>b</sup> Ruthenium bound to pyridyltriazole arm,

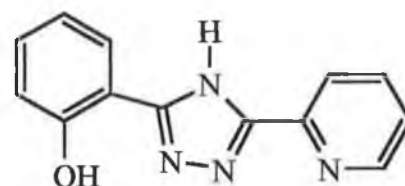
<sup>c</sup> Osmium bound to pyridyltriazole arm

One of the most important applications of  $^1\text{H-NMR}$  in the structural characterisation of metal complexes containing pyridyltriazole ligands is the elucidation of the coordination mode of the ligand. For all the complexes coordination of the  $\text{M}(\text{bpy})_2$ -unit to the bridging ligand can occur via N1 or N4 of the triazole ring. Analysis of the NMR data obtained for both mononuclear and dinuclear complexes and comparison of the chemical shifts observed for N1-bound complexes of other similar pyridyltriazole-based systems indicate that coordination does indeed occur through N1 of the triazole moiety. If the ligand was bound via N4, the phenyl ring would be in close proximity to a bpy ligand, and as a result of this, the chemical shift associated

with the phenyl ring would be noticeably shifted to higher field as is observed for the pyridyl H6 proton. This is not the case. Furthermore the crystal structures of analogous pyridyltriazole complexes containing the ligands 3-methyl-5-(2-pyridyl)-4*H*-1,2,4-triazole<sup>21</sup> and 3-(2-hydroxyphenyl)-5-(2-pyridyl)-4*H*-1,2,4-triazole<sup>22</sup> (Fig. 4.6) have been solved and in all cases showed that the Ru(bpy)<sub>2</sub> unit is coordinated via N1. Since the chemical shifts associated with the methyl and phenolic moieties of these ligands of these complexes are comparable to those found for the phenyl ring of the H<sub>2</sub>L1/H<sub>2</sub>L2 complexes, this strongly implies coordination in the same manner. This finding is not surprising, as it would be expected that due to steric reasons coordination of the Ru(bpy)<sub>2</sub> moiety to N4 would place the bipyridine rings too close to the central phenyl ring.



3-methyl-5-(2-pyridyl)-4*H*-1,2,4-triazole



3-(2-hydroxyphenyl)-5-(2-pyridyl)-4*H*-1,2,4-triazole

*Figure 4.6 Structures of pyridyltriazole ligands which feature N1 coordination.*

It was noted that in general the resonances of the osmium-bound complexes are found at higher field than those of the analogous ruthenium-bound compounds. The greater shielding effect in osmium(II) complexes is due to relatively stronger metal  $d\pi - \pi^*$  (bpy) back-donation compared to Ru(II), due to the higher energy of Os(II) orbitals. The difference in chemical shifts between the pyridyltriazole arm bound to

$\text{Ru}(\text{bpy})_2$  and that bound to  $\text{Os}(\text{bpy})_2$  can also be observed in the NMR spectra of the heterodinuclear complexes (Fig. 4.4).

### 4.3.3. Electronic and Photophysical Properties.

#### 4.3.3.1. Absorption Spectra.

The electronic absorption spectra of all the complexes are quite similar and are dominated in the visible region by  $d\pi - \pi^*$  metal-to-ligand charge transfer (MLCT) transitions typical of complexes of this type<sup>23</sup> and in the UV region (250-350 nm) by intense  $\pi-\pi^*$  transitions associated with the bipyridyl and bridging ligands. The absorbances of the deprotonated complexes are all red-shifted with respect to  $\text{Ru}(\text{bpy})_3^{2+}$  as a result of strong  $\sigma$ -donation of the negatively charged triazole moiety. Upon protonation the coordinated ligand becomes a weaker  $\sigma$ -donor and a stronger  $\pi$ -acceptor. As a consequence, the metal  $d\pi$  ( $t_{2g}$ ) orbitals are stabilised and the  $t_{2g} - {}^3\text{MLCT}$  energy gap is increased, resulting in the observed blue shift in the absorption spectrum (Fig. 4.7).

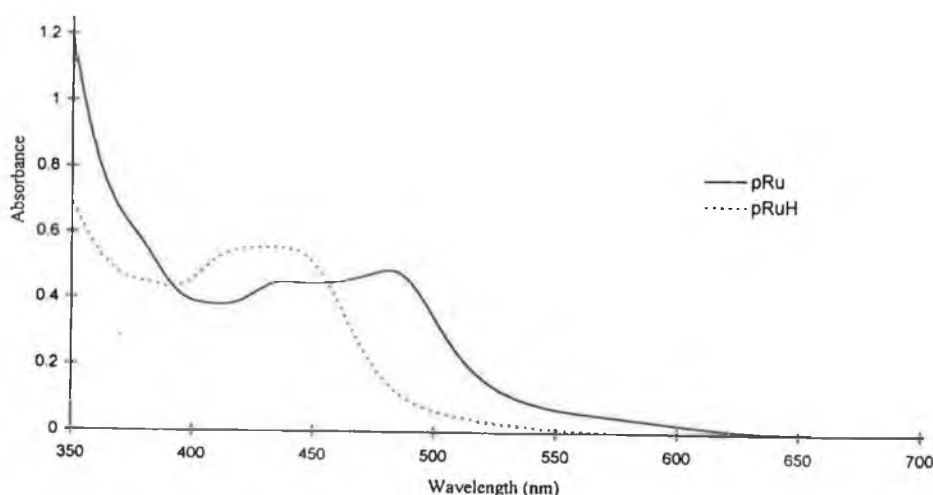


Figure 4.7 Absorption spectra in acetonitrile of pRu and pRuH.

Table 4.3 lists the absorption and emission data for the mononuclear and dinuclear complexes in their protonated and deprotonated forms.

**Table 4.3** *Absorption and Emission Data for the complexes\*. Unless otherwise stated all measurements were carried out in acetonitrile. Protonation of the complexes was achieved by the addition of perchloric acid.*

| Complex       | Absorbance $\lambda_{\max}$ , nm<br>( $10^4 \epsilon$ ) | Emission $\lambda_{\max}$ , nm |                   | Lifetime (ns)<br>at 300K <sup>b</sup> |
|---------------|---|--------------------------------|-------------------|---------------------------------------|
|               |   | 300 K                          | 77 K <sup>a</sup> |                                       |
| <b>mRu</b>    | 482 (0.85)  | 688                            | 612               | 125                                   |
| <b>mRuH</b>   | 440   | 613                            | 578               | <20                                   |
| <b>mRuRu</b>  | 482 (2.00)  | 687                            | 618               | 85                                    |
| <b>mRuRuH</b> | 440   | 611                            | 581               | <20                                   |
| <b>mOs</b>    | 503 (1.13), 652 (0.23)                                  | 813                            | 759               | 23                                    |
| <b>mOsH</b>   | 576, 468, 431   | 726                            | 719               | 38                                    |
| <b>mOsOs</b>  | 502 (2.20), 660 (0.49)                                  | 811                            | 759               | <20                                   |
| <b>mOsOsH</b> | 679, 472, 431   | 736                            | 711               | 46                                    |
| <b>mRuOs</b>  | 485 (1.95), 660 (0.22)                                  | 688, 806                       | 615, 750          | <20 <sup>c</sup>                      |
| <b>mRuOsH</b> | 565, 431  | 727                            | 581 (w), 705      | 35 <sup>d</sup>                       |
| <b>pRu</b>    | 482 (0.98)  | 685                            | 610               | 20                                    |
| <b>pRuH</b>   | 432   | 612                            | 580               | <20                                   |
| <b>pRuRu</b>  | 481 (2.03)  | 690                            | 610               | 54                                    |
| <b>pRuRuH</b> | 420   | 614                            | 584               | <20                                   |
| <b>pOs</b>    | 501 (1.05), 644 (0.22)                                  | 814                            | 761               | <20                                   |
| <b>pOsH</b>   | 576, 463, 427   | 737                            | 720               | 34                                    |
| <b>pOsOs</b>  | 502 (2.43), 648 (0.53)                                  | 814                            | 753               | <20                                   |
| <b>pOsOsH</b> | 581, 429  | 725                            | 718               | 45                                    |
| <b>pRuOs</b>  | 483 (2.25), 629 (0.35)                                  | 684, 795                       | 615 (w), 750      | <20 <sup>c</sup>                      |
| <b>pRuOsH</b> | 568, 424  | 725                            | 585, 710          | 41 <sup>d</sup>                       |

<sup>a</sup> Measured in Ethanol/Methanol 4:1 <sup>b</sup> Samples degassed using N<sub>2</sub>.

<sup>c</sup> Lifetime measured at 680 nm, <sup>d</sup> Lifetime measured at 750 nm.

\* mRuH, pOsH etc. refer to complexes in their protonated forms.

Replacement of a Ru-containing unit with a Os-unit causes a shift to lower energy of the MLCT absorption bands. This has been observed for other osmium systems and is caused by the higher energy of the Os 5d orbitals compared to the Ru 4d orbitals<sup>24</sup>. For the osmium complexes, additional absorption bands are observed at 600-660 nm, which can be assigned to formally forbidden triplet  $d\pi - \pi^*$  bpy MLCT transitions<sup>25</sup>(Fig. 4.8). For Os(II)-polypyridyl complexes, excited state properties at room temperature are determined by a series of three low energy Boltzmann populated MLCT states which have considerable triplet character and which behave kinetically as a single state, while the fourth state is predominantly singlet in nature<sup>26</sup>. It was found that the “triplet” states of osmium have 2-5 times as much singlet character as ruthenium analogues<sup>27</sup>.

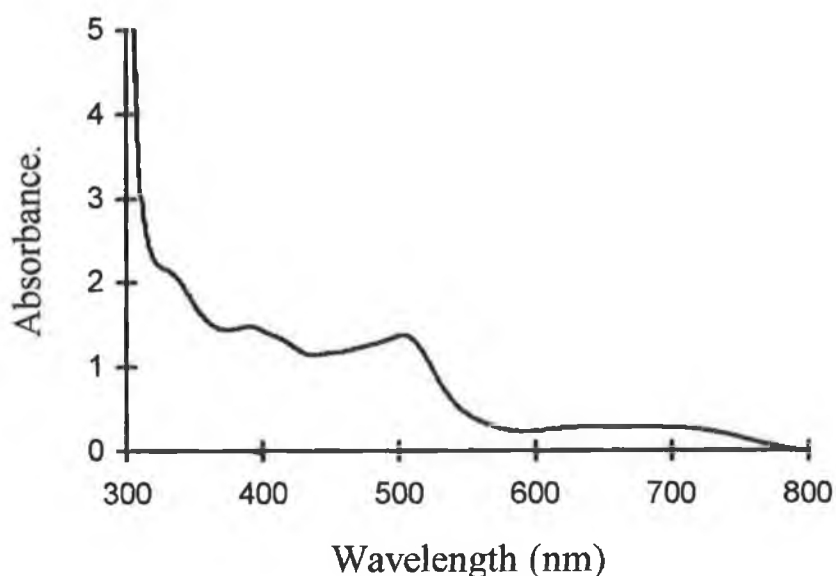


*Figure 4.8 Absorption spectrum in acetonitrile of mOs*

A comparison of the absorption spectra of the mononuclear and dinuclear complexes in their protonated and deprotonated forms reveals that the energies of the absorption bands are not altered much in going from the mononuclear to the dinuclear

complexes. Furthermore, the absorption spectra of equimolar solutions of the heterometallic dinuclear complexes **mRuOs** and **pRuOs** and 1:1 mixtures of the corresponding homometallic dinuclear species, **pRuRu/pOsOs** and **mRuRu/mOsOs** were found to be identical. These observations indicate that any interaction, if present, between the metal centres is at best very weak.

#### 4.3.3.2. Emission Properties.

All the complexes exhibit room temperature emissions in acetonitrile in their protonated and deprotonated forms (Fig. 4.9). The emission maxima of the deprotonated complexes occur at lower energy than that of their corresponding  $M(\text{bpy})_3^{2+}$  counterparts. This behaviour can be explained by the strong  $\sigma$ -donor properties of the anionic bridging ligands, leading to increased electron density on the metal centre, a consequent decrease in the  $t_{2g} - {}^3\text{MLCT}$  energy gap and so a lowering of the emission energy. As with the absorption spectra, and for the same reasons, protonation of the complexes results in a blue shift of the emission maxima. The ruthenium mononuclear and homodinuclear complexes have emission maxima in the region 610 nm. The emission maxima of the osmium complexes occur, as expected, at lower energy than those of the analogous ruthenium complexes. The energy difference between the metal  $t_{2g}$  and  $\text{bpy } \pi^*$  orbitals is smaller for osmium than ruthenium and the MLCT energies are therefore lower (Fig. 4.10). The emission spectral features of the heterodinuclear **mRuOs** and **pRuOs** complexes are more complicated and will be discussed in Section 4.3.3.3.

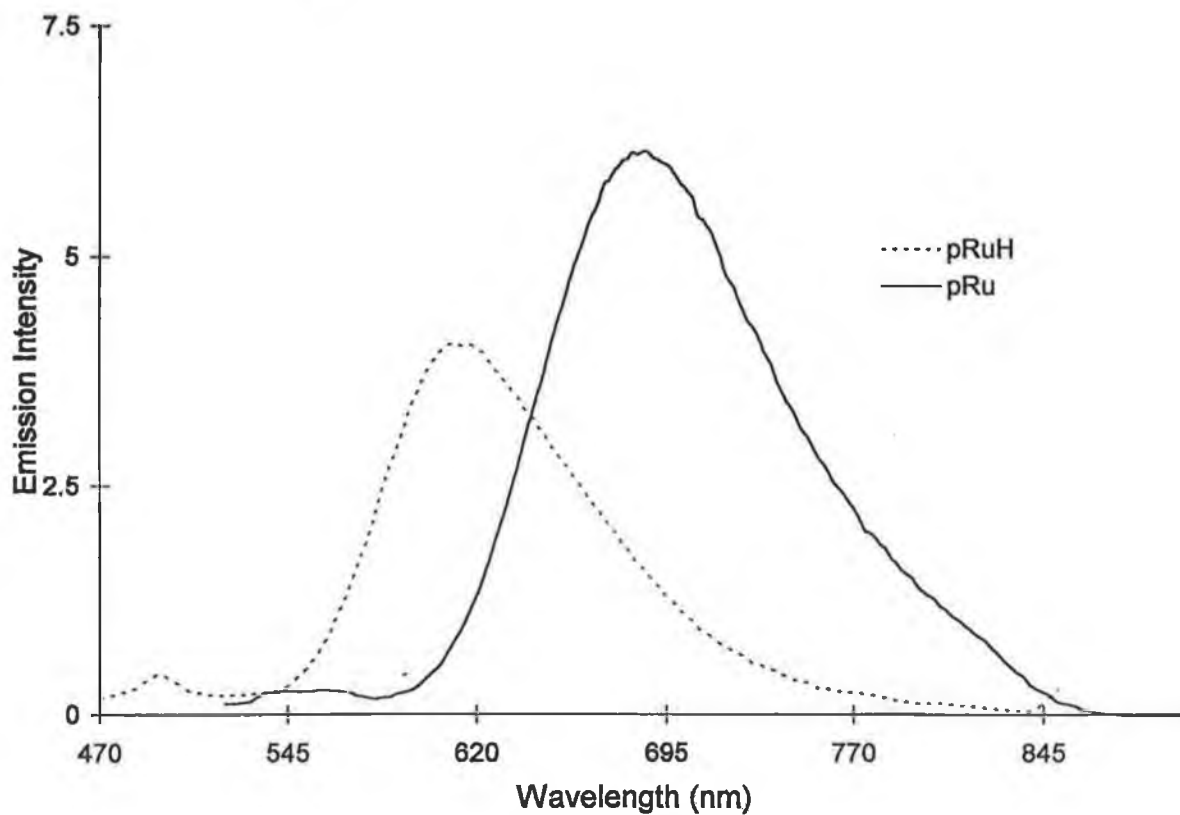


Figure 4.9 Room temperature emission spectra of pRu and pRuH in acetonitrile.

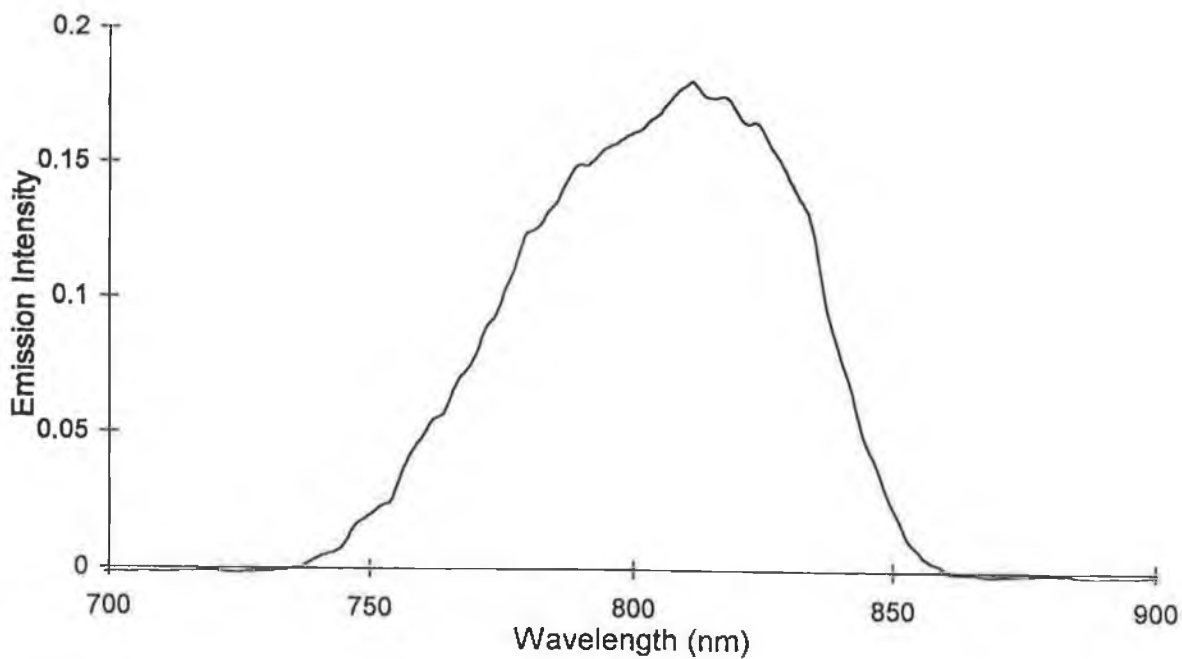
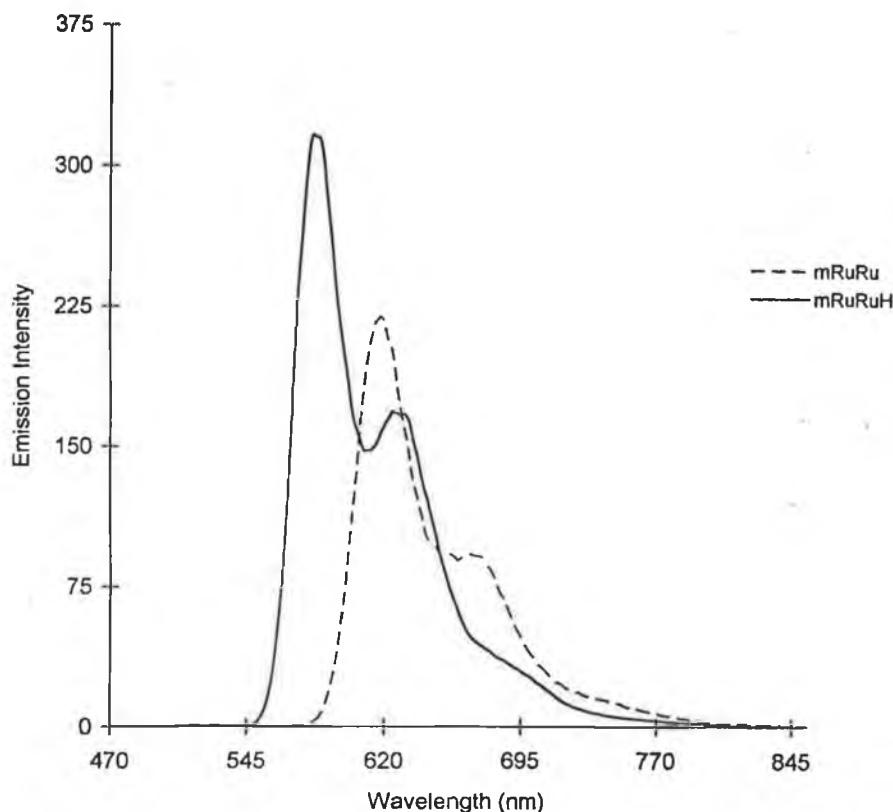


Figure 4.10 Room temperature emission spectrum of mOsOs in acetonitrile.

At 77 K all the complexes exhibit a strong emission with vibrational structure (Fig 4.11). This vibrational fine structure, which has been attributed to relaxation via bipyridine-based vibrations<sup>28</sup>, is common for ruthenium and osmium polypyridyl complexes. Cooling to 77 K leads to a blue shift in the emission maxima in both protonated and deprotonated complexes. This is associated with a phenomenon termed “rigidchromism” by Wrighton and coworkers who were one of the first to report on it<sup>29</sup>. In the alcoholic glasses formed at 77 K, the solvent dipoles are immobile on the timescale of the excited state and therefore cannot respond to the change in electronic configuration between the ground and excited state. The result is an increase in the emission energy as manifested by the blue shift in the emission spectra. Another influence of low temperature on the emission spectra of the complexes is to cause an increase in the intensity of the emission observed. This is associated with two factors, the first of which is solvent dependent. At low temperature, the complex and its environment are rigid, making it less susceptible to vibronic coupling to low frequency, high amplitude Ru - N vibrations which contribute to radiationless decay,  $k_{nr}$ . Solvent interactions which may contribute to  $k_{nr}$  are also considerably reduced in the frozen matrix, as too is quenching of the excited state by oxygen, since diffusion of oxygen to the excited state is restricted. The second factor is related to the  $^3MLCT - ^3MC$  energy gap. Since this transition is thermally activated, at 77 K there will be insufficient thermal energy to populate the  $^3MC$  level, and as a consequence, the intensity of the emission increases.



*Figure 4.11 Emission spectra of mRuRu and mRuRuH at 77 K in ethanol/methanol (4:1)*

An examination of the room temperature lifetimes under anaerobic conditions reveals that the complexes are all generally very short-lived. Room temperature luminescent decay and consequently lifetimes of MLCT excited states of ruthenium and osmium polypyridyl complexes at room temperature in fluid solution are typically dominated by nonradiative processes<sup>23</sup>. As predicted by the energy gap law<sup>30</sup>, the rate of nonradiative decay typically increases as the energy gap between the ground and excited state decreases. Because of this complexes with low energy absorption bands are generally weak emitters with short-lived excited states<sup>31</sup>. On this basis, it would therefore be expected that the deprotonated complexes would have shorter lifetimes

than their protonated analogues. However, with the exception of the osmium-containing complexes, the opposite is actually the case. The deprotonated complexes exhibit longer lifetimes, most noticeably in the case of **mRu**, **mRuRu** and **pRuRu**. For all the protonated ruthenium mononuclear and homodinuclear complexes, the lifetimes fall outside the range of the instrumentation used. As stated previously, protonation of the triazole decreases the  $\sigma$ -donor capacity of the ligand. Consequently the ligand field splitting ( $\Delta_o$ ) is decreased which favours thermal population of the strongly deactivating  $e_g^*$  ( $^3MC$ ) state and faster radiationless decay, resulting in shorter lifetimes. This trend is one which has been observed before by Hage in complexes of the ligand 1,3,5-tris(5-(2-pyridyl)-4H-1,2,4-triazol-3-yl)benzene<sup>32</sup> (Fig. 4.12). This ligand bears a strong structural resemblance to H<sub>2</sub>L1 and H<sub>2</sub>L2 and therefore the lifetime results are not unexpected.

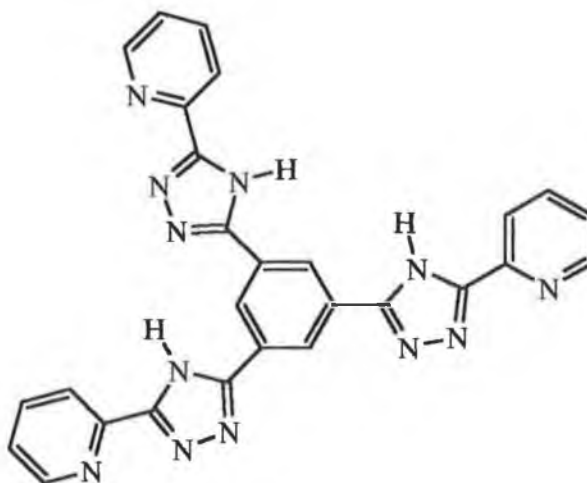


Figure 4.12 Structure of 1,3,5-tris(5-(2-pyridyl)-4H-1,2,4-triazol-3-yl)benzene<sup>32</sup>.

#### 4.3.3.3 Emission properties of the mixed-metal RuOs complexes and the possibility of electron/energy transfer.

At room temperature both **mRuOs** and **pRuOs** exhibit a very weak luminescence at around 680 nm and 800 nm when deprotonated, which by comparison with data for the mononuclear and homodinuclear complexes may be assigned as being due to the Ru-bound and Os-bound sites, respectively (Fig 4.13). For both complexes, the emission from the Ru-based component is stronger than that from the Os-based unit. At 77 K, however, although once again emission from both sites can be seen, the Os-based luminescence is found to be the stronger component- by a ratio of approximately Ru:Os = 1:2 (Fig. 4.14). Such dual luminescence is not uncommon and has been reported by de Cola et al for the RuOs complex of a bis(pyridine) bridging ligand containing a rigid bicyclooctane spacer<sup>9</sup> and more recently by Barigelletti and coworkers for rodlike cyclometalated Ru(II)/Os(II) dinuclear complexes where the biscyclometalating bridging ligand contains dipyriddybenzene fragments separated by phenylene spacers<sup>33,34</sup>. Furthermore, examination of the emission spectra of the protonated **mRuOs** and **pRuOs** complexes reveals that in both cases emission from the Os-based site is the predominant spectral feature. The Ru-based emission appears as a very weak band preceding the tail of the osmium luminescence (Fig. 4.15 ). At 77 K when protonated, the situation is somewhat similar, except that the Ru-based emission, although very weak, may be more clearly identified (Fig. 4.16). This apparent quenching of the ruthenium-based luminescence and sensitization of the Osmium-based luminescence indicates that either an energy- or electron-transfer process is present in these systems.

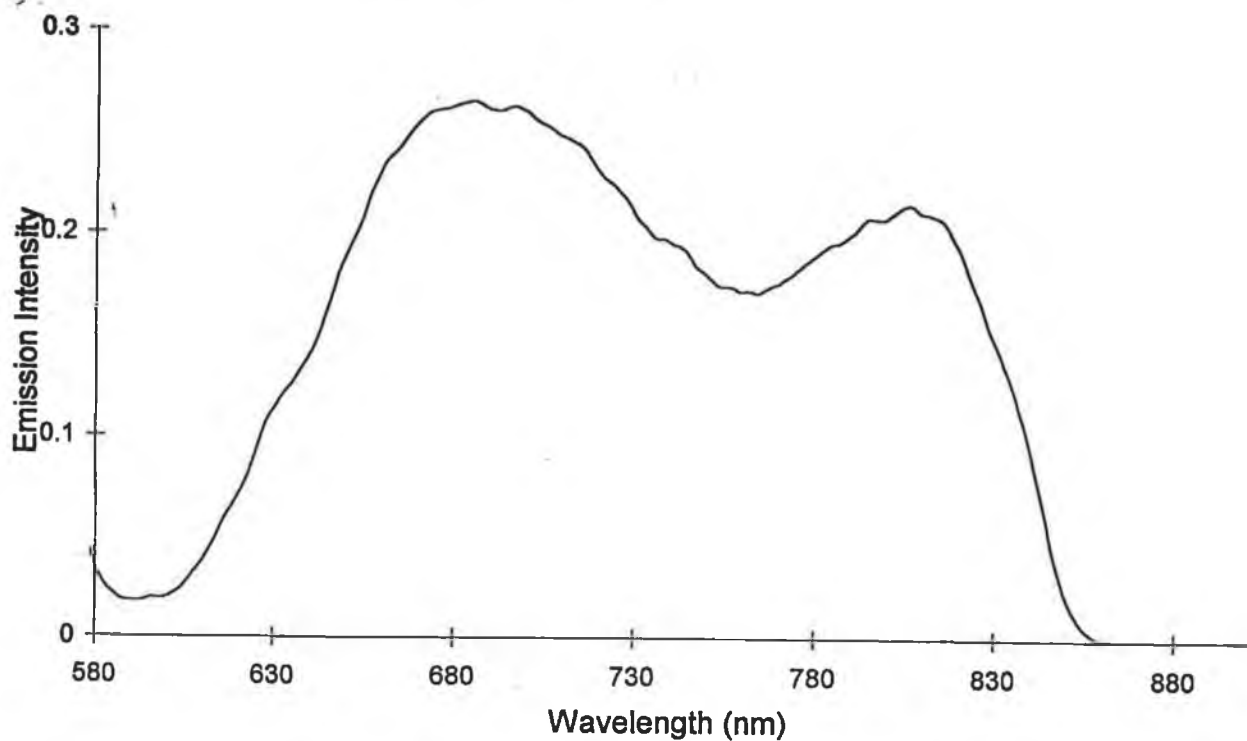


Figure 4.13 Room Temperature emission spectrum of mRuOs in acetonitrile.

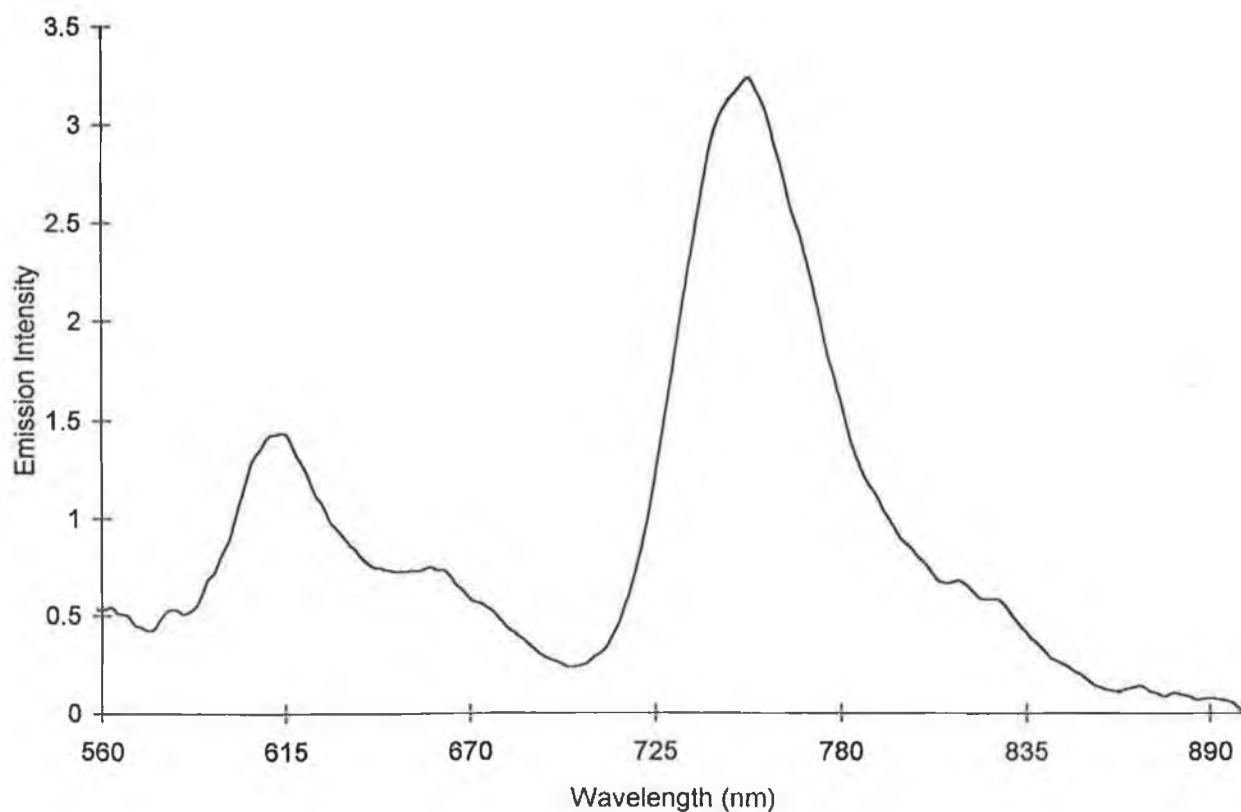


Figure 4.14 Emission spectrum of mRuOs at 77 K in ethanol/methanol (4:1)

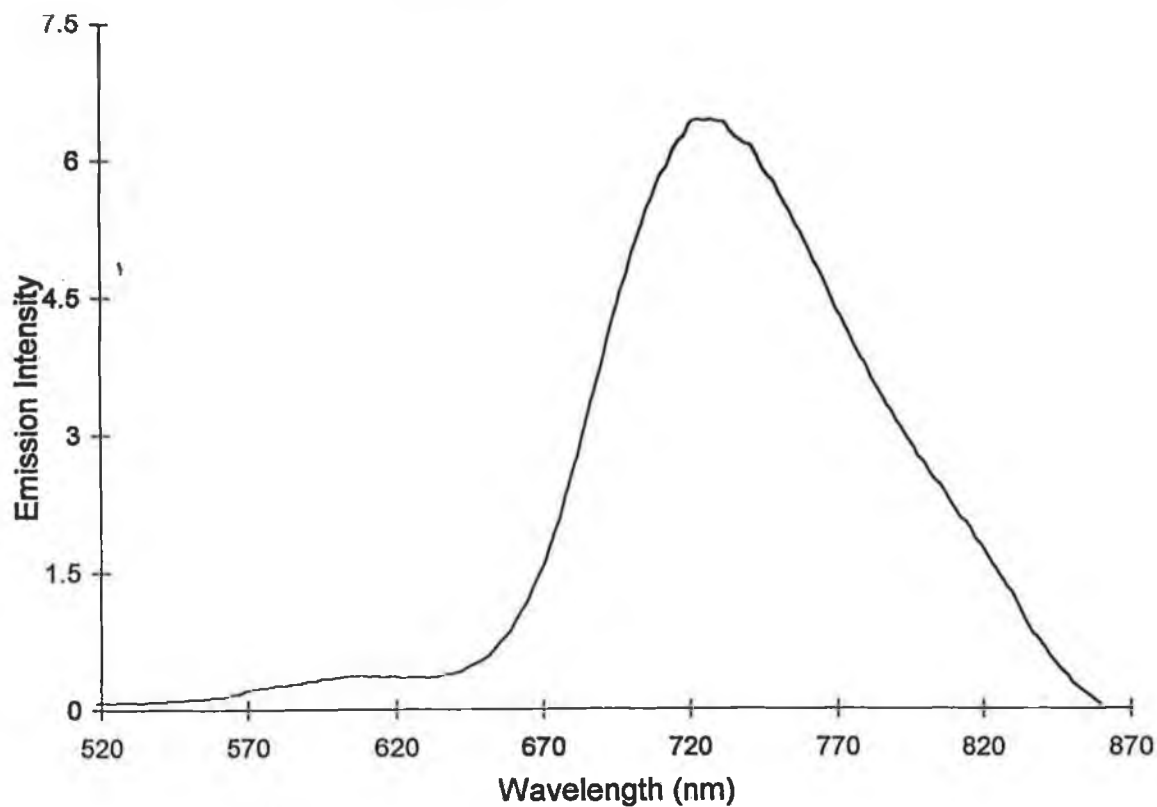


Figure 4.15 Room temperature emission spectrum of **mRuOsH** in acetonitrile.

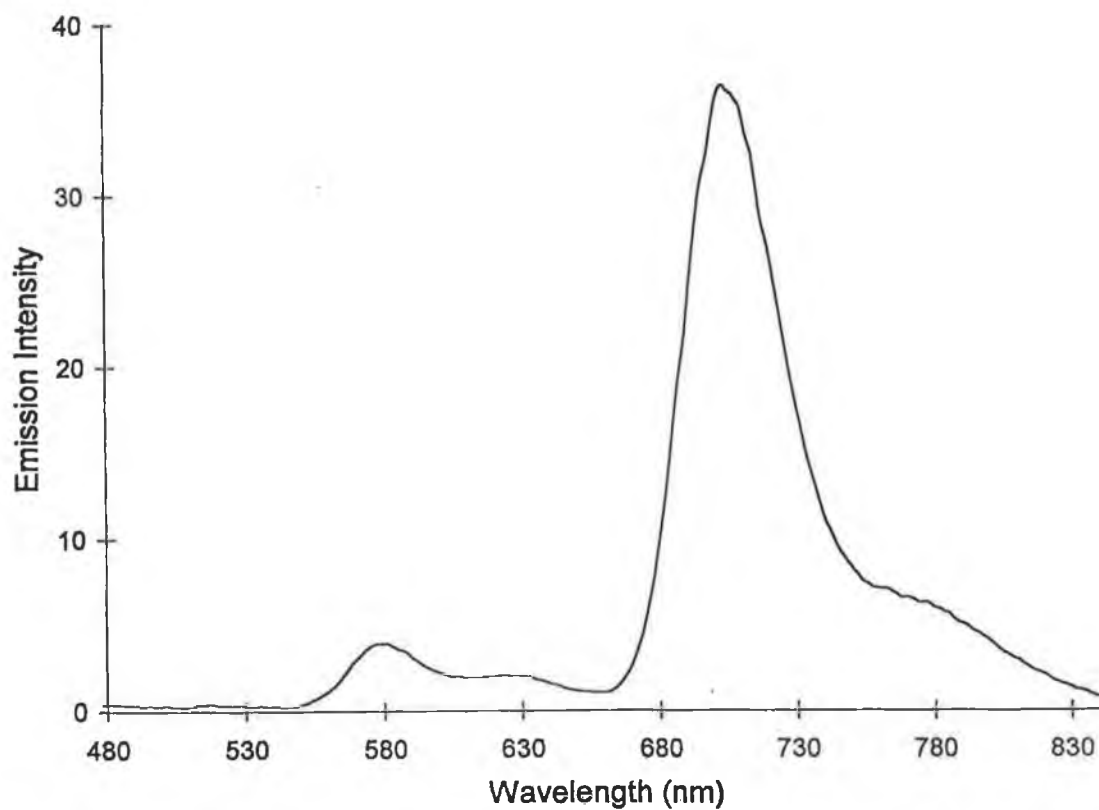
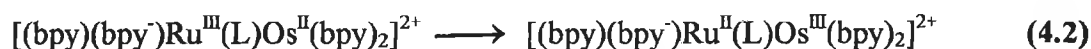


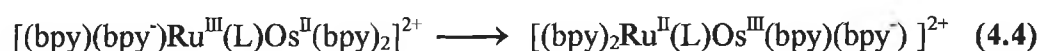
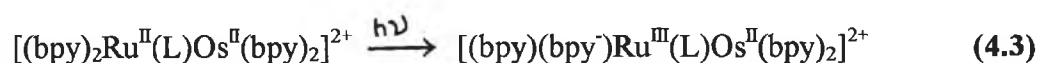
Figure 4.16 Emission spectrum of **mRuOsH** at 77 K in ethanol/methanol (4:1).

In an electron-transfer process in a mixed-metal RuOs complex, an electron may be transferred from the osmium(II) ion to the ruthenium(III) moiety after excitation of the Ru-based unit, as follows:



Since the osmium centre has a lower oxidation potential than the ruthenium centre, this process is feasible. After electron transfer, the “remote” MLCT state decays to the ground state *via* a nonradiative pathway and consequently, whilst the ruthenium-based emission is quenched, the intensity of the osmium-based luminescence is not enhanced.

In an energy-transfer process however, the following processes occur:



Following excitation of the ruthenium unit, one electron is transferred from the osmium(II) unit to the Ru(III) moiety and, at the same time, an electron transfer from a bpy ligand of the Ru(bpy)<sub>2</sub> centre to a bpy ligand of the Os(bpy)<sub>2</sub> centre also takes place. The net result of this simultaneous transfer of two electrons is energy transfer. In this case what remains is a species in which the osmium centre is formally oxidised and a bpy ligand associated with it is reduced. As a result luminescence from the Os-unit may be observed, even though it was not itself excited initially.

From the luminescence maxima at 77 K, it can be seen that the Ru→Os energy transfer step in **mRuOs** and **pRuOs** is energetically allowed by approximately 0.36 eV. In order to investigate the possibility of electron/energy transfer in **mRuOs** and **pRuOs** using luminescence spectroscopy, only the ruthenium centre should be selectively excited. Unfortunately, the two metal centres have too much overlap in the absorption spectra to allow selective excitation of one over the other. Instead, solutions of **mRuRu**, **mOsOs** and **mRuOs** and **pRuRu**, **pOsOs** and **pRuOs** all having the same optical density at a particular wavelength were excited at that wavelength. The procedure paralleled that used by Belser and coworkers<sup>9,35</sup>. The absorption spectra of equimolar ( $1.5 \times 10^{-5}$  M) solutions of **pRuRu**, **pOsOs** and **pRuOs** were recorded and were found to exhibit an isobestic point at 486 nm. The luminescence spectra of these solutions were recorded with excitation at this wavelength under identical instrumental conditions. In this way 50 % of the excited dinuclear species has excitation centred on the ruthenium-based chromophore and 50 % has excitation centred on the osmium-based unit. Comparison of the heights of the emission bands at 680 nm, where the luminescence of the Os-unit is negligible, facilitated quantification of the quenching of the Ru-based luminescence. The results obtained revealed that 94 % of the luminescence intensity of the Ru-based component is quenched by the Os-based unit. The measurement of the sensitisation of the Os-based moiety on the other hand was more difficult, since the tail of the residual luminescence of the Ru-based component interferes considerably with the measurement of the luminescence of the Os-based unit even at the emission maximum (Figure 4.17). However by subtracting a normalised spectrum of **pRuRu** (at 680 nm) from **pRuOs**, the contribution of the Os-based luminescence to the **pRuOs** emission at 800 nm could be estimated and directly

compared with the height of the luminescence band in **pOsOs**. It was found that the Os-based luminescence in **pRuOs** is as intense as that of an equimolar **pOsOs** solution, a finding consistent with energy transfer<sup>9</sup>.

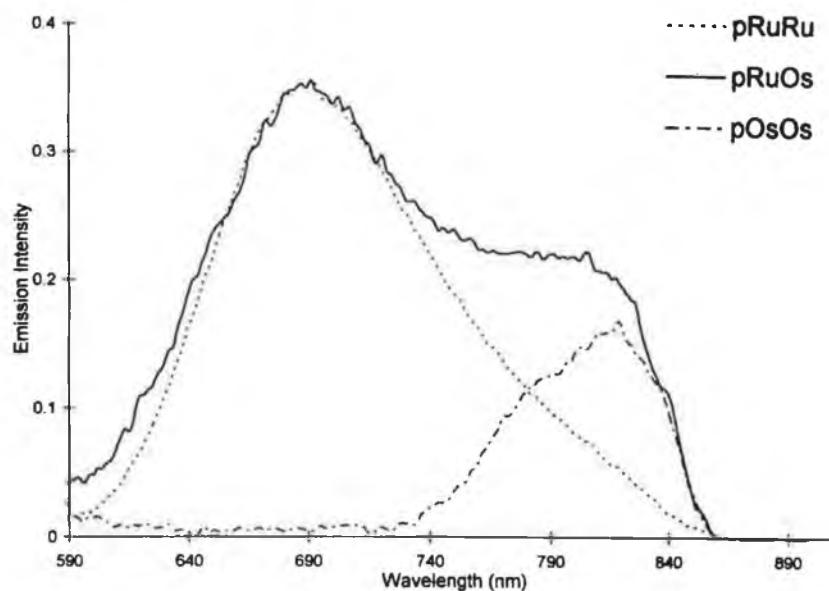


*Figure 4.17* Room temperature emission spectra of isoabsorptive solutions of **pRuOs**, **pOsOs** and **pRuRu** (normalised to **pRuOs**).

As can be seen in Figure 4.18, the luminescence intensity of the Ru-based moiety of a 1:1 mixture of **pRuRu** and **pOsOs** is approximately 50 % that of an isoabsorptive **pRuRu** solution ( $\lambda_{\text{excit}} = 486 \text{ nm}$  (isobestic point)). This indicates that intermolecular quenching does not occur under the experimental conditions used. However the Ru-based luminescence intensity in **pRuOs** is only 10 % that of an equimolar 1:1 **pRuRu/pOsOs** mixture, indicating that in **pRuOs** the luminescence of the Ru-based component is intramolecularly quenched by the Os-component. Similar results were obtained for the measurements performed on the analogous **m**-complexes.

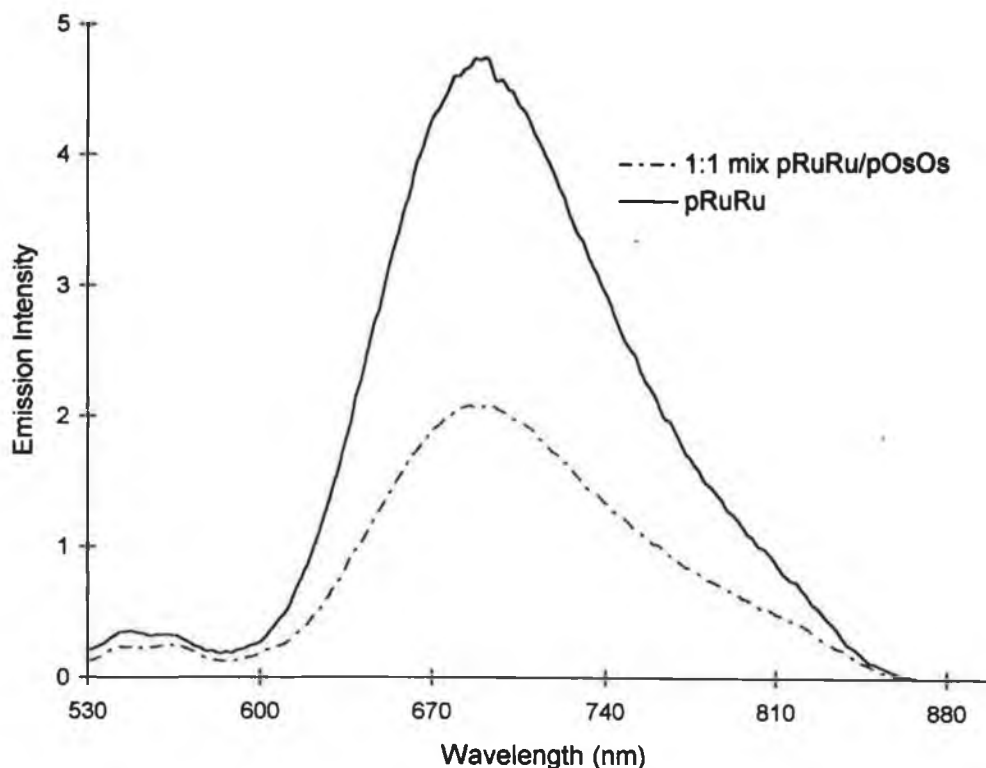


Figure 4.18 Room temperature emission spectra of **pRuRu** and 1:1 mixture of **pRuRu/pOsOs**.

As was found for **pRuOs**, the intensity of the Os-based luminescence in **mOsOs** coincides with the intensity of the osmium luminescence in **mRuOs** (after correction for the tail of the residual Ru-based luminescence) (Fig. 4.19). The ruthenium-based luminescence in **mRuOs** is 16 % that of a 1:1 **mRuRu/mOsOs** mixture, whilst the Os-based luminescence is sensitized by 84 %. In the case of the protonated complexes similar results were obtained. 98 % of the ruthenium-based luminescence is quenched in **pRuOsH**. The luminescence spectra obtained for **pRuRuH**, **pOsOsH**, **pRuOsH** and a 1:1 mixture of **pRuRuH/pOsOsH** (isoabsorptive at 457 nm) are shown in Figure 4.20. Evidence for energy transfer arises from a comparison of corrected luminescence intensities of **pOsOsH** and **pRuOsH** which shows that quenching of the Ru-based unit is accompanied quantitatively by sensitisation of the Os-based luminescence.

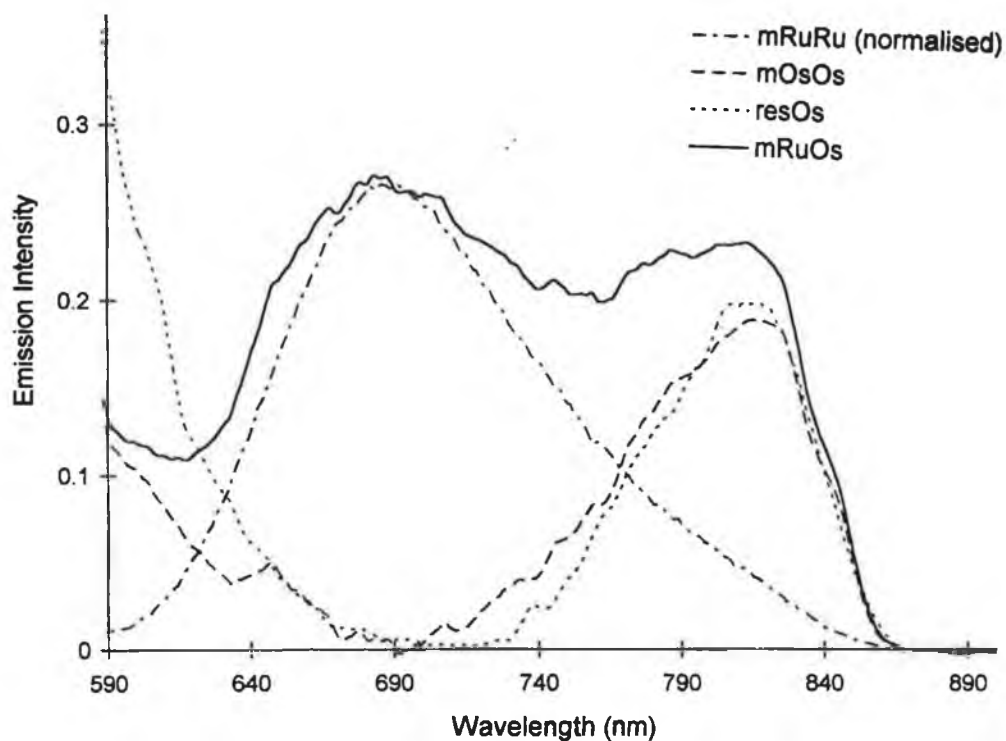


Figure 4.19 Room temperature emission spectra of **mRuRu** (normalised to the spectrum of **mRuOs**), **mOsOs**, **mRuOs** and of residual Os-based luminescence in **mRuOs** (**resOs**).

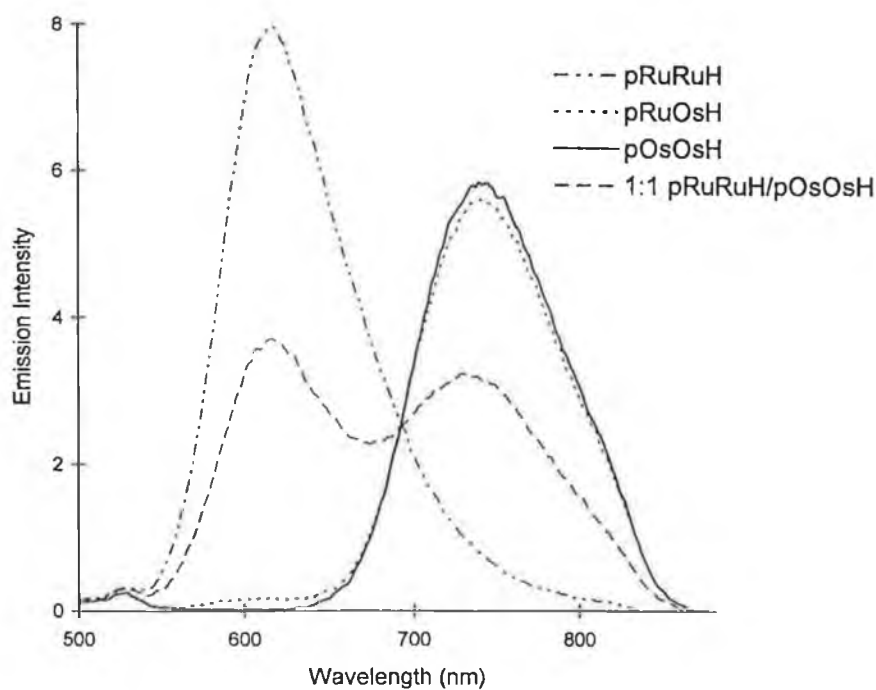


Figure 4.20 Room temperature emission spectra of **pRuOsH**, **pOsOsH**, **pRuRuH**, and 1:1 mixture **pRuRuH/pOsOsH**.

It should be noted however that the luminescent intensity measurements are prone to error and only provide a qualitative assessment of the energy transfer step. In addition, for the deprotonated **pRuOs** and **mRuOs** complexes, the observed emission is very weak and this means that the slightest impurity may alter the results and prevent any meaningful analysis<sup>36</sup>. A detailed analysis of lifetime measurements is necessary. Unfortunately, as the lifetime values of **pRuOs** and **mRuOs** lie outside the range of the equipment used, this is not possible. However the luminescence decay of **pRuOs** and **mRuOs** yield lifetimes which are substantially smaller than those of the parent homodinuclear complexes **pRuRu** and **mRuRu**, thereby indicating that another deactivation pathway is present in the mixed-metal dinuclear complexes.

#### 4.3.4 Acid-Base Properties.

As previously described in Section 4.3.3, protonation/deprotonation alters the  $\sigma$ -donor and  $\pi$ -acceptor properties of the ligands  $H_2L1$  and  $H_2L2$ . An investigation of the acid-base behaviour of their  $Ru(bpy)_2^-$  and  $Os(bpy)_2^-$  complexes can therefore yield important information about their electronic properties. In ruthenium and osmium polypyridyl complexes, the M-N bond ( $M = Ru/Os$ ) is mainly  $\sigma$  in nature, but in addition it is stabilised by backbonding between the  $t_{2g}$  and  $\pi^*$  orbitals of the metal and ligand, respectively. Determination of the  $pK_a$  of a complex yields information about the extent of backbonding from the metal and the  $\sigma$ -donor and  $\pi$ -acceptor properties of the ligands, while determination of the excited state  $pK_a$ ,  $pK_a^*$ , offers an insight into the nature of the emitting state. The acid-base properties of the excited state can

give information about the charge redistribution which occurs upon excitation, and furthermore, the excited state acidity can be related to the nature of the emitting state.

By monitoring the spectral changes as a function of pH, titration curves were obtained from which were determined pKa values. For both the mononuclear and dinuclear complexes the only spectral changes which occur are those associated with (de)protonation of the coordinated triazole ring. The mononuclear complexes also have an equilibrium associated with the free triazole ring. However, spectral changes associated with this step could not be readily identified. An example of a typical set of spectra, which shows the pH dependence of the absorption spectra of **pOsOs**, is given in Fig. 4.21. All the complexes show reversible behaviour in the pH range 1-11. In all cases lowering the pH results in a blue shift of the MLCT band due to stabilisation of the  $t_{2g}$  orbitals and the consequent increase in the  $^3\text{MLCT}-t_{2g}$  energy gap. Isobestic points are observed at around 460 nm, 388 nm and 315 nm and at around 411 nm, 485 nm, 545 nm and 655 nm for the ruthenium and osmium homonuclear compounds, respectively. As can be seen from Table 4.4, the ground state pKa values of the triazole moiety of the ligands decrease upon coordination. This is to be expected and can be explained by strong  $\sigma$ -donation effects from the ligand to the metal centre. Upon coordination less electron density is present on the triazole ring and as a result the acidity of the ligand in the ground state increases. The observations that only one pKa value is found for the dinuclear complexes and that no significant changes occur in the spectra of the mononuclear complexes in the pH range 8-11 (where, on the basis of the pKa of the free ligand deprotonation of the free triazole ring would be expected to occur) further confirms the very weak metal-metal interaction.

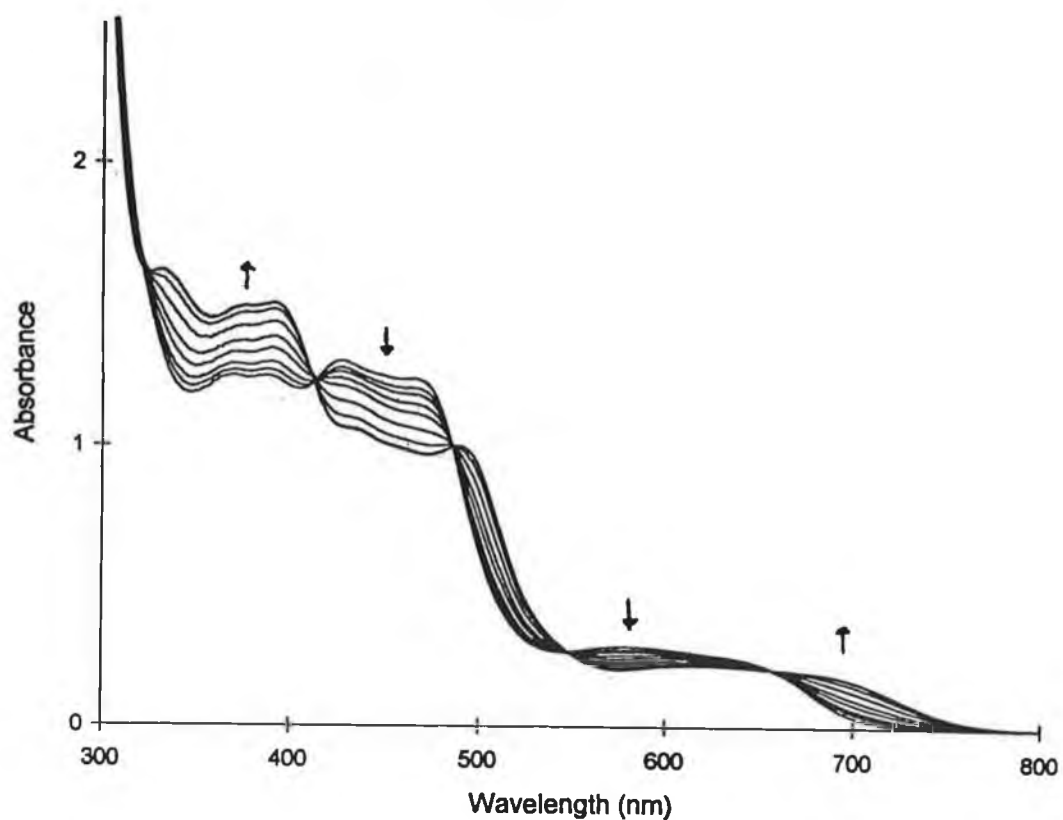


Figure 4.21 pH dependent absorbance of pOsOs in pH range 1-7.

Table 4.4 Ground and Excited State pKa values for the complexes of the ligands H<sub>2</sub>L1 and H<sub>2</sub>L2.

| Complex           | pKa±0.1 | pHi <sub>1</sub> ±0.1 <sup>b</sup> | pKa*±0.1 |
|-------------------|---------|------------------------------------|----------|
| mRu               | 3.3     | 2.5                                | 1.7      |
| mOs               | 3.0     | 2.4                                | 1.6      |
| mRuRu             | 3.5     | 2.5                                | 1.5      |
| mOsOs             | 3.1     | 2.7                                | 1.4      |
| mRuOs             | 3.2     | 2.7                                | 1.5      |
| pRu               | 3.6     | 2.8                                | 1.8      |
| pOs               | 3.3     | 2.7                                | 1.8      |
| pRuRu             | 3.6     | 2.2                                | 2.1      |
| pOsOs             | 3.4     | 2.4                                | 1.9      |
| pRuOs             | 3.4     | 2.3                                | 1.9      |
| H <sub>2</sub> L1 | 9.5     |                                    |          |
| H <sub>2</sub> L2 | 9.1     |                                    |          |

<sup>b</sup> pHi = inflection point of emission intensity titration.

In order to investigate the excited state acidity, the emission titrations were carried out by excitation at the isobestic point taken from the ground state pKa titration. A representative example of the spectra obtained is shown in Figure 4.22, which shows the pH dependence of the emission of **mRuRu**. It is noteworthy that for the ruthenium homonuclear compounds the intensity of the emission is found to decrease as the pH decreases, whereas for the osmium compounds, the intensity increases with decreasing pH. The decrease in emission intensity with an increase in the acidity of the solution is probably due to a thermally populated  $^3\text{MC}$  state and proton-induced quenching as suggested by Rillema and others and previously discussed in Section 4.5<sup>37,38</sup>. In the osmium compounds, which have a greater  $t_{2g} - ^3\text{MC}$  energy gap, thermal population of deactivating dd states is avoided and their luminescent behaviour follows the trends predicted by the Energy Gap Law<sup>39</sup>. As explained in Section 4.3.3.2, protonation results in a greater  $t_{2g} - ^3\text{MLCT}$  energy gap and a decrease in the rate of non-radiative decay, which consequently results in an increase in emission intensity.

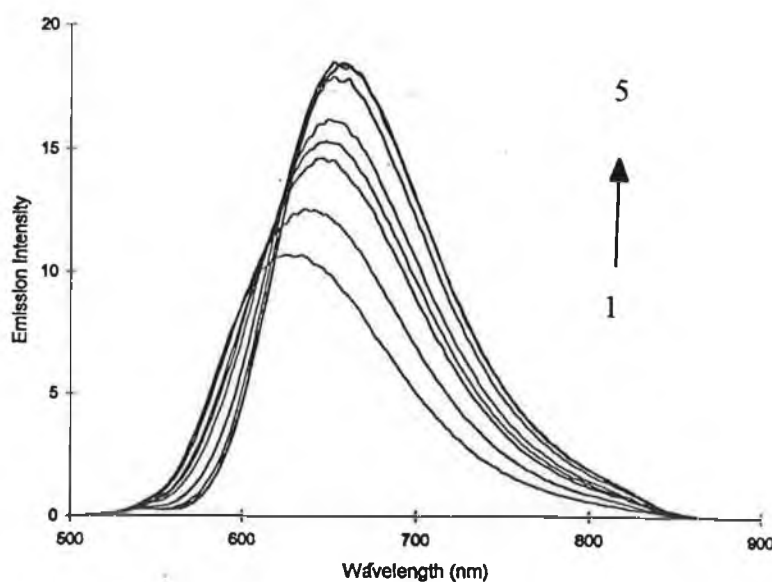


Figure 4.22 pH dependant emission spectra of **mRuRu** in pH range 1-5.

Using the spectroscopic data obtained for the protonated and deprotonated compounds, an estimate of  $pK_a^*$  can be made using the Forster cycle<sup>40</sup> as follows:

$$pK_a^* = pK_a + 0.625(\nu^- - \nu) / T \quad (4.5)$$

where T is the absolute temperature and  $\nu^-$  and  $\nu$  are the energies (in  $\text{cm}^{-1}$ ) of the 0-0 transition of the deprotonated and protonated forms, respectively. These values were taken from the emission frequencies obtained at 77 K as they are the best means to obtain an estimate for the energy difference involved in the 0-0 transition.

The  $pK_a^*$  values can also be calculated using the inflection point of the luminescence intensity vs pH titration curve ( $\text{pH}_i$ ), which is corrected for differences in excited state lifetimes of the deprotonated and protonated forms according to the equation derived by Ireland and Wyatt<sup>40</sup>:

$$pK_a^* = \text{pH}_i + \log [\tau / \tau^-] \quad (4.6)$$

Since the lifetimes of the protonated complexes are so short ( $< 20$  ns) and lie outside the range of the equipment, they are therefore unreliable and so it was not possible to use Equation 4.6 for an estimate of the  $pK_a^*$  values. The Forster equation has been used instead. It should be borne in mind that the main difficulty in using the Forster cycle as a means of determining  $pK_a^*$  is the accurate assessment of  $E_{0-0}$  for  $\nu^-$  and  $\nu$  since small errors in these values produce considerable errors in  $pK_a^*$ <sup>41</sup>. The best evaluation for the 0-0 energy should come from a detailed analysis of the vibrational structure by low temperature emission curve fitting, as demonstrated by Meyer and coworkers<sup>42,43</sup>. Therefore the Forster equation can only really be considered as a guideline with limited quantitative applicability. Nonetheless, from the values calculated, the direction of change in  $pK_a$  when going from the ground state to the excited state can be obtained.

As can be seen from Table 4.4, the  $pK_a^*$  values are more acidic than the ground state values. This means that the ligands H<sub>2</sub>L1 and H<sub>2</sub>L2 are spectator ligands and are not directly involved in the excited state. It is generally accepted that acidity of the excited state increases with respect to the ground state when the ligand involved in the acid-base reaction is not directly involved in the emission process. This is based on the knowledge that upon excitation of a ruthenium polypyridyl complex, a metal-based electron is promoted to a ligand  $\pi^*$  orbital. This results in the creation of a Ru centre with a formal valency of 3+. A decreased basicity is rationalised by a reduced electron density on the spectator ligand as a result of electron donation to the metal centre<sup>44</sup>. If on the other hand the basicity of a coordinated ligand in the excited state increases, the excited electron is thought to be localised on this ligand, and it is therefore directly involved in the emission process of the complex. The bipyrazine ligands represent such a case<sup>45</sup>.

#### 4.3.5 Electrochemical Properties.

From a number of investigations on mono- and polynuclear complexes containing polypyridine-type ligands, it is well established that oxidation and reduction processes are metal-centred and ligand-centred, respectively<sup>23</sup>. The oxidation and reduction potentials of the complexes are given in Table 4.5. All values have been corrected using the redox potential of ferrocene under the same experimental conditions as a secondary reference. Its potential was taken to be +0.38 V vs SCE<sup>46,47</sup>.

The anodic region of the cyclic voltammograms (Fig 4.23-4.24) feature reversible metal-centred oxidations, while the cathodic region exhibits poorly defined

waves resulting from the reduction of the coordinated polypyridyl ligands. The oxidation potentials are, without exception, significantly lower than that of  $M(\text{bpy})_3^{2+}$  ( $E_{1/2} = 1.26$  V for  $M = \text{Ru}$ ,  $E_{1/2} = 0.83$  V for  $M = \text{Os}$  (vs. SCE)) which indicates that the ligands  $\text{H}_2\text{L1}$  and  $\text{H}_2\text{L2}$  are stronger  $\sigma$ -donor ligands than  $\text{bpy}$  in both their protonated and deprotonated forms. The protonated complexes show an anodic shift of between 250 and 300 mV compared to the deprotonated compounds. Since in its protonated form the coordinated ligand is a better  $\pi$ -acceptor and weaker  $\sigma$ -donor, this results in a decrease in electron density at the metal centre which then becomes more difficult to oxidise. As expected the oxidation potentials of the osmium compounds are approximately 400 mV lower than those of the analogous ruthenium complexes. This has been reported for other complexes and is caused by the slightly higher energy of the 5d orbitals of osmium compared to the 4d orbitals of ruthenium<sup>48</sup>. For the heterodinuclear complexes, **pRuOs** and **mRuOs**, two reversible waves are observed with a 1:1 intensity as expected for oxidation of the  $\text{Os}^{\text{II}}$  centre, followed by the  $\text{Ru}^{\text{II}}$  centre (Fig. 4.24).

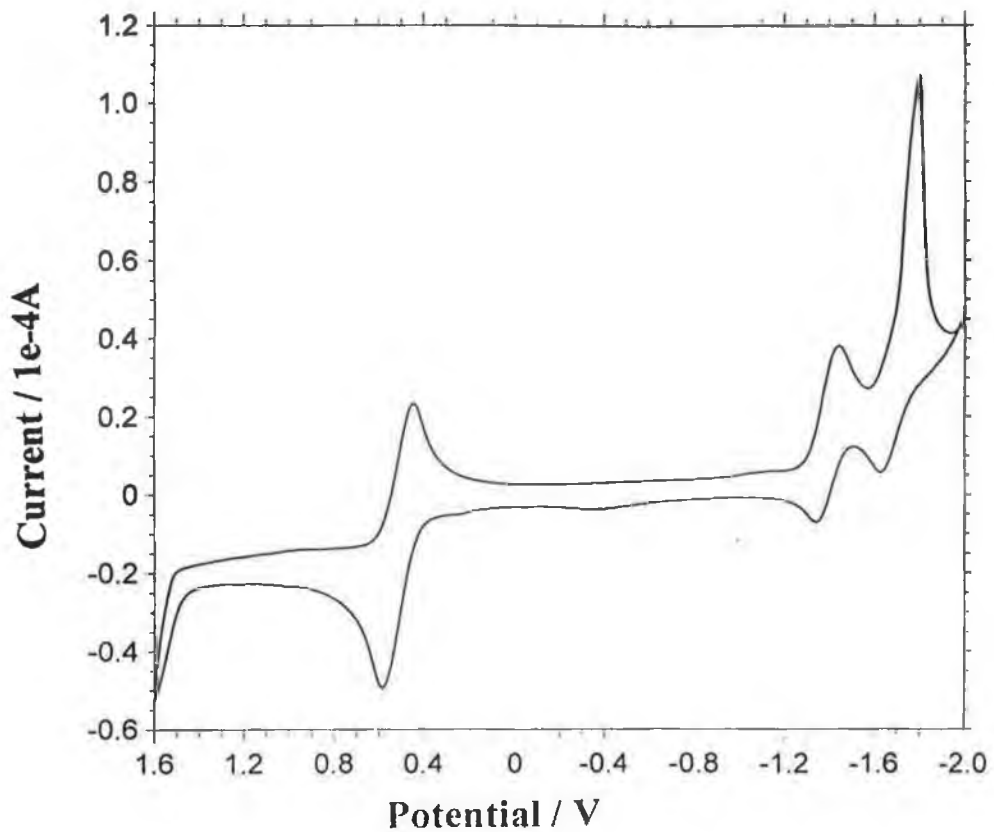


Figure 4.23 Cyclic voltammogram of pOs in acetonitrile.

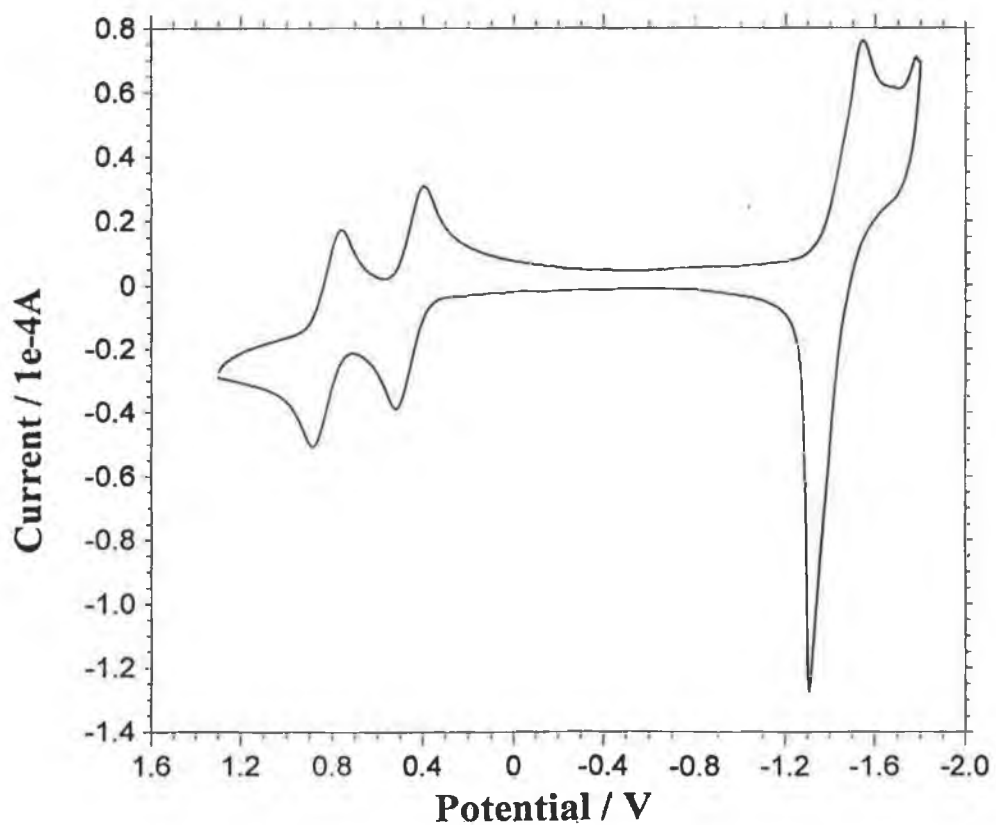


Figure 4.24 Cyclic voltammogram of pRuOs in acetonitrile.

**Table 4.5** *Oxidation and Reduction potentials of the mononuclear and dinuclear complexes with H<sub>2</sub>L1 and H<sub>2</sub>L2 (V vs SCE). All measurements carried out in acetonitrile with 0.1 M TEAP.*

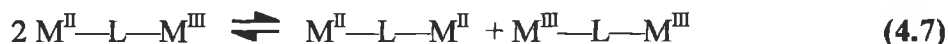
| Complex       | Oxidation Potentials |          | Reduction Potentials     |
|---------------|----------------------|----------|--------------------------|
|               | Ru-based             | Os-based |                          |
| <b>mRu</b>    | 0.84                 |          | -1.45, -1.60             |
| <b>mRuH</b>   | 1.18                 |          | -1.47                    |
| <b>mOs</b>    |                      | 0.48     | -1.39, -1.71             |
| <b>mOsH</b>   |                      | 0.76     | -1.46 (irr)              |
| <b>mRuRu</b>  | 0.84                 |          | -1.40, -1.69             |
| <b>mRuRuH</b> | 1.18                 |          | -1.53                    |
| <b>mOsOs</b>  |                      | 0.48     | -1.41, -1.71             |
| <b>mOsOsH</b> |                      | 0.72     | -1.43, -1.71 (irr)       |
| <b>mRuOs</b>  | 0.83                 | 0.47     | -1.44, -1.60             |
| <b>mRuOsH</b> | 1.16                 | 0.76     | -1.56 (irr), -1.72 (irr) |
| <b>pRu</b>    | 0.84                 |          | -1.45, -1.61             |
| <b>pRuH</b>   | 1.15                 |          | -1.47                    |
| <b>pOs</b>    |                      | 0.49     | -1.37, -1.54             |
| <b>pOsH</b>   |                      | 0.75     | -1.48 (irr), -1.69       |
| <b>pRuRu</b>  | 0.84                 |          | -1.50, -1.71 (irr)       |
| <b>pRuRuH</b> | 1.14                 |          | -1.52, -1.79 (irr)       |
| <b>pOsOs</b>  |                      | 0.49     | -1.36, -1.52, -1.75      |
| <b>pOsOsH</b> |                      | 0.73     | -1.39, -1.66             |
| <b>pRuOs</b>  | 0.85                 | 0.48     | -1.47, -1.68 (irr)       |
| <b>pRuOsH</b> | 1.14                 | 0.73     | -1.47, -1.60 (irr)       |

The oxidation potentials of the complexes are very similar to those found for the N1-bound isomers of the ligands 5-(2-pyridyl)-1,2,4-triazole and Hbpt<sup>18</sup>. This observation

further supports the conclusion made from the analysis of the  $^1\text{H-NMR}$  spectra that the metal centres are bound via N1 of the triazole ring.

Of particular interest is the finding that for the homodinuclear complexes a single redox wave without any sign of splitting is obtained, which by comparison with the oxidation peaks of the corresponding mononuclear species is attributed to the simultaneous oxidation of the two metal units. It is known that molecules containing a number of identical noninteracting centres exhibit current-potential responses having the same shape as that obtained with the corresponding molecule containing a single centre<sup>49</sup>. The presence of additional electroactive centres only enhances the magnitude of the current. Furthermore the oxidation potentials of the osmium and ruthenium metal centres in their respective mononuclear and dinuclear complexes are identical, within experimental error. No shift in the metal redox potential occurs upon formation of the dinuclear complex. This is a characteristic feature of mixed-valence dinuclear complexes where electrostatic and resonance stabilisation effects are small and therefore serves as evidence of small electronic coupling between the two metal centres in the ground state<sup>50</sup>. A metal-metal interaction would lead to stabilisation of the mixed-valence complex and the presence of discrete oxidation waves for each metal centre<sup>51</sup>. Electrostatic effects are also a factor in the separation of redox waves of metal units in polynuclear compounds<sup>52,53</sup>. However with increasing distance between metal centres, electrostatic effects play a negligible role and the difference in redox potentials between the  $\text{M}^{\text{II}}\text{-L-M}^{\text{II}}/\text{M}^{\text{II}}\text{-L-M}^{\text{III}}$  and  $\text{M}^{\text{II}}\text{-L-M}^{\text{III}}/\text{M}^{\text{III}}\text{-L-M}^{\text{III}}$  species falls below the resolution limit, resulting in a single redox wave<sup>54</sup>. The intermediate species exist in a comproportionation equilibrium shown in Equation 4.7. The stability of the mixed-valence complex  $\text{M}^{\text{II}}\text{-L-M}^{\text{III}}$  towards redox dissociation or

comproportionation as measured by the comproportionation equilibrium constant,  $K_c$ , is directly related to the difference in the  $M^{II}-L-M^{II}/M^{II}-L-M^{III}$  and  $M^{II}-L-M^{III}/M^{III}-L-M^{III}$  redox potentials ( $\Delta E$ ) as shown in Equation 4.8.



$$K_c = e^{\Delta E \text{ (mV)} / 25.69} \quad \text{at } T = 298 \text{ K.} \quad (4.8)$$

The presence of a single oxidation wave for the homodinuclear complexes means that  $K_c$  is very close or at the statistical limit of  $4^{55}$ .

The reduction waves observed for all the complexes are bpy-based. The ligands  $H_2L1$  and  $H_2L2$ , being weaker  $\pi$ -acceptors than bpy, are consequently more difficult to reduce and their redox couples lie outside the potential window investigated. Resonance Raman measurements on  $[Ru(bpy)_2bpt]^+$  have shown that the lowest unoccupied molecular orbital (LUMO) is located on the bpy ligands. The similar reduction potentials observed for the complexes of  $H_2L1$  and  $H_2L2$  support the assignment of bpy reduction. The bpy-based reductions occur at a more negative potential than their  $M(bpy)_3^{2+}$  analogues. It may be argued that the  $\sigma$ -donor properties of the ligands  $H_2L1/H_2L2$  enhance not only the electron density at the metal centre, but also metal — bpy back-bonding. As a consequence of this it is more difficult to add electron(s) to the bipyridyl ligands and more negative reduction potentials are observed. The weak interaction of the metal units indicated by the oxidation behaviour in the dinuclear complexes is also reflected in the reduction patterns observed. In the homodinuclear complexes the first peak is attributed to simultaneous one-electron reduction of a bpy ligand of each of the two different metals<sup>52</sup>. As has been found for

other diimine complexes, irreversible waves corresponding to the second reduction process of the bpy ligands and desorption spikes are observed at negative potentials<sup>56,57</sup>. This situation is particularly aggravated for measurements involving the protonated complexes. As found before by Hage<sup>18</sup> and others, it is very difficult to obtain satisfactory reduction potentials in acidic solutions. Adsorption onto the electrode surface is a problem as is the fact that the protonated complexes can be deprotonated when scanning to a negative potential.

#### 4.3.6 Spectroelectrochemical Measurements.

The electrochemical and spectroscopic data for the complexes suggest very weak communication between the metal centres in the ground state. It should be recalled however that fast electron transfer processes need only electronic couplings as small as tens of wavenumbers<sup>58</sup>. Whilst  $K_c$  may in principle serve as a measure of electronic interaction between two metal sites in a binuclear complex, the most direct measure of metal-metal electronic coupling in a mixed-valence system lies in an analysis of intervalence transitions associated with the species. There are many examples reported in the literature of dinuclear systems exhibiting only one redox couple associated with oxidation of the metal centres where intervalence transitions are observed<sup>59,60,61</sup>. As discussed in Chapter 1, intramolecular electron transfer can be monitored by the study of intervalence transitions occurring in mixed-valence complexes<sup>62</sup>. The interaction between two metal atoms connected through a bridging ligand is characterised by the electronic matrix element,  $V_{ab}$ , which has a dimension of energy and corresponds to the effective coupling between metal localised orbitals.  $V_{ab}$

can be obtained from the position, intensity and width of the intervalence transition which generally occurs in the near infrared region of the spectrum (Equation 4.9)<sup>63</sup>.

$$V_{ab} = 2.05 \times 10^{-2} (\epsilon_{\max} \nu_{\max} \Delta\nu_{1/2})^{1/2} / R_{MM} \quad (4.9)$$

where  $\epsilon_{\max}$  is the maximum extinction coefficient,  $\nu_{\max}$  is the band position in  $\text{cm}^{-1}$ ,  $\Delta\nu_{1/2}$  is the band width at half maximum ( $\text{cm}^{-1}$ ) and  $R_{MM}$  is the metal—metal distance in Å.

Spectroelectrochemical measurements were therefore carried out on the mononuclear and dinuclear complexes in their protonated and deprotonated forms. In a typical experiment the UV/Vis/near-IR spectra were recorded at given intervals during controlled potential electrolysis in the OTTLE cell described in Chapter 2. The reversibility of the process was ascertained at the end of the experiment by electrolysis to the original oxidation state and analysis of the absorption spectrum. In all cases 100 % regeneration of the parent complex was observed. The relevant spectral parameters for the oxidised metal complexes are reported in Table 4.6.

Oxidative spectroelectrochemistry of the mononuclear complexes sees in each case the gradual disappearance of the MLCT band and a decrease in intensity and red-shift in the  $\pi\text{-}\pi^*$  transition around 280 nm. With the bleach of the MLCT band a concurrent increase in intensity of bands in the region 520-1000 nm appears which persists when the oxidation process is complete. These have been assigned as a ligand-to-metal charge transfer (LMCT) bands on the basis of their energy and intensity and comparison with spectroelectrochemical experimental data for the complex  $[\text{Ru}(\text{bpy})_2\text{pptr}]^+$ , where Hpptr is 3-phenyl-5-(2-pyridyl)-4H-1,2,4-triazole (Figure

4.25). The spectral changes observed upon the gradual oxidation of **mRu** are shown in Figure 4.26. It can be seen that the changes occurring upon oxidation are clean, with isobestic points being observed at 321 nm and 515 nm. In the UV region, the characteristic splitting and shift to lower energy of the band originally at 280 nm is indicative of oxidation of metal centres bound to bpy ligands<sup>64</sup>.

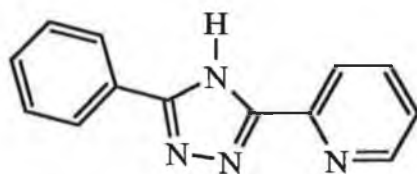


Figure 4.25 Structure of 3-phenyl-5-(2-pyridyl)-4H-1,2,4-triazole.

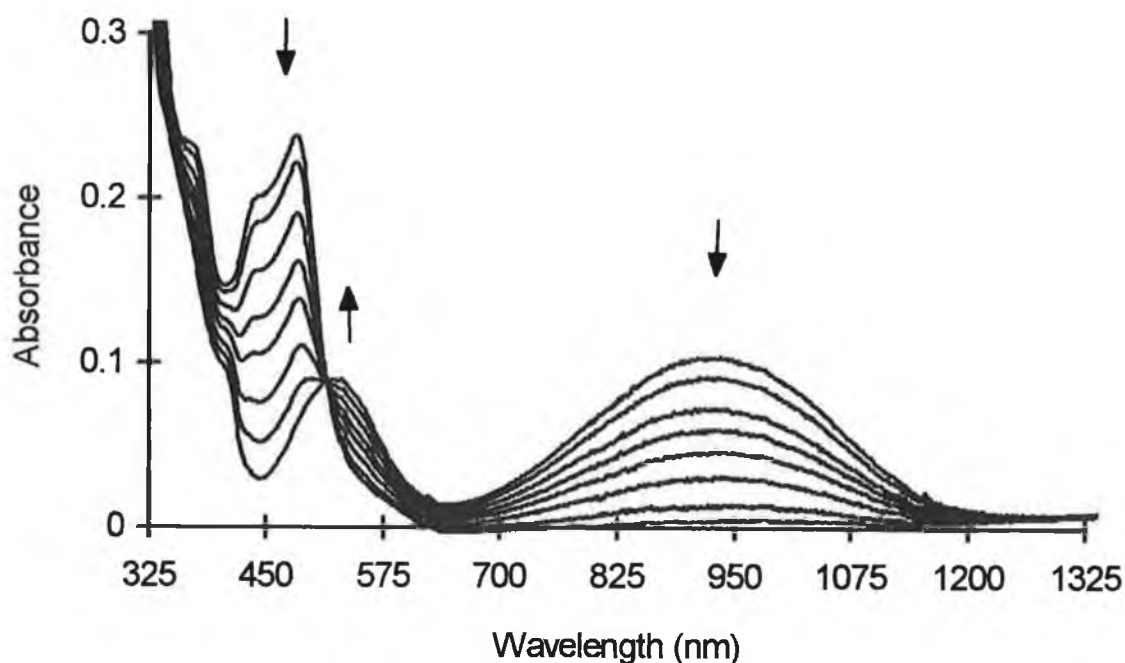
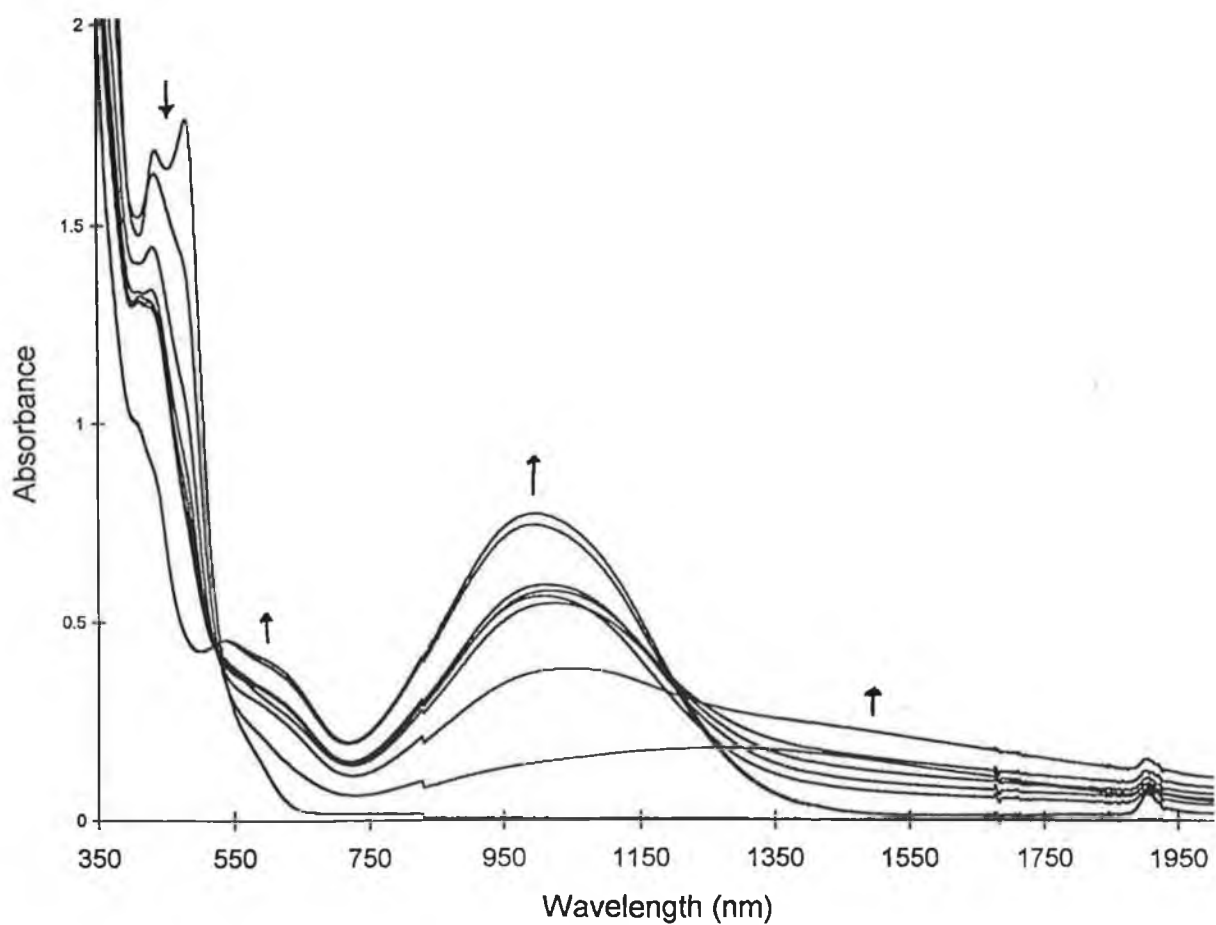


Figure 4.26 Spectral changes for oxidative spectroelectrochemistry of **mRu**.

**Table 4.6** *UV/Vis/NIR absorption data for the complexes of H<sub>2</sub>L1 and H<sub>2</sub>L2 in their protonated and deprotonated forms. All measurements carried out using CH<sub>3</sub>CN with 0.1 M TEAP. Solutions were acidified using HClO<sub>4</sub>.*

| <b>Complex</b>                                  | <b>M(III) absorption bands/ nm (<math>\epsilon/M^{-1}cm^{-1}, \nu_{1/2}/cm^{-1}</math>)</b> |
|---|---|
| <b>mRu</b>                                      | 530 (3094, 3499); 923 (3698, 3541)  |
| <b>mRuH</b>                                     | 520 (2310, 5323); 850 (2140, 5191)  |
| <b>mOs</b>                                      | 734 (2123, 4078); 1680 (222); 2320 (1235)   |
| <b>mOsH</b>                                     | 573 (1395); 1674 (119); 2310 (800)  |
| <b>mRuRu</b>                                    | 525 (8115, 3643); 927 (7540, 3945)  |
| <b>mRuRuH</b>                                   | 500 (3210); 755 (3816, 5610)  |
| <b>mOsOs</b>                                    | 730 (4183, 4003); 1700 (550); 2320 (2578)   |
| <b>mOsOsH</b>                                   | 566 (2463, 5319)  |
| <b>mRuOs</b>                                    | 741 (2369, 4170); 930 (4625, 3471);<br>1685 (300); 2315 (1581)                              |
| <b>mRuOsH</b>                                   | 706 (1871, 4272); 912 (3994, 3996); 530 (4376);<br>1750 (259); 2328 (1659)                  |
| <b>pRu</b>                                      | 578 (2743, 3418); 978 (5114, 3200)  |
| <b>pRuH</b>                                     | 550 (2608, 4293); 900 (2643, 4355)  |
| <b>pOs</b>                                      | 770 (3027, 4055); 1650 (548); 2271 (1370)   |
| <b>pOsH</b>                                     | 624 (1278, 4623); 1678 (165); 2305 (850)  |
| <b>pRuRu</b>                                    | 535 (5242); 998 (8733, 3988)  |
| <b>pRuRuH</b>                                   | 537 (2593); 870 (3048, 6210)  |
| <b>pOsOs</b>                                    | 800 (6593, 2654); 1700 (420); 2343 (3390)   |
| <b>pOsOsH</b>                                   | 740 (2302, 4080); 1709 (224); 2320 (1531)   |
| <b>pRuOs</b>                                    | 560 (3398); 782 (2808, 4760); 1018 (7883, 4058);<br>1691 (358); 2316 (2050)                 |
| <b>pRuOsH</b>                                   | 772 (1877, 1305); 942 (6292, 1689);<br>1816 (245); 2319 (1603)                              |
| <b>[Ru(bpy)<sub>2</sub>(pptr)]<sup>2+</sup></b> | 920 (4523, 3118)  |

For the dinuclear complexes similar changes occur in the UV/Vis/Near IR spectra upon oxidation. The spectral changes which occur for the complexes **pRuRu**, **mRuRu** and **pOsOs** upon oxidation are shown in Figs. 4.27-4.29, respectively.



*Figure 4.27* Spectral changes for oxidative spectroelectrochemistry of **pRuRu**.

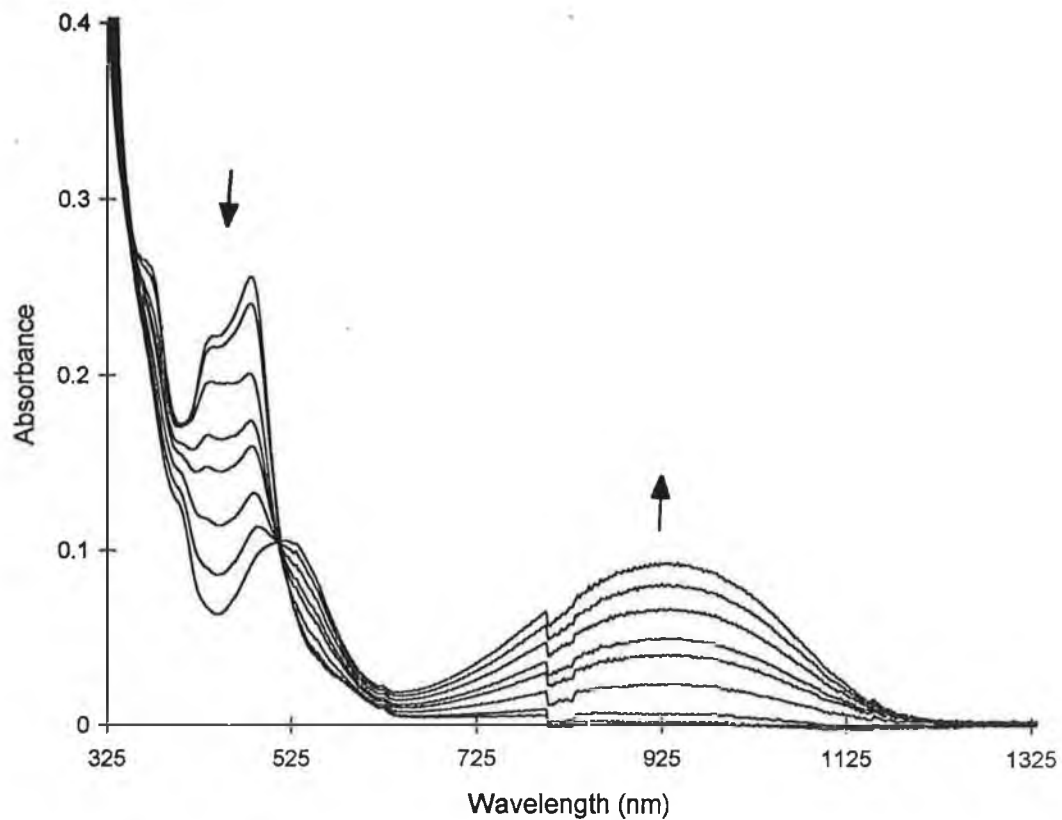


Figure 4.28 Spectral changes for oxidative spectroelectrochemistry of mRuRu.

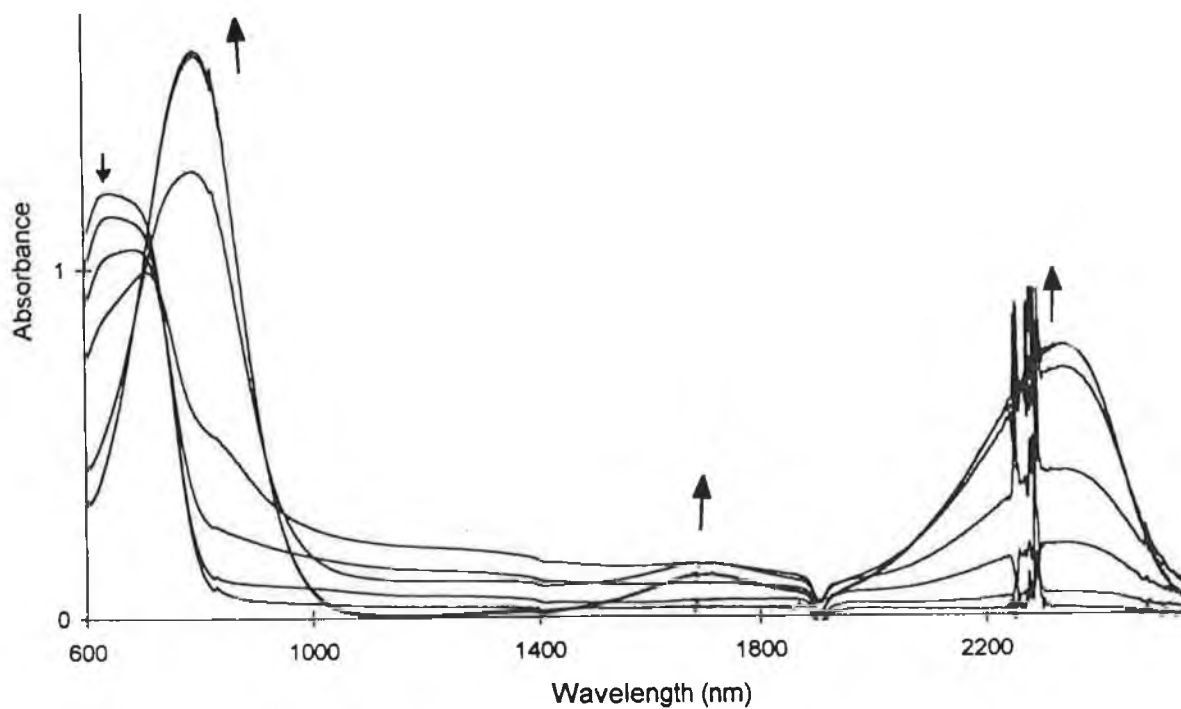


Figure 4.29 Spectral changes for oxidative spectroelectrochemistry of pOsOs.

As with the mononuclear complexes, gradual oxidation showed the progressive decay of the MLCT band the concomitant grow-in of bands in the red end of the spectrum. Since these are very similar in energy to those found for the mononuclear parent compounds and persist in the fully oxidised species they are attributed to ligand-to-metal charge transfers from the bridging ligand to the M(III) centres. In the case of **pRuRu**, however, an additional feature appears in the near infrared region of the spectrum. Initial oxidation sees the appearance of a very broad weak band centred at 1271 nm (Fig 4.30).

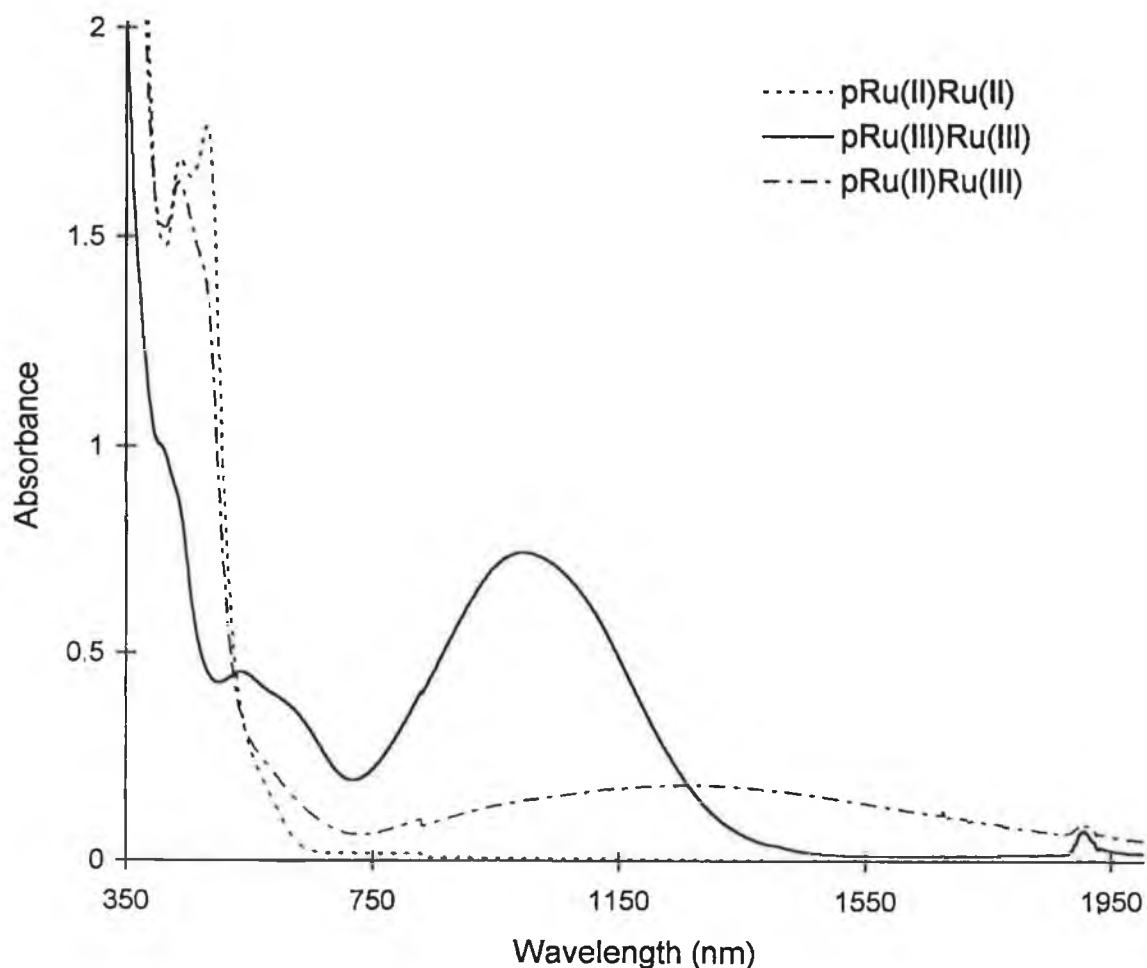


Figure 4.30 Visible/Near-IR Absorption Spectra of  $\text{pRu}^{\text{II}}\text{Ru}^{\text{II}}$ ,  $\text{pRu}^{\text{III}}\text{Ru}^{\text{II}}$ , and  $\text{pRu}^{\text{III}}\text{Ru}^{\text{III}}$ .

As the oxidation progresses this decreases in intensity and a more intense, structured, higher energy band at 1000 nm develops, which by comparison with **pRu** is assigned as a LMCT band. The increase and subsequent decrease of the 1271 nm band during the oxidation process, together with its position and intensity, strongly suggests that this absorption feature represents an intervalence transition. The situation is reminiscent of that found by Bonvoisin and coworkers who studied the intervalence transition in the mixed-valence forms of the aromatic amine [4-[bis(4-ethylphenyl)amino]phenyl]-*N,N,N',N'*-tetrakis(4-ethylphenyl)-[1,1':3',1''-terphenyl]-4,4''-diamine<sup>65</sup>. Similarly, upon close examination of the spectral changes which occur during the oxidation of **pOsOs**, a weak band at 1066 nm appears and subsequently disappears during the course of the oxidation. However no evidence of such intervalence features can be identified for **pRuOs** or any of the meta complexes, **mRuRu**, **mOsOs** and **mRuOs**. It is difficult to explain why this is so. It may be due to the fact that IVCT bands, if present, are extremely weak or coincide in terms of position with the LMCT bands associated with the complexes. Because of the redox asymmetry of the mixed-metal system, it is expected that the energy of an IVCT band for **pRuOs** would be higher than  $\nu_{\max}$  for the analogous **pRuRu** complex<sup>66</sup>. Using the relationship shown in Equations 4.10 and 4.11 between intervalence absorption energies ( $\Delta\nu_{\max}$ ) and the difference in redox potentials  $\Delta(\Delta E_{1/2})$  devised by Goldsby and Meyer<sup>67</sup>, an IVCT band associated with **pRuOs** would be predicted to occur around 950 nm.

$$\Delta\nu_{\max} = \Delta(\Delta E_{1/2}) = \Delta E_{1/2}(\text{Ru/Os}) - \Delta E_{1/2}(\text{Ru/Ru}) \quad (4.10)$$

$$\Delta\nu_{\max} = \nu_{\max}(\text{Ru}^{\text{II}}\text{-Os}^{\text{III}}) - \nu_{\max}(\text{Ru}^{\text{II}}\text{-Ru}^{\text{III}}) \quad (4.11)$$

It would therefore be hidden underneath the Os(III) and Ru(III) LMCT bands. In the case of the meta complexes, **mRuRu**, **mOsOs** and **mRuOs**, the lack of evidence for IVCT bands may be as a result of extremely weak coupling which means that intervalence transitions cannot be observed under the experimental conditions used. The observation that electronic coupling is not as efficient for meta substituted aromatic rings has already been noted by several groups<sup>68,69</sup>.

The analysis of the IVCT bands provides some insight into the degree of metal-metal coupling in **pRuRu** and **pOsOs** (Table 4.7). In reporting the extinction coefficient for the intervalence band, the intensity has been corrected by a factor of  $(2 + (K_c)^{1/2})/(K_c)$  to account for comproportionation<sup>70</sup>. Thus when half the total ruthenium has been oxidised the solution actually contains 50 % of the dimer as the mixed-valence species, the remaining being an equimolar mixture of homovalent species (each 25 %). If the concentration of mixed-valence species were taken to equal the total dinuclear content, this would introduce a considerable error<sup>71</sup>. The bandwidth at half maximum has been obtained by doubling the half-width on one side of the band. The value of  $K_c$  has been taken to be 4. This is reasonable as Taube and coworkers have shown that when the metal-metal distance reaches ca. 12 Å,  $K_c$  is near the statistical limit<sup>70</sup>. Molecular models of the dinuclear complexes using Hyperchem predicts a metal—metal distance of 13 Å. Whilst this is only an approximation, it nonetheless allows an estimate of the degree of coupling between the metal centres. The electronic coupling factors,  $V_{ab}$ , calculated for **pRuRu** and **pOsOs** are similar to those found by Collin *et al.* for dinuclear Ru(II) complexes containing back-to-back bisterpyridine ligands linked by phenylene spacers<sup>72</sup>. It could be argued that aromatic groups do not necessarily promote a strong electronic coupling between redox centres.

Kim and Lieber found that pentaamineruthenium groups connected through dipyridylbenzene and dipyridylphenyl units showed very weak intervalence spectra<sup>6</sup>. It has been suggested by Ribou and coworkers, who examined intervalence electron transfer in similar pentaamineruthenium complexes of dipyridylpolyenes, dipyridylthiophene and dipyridylfuran and observed stronger, more defined IVCT transitions, that the phenylene group, because of its strong aromaticity, is unfavourable as a mediator of intervalence electron transfer since conjugative interaction with attached units may be realized at the expense of its own aromaticity<sup>59</sup>.

**Table 4.7** *Intervalence band parameters for pRuRu and pOsOs.*

| <b>Complex</b> | $\nu_{\max}$ (cm <sup>-1</sup> ) | $\Delta\nu_{1/2}$ (cm <sup>-1</sup> ) | $\epsilon$ (M <sup>-1</sup> cm <sup>-1</sup> ) | $V_{ab}$ (cm <sup>-1</sup> ) |
|----------------|----------------------------------|---------------------------------------|--|------------------------------|
| <b>pRuRu</b>   | 7870                             | 4262                                  | 1042   | 295                          |
| <b>pOsOs</b>   | 9381                             | 5544                                  | 435  | 237                          |

For the osmium compounds additional bands are observed at around 2200 nm and 1800 nm. These are assigned as Os(III) d $\pi$ - d $\pi$  transitions and occur as a result of the larger spin-orbit coupling found in osmium systems<sup>73</sup> (Fig. 4.31). The vertical lines are artifacts as a result of the solvent absorption exceeding the compensation capability of the spectrophotometer<sup>74</sup>.

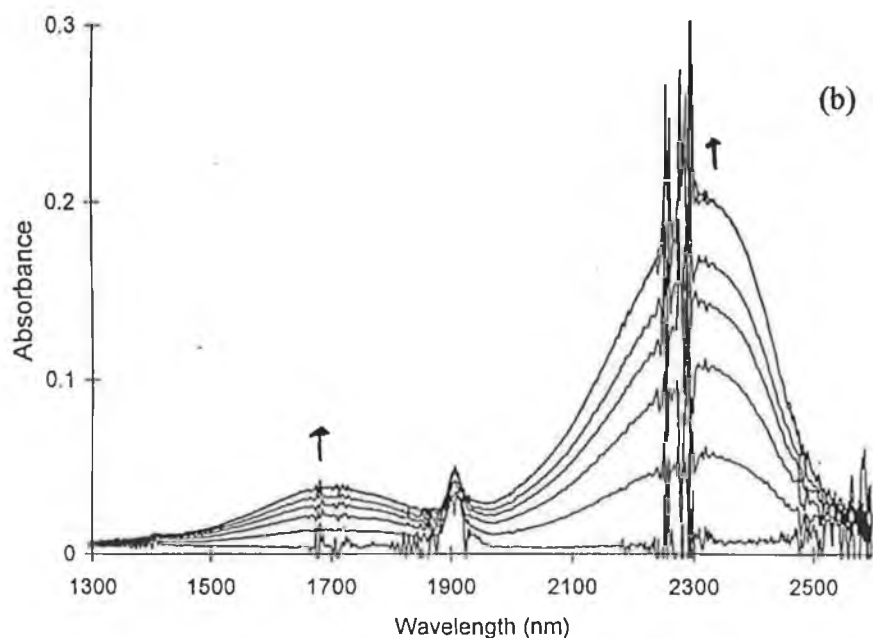
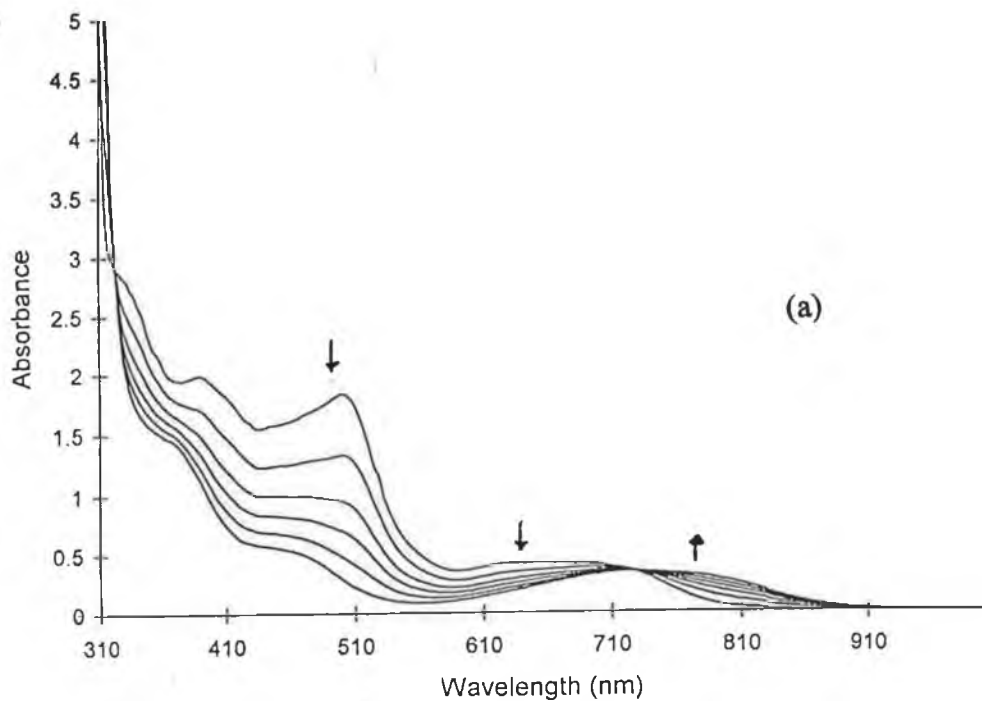


Figure 4.31 Spectral changes which occur for mOs during oxidation in (a) visible/near- IR region and (b) near-IR region.

The spectroelectrochemistry of the mixed-metal Ru/Os dinuclear complexes affords an opportunity to examine more closely the electronic transitions associated with each metal centre, since the two metals oxidise at substantially different

potentials. Upon oxidation of the Os site the transitions that remain in the visible may be attributed to the MLCT transitions involving the Ru(II) centre. Likewise the LMCT bands observed may be distinguished as belonging to the Os(III) or the Ru(III) centres (Fig. 4.32). It is noteworthy that the LMCT bands of the Os(III) centres are at higher energy than those associated with the Ru(III) sites. This is due to the fact that Os(III) is a less powerful oxidant than Ru(III).

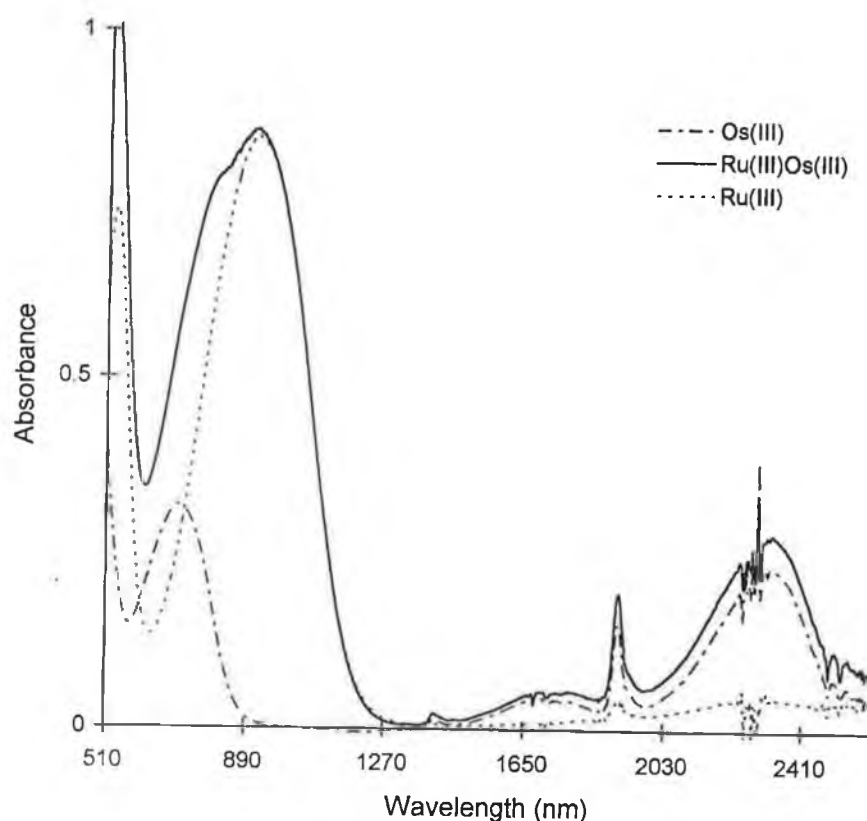


Figure 4.32 Spectra associated with the Ru(III) and Os(III) centres in  $m\text{Ru}^{\text{III}}\text{Os}^{\text{III}}$ .

As can be seen in Table 4.6 the Ru(III) and Os(III) complexes show fairly intense LMCT bands in the visible/near IR region. Ru(III) and Os(III) complexes (octahedral, low-spin with  $d^5$  electronic configuration) are known to exhibit LMCT bands. The  $d^5$  Ru(III) centres may be regarded as  $\pi$ -acceptors by virtue of their high

charge and half-vacant  $\pi$ d-acceptor orbital<sup>75</sup>. With a few notable exceptions, very little work has been carried out on the study of LMCT states. This may be because of their weak intensities ( $\epsilon \leq 500 \text{ M}^{-1}\text{cm}^{-1}$ ) in the archetypal  $[\text{Ru}(\text{bpy})_3]^{2+}$  and  $[\text{Os}(\text{bpy})_3]^{2+}$  complexes and their nonemissive nature. Nazeeruddin and coworkers studied the variations in the energies and intensities of LMCT bands in twenty complexes of the type  $[\text{M}(\text{X}_2\text{-bpy})_3]^{3+}$  and  $[\text{M}(\text{bpy})_n(\text{X}_2\text{-bpy})_{3-n}]^{3+}$  ( $\text{M} = \text{Ru}$  or  $\text{Os}$ ,  $\text{X} = \text{Me}$ ,  $\text{OMe}$ ,  $\text{NH}_2$  and  $\text{NMe}_2$ )<sup>76</sup>. The results found for the complexes of  $\text{H}_2\text{L1}$  and  $\text{H}_2\text{L2}$  will be discussed in the context of their findings.

LMCT transitions involve the removal of an electron from the HOMO of the donor ligand to one of the partially filled  $t_{2g}$  orbitals of the metal ion i.e.  $\pi_L \rightarrow t_{2g}^*(\text{M})$ . Whilst the MLCT transition in mixed-ligand complexes of the type  $[\text{M}(\text{bpy})_n(\text{L})_{3-n}]^{2+}$  involve the acceptor ligand bpy, the LMCT transition involves the electron-rich donor ligand. LMCT bands of moderate intensity in the red/near IR region have previously been observed in the mixed-ligand complexes of Ru(III) containing electron-rich donor ligands such as bibenzimidazole<sup>77</sup> and Hbpt<sup>78</sup>. The position and intensity of these LMCT bands correlate well with those found here.

Spectroelectrochemistry on the protonated complexes results in the LMCT bands moving to higher energy. This observation can be rationalised in terms of the relative energies of the donor ( $\pi_L$ ) and acceptor ( $t_{2g}^*$ ) orbitals (Fig. 4.33). To a first approximation, the energy of the acceptor  $t_{2g}$  orbital can be estimated using the first oxidation potential  $E[\text{Ru}(\text{III})/\text{Ru}(\text{II})]$ . The energy of the donor level in the Ru and Os complexes on the other hand is more difficult to determine and has been estimated using the energy of the LMCT transition. The spectroscopic (0-0) energy of the charge transfer transition has been estimated as the energy at which the absorption

intensity at the band maximum drops to 1 % of the intensity at the band maximum on the high energy side of the band<sup>79</sup>. This point is given by  $\nu_{1\%} = \nu_{\max} + 1.29 \Delta\nu_{1/2}$ , where  $\Delta\nu_{1/2}$  is the bandwidth at half-height for a gaussian band shape.

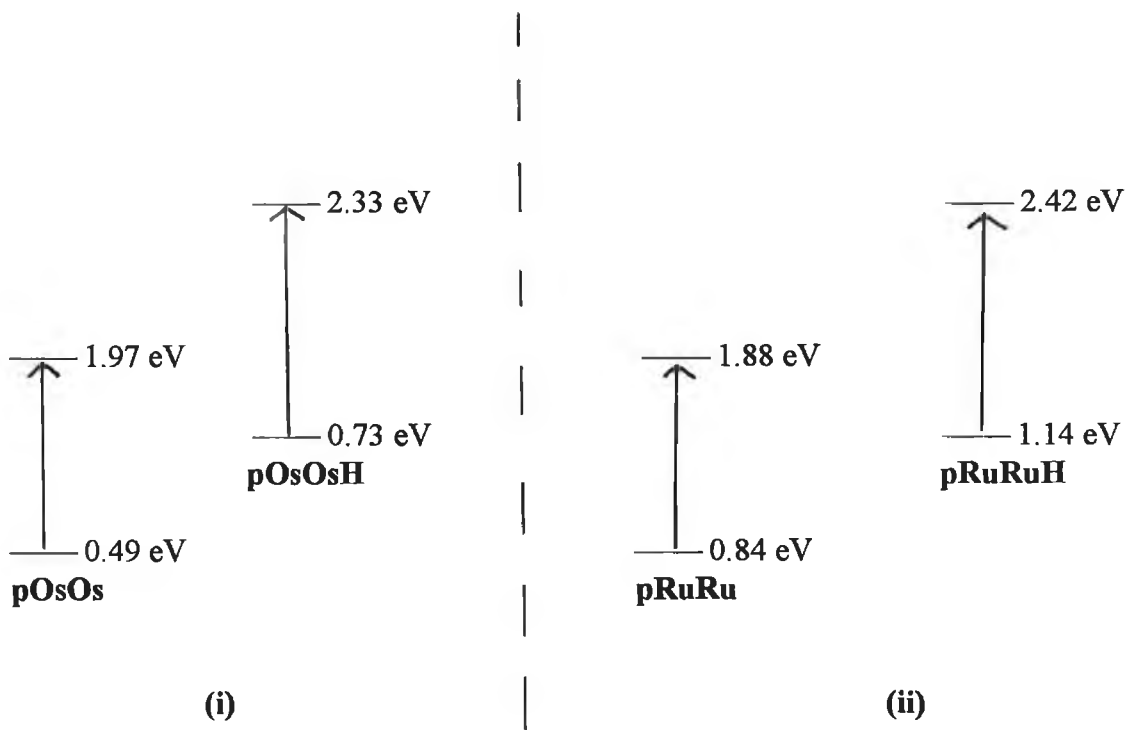


**Fig. 4.34.** Schematic correlation of the LMCT transition energies with the energies of the metal and ligand orbitals for pOsOs/pOsOsH (i) and pRuRu/pRuRuH (ii).

The effect of protonation and the subsequent decrease in the  $\sigma$ -donor properties of the bridging ligand is to increase the energy of both the donor and acceptor orbitals, leading to the observed shift in the LMCT transition.

In addition, upon protonation there is a noticeable decrease in intensity of the LMCT band. This is consistent with the findings of Nazeeruddin and coworkers who

concluded that the intensity of the LMCT transition increases with increasing electron-donating capacity of the donor ligand.

#### 4.4 Concluding Comments.

The ruthenium and osmium bipyridyl complexes of the ligands 1,3-bis(5-(2-pyridyl)-4*H*-1,2,4-triazol-3-yl)benzene (H<sub>2</sub>L1) and 1,4-bis(5-(2-pyridyl)-4*H*-1,2,4-triazol-3-yl)benzene (H<sub>2</sub>L2) have been synthesised and characterised using a combination of electrochemical and spectroscopic techniques.

The substantial additivity of the spectroscopic and electrochemical properties of the metal-containing units in the dinuclear complexes points towards a relatively weak degree of metal-metal interaction. The oxidation potentials, absorption maxima and luminescence properties of the mononuclear and homodinuclear complexes are identical (within experimental error). In addition, the absorption spectra exhibited by the heterometallic RuOs complex and a 1:1 mixture of their homometallic “parent” complexes coincide completely with each other. However the observation of very weak intervalence band transitions in the region 1000-1500 nm for the RuRu and OsOs complexes indicates that an interaction, albeit weak, does exist for these compounds.

The luminescence spectra obtained for the mixed-metal complexes in their deprotonated and protonated forms indicate that electronic energy transfer occurs from the Ru-based unit to the Os-based component. However more detailed measurements are necessary before any conclusions as to a mechanism for this process can be made.

## 4.5 References

---

- 1 L.A. Worl, G.F. Strouse, J.N. Younathan, S.M. Baxter and T.J. Meyer, *J. Am. Chem. Soc.*, 1990, 112, 7571.
- 2 V. Balzani, *Tetrahedron*, 1992, 48, 10443.
- 3 V. Balzani, S. Campagna, G. Denti, A. Juris, S. Serroni and M. Venturi, *Acc. Chem. Res.*, 1998, 31, 26.
- 4 V. Balzani and F. Scandola, *Supramolecular Photochemistry*; Horwood: Chichester, UK, 1991.
- 5 F. Scandola, M.T. Indelli, C. Chiorboli and C.A. Bignozzi, *Top. Curr. Chem.*, 1990, 158, 73.
- 6 Y. Kim and C.M. Lieber, *Inorg. Chem.*, 1989, 28, 3990.
- 7 F. Barigelletti, L. Flamigni, V. Balzani, J.-P. Collin, J.-P. Sauvage, A. Sour, E.C. Constable and A.M.W. Cargill Thompson, *J. Chem. Soc., Chem. Commun.*, 1993, 942.
- 8 F. Voegtle, M. Frank, M. Nieger, P. Belser, A. von Zelewsky, V. Balzani, F. Barigelletti, L. de Cola, L. Flamigni, *Angew. Chem. Int. Ed. Engl.*, 1993, 32, 1643.
- 9 L. de Cola, V. Balzani, F. Barigelletti, L. Flamigni, P. Belser, A. von Zelewsky, M. Frank and F. Voegtle, *Inorg. Chem.*, 1993, 32, 5228.
- 10 R. Hage, A.H.J. Dijkhuis, J.G. Haasnoot, R. Prins, J. Reedijk, B.E. Buchanan and J.G. Vos, *Inorg. Chem.*, 1988, 27, 2185.
- 11 F. Barigelletti, L. de Cola, V. Balzani, R. Hage, J.G. Haasnoot, J. Reedijk and J.G. Vos, *Inorg. Chem.*, 1989, 28, 4344; *ibid.* 1991, 30, 641.

- 
- 12 E. Gunnewegh, Unpublished results, Leiden University, 1988.
  - 13 B.P. Sullivan, D.J. Salmon, T.J. Meyer, *Inorg. Chem.*, 1978, 17, 3334.
  - 14 J.M. Kelly, C.M. O'Connell and J.G. Vos, *J. Chem. Soc. Dalton Trans.*, 1986, 253.
  - 15 D.A. Buckingham, F.P. Dwyer, H.A. Goodwin and A.M. Sargeson, *Aust. J. Chem.*, 1964, 17, 325.
  - 16 G.D. Marco, A. Bartolotta, V. Ricevuto, S. Campagna, G. Denti, L. Sabatino, and G. D. Rosa, *Inorg. Chem.*, 1991, 30, 270.
  - 17 G. Denti, S. Campagna, S. Serroni, M. Ciano and V. Balzani, *J. Am. Chem. Soc.*, 1992, 114, 2944.
  - 18 R. Hage, Ph.D Thesis 1991, Leiden University.
  - 19 P. Belser and A. von Zelewsky, *Helv. Chim. Acta.*, 1980, 63, 1675.
  - 20 E.C. Constable and J. Lewis, *Inorg. Chim. Acta.*, 1983, 70, 251.
  - 21 B.E. Buchanan, J.G. Vos, M. Kaneko, W.J.M. van der Putten, J.M. Kelly, R. Hage, R.A.G. de Graaf, R. Prins, J.G. Haasnoot and J. Reedijk, *J. Chem. Soc. Dalton Trans.*, 1990, 2425.
  - 22 R. Hage, J.G. Haasnoot, J. Reedijk, R. Wang, E.M. Ryan, J.G. Vos, A.L. Spek and A.J.M. Duisenberg, *Inorg. Chim. Acta*, 1990, 174, 77.
  - 23 A. Juris, V. Balzani, F. Barigelletti, S. Campagna, P. Belser and A. von Zelewsky, *Coord. Chem. Rev.*, 1988, 84, 85.
  - 24 S. Ernst, V. Kasack and W. Kaim, *Inorg. Chem.*, 1989, 28, 1520.
  - 25 M. Haga, T. Matsumura-Inoue and S. Yamabe, *Inorg. Chem.*, 1987, 26, 4148.
  - 26 W.J. Vining, J.V. Caspar and T.J. Meyer, *J. Phys. Chem.*, 1985, 89, 1095.

- 
- 27 E.M. Kober, J.P. Caspar, B.P. Sullivan and T.J. Meyer, *Inorg. Chem.*, 1988, 27, 4587.
- 28 R.S. Lumpkin, E.M. Kober, L. Worl, Z. Murtaza and T.J. Meyer, *J. Phys. Chem.*, 1990, 94, 239.
- 29 M. Wrighton and D.L. Morse, *J. Am. Chem. Soc.*, 1974, 96, 996.
- 30 E.M. Kober, J.V. Caspar, R.S. Lumpkin and T.J. Meyer, *J. Phys. Chem.*, 1986, 90, 3722.
- 31 G.E. Strouse, J.R. Schoonover, R. Duesing, S. Boyde, W.E. Jones Jr. and T.J. Meyer, *Inorg. Chem.*, 1995, 34, 473.
- 32 J. M. de Wolf, R. Hage, J.G. Haasnoot, J. Reedijk and J.G. Vos, *New. J. Chem.*, 1991, 15, 501.
- 33 F. Barigelletti, L. Flamigni, M. Guardigli, A. Juris, M. Beley, S. Chodorowski-Kimmes, J.-P. Collin and J.-P. Sauvage, *Inorg. Chem.*, 1996, 35, 136.
- 34 F. Barigelletti, L. Flamigni, J.-P. Collin and J.-P. Sauvage, *J. Chem. Soc., Chem. Commun.*, 1997, 333.
- 35 P. Belser, A. von Zelewsky, M. Frank, C. Seel, F. Voegtle, L. de Cola, F. Barigelletti and V. Balzani, *J. Am. Chem. Soc.*, 1993, 115, 4076.
- 36 M.T. Indelli, F. Scandola, J.-P. Collin, J.-P. Sauvage and A. Sour, *Inorg. Chem.*, 1996, 35, 303.
- 37 R.J. Crutchley, N. Kress and A.B.P. Lever, *J. Am. Chem. Soc.*, 1983, 105, 1170.
- 38 G.H. Allen, R.P. White, D.P. Rillema and T.J. Meyer, *J. Am. Chem. Soc.*, 1984, 106, 2613.

- 
- 39 E.M. Kober, J.C. Marshall, W.J. Dressick, B.P. Sullivan, J.V. Caspar and T.J. Meyer, *Inorg. Chem.*, 1985, 24, 2755.
- 40 J.F. Ireland and P.A.H. Wyatt, *Adv. Phys. Org. Chem.*, 1976, 12, 32.
- 41 J.G. Vos, *Polyhedron*, 1992, 11, 25.
- 42 J.V. Caspar and T.J. Meyer, *J. Am. Chem. Soc.*, 1983, 105, 5583.
- 43 J.V. Caspar and T.J. Meyer, *Inorg. Chem.*, 1983, 22, 2444.
- 44 S.H. Peterson and J.N. Demas, *J. Am. Chem. Soc.*, 1979, 101, 6571.
- 45 P. Ford, D.F.P. Rudd, R. Gaunder and H. Taube, *J. Am. Chem. Soc.*, 1968, 90, 1187.
- 46 J.P. Chang, E.Y. Fung and J.C. Curtis, *Inorg. Chem.*, 1986, 25, 4233.
- 47 N.G. Connelly and W.E. Geiger, *Chem. Rev.*, 1996, 96, 877.
- 48 K.A. Goldsby and T.J. Meyer, *Inorg. Chem.*, 1984, 23, 3002.
- 49 J.B. Flanagan, S. Margel, A.J. Bard, F.C. Anson, *J. Am. Chem. Soc.*, 1978, 100, 4248.
- 50 J.C. Curtis, J.S. Bernstein and T.J. Meyer, *Inorg. Chem.*, 1985, 24, 385.
- 51 C. Creutz and H. Taube, *J. Am. Chem. Soc.*, 1969, 91, 3988.
- 52 G. Giuffrida, G. Calogero, G. Guglielmo, V. Ricevuto, M. Ciano and S. Campagna, *Inorg. Chem.*, 1993, 32, 1179.
- 53 R. Hage, J.G. Haasnoot, J. Reedijk and J.G. Vos, *Inorg. Chim. Acta.*, 1986, 118, 73.
- 54 S. Woitellier, J.-P. Launay and C.W. Spangler, *Inorg. Chem.*, 1989, 28, 758.
- 55 D.E. Richardson and H. Taube, *Inorg. Chem.*, 1981, 20, 1278.

- 
- 56 R.L. Cleary, K.J. Byrom, D.A. Bardwell, J.C. Jeffrey, M.D. Ward, G. Calogero, N. Armoli, L. Flamigni and F. Barigelletti, *Inorg. Chem.*, 1997, 36, 2601.
- 57 N.E. Tokel-Takvoryan, R.E. Hemingway and A.J. Bard, *J. Am. Chem. Soc.*, 1973, 95, 6582.
- 58 V. Balzani, A. Juris, M. Venturi, S. Campagna and S. Serroni, *Chem. Rev.*, 1996, 96, 759.
- 59 A.-C. Ribou, J.-P. Launay, K. Takahashi, T. Nihira, S. Tarutani and C.W. Spangler, *Inorg. Chem.*, 1994, 33, 1325.
- 60 P. Laine, V. Marvaud, A. Gourdon, J.-P. Launay, R. Argazzi and C. A. Bignozzi, *Inorg. Chem.*, 1996, 35, 711.
- 61 A.-C. Ribou, J.-P. Launay, M.L. Sachtleben, H. Li and C.W. Spangler, *Inorg. Chem.*, 1996, 35, 3735.
- 62 C. Creutz, *Prog. Inorg. Chem.*, 1983, 30, 1.
- 63 N.S. Hush, *Coord. Chem. Rev.*, 1985, 64, 135.
- 64 E. Brauns, S.W. Jones, J.A. Clark, S.M. Molnar, Y. Kawanishi and K.J. Brewer, *Inorg. Chem.*, 1996, 35, 1737.
- 65 J. Bonvoisin, J.-P. Launay, M. Van der Auweraer and F.C. De Schriver, *J. Phys. Chem.*, 1994, 98, 5052; Correndum:*ibid.*, 1996, 100, 18006.
- 66 M.M. Richter and K.J. Brewer, *Inorg. Chem.*, 1993, 32, 2827.
- 67 K.A. Goldsby and T.J. Meyer, *Inorg. Chem.*, 1984, 23, 3002.
- 68 C. Patoux, J.-P. Launay, M. Beley, S. Chodorowski-Kimmes, J.-P. Collin, S. James and J.-P. Sauvage, *J. Am. Chem. Soc.*, 1998, 120, 3717.

- 
- 69 C. Patoux, C. Coudret, J.-P. Launay, C. Joachim and A. Gourdon, *Inorg. Chem.*, 1997, 36, 5037.
- 70 D.E. Richardson and H. Taube, *J. Am. Chem. Soc.*, 1983, 105, 40.
- 71 J.E. Sutton, P.M. Sutton and H. Taube, *Inorg. Chem.*, 1979, 18, 1017.
- 72 J.-P. Collin, P. Laine, J.-P. Launay, J.-P. Sauvage and A. Sour, *J. Chem. Soc., Chem. Commun.*, 1993, 434.
- 73 M. Haga, Md. Meser Ali and R. Arakawa, *Angew. Chem. Int. Ed. Engl.*, 1996, 35, 76.
- 74 A.-C. Ribou, J.-P. Launay, M.L. Sachtleben, H. Li, C.W. Spangler, *Inorg. Chem.*, 1996, 35, 3735.
- 75 S. Roffia, C. Paradisi and C.A. Bignozzi, *J. Electroanal. Chem.*, 1986, 200, 105.
- 76 M.K. Nazeeruddin, S.M. Zakeeruddin and K. Kalyananundaram, *J. Phys. Chem.*, 1993, 97, 9607; *Coord. Chem. Rev.*, 1994, 132, 259.
- 77 T. Ohno, K. Nozaki and M. Haga, *Inorg. Chem.*, 1992, 31, 548.
- 78 R. Hage, J.G. Haasnoot, H.A. Nieuwenhuis, J. Reedijk, D.J.K. de Ridder and J.G. Vos, *J. Am. Chem. Soc.*, 1990, 112, 9245.
- 79 M. Nishizawa, T.M. Suzuki, S. Sprouse, R.J. Watts and P.C. Ford, *Inorg. Chem.*, 1984, 23, 1837.

## **Chapter Five**

### **The Synthesis and Characterisation of Ruthenium and Osmium Complexes Containing 1-Methyl-3-(2- pyridyl)-1,2,4-Triazole Moieties Connected by a Phenyl Spacer**

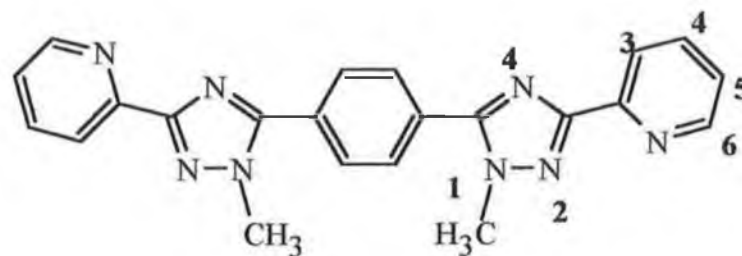
## 5.1 Introduction.

In Chapter 4 the synthesis and characterisation of complexes of symmetric ligands, H<sub>2</sub>L1 and H<sub>2</sub>L2, containing anionic triazolate bridges were discussed. Spectroscopic and electrochemical measurements indicated that the metal-metal interaction in the dinuclear complexes was very weak. Emission experiments, however, indicated that Ru→Os energy transfer occurred in the mixed-metal RuOs complexes, especially when protonated.

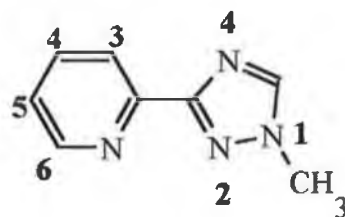
This chapter describes the synthesis and characterisation of the mononuclear and dinuclear Ru(bpy)<sub>2</sub>- and Os(bpy)<sub>2</sub>- complexes of the methylated analogue of H<sub>2</sub>L2, 1,4-bis(1-methyl-3-(2-pyridyl)-1,2,4-triazol-5-yl)benzene (L3) (Fig. 5.1).

Extensive studies carried out over the years on pyridyltriazole-based ligands have confirmed that the N1 (or N2) atom and the N4 atom of the triazole ring are not equivalent<sup>1</sup>. An interesting feature of triazole ligands is the observation that the position of substituents on the triazole ring determines which coordination mode *i.e.* N1 (N2) or N4 prevails. Previous reports on *N*-methylated pyridyltriazole ligands revealed that steric considerations were of great importance in determining the preferred mode of coordination. Buchanan *et al* reported that the N4-coordinated mononuclear complex [Ru(bpy)<sub>2</sub>L]<sup>2+</sup> was the only isomer isolated for the ligand L = 1-methyl-3-(2-pyridyl)-1,2,4-triazole (1M3ptr)<sup>2</sup>, the structure of which is shown in Fig. 5.1. However in a subsequent study carried out by E. Ryan on the corresponding [Ru(phen)<sub>2</sub>(1M3ptr)]<sup>2+</sup> and [Ru(dmbpy)<sub>2</sub>(1M3ptr)]<sup>2+</sup> complexes (phen = 1,10-phenanthroline; dmbpy = 4,4'-dimethyl-2,2'-bipyridyl), it was found that coordination occurred via both N4 and N2 in a ratio of approximately 90:10<sup>3</sup>. From the results of the previous chapter it was found that coordination only occurred via the pyridine

nitrogen and N1 of the triazole ring and this was considered to be as a result of steric hindrance by the phenyl ring. In L3 the methyl substituent presents an added steric restriction to binding of the  $M(\text{bpy})_2$ -unit. Therefore it is anticipated that more than one coordination isomer will be formed for complexes of this ligand. It is possible that in the mononuclear complexes the  $M(\text{bpy})_2$ -unit can coordinate via N2 or N4 of the triazole ring. For the dinuclear complexes there are potentially three products, namely, the N2/N2, N4/N4 and N2/N4 coordinated isomers. This chapter details the synthesis, purification and characterisation of the mononuclear and dinuclear complexes of L3. The structure of the complexes are elucidated with the aid of  $^1\text{H-NMR}$  spectroscopy, X-Ray data and by comparison with analogous complexes. The influence of the coordination geometry on the electrochemical and photophysical properties of the complexes is also discussed. As in the previous chapter the extent of metal-metal interaction in the ground and excited state is investigated. Furthermore the effect of methylation of the triazole ring on the properties of the complexes compared to their unmethylated counterparts (discussed in Chapter 4) is examined.



1,4-bis(1-methyl-3-(2-pyridyl)-1,2,4-triazol-5-yl)benzene



1-methyl-3-(2-pyridyl)-1,2,4-triazole (IM3ptr)<sup>2</sup>

Figure 5.1 Structures of ligands L3 and IM3ptr.

## 5.2 Experimental.

### 5.2.1 Synthesis of the Metal Complexes.

Unless otherwise stated, all materials and solvents used were of commercial grade.  $\text{cis-[Ru(bpy)}_2\text{Cl}_2\text{]}\cdot 2\text{H}_2\text{O}$  and  $\text{cis-[Os(bpy)}_2\text{Cl}_2\text{]}\cdot 2\text{H}_2\text{O}$  were prepared as described in Section 4.2. The preparation of the ligand 1,4-bis(1-methyl-3-(2-pyridyl)-1,2,4-triazol-5-yl)benzene (L3) has already been described in Chapter 3.

#### [Ru(bpy)<sub>2</sub>L3](PF<sub>6</sub>)<sub>2</sub>

L3 (0.789 g, 2 mmol) was dissolved in hot methanol/water (2:1 v/v). To the solution was added  $\text{cis-[Ru(bpy)}_2\text{Cl}_2\text{]}\cdot 2\text{H}_2\text{O}$  (0.312 g, 0.6 mmol) and the mixture was heated at reflux for 6 hours. Following removal of most of the solvent by rotary evaporation and the addition of saturated aqueous  $\text{NH}_4\text{PF}_6$  solution, the resulting precipitate was filtered off and dried. HPLC analysis revealed that the product consisted of two isomers in approximately a 30:70 ratio (Isomer 1:Isomer 2), based on their integrated absorbance areas at 280 nm. These were purified by semi-preparative HPLC using 80:20 acetonitrile/water containing 0.11 M  $\text{KNO}_3$  and a flow rate of 1.7  $\text{cm}^3/\text{min}$ . Yield = 0.20 g (30 %).

Isomer 1: Calcd. for  $\text{Ru}_1\text{C}_{42}\text{H}_{34}\text{N}_{12}\text{P}_2\text{F}_{12}\cdot 3\text{H}_2\text{O}$  = C: 45.78; H: 3.50; N; 14.58 %. Anal.

Found: C: 45.24; H: 3.12; N: 14.14 %.

Isomer 2: Calcd. for  $\text{Ru}_1\text{C}_{42}\text{H}_{34}\text{N}_{12}\text{P}_2\text{F}_{12}\cdot \text{H}_2\text{O}$  = C: 45.19; H: 3.23; N; 15.06 %. Anal.

Found: C: 45.41; H: 3.15; N: 14.93 %.

[Os(bpy)<sub>2</sub>L3](PF<sub>6</sub>)<sub>2</sub>

L3 (0.388 g, 0.98 mmol) was dissolved in hot methanol/water (2:1 v/v). cis-[Os(bpy)<sub>2</sub>Cl<sub>2</sub>].2H<sub>2</sub>O (0.20 g, 0.33 mmol) and a small amount of zinc metal (to reduce any [Os<sup>III</sup>(bpy)<sub>2</sub>Cl<sub>3</sub>] to [Os<sup>II</sup>(bpy)<sub>2</sub>Cl<sub>2</sub>]) was added to the solution and the mixture was heated at reflux. After 3 hours HPLC analysis of the reaction mixture showed that all the cis-[Os(bpy)<sub>2</sub>Cl<sub>2</sub>].2H<sub>2</sub>O had reacted and two products in approximately a 30:70 ratio were present as found for [Ru(bpy)<sub>2</sub>L3](PF<sub>6</sub>)<sub>2</sub>. Upon cooling the reaction mixture was filtered (to remove unreacted ligand and Zn metal). The solvent was concentrated to approx. 15 cm<sup>3</sup> and saturated aqueous NH<sub>4</sub>PF<sub>6</sub> solution added. The resulting precipitate was filtered and dried. The isomers were purified by semi-preparative HPLC using 80:20 acetonitrile/water containing 0.11 M KNO<sub>3</sub> and a flow rate of 1.7 cm<sup>3</sup>/min. Yield = 0.10 g (25 %).

Isomer 1: Calcd. for Os<sub>1</sub>C<sub>42</sub>H<sub>34</sub>N<sub>12</sub>P<sub>2</sub>F<sub>12</sub>.4H<sub>2</sub>O = C: 40.06; H: 3.36; N: 13.35 %. Anal. Found: C: 39.48; H: 2.88; N: 12.88 %.

Isomer 2: Calcd. for Os<sub>1</sub>C<sub>42</sub>H<sub>34</sub>N<sub>12</sub>P<sub>2</sub>F<sub>12</sub>.H<sub>2</sub>O = C: 41.86; H: 3.01; N: 13.95 %. Anal. Found: C: 42.03; H: 3.07; N: 13.78 %.

[(Ru(bpy)<sub>2</sub>)<sub>2</sub>L3](PF<sub>6</sub>)<sub>4</sub>      **(RuRu)**

cis-[Ru(bpy)<sub>2</sub>Cl<sub>2</sub>].2H<sub>2</sub>O (0.624 g, 1.2 mmol) and L3 (0.197 g, 0.5 mmol) were heated at reflux in ethanol/water (2:1 v/v) for 6 hours. Upon cooling of the reaction mixture, a few drops of a saturated ammonium hexafluorophosphate aqueous solution were added, whereupon a bright orange precipitate was obtained. This was filtered and recrystallised from acetone/water (2:1 v/v). The product, obtained by recrystallisation,

was found by HPLC analysis to contain only one isomer and so was isolated without need for any further purification. Yield = 0.30 g (33 %).

Calcd. for  $\text{Ru}_2\text{C}_{62}\text{H}_{50}\text{N}_{16}\text{P}_4\text{F}_{24}\cdot 3\text{H}_2\text{O}$  = C: 40.11; H: 3.04; N: 12.07 %. Anal. Found: C: 40.27; H: 3.08; N: 12.02 %.

$[(\text{Os}(\text{bpy})_2)_2\text{L3}](\text{PF}_6)_4$             **(OsOs)**

This complex was prepared as described for the mononuclear compound except that  $\text{cis}[\text{Os}(\text{bpy})_2\text{Cl}_2]\cdot 2\text{H}_2\text{O}$  (0.20 g, 0.33 mmol) and L3 (0.05g, 0.13 mmol) were heated at reflux in ethanol/water (2:1 v/v) for 6 hours. 0.215 g of product, containing mononuclear complex and the desired dinuclear product as two isomers were isolated. However many attempts to purify the isomers by semi-preparative HPLC and column chromatography (neutral alumina) failed. One pure fraction (corresponding to Isomer 2 of the dinuclear species) was obtained by fractional recrystallisation of the mixture from ethanol/water (1:1 v/v). Yield = 0.02 g (3 %).

Calcd. for  $\text{Os}_2\text{C}_{62}\text{H}_{50}\text{N}_{16}\text{P}_4\text{F}_{24}\cdot 4\text{H}_2\text{O}$  = C: 36.30; H: 2.85; N: 10.92 %. Anal. Found: C: 36.24; H: 2.68; N: 10.73 %.

$[\text{Ru}(\text{bpy})_2(\text{L3})\text{Os}(\text{bpy})_2](\text{PF}_6)_4$             **(RuOs)**

$[\text{Ru}(\text{bpy})_2\text{L3}](\text{PF}_6)_2\cdot 3\text{H}_2\text{O}$  (Isomer 2) (0.08g, 0.07 mmol) and  $\text{cis}[\text{Os}(\text{bpy})_2\text{Cl}_2]\cdot 2\text{H}_2\text{O}$  (0.05 g, 0.08 mmol) were dissolved in ethanol/water (2:1 v/v). A small amount of Zn metal was added as before and the mixture was heated at reflux for 6 hours. HPLC analysis of the reaction mixture revealed the presence of two isomers of the desired product in a ratio of approximately 60:40. Upon cooling, a few drops of saturated ammonium hexafluorophosphate solution were added to the solution. The solvent was

allowed to evaporate slowly and the first fraction of product to fall out of solution was found to contain only one isomer. This was recrystallised from acetone/water.

Yield = 0.06 g (43 %). Calcd. for  $\text{Ru}_1\text{Os}_1\text{C}_{62}\text{H}_{50}\text{N}_{16}\text{P}_4\text{F}_{24}\cdot 4\text{H}_2\text{O}$  = C: 37.93; H: 2.98; N: 11.42 %. Anal. Found: C: 37.77; H: 2.65; N: 11.28 %.

### 5.2.2 X-Ray data collection and structure determination.

Crystals of Isomer 2 of  $[\text{Ru}(\text{bpy})_2\text{L3}]^{2+}$  were isolated from a fraction eluted from a silica column using 80/20  $\text{CH}_3\text{CN}/\text{H}_2\text{O}$  containing 0.12 M  $\text{KNO}_3$ . Data were collected using a Siemens P4 four circle diffractometer with graphite monochromated  $\text{Mo-K}_\alpha$  radiation. The crystals stability was monitored every 100 reflections and there were no significant variations ( $\pm 1\%$ ). Cell parameters were obtained from 35 accurately centred reflections in the two-theta range  $10^\circ - 18^\circ$ . Data were collected at room temperature. Omega scans were employed for data collection and Lorentz and polarisation corrections were applied.

The structure was solved by direct methods and the non hydrogen atoms were refined with isotropic thermal parameters. Hydrogen atom positions were added at idealised positions and a riding model with fixed thermal parameters, ( $U_{ij} = 1.2 U_{ij}(\text{eq})$ ), was used for subsequent refinement. The function minimised for wR2 was  $\Sigma[w(|F_o|^2 - |F_c|^2)]$  with reflection weights  $w^{-1} = [\sigma^2 |F_o|^2 + (g_1 P)^2 + g_2 P]$  where  $P = [\max |F_o|^2 + 2|F_c|^2] / 3$  for all  $F^2$  and the function minimised for R1 was  $\Sigma[w(|F_o| - |F_c|)]$ . The XSCANS, SHELXTL PC\* and SHELXL-93\* packages were used for data collection, reduction, structure solution and refinement. A total of 4449 reflections were measured for  $4 < 2\theta < 40$  and 2369 unique reflections were used in the refinement.

## 5.3 Results and Discussion.

### 5.3.1 Synthesis of the complexes.

The methods used for the synthesis and purification of the complexes were similar to methods previously employed for other pyridyltriazole-based complexes. High performance liquid chromatography proved invaluable in the analysis of reaction mixtures and the purification of products. HPLC analysis of the reaction mixture and products isolated for the ruthenium and osmium mononuclear complexes revealed the presence of two isomers, differing in retention time by approximately 1 minute. Figure 5.2 shows the chromatogram trace and the associated UV/Vis spectra of the isomers of  $[\text{Ru}(\text{bpy})_2\text{L3}](\text{PF}_6)_2$ .

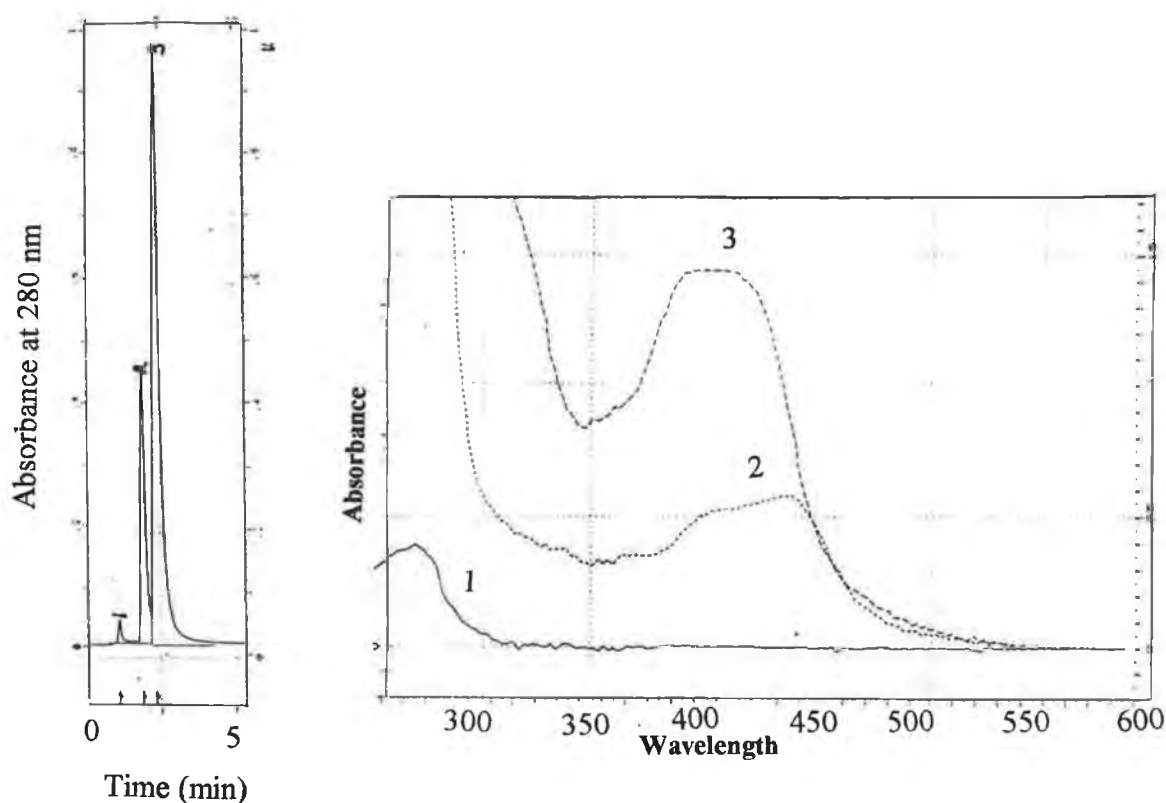


Figure 5.2 Chromatogram trace and associated UV/Vis spectra of the isomers of  $[\text{Ru}(\text{bpy})_2\text{L3}]^{2+}$ .

These were separated and isolated in mg quantities using semi-preparative HPLC. It was found previously for the complexes of the ligand 1M3ptr that the N4-coordinated complexes eluted before those coordinated via N2 of the triazole ring<sup>4</sup>. On this basis and also by comparison of the absorption spectra obtained using the photodiode array detector with those obtained for the N2- and N4-coordinated isomers of 1M3ptr, Isomer 1 and Isomer 2 are at this stage tentatively assigned as being N4-coordinated and N2-coordinated, respectively.

In the case of the dinuclear complexes, however, there are a number of coordination possibilities. For the homodinuclear complexes **RuRu** and **OsOs** coordination of the two metal units may occur via N2/N2, N4/N4 or N2/N4 of the triazole ring. For the heterodinuclear complex **RuOs** the possibility exists for a total of four coordination isomers- N2(Ru)/N2(Os), N4(Ru)/N4(Os), N2(Ru)/N4(Os) and N2(Os)/N4(Ru). HPLC analysis of the reaction mixtures of the dinuclear complexes revealed in all cases the formation of two products, differing in retention time by between 0.5-1.5 min, which on the basis of integrated areas of the peaks detected at 280 nm were in a ratio of approximately 50:50. The first isomer was the main product and this was isolated in its pure form by fractional recrystallisation. This was rather fortuitous, particularly in the case of **OsOs**, where several attempts to purify the isomers by column chromatography (neutral alumina and silica) and semi-preparative HPLC (mobile phases of varying CH<sub>3</sub>CN/H<sub>2</sub>O ratios and concentrations of KNO<sub>3</sub> in the range 0.12-0.20M) were all unsuccessful. Figure 5.3 shows the chromatogram trace and associated UV/Vis absorption spectra of the crude product isolated from the **OsOs** reaction mixture. Peaks 2 and 3 are the mononuclear complexes, whilst the main peaks represent two isomers of the dinuclear complexes. It can be seen that the

resolution between both isomers is quite poor. Attempts made to improve the resolution were hampered by the long retention time of the dinuclear +4 species, which resulted in band broadening and co-elution of both isomers on a semi-preparative scale. Careful fractional recrystallisation using ethanol/water proved to be the only means of obtaining the main isomer in its pure form.

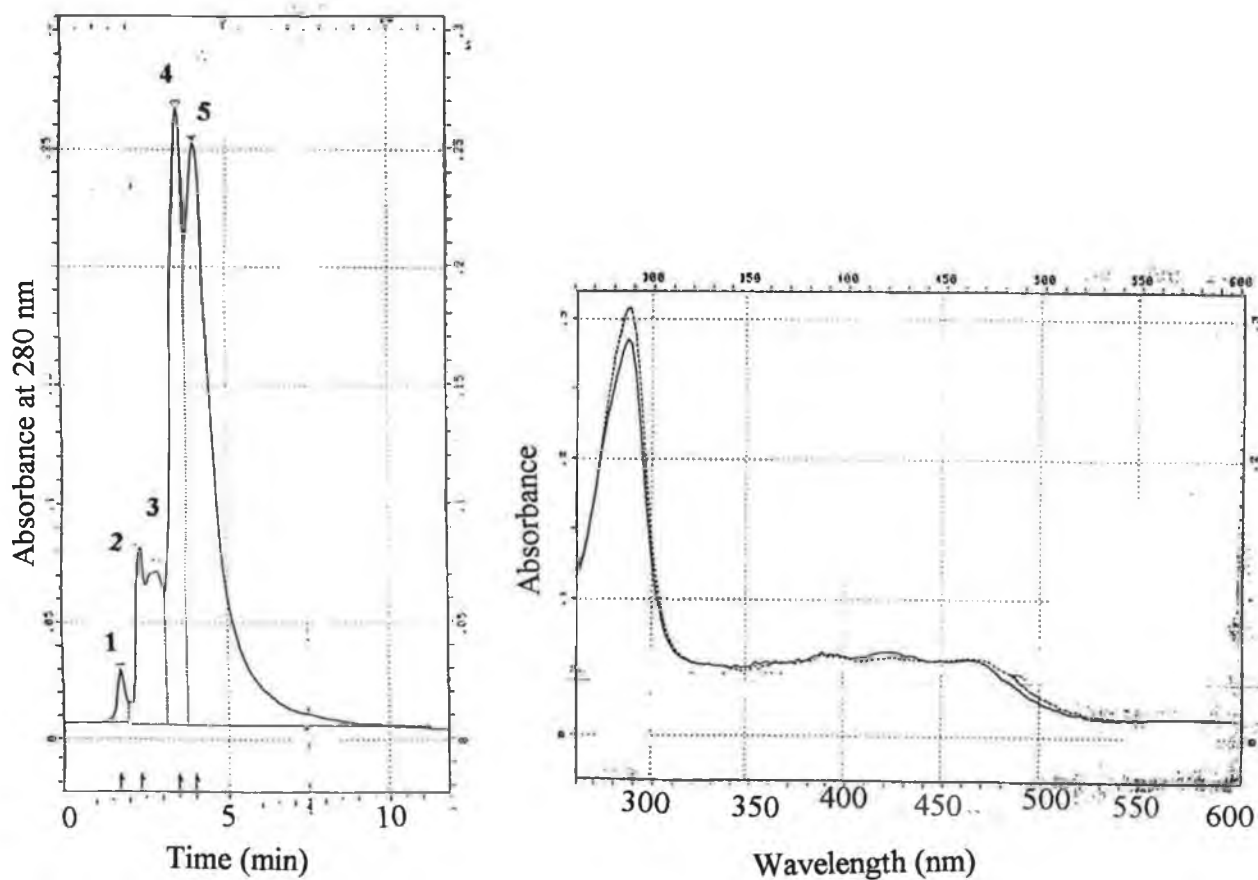


Figure 5.3 Chromatogram trace and associated UV/Vis spectra of the isomers of  $[(Os(bpy)_2)_2 L3]^{4+}$  (4, 5)

The mixed-metal **RuOs** complex was prepared using the N2-bound isomer of the  $[\text{Ru}(\text{bpy})_2\text{L3}]^{2+}$  complex. As was found for the other dinuclear complexes two products were identified in the reaction mixture in approximately a 60:40 ratio, corresponding to the N2/N2 and N2/N4 coordinated isomers, respectively. However only the first isomer was isolated in its pure form. It is of interest to note that the direct reaction of L3 with two equivalents of  $\text{cis-}[\text{Ru}(\text{bpy})_2\text{Cl}_2]\cdot 2\text{H}_2\text{O}$  resulted also in the formation of only two products, the main fraction being the N2/N2-coordinated dimer (established by NMR, *vide infra*).

It should be pointed out that for the dinuclear complexes only the main fraction from the reaction mixture was isolated and used for further characterisation. It will be seen that this corresponded to the complex in which both metal units were bound via N2 of the triazole ring.

### 5.3.2 $^1\text{H-NMR}$ Spectroscopy.

Proton NMR spectroscopy has been shown to be a valuable tool in yielding information about the structure and isomer formation of triazole systems<sup>5</sup>. Since for the monomeric  $\text{Ru}(\text{bpy})_2$  and  $\text{Os}(\text{bpy})_2$  complexes isomers have been obtained, it is necessary to establish whether the  $\text{M}(\text{bpy})_2$  moieties are bound via N2 or N4 of the triazole moiety. It has been found that the coordination mode exerts an effect on the electronic properties of the ligand *e.g.* its  $\pi$ -acceptor properties, because of the localised nature of the double bond in 1,2,4-triazoles. Therefore it is important to determine which triazole nitrogen is, in addition to the N atom of the pyridine ring,

coordinated to the  $M(\text{bpy})_2$  unit. In general it may be said that the chemical shifts of the protons of the ligands are influenced by three factors<sup>6</sup>:

- (i) the electron density on the ligands is reduced upon coordination, inducing a downfield shift.
- (ii) steric effects result in a downfield shift.
- (iii) alignment of a proton above an adjacent aromatic ring leads to a dramatic upfield shift (diamagnetic anisotropy).

In the previous chapter it was concluded for complexes of the ligands  $\text{H}_2\text{L1}$  and  $\text{H}_2\text{L2}$  that coordination of the  $M(\text{bpy})_2$  moiety occurred via N2 of the triazole ring. This was in agreement with expectations based on steric reasons, as coordination through N4 would place the bipyridine rings too close to the central benzene ring. However in the case of L3, the presence of a methyl substituent on N1 of the triazole causes an additional steric effect. If a nitrogen atom is coordinated to a metal centre, the neighbouring group will be affected, not only by a change in electron density in the five-membered ring, but also by the shielding cone of a bpy ring. The latter gives rise to a diamagnetic anisotropic interaction which results in an upfield shift of the resonance associated with the neighbouring group<sup>4</sup>. Therefore the resonance position of the methyl group is indicative of the manner in which the pyridyltriazole moiety is coordinated to the  $M(\text{bpy})_2$  unit. It is expected in the case of L3 that coordination through N4 will result in the phenyl resonances being shielded, while in the case of N2 coordination, the resonance for the methyl substituent will be found at significantly higher field than for the free ligand. This effect has been shown previously by Steel *et al* for the complex  $[\text{Ru}(\text{bpy})_2\text{L}]^{2+}$  where  $\text{L} = 3,5\text{-dimethyl-1-(2-pyridyl)pyrazole}$ <sup>7</sup>.

The  $^1\text{H-NMR}$  data obtained for the ruthenium and osmium complexes of the ligand L3 are presented in Table 5.1. Some representative spectra are depicted in Figures 5.4 - 5.7. Assignments were made using 2D-COSY techniques (see for example Fig. 5.7) and also by comparison with the chemical shifts for the free ligand and for the complexes  $[\text{Ru}(\text{bpy})_2\text{1M3ptr}]^{2+2}$  and  $[\text{Ru}(\text{phen})_2\text{1M3ptr}]^{2+3}$ . Coordination induced shifts (C.I.S) of the pyridyltriazole resonances in the complex compared to the free ligand are also given.

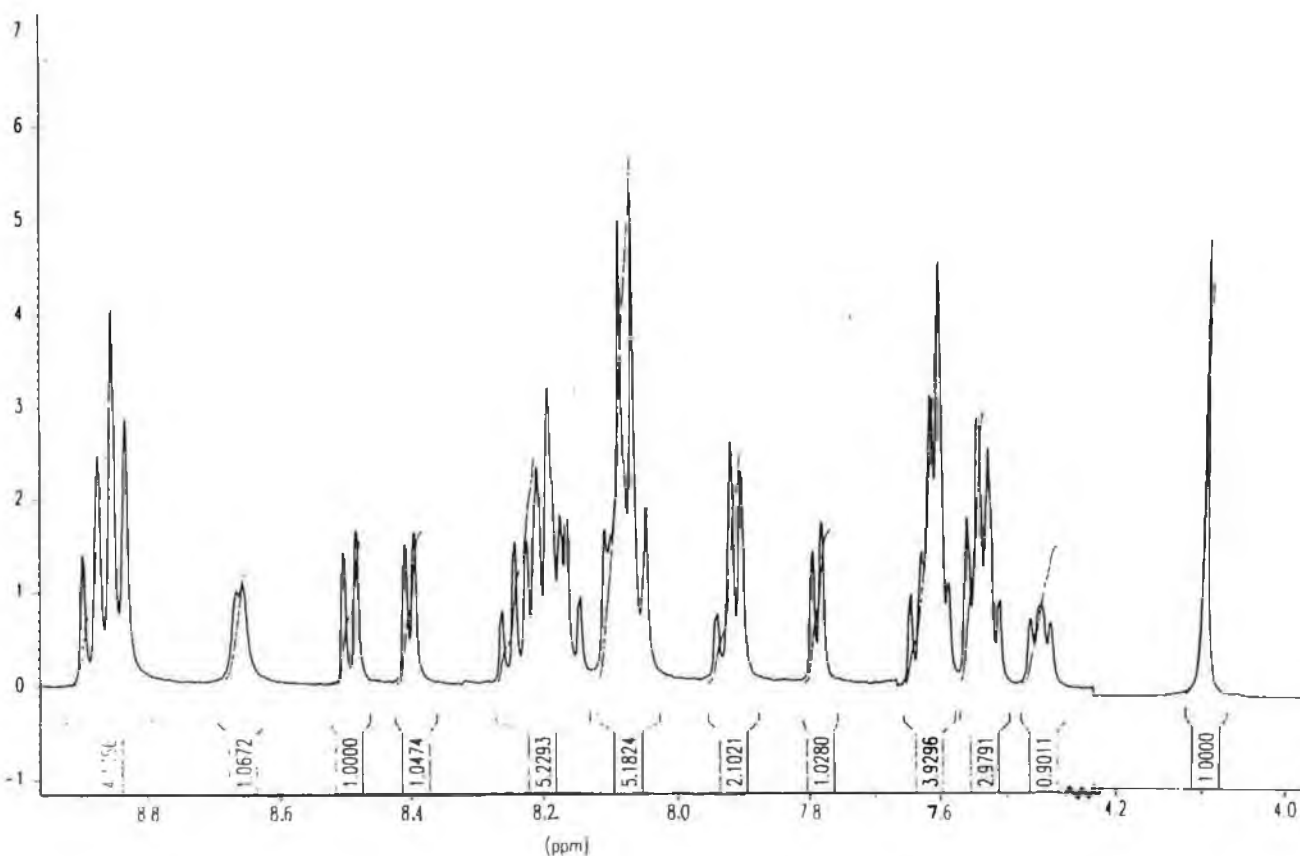


Figure 5.4  $^1\text{H-NMR}$  spectrum of N4-Ru (Isomer 1) in  $d_6$ -dimethyl sulphoxide.

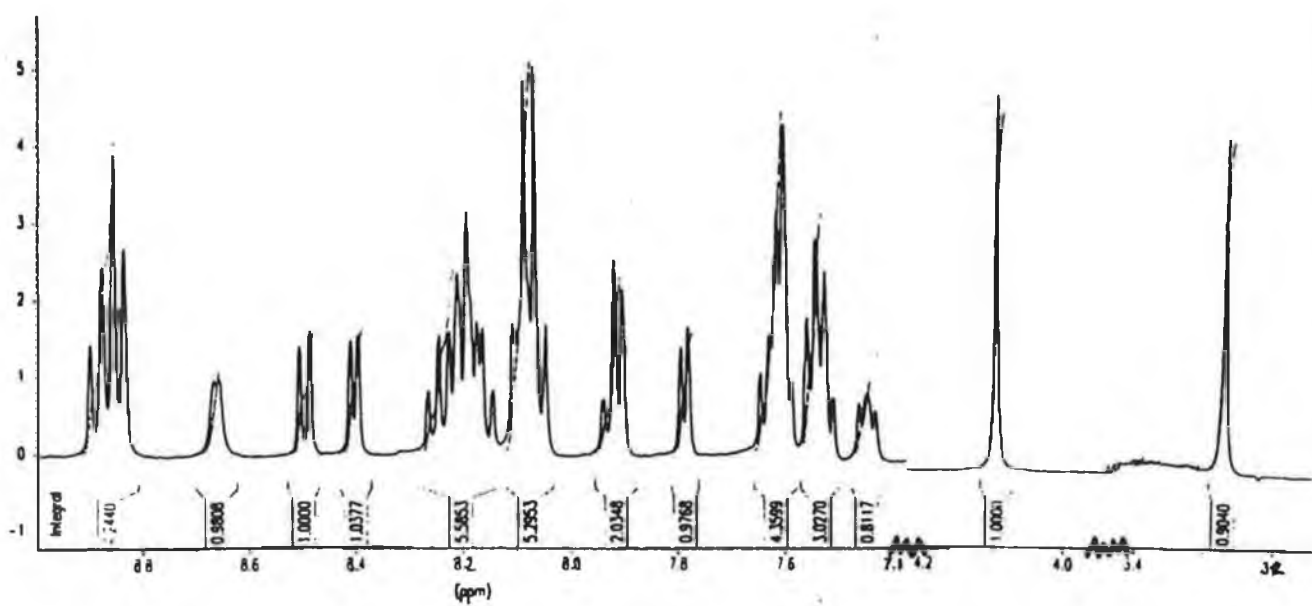


Figure 5.5  $^1\text{H-NMR}$  spectrum of  $\text{N}_2\text{-Ru}$  (Isomer 2) in  $d_6$ -dimethyl sulphoxide.

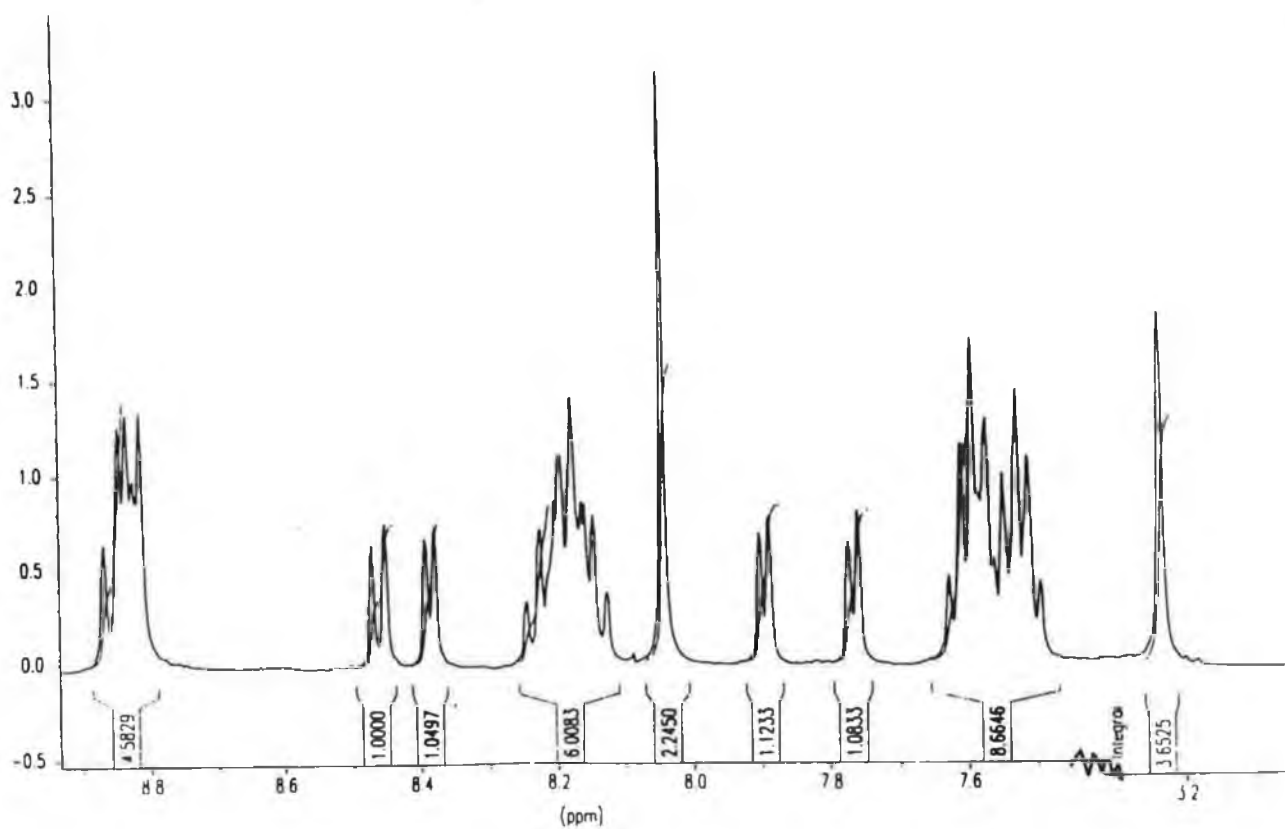


Figure 5.6  $^1\text{H-NMR}$  spectrum of  $\text{RuRu}$  in  $d_6$ -dimethyl sulphoxide.

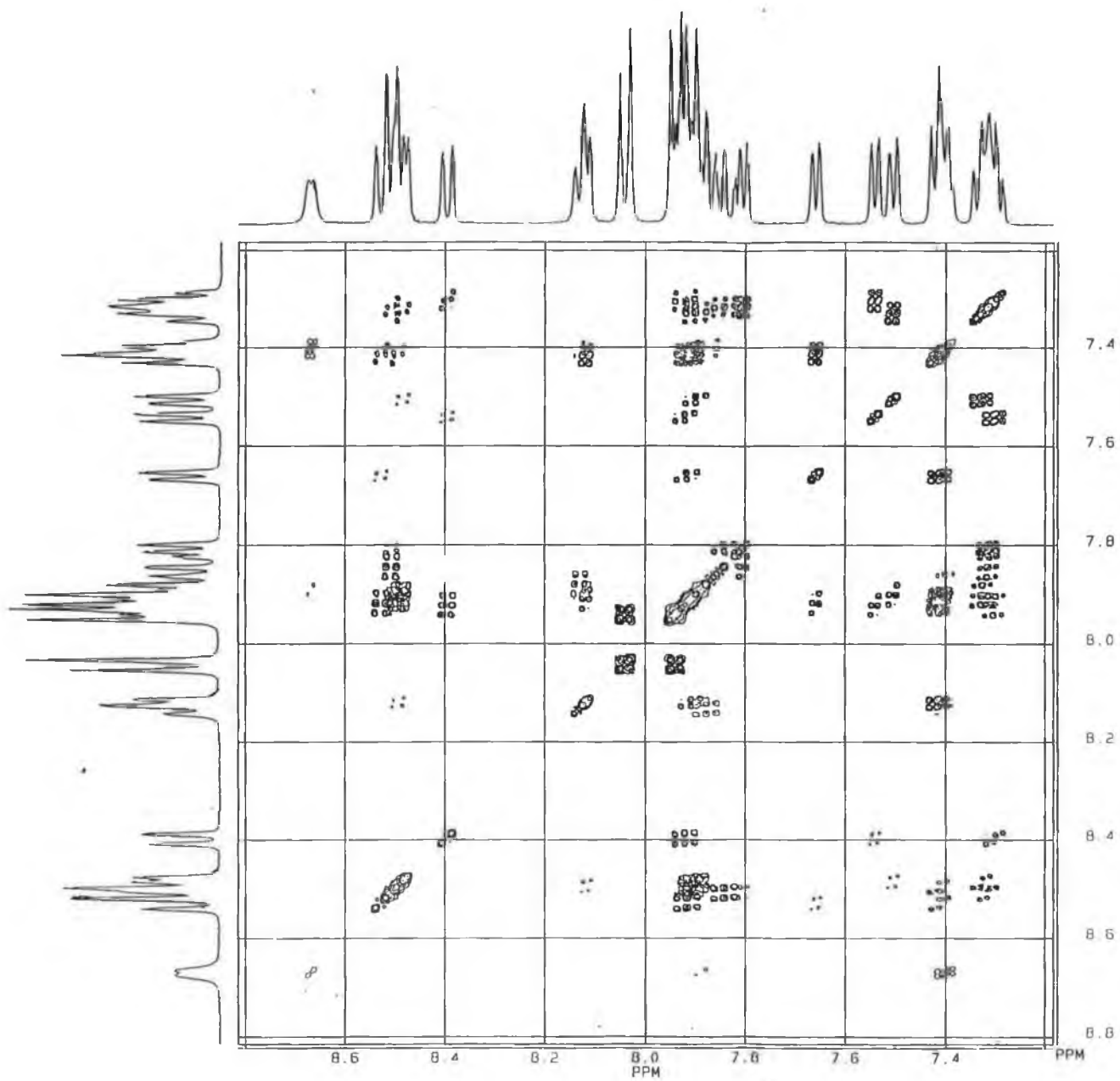


Figure 5.7 COSY spectrum of N<sub>2</sub>-Os in d<sub>3</sub>-dimethyl sulphoxide.

**Table 4.1** *Chemical shifts (ppm) for the Ru and Os complexes with L3. Measurements carried out in CD<sub>3</sub>CN unless otherwise stated. C.I.S values are given in parentheses. (f) and (b) refer to the free and bound pyridyltriazole ring, respectively.*

| Compound                            |                         | H3                        | H4                        | H5                        | H6                        | Phenyl                    | CH <sub>3</sub>           |
|-------------------------------------|-------------------------|---------------------------|---------------------------|---------------------------|---------------------------|---------------------------|---------------------------|
| <b>Isomer 1 (N4-Ru)<sup>a</sup></b> | (f)                     | 8.21                      | 7.90                      | 7.43                      | 8.66                      |                           | 4.07                      |
|                                     | (b)                     | 8.46 (+0.36)              | 8.09 (+0.17)              | 7.50 (+0.05)              | 7.57 (-1.10)              | 7.60 (-0.47)              | 3.82 (-0.40)              |
| <b>Isomer 2 (N2-Ru)<sup>a</sup></b> | (f)                     | 8.09                      | 7.92                      | 7.45                      | 8.66                      |                           | 4.10                      |
|                                     | (b)                     | 8.49 (+0.39)              | 8.20 (+0.28)              | 7.51 (+0.06)              | 7.64 (-1.03)              | 8.06 (-0.01)              | 3.27 (-0.85)              |
| <b>Isomer 1 (N4-Os)</b>             | (f)                     | 8.25                      | 8.03                      | 7.51                      | 8.71                      |                           | 4.05                      |
|                                     | (b)                     | 8.34                      | 7.90                      | 7.29                      | 7.40                      | 7.55                      | 3.79                      |
| <b>Isomer 2 (N2-Os)</b>             | (f)                     | 8.13                      | 7.88                      | 7.41                      | 8.67                      |                           | 4.09                      |
|                                     | (b)                     | 8.39                      | 7.91                      | 7.30                      | 7.54                      | 7.93-8.04                 | 3.23 (-0.89)              |
| <b>RuRu (in DMSO)</b>               |                         | 8.46 (+0.36) <sup>a</sup> | 8.14 (+0.22) <sup>a</sup> | 7.50 (+0.05) <sup>a</sup> | 7.90 (-0.77) <sup>a</sup> | 8.05 (-0.02) <sup>a</sup> | 3.23 (-0.89) <sup>a</sup> |
|                                     | (in CD <sub>3</sub> CN) | 8.39                      | 8.03                      | 7.41                      | 7.77                      | 7.94                      | 3.17                      |
| <b>OsOs</b>                         |                         | 8.36                      | 7.82                      | 7.28                      | 7.53                      | 7.93                      | 3.19                      |
| <b>RuOs</b>                         |                         | 8.39 <sup>b</sup>         | 8.02 <sup>b</sup>         | 7.39 <sup>b</sup>         | 7.77 <sup>b</sup>         |                           | 3.17 <sup>b</sup>         |
|                                     |                         | 8.35 <sup>c</sup>         | 7.82 <sup>c</sup>         | 7.29 <sup>c</sup>         | 7.52 <sup>c</sup>         | 7.93                      | 3.19 <sup>c</sup>         |
| <b>bpy rings</b>                    |                         | 8.31-8.45                 | 7.60-8.05                 | 7.12-7.50                 | 7.70-7.90                 |                           |                           |

<sup>a</sup> measured in (CD<sub>3</sub>)<sub>2</sub>SO

<sup>b</sup> pyridyltriazole ring bound to Ru(bpy)<sub>2</sub> unit

<sup>c</sup> pyridyltriazole ring bound to Os(bpy)<sub>2</sub> unit.

Like 1M3ptr, L3 can chelate via the pyridyl N and via N2 or via N4 of the triazole ring. In the case of  $[\text{Ru}(\text{bpy})_2\text{1M3ptr}]^{2+}$  it was found from NMR studies that coordination occurred at the N4 site<sup>8</sup>. This finding was rationalised on the basis of steric hindrance due to the presence of the methyl group. However for analogous  $[\text{Ru}(\text{phen})_2\text{1M3ptr}]^{2+}$  and  $[\text{Ru}(\text{dmbpy})_2\text{1M3ptr}]^{2+}$  complexes two isomers were isolated in approximately a 90:10 % ratio<sup>3</sup>. The main isomer was the expected N4 coordinated isomer, whilst the minor product was the complex where coordination to the ruthenium was sterically hindered *ie.* through the N2 site of the triazole ring. For the N2-coordinated complexes the methyl group was found to move upfield by -0.53 and -0.72 ppm for L = dmbpy and phen, respectively. For the N4-bound compounds the methyl resonance occurred at lower field relative to the free ligand. The shift was +0.11 and +0.06 ppm for the dmbpy and phen complexes, respectively.

All the compounds show a series of resonances in the 7.2-8.5 ppm range which can be attributed to the bipyridine ligands and the pyridyl moiety of L3. The methyl signals are observed between 3-4 ppm. The resonances in the mononuclear complexes associated with the free end of the ligand L3 are, as expected, very similar to those of the free ligand and are readily assigned.

For Isomer 2 of  $[\text{Ru}(\text{bpy})_2(\text{L3})]^{2+}$  the methyl resonance associated with the coordinated pyridyltriazole is shifted upfield by -0.85 ppm, relative to the free ligand (Fig. 5.5). This suggests that in this case coordination to the metal atom is through the N2 position of the triazole ring. For Isomer 1, on the other hand, the methyl resonance is only shifted by -0.4 ppm, suggesting that coordination is via the N4 of the triazole unit (Fig. 5.4). A similar case is found for the osmium mononuclear complexes-

Isomer 1 is the N4-coordinated complex, while Isomer 2 is bound via N2 of the triazole ring.

An examination of the methyl resonances for the dinuclear complexes which were isolated reveals two important points. Firstly, for the homodinuclear complexes only one methyl resonance is observed, thereby indicating the presence of only one coordination isomer. This is also reflected by the simplicity of the NMR spectra obtained. Secondly the resonance position of the methyl protons are in all cases shifted upfield by approximately -0.9 ppm relative to the free ligand (Fig. 5.6, Table 5.1). This implies that the  $M(\text{bpy})_2$  units are coordinated via N2 of the triazole ring.

The NMR assignments for the mononuclear complexes confirm the tentative assignments made on the basis of HPLC data in Section 5.3.1, where the order of elution, based on previous work, suggested that Isomer 1 was N4 coordinated and Isomer 2 was N2-bound. The ratio of Isomer 1:Isomer 2 was found to be approximately 30:70. If steric reasons alone are considered, this is not surprising. The steric effect of the phenyl group would be expected to be much greater than that of the methyl group. As a result, the preferred mode of coordination is through N2, since this leads to less steric hindrance. Furthermore, this finding also supports the coordination assignments made for the complexes of the ligands  $\text{H}_2\text{L1}$  and  $\text{H}_2\text{L2}$  in the previous chapter.

As before, upon coordination the H6 proton of the pyridyl ring is shifted upfield by over 1 ppm due to a diamagnetic anisotropic interaction of this proton with the ring current of the bpy ligands. The resonances for the osmium-coordinated units are in all cases located at higher field to the ruthenium analogues. This is a common observation and is explained by the stronger metal  $d\pi - \pi^*(\text{bpy})$  back-donating

properties of Os(II) compared to Ru(II). This difference in resonances for the ruthenium and osmium units greatly facilitates the assignment of the mixed-metal RuOs complex. The resonances associated with the Ru- and Os-bound moieties correlate very well with those found for their respective homodinuclear complexes.

### 5.3.3 X-Ray Data for N2-Ru.

Figure 5.8 shows a projection of the structure of **N2-Ru**. Relevant bond lengths and angles are presented in Appendix 1. Unfortunately the crystal quality was rather poor. Despite using four separate crystals with the best being used for data collection, it was not possible to completely solve the structure. The x-ray data was not good enough to locate the nitrate counterion accurately and an examination of the anion sites indicated that there was substantial disorder within these positions. No attempt was made to model this disorder as the primary reason for the data collection was to determine the ligands mode of binding to the ruthenium centre. It can be seen in Figure 5.8 that the ruthenium centre is coordinated via the pyridine nitrogen and N2 of the triazole ring. This confirms the assignments made using <sup>1</sup>H-NMR spectroscopy in Section 5.3.2. Preliminary crystal data for [**N2-Ru**]: Orthorhombic, space group *Pnma*,  $a = 31.254(8)$ ,  $b = 27.204(5)$  Å,  $c = 11.075(3)$  Å,  $U = 9416(4)$  Å<sup>3</sup>,  $Z = 8$ ,  $\mu = 0.536$  mm<sup>-1</sup>, crystal dimensions = 0.26 x 0.12 x 0.12 mm.

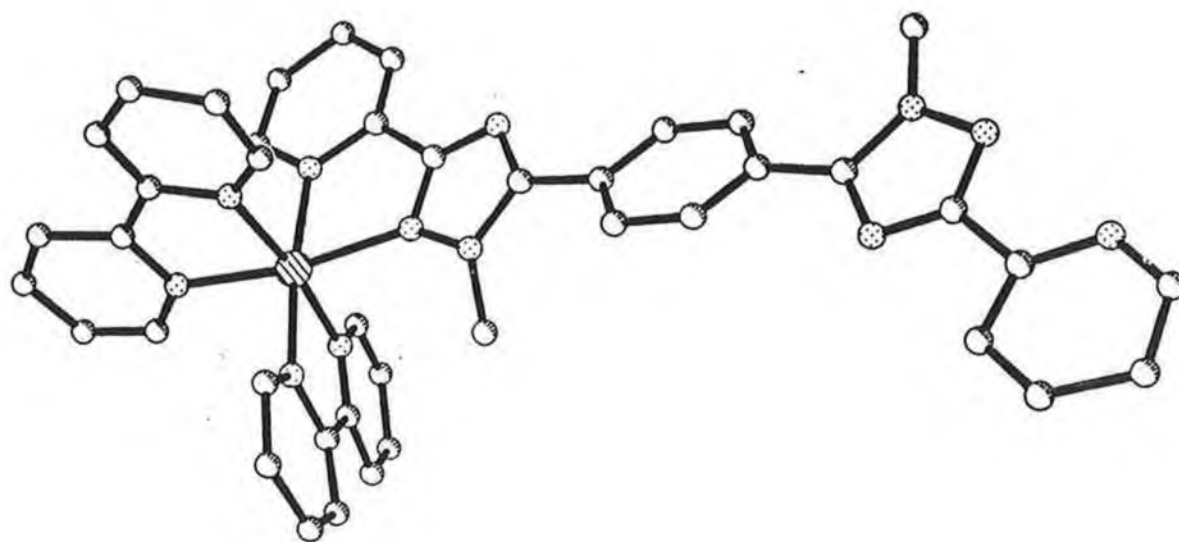


*Figure 5.8 Schematic representation of the structure of N<sub>2</sub>-Ru determined using X-Ray data.*

### 5.3.4 Electronic and Redox Properties.

#### 5.3.4.1 Redox properties.

All the complexes show well-behaved electrochemistry under the experimental conditions used. Representative diagrams of electrochemical measurements, showing oxidation and reduction processes of the complexes are shown in Figures 5.9 - 5.10. The redox processes are reversible, with peak to peak separations of 60-100 mV. All redox potentials measurements were made using ferrocene as an internal reference<sup>9</sup>.  $[\text{Ru}(\text{bpy})_3]^{2+}$  and  $[\text{Os}(\text{bpy})_3]^{2+}$  were also used as internal standards. An examination of the electrochemical data in Table 5.2 reveals some interesting features. As found for the complexes of  $\text{H}_2\text{L1}$  and  $\text{H}_2\text{L2}$  in Chapter 4, the homodinuclear complexes exhibit a single oxidation wave, without any sign of splitting. Furthermore, the oxidation potentials of the dinuclear complexes and their mononuclear substituents are very similar, indicating that the interaction between the metal centres is at best very weak.

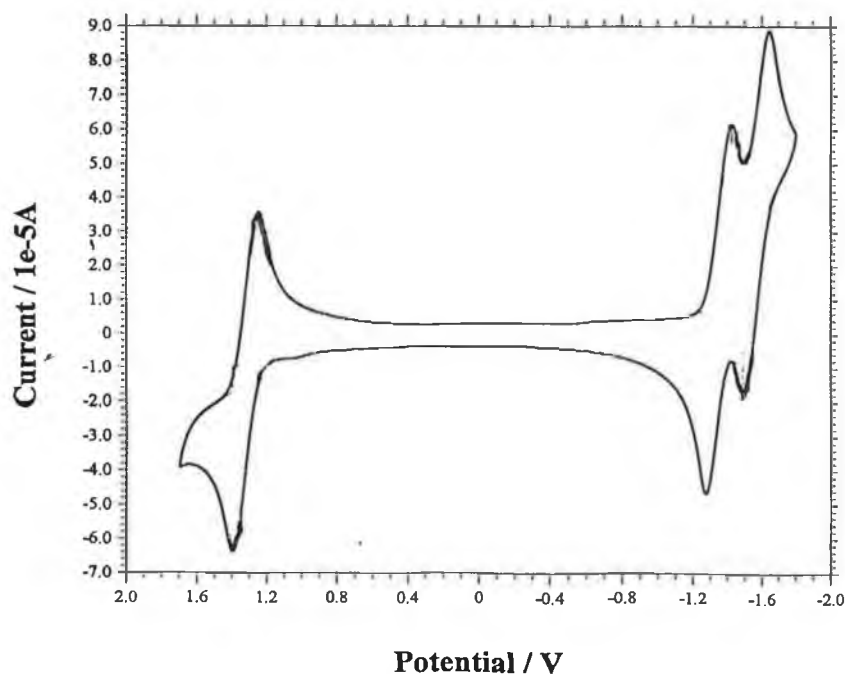


Figure 5.9 Cyclic voltammogram of  $\text{N2-Ru}$  in acetonitrile.

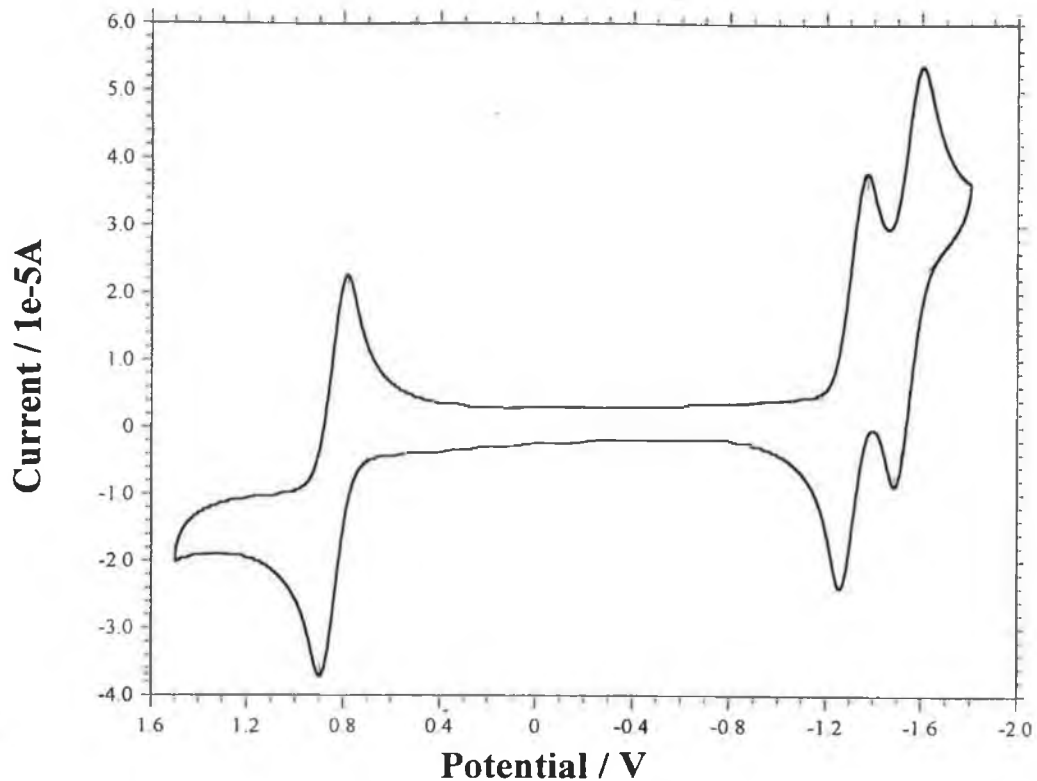


Figure 5.10 Cyclic voltammogram of N2-Os in acetonitrile.

Table 5.2 Electrochemical data for the mononuclear and dinuclear complexes with L3. All measurements carried out in acetonitrile with 0.1M TEAP.

| Complex                               | Oxidation Potential (V vs S.C.E) | Reduction Potential (V vs S.C.E)  |
|---------------------------------------|----------------------------------|-----------------------------------|
| N2-Ru                                 | 1.31                             | -1.35, -1.56                      |
| N4-Ru                                 | 1.20                             | -1.35, -1.58                      |
| N2-Os                                 | 0.80                             | -1.35, -1.59                      |
| N4-Os                                 | 0.76                             | -1.36, -1.64                      |
| RuRu                                  | 1.29                             | -1.38, -1.56                      |
| OsOs                                  | 0.85                             | -1.39, -1.57                      |
| RuOs                                  | 0.80, 1.26                       | -1.39, -1.59                      |
| [Ru(bpy) <sub>3</sub> ] <sup>2+</sup> | 1.26                             | -1.35, -1.55, -1.80               |
| [Os(bpy) <sub>3</sub> ] <sup>2+</sup> | 0.83 <sup>8</sup>                | -1.29, -1.46, -1.79 <sup>10</sup> |

The oxidation potentials of the ruthenium and osmium mono- and dinuclear complexes are very similar to those of  $[\text{Ru}(\text{bpy})_3]^{2+}$  and  $[\text{Os}(\text{bpy})_3]^{2+}$ , respectively. The N4-coordinated complexes exhibit lower oxidation potentials than their  $[\text{M}(\text{bpy})_3]^{2+}$  analogues. Lower oxidation potentials imply that the metal ion has more electron density which means that the ligand L3 has better  $\sigma$ -donor/weaker  $\pi$ -acceptor properties than bpy when coordinated through its N4 position. The case for L3 in its N2 coordination mode is less clear. **N2-Ru** and **RuRu** each have an oxidation potential somewhat greater than that of  $[\text{Ru}(\text{bpy})_3]^{2+}$  (1.26 V vs S.C.E). Similarly the **OsOs** complex has a slightly higher oxidation potential than  $[\text{Os}(\text{bpy})_3]^{2+}$  (0.83 V vs S.C.E.)<sup>8</sup>. At first this might appear to indicate that in the N2 coordination mode, L3 may act as a stronger  $\pi$ -acceptor than bpy. This would have important implications for the photophysical properties of the complexes. It is therefore important to determine the nature of the lowest  $\pi^*$  orbital. In ruthenium and osmium polypyridyl complexes reduction involves the transfer of an electron to the LUMO (lowest unoccupied molecular orbital) of the complex. Therefore the first reduction potential enables the identification of the LUMO. For the N2-coordinated complexes the first two reduction potentials observed occur at the same or more negative potentials to those of their  $[\text{M}(\text{bpy})_3]^{2+}$  counterparts. If L3 were a stronger  $\pi$ -acceptor than bpy it would be easier to reduce and its first reduction potential would therefore occur at a less negative potential. The similarity suggests that in all cases a bpy-based reduction is observed. This conclusion correlates well with results obtained by Ryan *et al*<sup>3</sup> and Forster<sup>11</sup>. The cyclic voltammogram of the ligand L3 in DMF is shown in Fig. 5.11. It has a reduction potential of -2.13 V vs SCE and is therefore reduced at a slightly more negative potential than 2,2'-bipyridine (-2.09 V vs SCE)<sup>12</sup>. It therefore appears likely

that although L3 possesses  $\pi$ -acceptor properties similar to 2,2'-bipyridine, the bipyridyl ligands in the metal complexes are first to be reduced.

The differences in oxidation potentials observed for the N2- and N4-coordination isomers also allows a comparison of the different coordination sites. Comparing the oxidation potentials of the isomeric  $[\text{Ru}(\text{bpy})_2(\text{L3})]^{2+}$  and  $[\text{Os}(\text{bpy})_2(\text{L3})]^{2+}$  complexes shows that the N4 coordinated isomer is oxidised more readily than the N2 isomer. This finding is in contrast to previous studies by Hage and coworkers on the ligands 5-(2-pyridyl)-1,2,4-triazole and 3,5-bis-(2-pyridyl)-1,2,4-triazole which showed that the pyridyltriazole ligand was a better  $\sigma$ -donor when bound *via* N1 (N2) than when bound *via* N4<sup>13</sup>. However the results agree with those obtained by Ryan *et al.* for the  $\text{Ru}(\text{phen})_2$  and  $\text{Ru}(\text{dmbpy})_2$  complexes of the ligand 1M3ptr and H3Mptr<sup>4</sup>. It then appears likely that the methyl substituent gives rise to different electronic and steric effects which may lead to shifts in the electrochemical potential. It may be concluded therefore that the three factors; coordination site, steric effects and electronic effects all influence the observed oxidation potential.

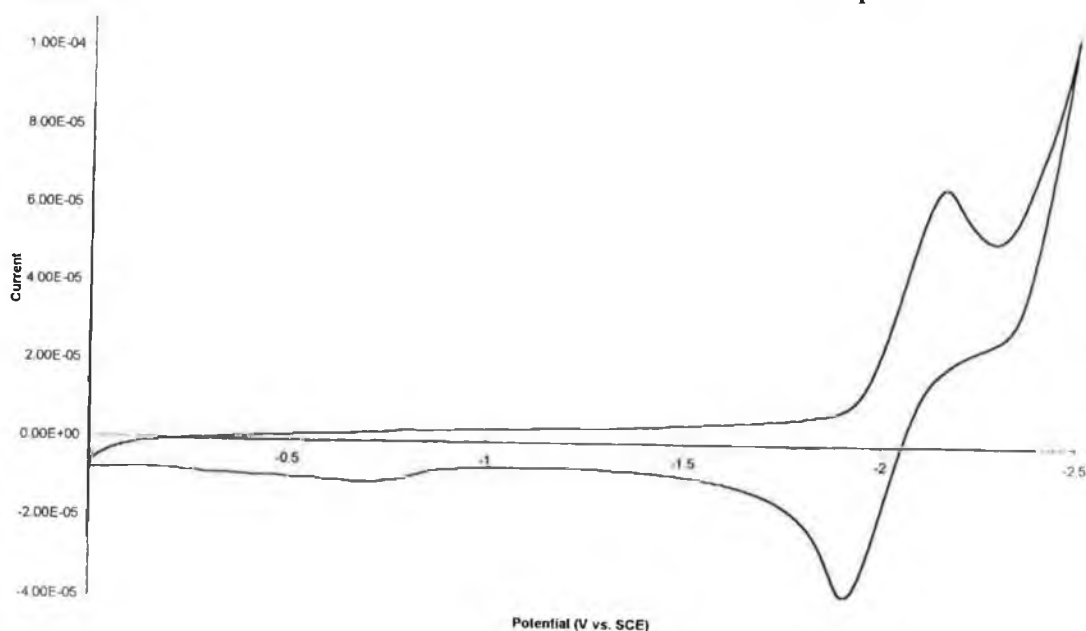


Figure 5.11 Cyclic voltammogram of L3 in DMF.

### 5.3.4.2 Electronic Properties.

As expected, the UV-Visible absorption spectra feature very intense bands in the region 220-330 nm associated with  $\pi-\pi^*$  transitions of the bpy and bridging ligands and absorption bands in the region 400-460 nm associated with  $d\pi-\pi^*$  MLCT bands. The position of the MLCT band can be taken as a measure of the  $\pi$ -acceptor/ $\sigma$ -donor properties of the ligands. If a ligand is a good  $\pi$ -acceptor, the metal  $d\pi$  orbitals are stabilised by back-donation of electron density from the filled metal orbitals to the unoccupied  $\pi^*$  level of the ligand and the MLCT band occurs at higher energy. If on the other hand, a ligand is a good  $\sigma$ -donor, this results in a smaller  $t_{2g}-\pi^*$  energy gap and the MLCT is present at low energy. The electronic properties of the complexes are listed in Table 5.3.

As can be seen from the data, the MLCT band for **N4-Ru** occurs at about the same energy as that of  $[\text{Ru}(\text{bpy})_3]^{2+}$ . However the N2-bound isomer has a MLCT band at around 415 nm (Fig 5.12), which suggests that in this coordination mode the  $\sigma$ -donor properties of the L3 ligand are greatly reduced and it becomes a stronger  $\pi$ -acceptor.

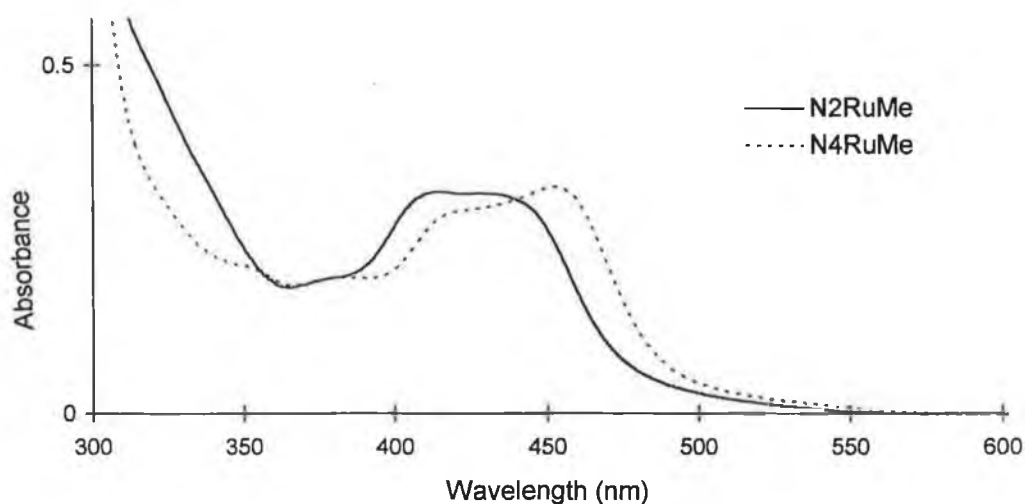


Figure 5.12 UV/Vis absorption spectra in acetonitrile of **N2-Ru** and **N4-Ru**.

**Table 5.3** *UV-Vis absorption and emission data for the ruthenium and osmium complexes of L3 and related compounds. All measurements in Acetonitrile unless otherwise stated.*

| Complex                                   | Absorption $\lambda_{\max}/\text{nm}$            | Emission $\lambda_{\max}/\text{nm}$ |                   | $\tau_{300\text{ K}}^{\text{b}}$ | $\Phi_{\text{em}} (300\text{ K})$ |
|---|--|-------------------------------------|-------------------|----------------------------------|-----------------------------------|
|   | ( $\epsilon/10^4\text{ M}^{-1}\text{ cm}^{-1}$ ) | 300 K                               | 77 K <sup>a</sup> | (ns)                             |                                   |
| <b>N2-Ru</b>                              | 415 (1.33)                                       | 611                                 | 570               | 30                               | $4.8 \times 10^{-4}$              |
| <b>N4-Ru</b>                              | 453 (0.90)                                       | 614                                 | 584               | 32                               | $1.6 \times 10^{-3}$              |
| <b>N2-Os</b>                              | 418 (1.43), 466 (1.33),<br>568 (0.35)            | 719                                 | 703               | 58                               | 0.006                             |
| <b>N4-Os</b>                              | 477 (1.06), 586 (0.24)                           | 744                                 | 723               | 45                               | 0.003                             |
| <b>RuRu</b>                               | 414 (2.60)                                       | 603                                 | 573               | 20                               | $3.1 \times 10^{-4}$              |
| <b>OsOs</b>                               | 419 (2.05), 464                                  | 718                                 | 698               | 65                               | 0.006                             |
| <b>RuOs</b>                               | 417 (2.00), 557 (0.25)                           | 716                                 | 693               | 48 <sup>c</sup>                  | $3.7 \times 10^{-3}$              |
| <b>[Ru(bpy)<sub>3</sub>]<sup>2+</sup></b> | 452 (1.30)                                       | 615                                 | 582               | 800                              | 0.028                             |
| <b>[Os(bpy)<sub>3</sub>]<sup>2+</sup></b> | 478  | 725                                 | 712               | 62                               | 0.005                             |

<sup>a</sup> measured in ethanol/methanol (4:1 v/v)      <sup>b</sup> deaerated solution.

<sup>c</sup> Lifetime measured at 750 nm.

The spectra observed for the osmium complexes are more complicated, showing more bands due to the appearance of formally forbidden singlet—triplet transitions which gain significant intensity by spin-orbit coupling induced mixing of excited singlet and triplet states<sup>14</sup> (Fig. 5.13).

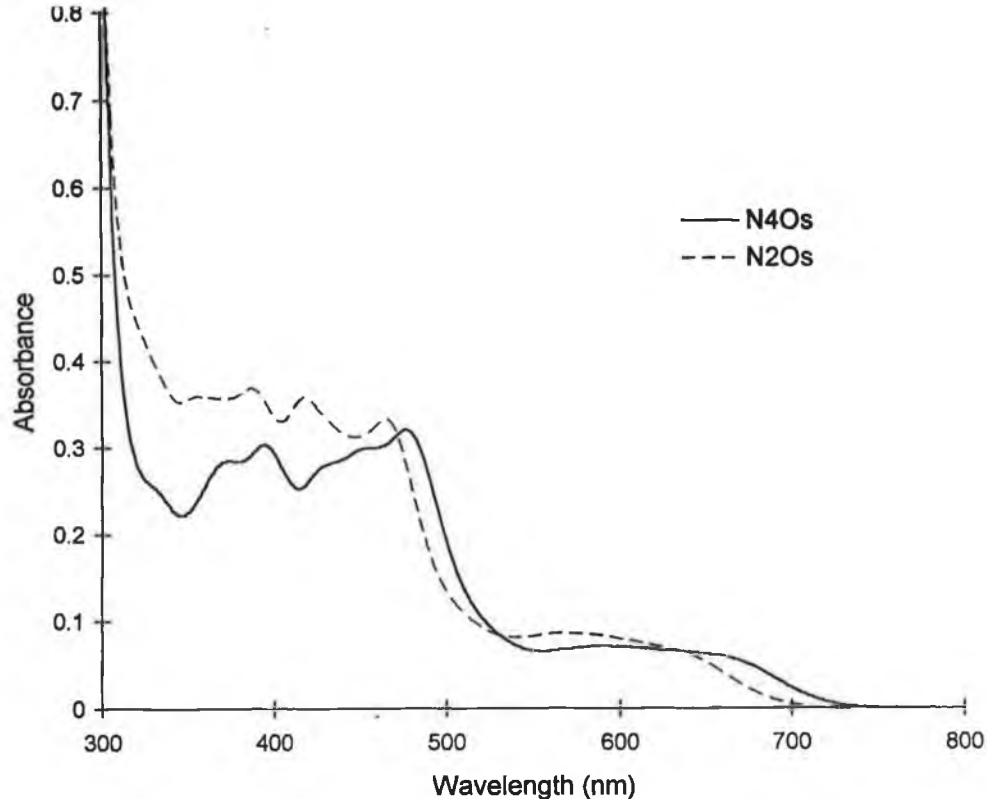


Figure 5.13 UV-Vis absorption spectra of N2-Os and N4-Os in acetonitrile.

It is interesting to note the spectral differences observed in going from a negatively charged triazolate ligand H<sub>2</sub>L2 to its methylated analogue, L3. Large blue shifts in the Ru(dπ) → bpy(π\*) MLCT band are induced by substitution with a methyl group. As stated previously, the blue shift reflects the decrease in electronic charge occurring on Ru(II) as a consequence of the higher π-acceptor ability and lower σ-donor properties of L3 relative to H<sub>2</sub>L2. It is also worth noting that the spectral features are very similar to those shown upon protonation of the ligand H<sub>2</sub>L2. The addition of a methyl substituent on the N1 site of the triazole ring results in Isomer 2 of the complexes having spectra which resemble those obtained for the protonated complexes of the ligand H<sub>2</sub>L2. As was found by Indelli and coworkers for cyanide ligands, from this point of view, methylation and protonation appear to have quite comparable consequences on the electronic properties of the complexes<sup>15</sup>.

A useful method to gauge the intercomponent electronic interaction in polynuclear metal complexes is the assessment of the additive properties of the absorption spectra of the components<sup>16</sup>. The sum of the absorption spectra of the homometallic dinuclear complexes **RuRu** and **OsOs** divided by two gives a spectrum which almost completely matches the absorption spectrum of **RuOs** (Fig. 5.14). This confirms that the metal units are only very weakly coupled as already suggested by electrochemical data. In addition, as expected for MLCT bands which are localised on electronically independent moieties, the band intensities are proportional to the number of metal centres<sup>17</sup>. The  $\lambda_{\text{max}}$  of **RuOs** occurs at an energy intermediate to that of **RuRu** and **OsOs**. Furthermore the observed band peaking in the **RuOs** complex at 417 nm is probably due to overlapping Ru→bpy and Os→bpy charge transfer transitions<sup>18</sup>.

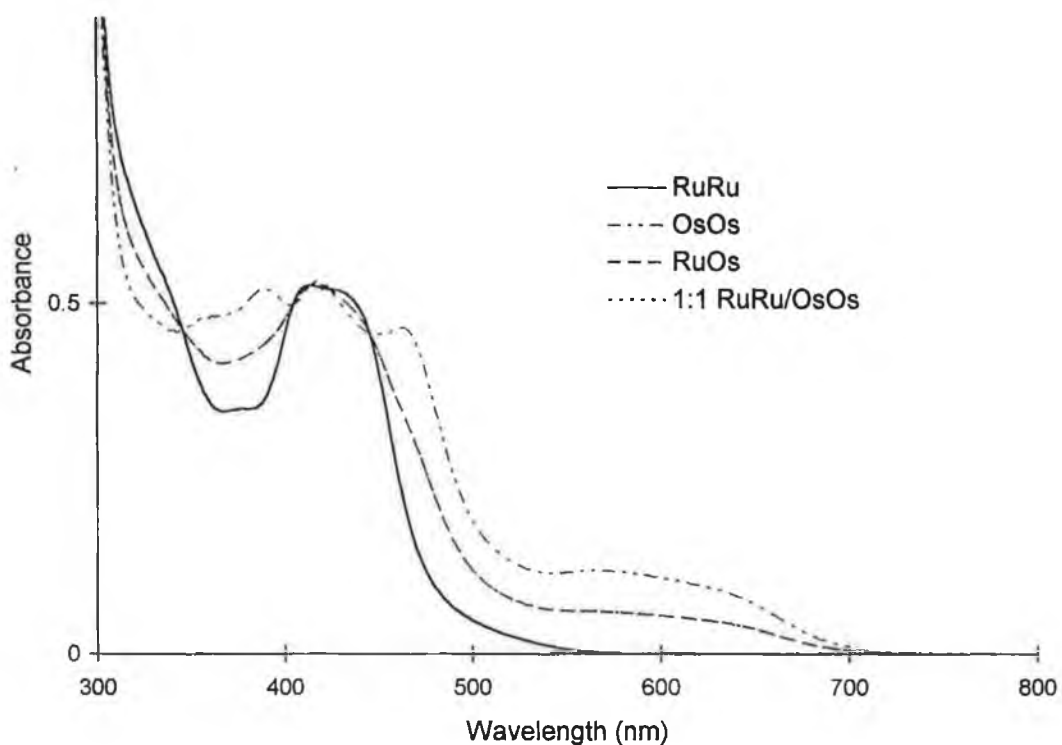


Figure 5.14 UV/Vis absorption spectra of **RuRu**, **OsOs**, **RuOs** and a 1:1 mixture of **RuRu/OsOs**.

All the compounds show emission at room temperature and at 77 K. As can be seen in Table 5.3 the emission wavelengths are similar to those obtained for the  $[M(\text{bpy})_3]^{2+}$  complexes. It is important to establish whether the emitting state is localised on the pyridyltriazole ligand L3 or on bpy. In the absence of resonance Raman data, the relationship between electrochemical potentials and emission maxima becomes useful in identifying the nature of the emitting state. It is known that a distinct relationship exists between the absorption/emission maxima and the difference in oxidation and reduction potentials for ruthenium polypyridyl systems<sup>19,20</sup> in that the energy of the MLCT absorption/emission band manifold increases in energy linearly with increases in  $\Delta E_{1/2}$  (the difference in the Ru(II)/Ru(III) oxidation potential and the first ligand-based reduction). By plotting  $\Delta E_{1/2}$  against  $\lambda_{\text{max}}$  of the emission in eV (calculated using  $\lambda_{\text{max}}$  of 77 K emission in 4:1 ethanol/methanol glass) for N2-Ru, N4-Ru and RuRu and complexes in which the LUMO is known to be bpy-based, a roughly linear correlation is observed (Fig. 5.15).

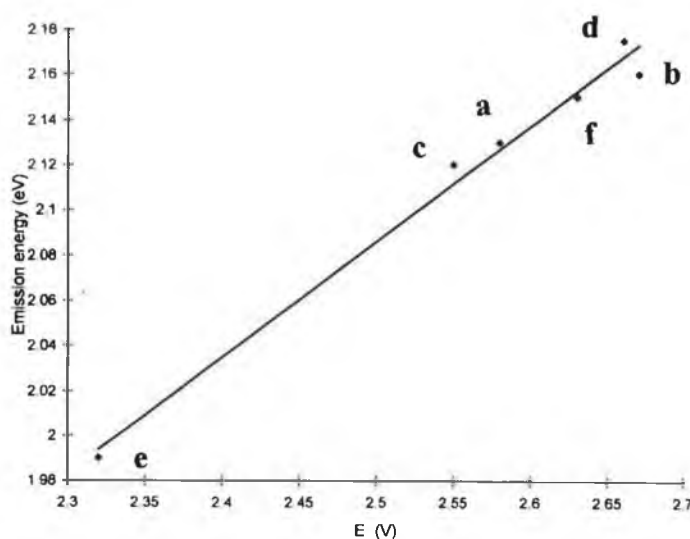


Figure 5.15 Redox dependence of optical electronic transitions for complexes

$[Ru(\text{bpy})_3]^{2+}$  (a), RuRu (b), N4-Ru (c), N2-Ru (d),  $[Ru(\text{bpy})_2\text{bpt}]^+$  (e) and  $[Ru(\text{bpy})_2\text{ptr}]^+$  (f).

The observation of a linear relationship demonstrates that throughout the series emission is occurring from states that have a common electronic origin<sup>20</sup>. Furthermore, as discussed in Section 5.3.4.1, the first reduction potentials of the Ru- and Os-complexes are all very similar to those of their  $[\text{Ru}(\text{bpy})_3]^{2+}$  and  $[\text{Os}(\text{bpy})_3]^{2+}$  analogues, respectively. This suggests that the reduction is bpy-based and indicates that the  $\pi^*$  level of L3 is at higher energy than that of bpy since it is harder to reduce. If this is the case, then the bipyridine ligand acts as the emitting ligand whilst L3 acts as a spectator ligand. However it should be pointed out that this assignment is rather tentative and that Resonance Raman data is necessary to confirm the above observations.

Strong emission with a distinct vibrational structure is observed for all the complexes at 77 K (Fig. 5.16). Similar behaviour has been observed before with other Ru-polypyridyl complexes and this vibrational fine-structure has been attributed to relaxation via bipyridine-based vibrations<sup>21</sup>. The lowest luminescent excited state is expected to be a <sup>3</sup>MLCT level, which for the Os(II) complexes should lie  $\sim 2000 \text{ cm}^{-1}$  lower than in the corresponding Ru(II) complexes<sup>22</sup>. This is found to be the case.

The emission spectrum of the mixed-metal complex **RuOs** is found to exhibit predominantly one band (Fig 5.17). Comparison of the spectra of **RuRu** and **OsOs** shows that the emission observed for **RuOs** is due to an emission from an Os $\rightarrow$ bpy charge transfer excited state.

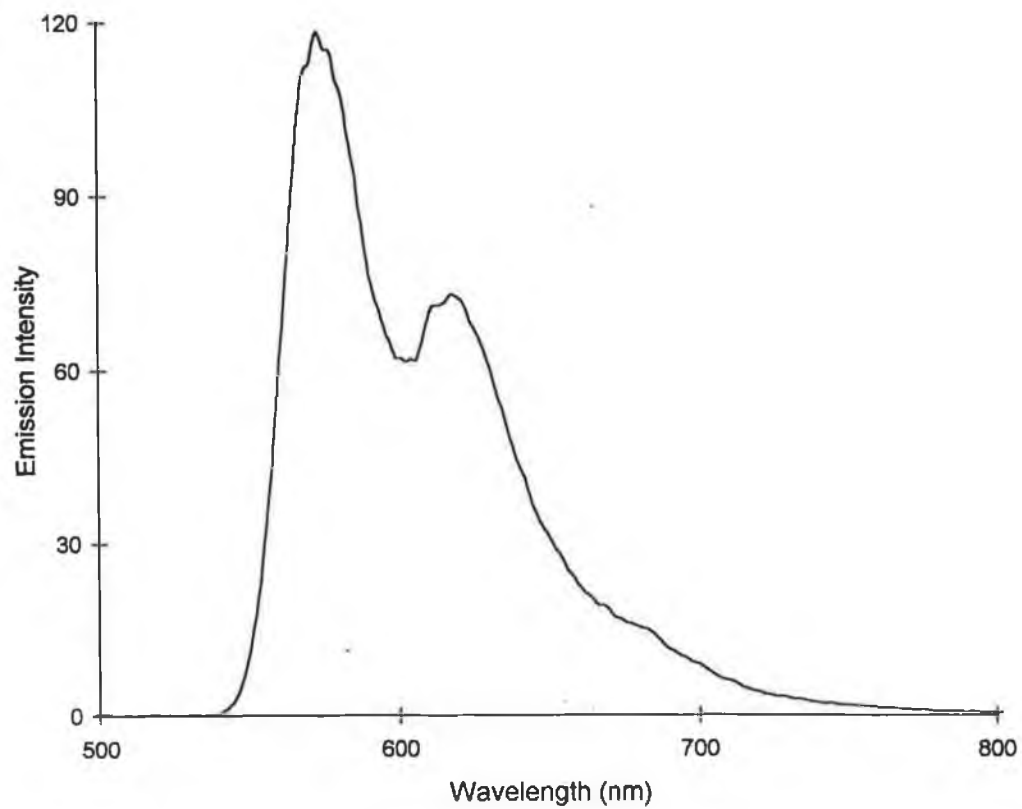


*Figure 5.16* Low temperature emission spectrum of **RuRu** in ethanol/methanol (4:1)

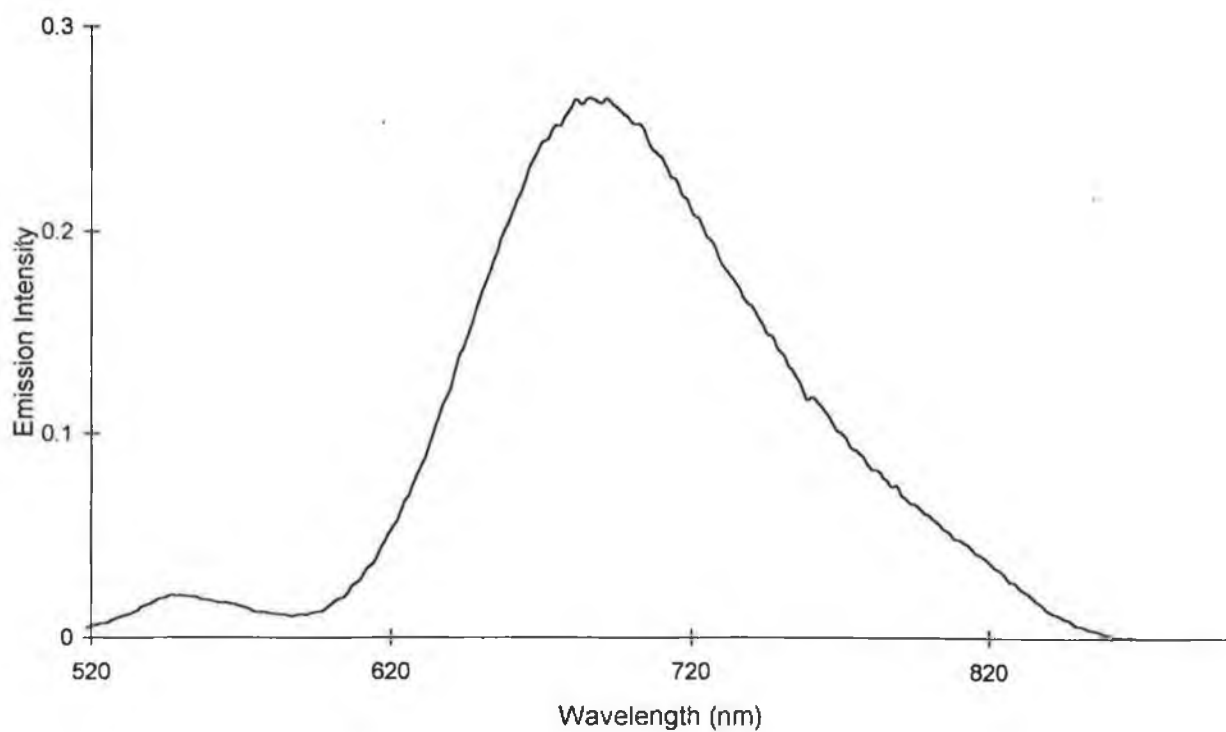


*Figure 5.17* Room temperature emission spectrum in  $\text{CH}_3\text{CN}$  of **RuOs**.

At 77 K emission is found to occur mainly from the osmium site, although a weak band associated with the Ru-based unit is also observed (Fig. 5.18).

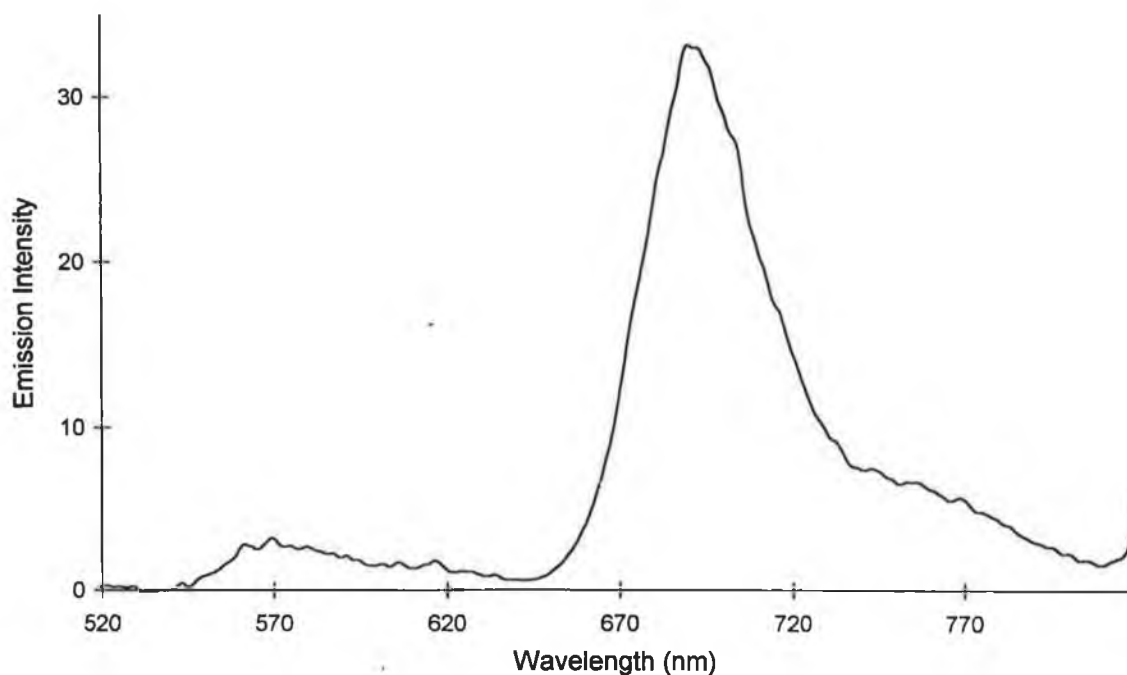


*Figure 5.18* Low temperature emission spectrum of **RuOs** in ethanol/methanol (4:1).

As has been found for many mixed-metal polypyridine complexes, the presence of Ru→bpy CT and Os→bpy CT excited states, each one located in a different subunit of the dinuclear structure, makes possible the occurrence of an electronic energy transfer from the upper-lying triplet Ru-based chromophore to the lower-lying osmium-based unit<sup>23,24</sup>. A quantitative comparison of the luminescence of **RuRu**, **OsOs** and **RuOs** in a manner similar to that described in Section 4.3.3.2 (excitation wavelength 446 nm; same optical density; identical instrumental conditions), shows that over 98 % of the potential luminescence intensity of the Ru-based unit (as measured for **RuRu**) is

quenched in **RuOs** (Fig. 5.19). That the quenching is intramolecular is indicated by the fact that the luminescence intensity of the Os-based chromophore in a 1:1 mixture of **RuRu** and **OsOs** is 50 % that of an isoabsorptive solution of **OsOs**. Therefore under the experimental conditions used ( $2 \times 10^{-5}$  M solutions) intermolecular quenching does not occur. However the luminescence intensity of the Ru-based unit in **RuOs** is only approximately 20 % that of an equimolar 1:1 **RuRu/OsOs** mixture, whilst the Os-based luminescence is sensitized by the same amount. This appears to suggest that the Ru-based luminescence is intramolecularly quenched by the Os-component. At 77 K the potential emission of the Ru-unit is quenched by over 97 % in **RuOs** (as estimated by the luminescence intensity of **RuRu**). In addition, when compared to an isoabsorptive **OsOs** solution the osmium-based luminescence is enhanced. Furthermore from the lifetimes and quantum yields of the **RuOs** and **OsOs** complexes it appears that there is an efficient conversion of the Ru→bpy and Os→bpy excited states, populated upon initial irradiation, to the lowest-lying, luminescent triplet Os → bpy charge transfer level. This result is not surprising, since in Chapter 4 an osmium-based emission was observed for the protonated **pRuOsH** complex of the analogous ligand H<sub>2</sub>L2. The quenching of the ruthenium-based luminescence indicates that energy transfer occurs from the Ru(bpy)<sub>2</sub> unit to the Os(bpy)<sub>2</sub> moiety.

It can be seen in Table 5.3 that the lifetimes and quantum yields of the osmium complexes are of a similar magnitude to those of [Os(bpy)<sub>3</sub>]<sup>2+</sup> and are in all cases greater than those of their ruthenium analogues. This indicates that in the osmium complexes the short-lived <sup>3</sup>MC levels cannot be populated at room temperature. The lifetime and quantum yield of emission depends, among other things on the energy difference between the deactivating antibonding dd orbitals and the emitting <sup>3</sup>MLCT

states. The  $^3\text{MLCT}$ - $^3\text{MC}$  energy gap is higher in the osmium compounds relative to their ruthenium analogues because of (i) the lower energy of the  $^3\text{MLCT}$  level, due to the fact that Os(II) is easier to oxidise than Ru(II) and (ii) the higher energy of the  $^3\text{MC}$  level because of the stronger ligand field splitting of Os(II) compared to Ru(II)<sup>25</sup>.

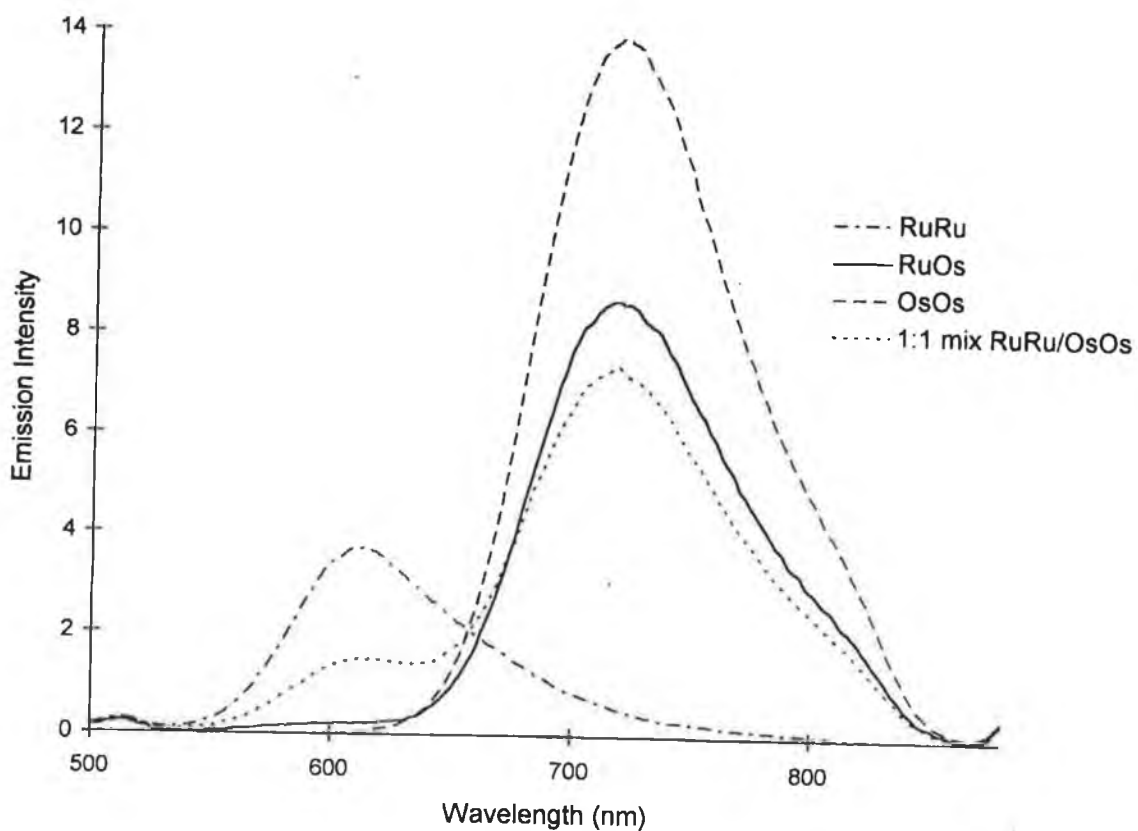


*Figure 5.19 Room Temperature emission spectra of RuRu, OsOs, RuOs and 1:1 RuRu/OsOs in Acetonitrile.*

### 5.3.4.3 Spectroelectrochemistry.

As was found for the dinuclear complexes of the analogous ligand H<sub>2</sub>L<sub>2</sub> in Chapter 4, the similarities in electrochemical and absorption data for the mononuclear and dinuclear complexes indicate that the interaction between the metal centres in the ground state is very weak. However, as pointed out by several authors<sup>16</sup> and shown by the presence of intervalence transitions for **pRuRu** and **pOsOs** in the preceding chapter, this does not mean that coupling between the metal centres is absent.

Oxidative spectroelectrochemistry was carried out on the mononuclear and dinuclear complexes. In all cases the oxidative process was found to be reversible with 100 % regeneration of the starting solution. As expected oxidation of the mononuclear complexes sees the collapse of the MLCT bands associated with the M(II) centre and the formation of weak, low energy bands at around 700 nm for the Ru-complexes and 550 nm for the osmium analogues. These are assigned as LMCT transitions.

In the case of the dinuclear complexes, similar spectral changes occur upon oxidation. However as was found for **pRuRu** ( in Section 4.3.6) a similar broad, very weak band centred at 1120 nm forms and subsequently diminishes as the oxidation progresses. The increase and decrease in intensity of this low energy band may be regarded as a “signature” of intervalence transition charge transfer bands<sup>26</sup> (Fig. 5.20). The parameters associated with this IVCT band are as follows:  $\nu_{\max} = 8929 \text{ cm}^{-1}$ ;  $\Delta\nu_{1/2} = 4786 \text{ cm}^{-1}$ ;  $\epsilon = 241 \text{ M}^{-1}\text{cm}^{-1}$ ,  $V_{\text{ab}} = 154 \text{ cm}^{-1}$ . In calculating the electronic coupling factor  $V_{\text{ab}}$ , the extinction coefficient has been corrected for comproportionation ( $K_c$  taken as 4)<sup>27</sup> and a metal-metal distance of 13.5 Å (based on

Hyperchem molecular model) has been used. The electronic coupling is weaker than that found for **pRuRu** (Section 4.3.6). This could possibly suggest that the negative charge on the triazole ring plays a role in facilitating intervalence electron transfer.

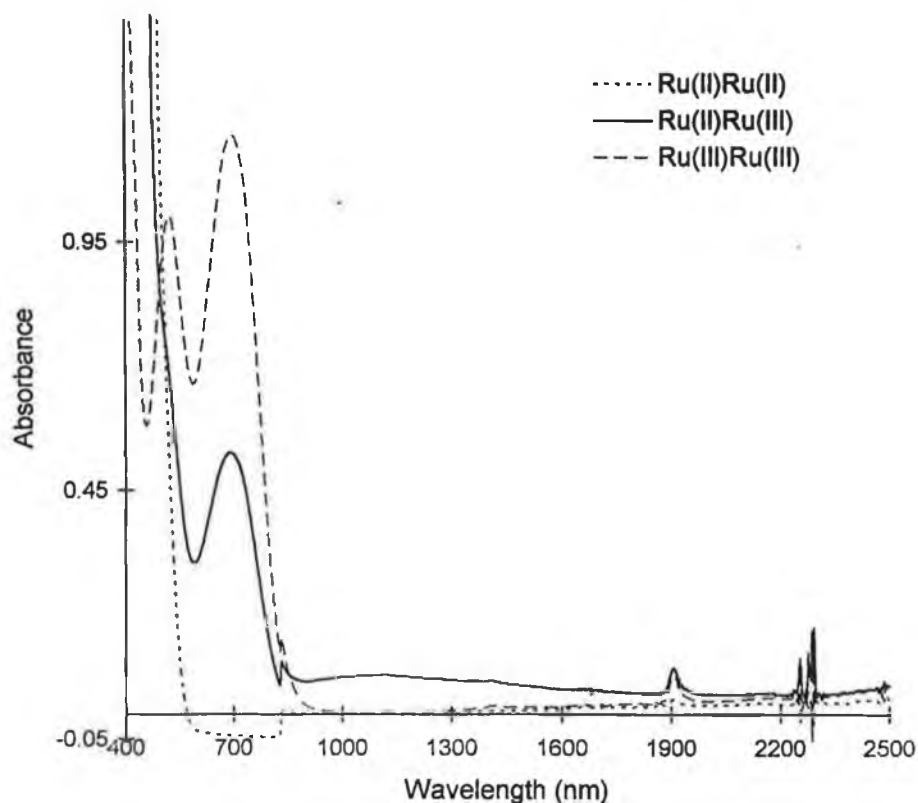


Figure 5.20 Spectra of  $Ru^{II}Ru^{II}$ ,  $Ru^{II}Ru^{III}$  and  $Ru^{III}Ru^{II}$  during oxidation.

No intervalence transitions were identified for the other dinuclear complexes, **OsOs** and **RuOs**. In the case of the former, although an extremely weak tail on the edge of the LMCT band could be detected, it was not possible to calculate any parameters associated with it. In practice, due to the dependence of the intensity of IVCT transitions on  $V_{ab}$ , optical electron transfers may only be observed in systems

with relatively strong intercomponent coupling<sup>28</sup>. It is established that for weakly interacting systems IVCT bands occur at high energy and are of low intensity-  $\lambda_{\max}$  values of <1000 nm and  $\epsilon$  values of a few hundred are common<sup>29</sup>. It is therefore possible that weakly coupled systems may undergo relatively fast electron transfers without exhibiting IVCT bands under the experimental conditions used. The relevant spectral data for the mononuclear and dinuclear complexes in their trivalent oxidation states are presented in Table 5.4.

**Table 5.4** *Visible/Near-IR absorption data for the complexes of L3. All measurements carried out using CH<sub>3</sub>CN with 0.1 M TEAP.*

| <b>Complex</b> | <b>M(III) absorption bands/nm (<math>\epsilon/M^{-1}cm^{-1}</math>, <math>\nu_{1/2}/cm^{-1}</math>)</b> |
|----------------|---|
| <b>N2-Ru</b>   | 408 (3855); 540 (1364); 725 (2618, 4401)  |
| <b>N4-Ru</b>   | 407 (1947); 675 (515, 3834)   |
| <b>N2-Os</b>   | 578 (1818, 4610); 1876 (305); 2320 (909)  |
| <b>N4-Os</b>   | 550 (1000, 4561); 1905 (400); 2218 (833)  |
| <b>RuRu</b>    | 404 (4500); 517 (2862, 4465); 694 (3383, 3636)  |
| <b>OsOs</b>    | 560 (3065, 4524); 1912 (735); 2320 (1176)   |
| <b>RuOs</b>    | 538 (864, 3979); 698 (1164, 3061); 1841 (100); 2310 (362)   |

Examination of the data in Table 5.4 shows that the LMCT bands associated with the complexes of L3 are located at higher energy to those observed for the analogous protonated complexes H<sub>2</sub>L2 (Section 4.5). In the case of the latter LMCT bands attributed to BL→Os(III) and BL→Ru(III) were located at around 700 nm and 900 nm, respectively. It is difficult to unambiguously identify the nature of the donor ligand involved in the LMCT transitions. It has already been established, using

electrochemical, absorption and emission data, that the ligand L3 is a poorer  $\sigma$ -donor than the corresponding ligand H<sub>2</sub>L2 in both its protonated and deprotonated forms. Kalyanasundaram and coworkers<sup>30,31</sup> found that in a series of mixed-ligand complexes, replacement of a donor ligand by a poorer donor ligand caused a blue shift in the observed LMCT transition. This is found to be the case here. However, that the LMCT bands for the complexes in this case are appreciably shifted may mean that the transition involves not the bridging ligand L3, but bpy. [Ru(bpy)<sub>3</sub>]<sup>3+</sup> and [Os(bpy)<sub>3</sub>]<sup>3+</sup> exhibit LMCT bands in the visible region at 676 nm<sup>32</sup> and 563 nm, respectively. These are very weak, with extinction coefficients of 409 M<sup>-1</sup>cm<sup>-1</sup> and 563 M<sup>-1</sup>cm<sup>-1</sup>. The LMCT bands observed for the complexes of L3 are more intense than those of the M(bpy)<sub>3</sub><sup>3+</sup> species (Fig 5.21). This may be due to the  $\sigma$ -donor properties of the pyridyltriazole ligand and the fact that the LMCT band actually originates from the ligand L3. Qualitatively the intensity of LMCT bands increases with increasing electron-donating capacity of the donor ligands<sup>22</sup>. As can be seen in Figure 5.22, additional bands associated with Os(III)  $d\pi$ - $d\pi$  transitions are observed in the spectra containing Os(III) species<sup>33</sup>.

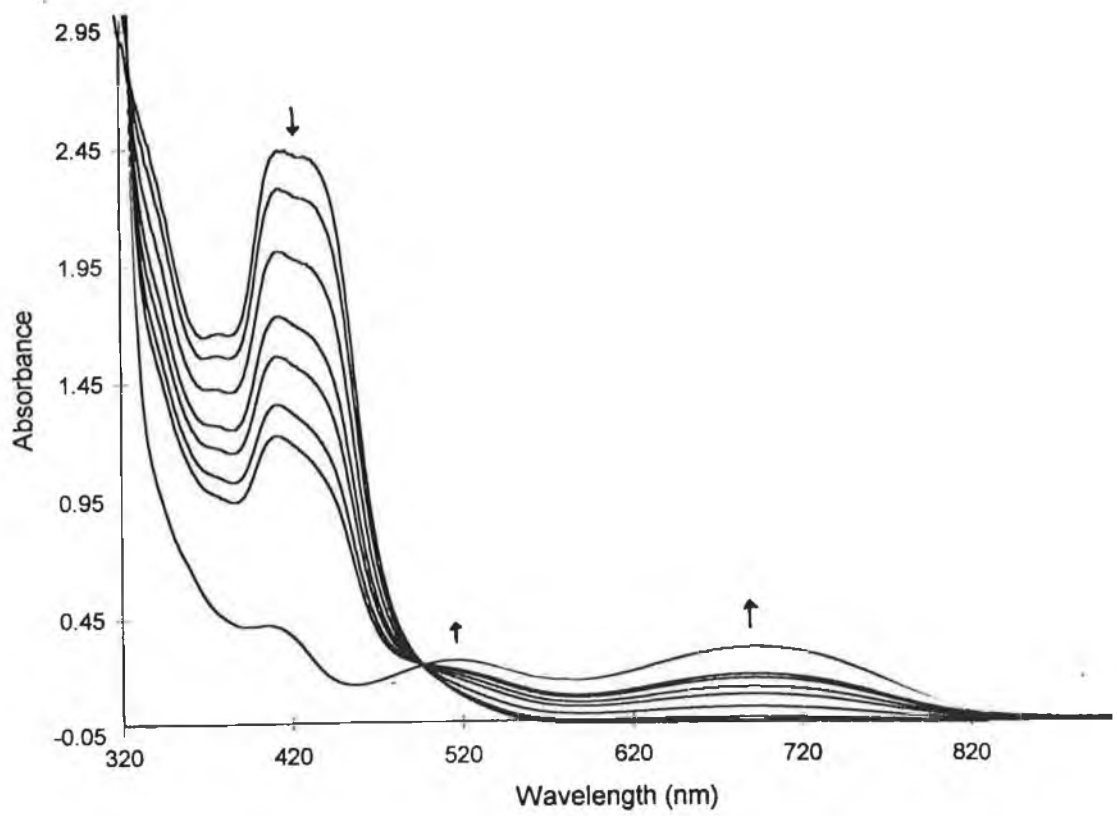


Figure 5.21 Spectral changes during oxidation of RuRu.

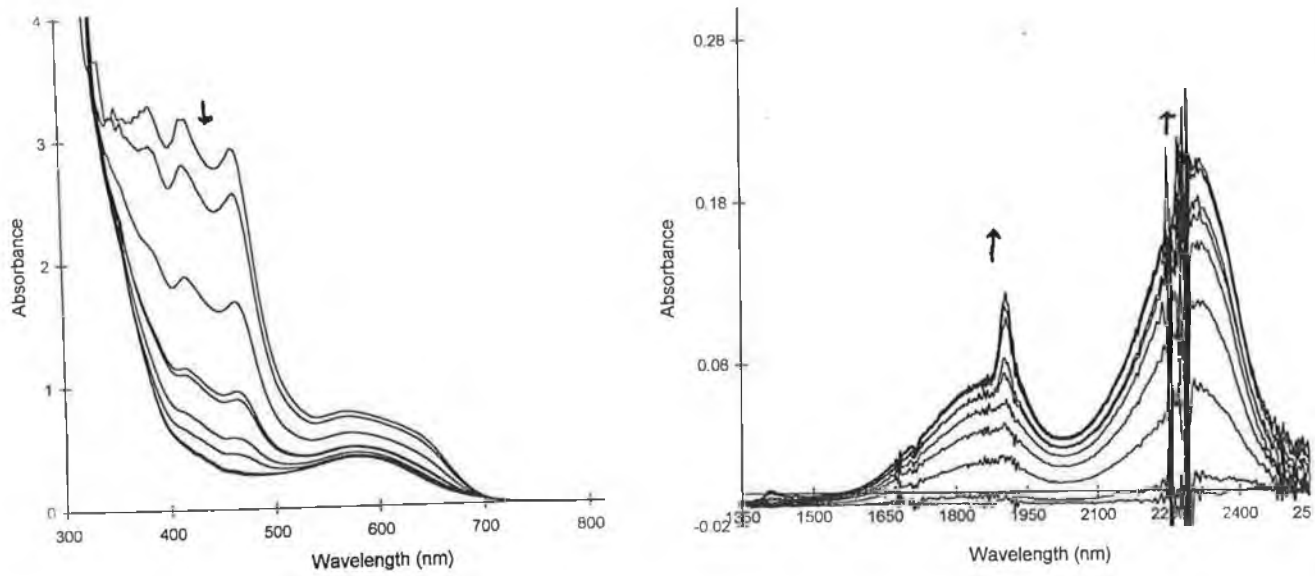


Figure 5.22 Spectral changes which occur during oxidation of N2-Os.

## 5.4 Concluding Comments.

The ruthenium and osmium bipyridyl complexes of the ligand 1,4-bis(1-methyl-3-(2-pyridyl)-1,2,4-triazol-5-yl)benzene, L3, have been synthesised and characterised using a combination of electrochemical and spectroscopic techniques.

All the complexes were found to have two coordination isomers, corresponding to the complexes in which coordination occurs via N2 of the triazole ring and pyridyl nitrogen and N4 of the triazole and pyridyl nitrogen, respectively. The main isomer was that in which coordination occurred via N2. This finding may be rationalised on the basis of steric effects. For the mononuclear complexes, semi-preparative HPLC was found to be invaluable for the separation of the isomers. In contrast, for the dinuclear species fractional recrystallisation proved to be the only method for isolation of the main isomer present.

Electrochemical and spectroscopic data indicate that there is a very weak interaction between metal centres in the dinuclear complexes. This is reflected for example by the presence of one redox wave in the homodinuclear complexes and similar absorption and emission maxima observed for the dinuclear complexes and their mononuclear parent compounds. In addition, the spectrum of **RuOs** is identical to that of a 1:1 mixture of **RuRu** and **OsOs**. The presence of a very weak intervalence band for **RuRu** further suggests a weak coupling between metal units. Initial experiments indicate that there is an interaction in the excited-state between the metal centres in the mixed-metal **RuOs** complex. Quenching of the ruthenium-based luminescence and sensitisation of the osmium-based emission is observed at both room temperature and 77 K. However a more detailed analysis of lifetimes and transient absorption spectra is required before assigning a mechanism to this energy transfer process.

## 5.5 References.

---

- 1 R. Hage, J.G. Haasnoot, H.A. Nieuwenhuis, J. Reedijk, R. Wang and J.G. Vos, *J. Chem. Soc. Dalton Trans.*, 1991, 3271.
- 2 B.E. Buchanan, J.G. Vos, M. Kaneko, W.J.M. van der Putten, J.M. Kelly, R. Hage, R.A.G. de Graaf, R. Prins, J.G. Haasnoot and J. Reedijk, *J. Chem. Soc., Dalton Trans.*, 1990, 2425.
- 3 E.M. Ryan, R. Wang, J.G. Vos, R. Hage and J.G. Haasnoot, *Inorg. Chim. Acta.*, 1993, 208, 49.
- 4 E.M. Ryan, Ph.D Thesis 1991, Dublin City University.
- 5 R. Hage, R. Prins, J.G. Haasnoot, J. Reedijk and J.G. Vos, *J. Chem. Soc. Dalton Trans.*, 1987, 1381.
- 6 P.J. Steel and E.C. Constable, *J. Chem. Soc., Dalton Trans.*, 1990, 1389.
- 7 P.J. Steel, F. Lahousse, D. Lerner and C. Marzin, *Inorg. Chem.*, 1983, 22, 1488.
- 8 R. Hage, J.G. Haasnoot, J. Reedijk and J.G. Vos, *Inorg. Chim. Acta*, 1986, 118, 73.
- 9 N.G. Connelly and W.E. Geiger, *Chem. Rev.*, 1996, 96, 877.
- 10 E.Z. Jandrasics and F.R. Keene, *J. Chem. Soc. Dalton Trans.*, 1997, 153.
- 11 R.J. Forster, A. Boyle, J.G. Vos, R. Hage, A.H.J. Dijkhuis, R.A.G. de Graaf, J.G. Haasnoot, R. Prins and J. Reedijk, *J. Chem. Soc. Dalton Trans.*, 1990, 121.
- 12 S. Roffia, M. Marcaccio, C. Paradisi, F. Paolucci, V. Balzani, G. Denti, S. Serroni and S. Campagna, *Inorg. Chem.*, 1993, 32, 3003.
- 13 R. Hage, Ph.D Thesis 1991, Leiden University.

- 
- 14 E.M. Kober and T.J. Meyer, *Inorg Chem.*, 1983, 22, 1614.
  - 15 M.T. Indelli, C.A. Bigozzi, A. Marconi and F. Scandola, *J. Am. Chem. Soc.*, 1988, 110, 7381.
  - 16 V. Balzani and F. Scandola, *Supramolecular Photochemistry*, Horwood; Chichester, 1991.
  - 17 C.A. Bigozzi, R. Argazzi, J.R. Schoonover, K.C. Gordon, R.B. Dyer and F. Scandola, *Inorg. Chem.*, 1992, 31, 5260.
  - 18 G. Giuffrida, G. Calgero, V. Ricevuto and S. Campagna, *Inorg. Chem.*, 1995, 34, 1957.
  - 19 E.S. Dodsworth and A.B.P. Lever, *Chem. Phys. Lett.*, 1985, 119, 61.
  - 20 F. Barigelletti, A. Juris, V. Balzani, P. Belser and A. von Zelewsky, *Inorg. Chem.*, 1987, 26, 4115.
  - 21 J.V. Caspar and T.J. Meyer, *Inorg. Chem.*, 1983, 22, 2444.
  - 22 S. Serroni, A. Juris, S. Campagna, M. Venturi, G. Denti and V. Balzani, *J. Am. Chem. Soc.*, 1994, 116, 9086.
  - 23 P. Belser, R. Dux, M. Baak, L. de Cola and V. Balzani, *Angew. Chem. Int. Ed. Engl.*, 1995, 34, 595.
  - 24 F. Barigelletti, L. Flamigni, V. Balzani, J.P. Collin, J.P. Sauvage, A. Sour, E.C. Constable and A.M.W. Cargill-Thompson, *J. Am. Chem. Soc.*, 1994, 116, 7692.
  - 25 E.M. Kober, J.L. Marshall, W.J. Dressick, B.P. Sullivan, J.V. Caspar and T.J. Meyer, *Inorg. Chem.*, 1985, 24, 2755.
  - 26 P.E. Sutton, M. R. Sutton, H. Taube, *Inorg. Chem.*, 1979, 18, 1017.

- 
- 27 D.E. Richardson and H. Taube, *Inorg. Chem.*, 1981, 20, 1278; *J. Am. Chem. Soc.*, 1983, 105, 40.
- 28 V. Balzani, A. Juris, M. Venturi, S. Campagna and S. Serroni, *Chem. Rev.*, 1996, 96, 759.
- 29 M.D. Ward, *Chem. Soc. Rev.*, 1995, 121.
- 30 M.K. Nazeeruddin, S.M. Zakeeruddin and K. Kalyanasundaram, *J. Phys. Chem.*, 1993, 97, 9607.
- 31 K.Kalyanasundaram, S.M. Zakeeruddin and Md. K. Nazeeruddin, *Coord. Chem. Rev.*, 1994, 132, 259.
- 32 P.S. Braterman, A. Harriman, G.A. Heath and L.J. Yellowlees, *J. Chem. Soc. Dalton Trans.*, 1983, 1801.
- 33 M. Haga, Md. Meser Ali and R. Arakawa, *Angew. Chem. Int. Ed. Engl.*, 1996, 35, 76.

## **Chapter Six**

### **Preliminary Studies on Ruthenium and Osmium Mononuclear and Dinuclear Complexes Containing Hydroquinone Bridged 3-(2-pyridyl)-1,2,4-Triazole Moieties**

## 6.1 Introduction.

It is well established that the electron transfer reactions of quinones and hydroquinones play an important role in biological transport chains. Quinones, for example, are the primary electron acceptors in Photosystem 1. There are a number of reasons why quinones find widespread use in nature as electron acceptors<sup>1</sup>- (i) they possess suitable redox potentials (ii) they can be converted into stable reduction products (hydroquinones) in a stepwise manner via semiquinones (iii) they can form hydrogen bonds and undergo protonation/deprotonation reactions with ease (iv) they are relatively small mobile molecules that can shuttle redox equivalents to the quinone pool. Given that the redox potentials can be systematically varied by altering substituents and that an extensive background chemistry exists for quinones<sup>2</sup>, they have found application as electron acceptors in studies of photoinduced electron transfer, particularly in systems incorporating porphyrin centres as models for artificial photosynthesis<sup>1,3,4</sup>. Since ruthenium(II) polypyridyl complexes are generally highly luminescent species capable of sensitising a wide variety of photoredox reactions, it seems likely that ruthenium polypyridyl complexes bound to hydroquinone/quinone moieties may have a role in the design artificial photosynthetic systems.

It is therefore hardly surprising that there has been a growing interest in ruthenium complexes containing quinoid moieties. Much of the focus in recent years has been on complexes of dioxolene ligands in which the quinone-based ligand acts as a 1,2-chelate through two metal-oxygen bonds, such as catechol and its oxidation products (semiquinone and quinone)<sup>5</sup>, 2,5-dihydroxy-1,4-benzoquinone<sup>6</sup> and dihydroxyanthraquinones<sup>7</sup>. Such ligands have orbitals of  $\pi$ -symmetry which lie close in energy to those of the metal  $d\pi$  orbitals. This "mixing" between metal and ligand

orbitals can play an important role in determining the physical and chemical properties of the complex<sup>8,9</sup>.

There are however relatively few examples in the literature of ruthenium(II) diimine complexes containing ligands with covalently linked pendant hydroquinone/quinone groups. One of the first examples of such systems was reported by Schanze and Sauer<sup>10</sup> who prepared a series of ruthenium(II) polypyridyl complexes which were covalently linked to *p*-benzoquinone by peptide bridges containing L-proline (Fig. 6.1). Luminescence experiments revealed that significant quenching of the ruthenium <sup>3</sup>MLCT excited state occurred which was ascribed to long-range electron transfer from the Ru MLCT state to the quinone. Despite the fact that the luminescence decay kinetics was complicated by the existence of conformation isomers of the peptide and the presence of hydroquinone impurities, it could be concluded that the rate of Ru to quinone electron transfer was strongly affected by the number of intervening peptide spacers.

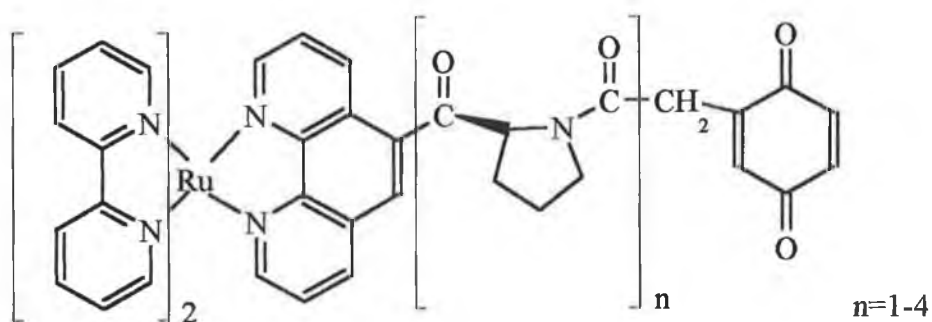


Figure 6.1 General structure of peptide-bridged quinone complexes investigated by Schanze and Sauer<sup>10</sup>.

In 1993 Colbran and coworkers studied N,N-coordinated  $\text{Ru}(\text{bpy})_2$ -complexes of phenanthrolyl ligands bearing pendant hydroquinone and quinone moieties and found that quenching occurred for the complex bearing a quinone substituent. Similarly Lehn *et al* reported luminescence quenching of the  $\text{Ru}(\text{bpy})_3^{2+}$  chromophore by the covalently connected quinone shown in Figure 6.2<sup>11</sup>. The quinone/hydroquinone redox couple built into complexes (i) and (ii) represents an electro-photoswitching device which displays a reversible electrochemical interconversion between the stable and isolable non-luminescent quinone and luminescent hydroquinone forms.

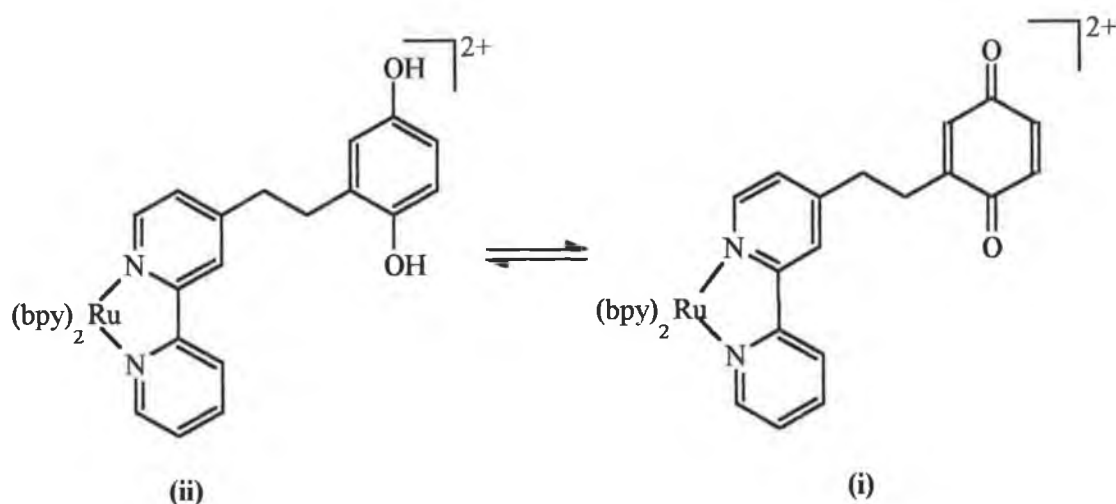


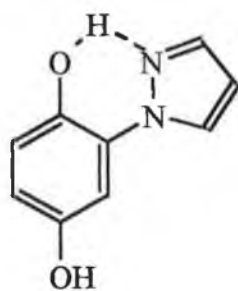
Figure 6.2 Hydroquinone/Quinone complexes studied by Lehn *et al*<sup>11</sup>.

Meyer and coworkers prepared a series of chromophore-quencher complexes that incorporated an anthraquinone-based acceptor ligand, *N*-((4'-methyl-2,2'-bipyridyl)-4-methyl)-9,10-anthraquinone-2-carboxamide (bpy-AQ), a phenothiazine-containing donor ligand (bpy-PTZ), and the ancillary ligands bpy, dmb (4,4'-dimethyl-2,2'-bipyridine) and tmb (4,4',5,5'-tetramethyl-2,2'-bipyridine)<sup>12</sup>. Whilst electron

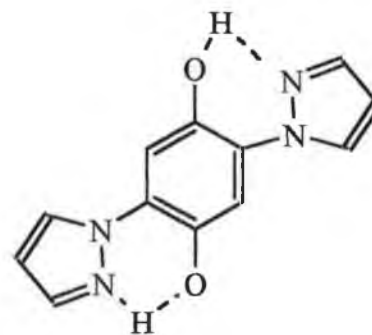
transfer quenching of the initial excited states of the  $[\text{Ru}(\text{bpy})_2(\text{bpy-AQ})]^{2+}$  and  $[\text{Ru}(\text{tmb})_2(\text{bpy-AQ})]^{2+}$  complexes was observed, back electron transfer to the ground state was rapid. However MLCT excitation of the donor-chromophore-acceptor complex  $[\text{Ru}(\text{bpy-AQ})_2(\text{bpy-PTZ})]^{2+}$  lead to the formation of the redox-separated state  $[\text{Ru}^{\text{II}}(\text{bpy-AQ})(\text{bpy-AQ}^{\cdot-})(\text{bpy-PTZ}^{\cdot+})]^{2+}$  in approximately 40 % yield.

It would appear from the literature that in all the cases reported for such quinone/hydroquinone systems the quenching moiety is bound either on, or, in close proximity to the luminophoric site. Recently our group has focussed some attention on a systematic study of complexes where hydroquinone units in combination with other coordinating groups are bound to metal centres in a bidentate, asymmetric fashion. T. Keyes carried out an extensive study of N,N-coordinated ruthenium(II) bipyridyl complexes bound to pyridyltriazole ligands bridged to pendant phenol, hydroquinone and quinone moieties and O,N-coordinated ruthenium(II) bipyridyl complexes of hydroquinone pyrazole ligands. Some of the ligands studied are depicted in Figure 6.3<sup>13</sup>.

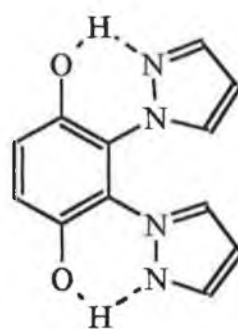
The O,N- coordinated complexes of these ligands were shown to have properties which would make them suitable candidates as sensitizers in artificial photosynthetic devices. They exhibit strong absorbances over a broad visible spectrum and show high levels of photostability. Furthermore, the dinuclear O,N-coordinated Ru(II) complexes produce stable mixed-valence species which show an electronic communication between the metal centres indicative of Class II behaviour<sup>14</sup>.



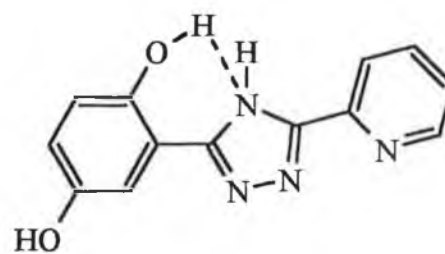
1,4-dihydroxy-2-(pyrazol-1-yl)benzene



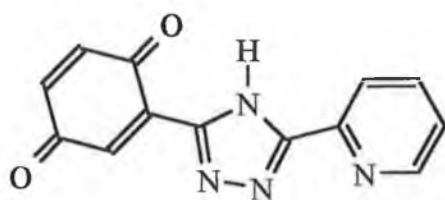
1,4-dihydroxy-2,3-bis(pyrazol-1-yl)benzene



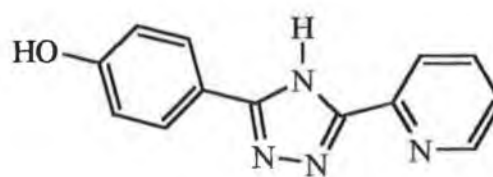
1,4-dihydroxy-2,3-bis(pyrazol-1-yl)benzene



3-(2,5-dihydroxyphenyl)-5-(2-pyridyl)-1,2,4-triazole



3-(2,5-benzoquinone)-5-(2-pyridyl)-1,2,4-triazole



3-(4-hydroxyphenyl)-5-(2-pyridyl)-1,2,4-triazole

Figure 6.3 Some of the ligands studied by T. Keyes<sup>13</sup>.

Hydroquinones and quinones are well known for their ability to quench the excited state of  $[\text{Ru}(\text{bpy})_3]^{2+}$  and related complexes. An examination of the electron transfer properties of the  $\text{Ru}(\text{bpy})_2$ -complexes of the aryl-substituted pyridyltriazole ligands such as those shown in Fig. 6.3 revealed that intramolecular electron transfer between the anionic  $\text{HQ}^-$ ,  $\text{Q}^{\cdot-}$  and  $\text{O}^-$  species and the  $\text{Ru}(\text{II})$  centre leading to a charge separated state occurred at high pH. These electron transfers showed a strong solvent dependence and were found to occur even at cryogenic temperatures. Electrochemical and spectroelectrochemical data indicated that the OH-containing complexes exhibited electrochemically induced proton transfer, whereby upon oxidation of the OH-containing group, the proton produced is accepted by the negative triazole. In the case of the complex  $[\text{Ru}(\text{bpy})_2\text{L}](\text{PF}_6)$  ( $\text{HL} = 3$ -(2,5-dihydroxyphenyl)-5-(2-pyridyl)-1,2,4-triazole) there is strong evidence to suggest that this facile reversible proton transfer occurs intramolecularly via hydrogen-bridge formation between the hydroquinone and the triazole<sup>15</sup>. In order to investigate the role played by the negative triazolate moiety it was of interest to synthesise a hydroquinone-containing ligand containing a neutral triazole ring. Therefore with this in mind, the ligand 1,4-dihydroxy-2,5-bis(3-(2-pyridyl)-1,2,4-triazol-1-yl)benzene,  $\text{H}_2\text{L}_4$ , (Figure 6.4) was prepared (Section 3.2.5).

This chapter describes the synthesis and initial investigation of the photophysical, redox and acid-base properties of the mononuclear and dinuclear  $\text{Ru}(\text{II})$  complexes of the ligand  $\text{H}_2\text{L}_4$ .

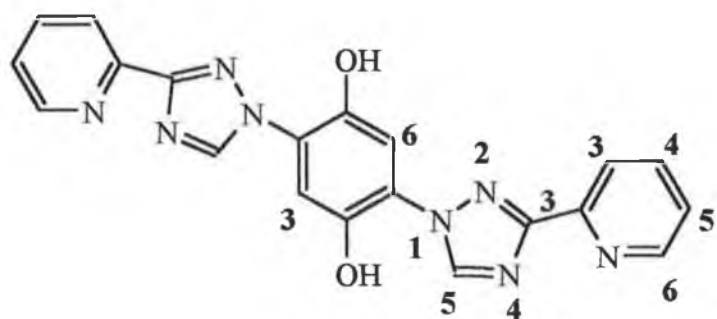


Figure 6.4. Structure of ligand H<sub>2</sub>L4.

## 6.2 Synthesis of the complexes.

The synthesis of the ligand H<sub>2</sub>L<sub>4</sub> has already been described in Chapter 3. All materials and solvents were of commercial grade unless otherwise stated. cis-[Ru(bpy)<sub>2</sub>Cl<sub>2</sub>].2H<sub>2</sub>O was prepared as described in Section 4.2.

### [Ru(bpv)<sub>2</sub>H<sub>2</sub>L<sub>4</sub>](PF<sub>6</sub>)<sub>2</sub>.3H<sub>2</sub>O.      **HQ-Ru**

H<sub>2</sub>L<sub>4</sub> (0.40 g, 1 mmol) was dissolved in ethanol/H<sub>2</sub>O (2:1 v/v) and cis-[Ru(bpy)<sub>2</sub>Cl<sub>2</sub>].2H<sub>2</sub>O (0.26 g, 0.5 mmol) was added. The mixture was heated at reflux for 6 hours. Upon cooling of the solution, unreacted ligand was removed by filtration. The solvent was reduced in volume to about 10 cm<sup>3</sup> and a few drops of aqueous NH<sub>4</sub>PF<sub>6</sub> added. The resulting precipitate was filtered and recrystallised from acetone/H<sub>2</sub>O. The mononuclear complex was obtained in its pure form by semi-preparative HPLC using 80:20 CH<sub>3</sub>CN/H<sub>2</sub>O containing 0.13 M KNO<sub>3</sub> and a flow rate of 1.8 cm<sup>3</sup>/min. Yield = 0.12 g (22 %).

Calcd. for Ru<sub>1</sub>C<sub>40</sub>H<sub>36</sub>N<sub>12</sub>O<sub>5</sub>P<sub>2</sub>F<sub>12</sub> = C: 41.54; H: 3.14; N: 14.54 %. Anal. Found: C: 41.64; H :2.87; N: 14.36 %.

### [(Ru(bpv)<sub>2</sub>)<sub>2</sub>H<sub>2</sub>L<sub>4</sub>](PF<sub>6</sub>)<sub>4</sub>.2H<sub>2</sub>O.      **HQ-RuRu**

The dinuclear complex was prepared as described for **HQ-Ru** except that cis-[Ru(bpy)<sub>2</sub>Cl<sub>2</sub>].2H<sub>2</sub>O (0.29 g, 0.55 mmol) and H<sub>2</sub>L<sub>4</sub> (0.10 g, 0.25 mmol) were heated at reflux in 40 cm<sup>3</sup> ethanol/water (2:1 v/v) for 6 hours. The dinuclear complex was obtained by semi-preparative HPLC using 80:20 acetonitrile/water containing 0.20 M KNO<sub>3</sub> as mobile phase and a flow rate of 2 cm<sup>3</sup>/min. Yield = 0.20 g (20 %).

Calcd. for  $\text{Ru}_2\text{C}_{60}\text{H}_{50}\text{N}_{16}\text{O}_4\text{P}_4\text{F}_{24}$  = C: 39.11; H: 2.74; N: 12.17 %. Anal. Found:  
C:39.36; H :2.69; N: 11.93 %.

## 6.3 Results and Discussion.

### 6.3.1 Synthesis.

The synthesis of the mononuclear and dinuclear complexes of H<sub>2</sub>L4 followed procedures previously employed in the preparation of analogous complexes. Analysis of the reaction mixtures and products indicated that the desired complexes were formed in approximately 60-65 % yield (based on integrated areas of peaks detected at 280 nm) with the main impurities being dinuclear species in the case of the mononuclear complex and vice versa. Purification by semi-preparative HPLC proved to be the method of choice for purification. The high charge on the dinuclear complex necessitated the use of a high concentration of potassium nitrate in the mobile phase, so as to avoid long run times and band spreading. Other methods of purification were investigated, including neutral alumina and silica column chromatography. However it was found that considerable adsorption of the complex occurred in the former, whilst no separation of mononuclear and dinuclear complex was obtained for the latter (using 80:20 CH<sub>3</sub>CN/H<sub>2</sub>O containing 0.10-0.20 M LiClO<sub>4</sub>).

For both the **HQ-Ru** and **HQ-RuRu** only the N,N-coordinated complexes were obtained. This was indicated by HPLC retention times and the UV/Vis absorption spectra of the complexes and was further confirmed by <sup>1</sup>H-NMR spectroscopy (*vide infra*). The UV/Vis absorption spectra did not show any low energy bands extending into the red which are indicative of O,N-coordinated complexes<sup>6</sup>. Attempts were made to synthesise the O,N-coordinated complexes by adding diethyl amine to the ligand solution before the addition of the metal<sup>13</sup>. It was hoped in this way to deprotonate the hydroxyl group of the hydroquinone ring and thereby facilitate formation of the O,N-species. However this proved unsuccessful.

As with the ligand L3 (Chapter 5), H<sub>2</sub>L4 can coordinate via N of the pyridine and either N2 or N4 of the triazole ring. HPLC analysis of the reaction mixture and product obtained for the mononuclear complexes provided evidence for the formation of only one mononuclear species. For the dinuclear complexes however, minor products (10-20 %) in addition to the main fraction of dinuclear species could be identified. It was not possible to isolate these as they had very long retention times (approx. 45 min) and eluted very slowly with band-spreading from the semi-preparative column.

### 6.3.2 <sup>1</sup>H-NMR Spectroscopy.

There are a number of coordination possibilities for these complexes, as represented in Fig. 6.5, which depicts the possible coordination modes of Ru(bpy)<sub>2</sub> which may occur in the mononuclear complex. The Ru(bpy)<sub>2</sub>-unit may bind via the pyridyl nitrogen and via N4 (i) or N2 (ii) of the triazole ring. There is also the possibility that the metal might bind via the oxygen of the hydroquinone and a triazole nitrogen (iii), although from preliminary HPLC/UV studies, this appears not to be the case.

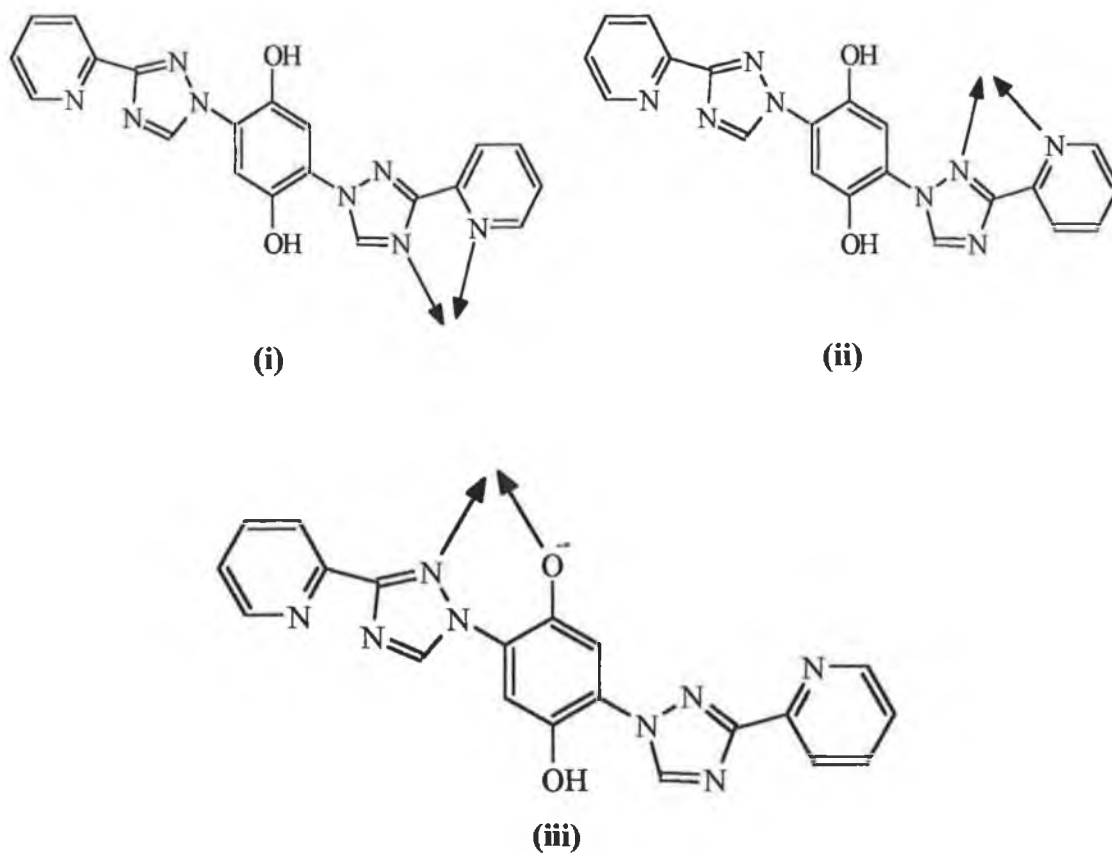


*Figure 6.5 Schematic representation of possible coordination modes for HQ-Ru.*

The  $^1\text{H-NMR}$  spectra of **HQ-Ru** and **HQ-RuRu** in dimethyl sulphoxide are shown in Figs. 6.6 and 6.7, respectively. The spectra are clean and well resolved and integrate to the expected number of protons. Although the bipyridyl resonances could be identified, they could not be assigned to individual rings. The assignments of resonances due to  $\text{H}_2\text{L}_4$  were made using COSY spectra and by comparison with the resonances of the free ligand.

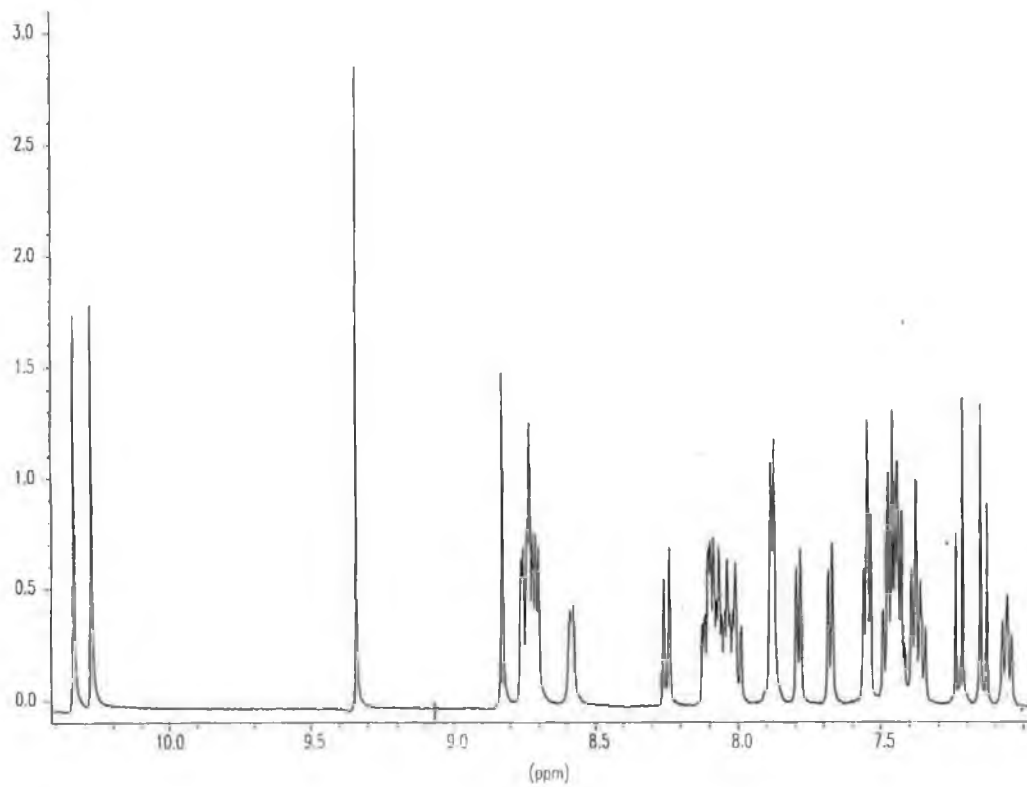


Figure 6.6.  $^1\text{H-NMR}$  spectrum of HQ-Ru in  $d_6$ -dimethyl sulphoxide

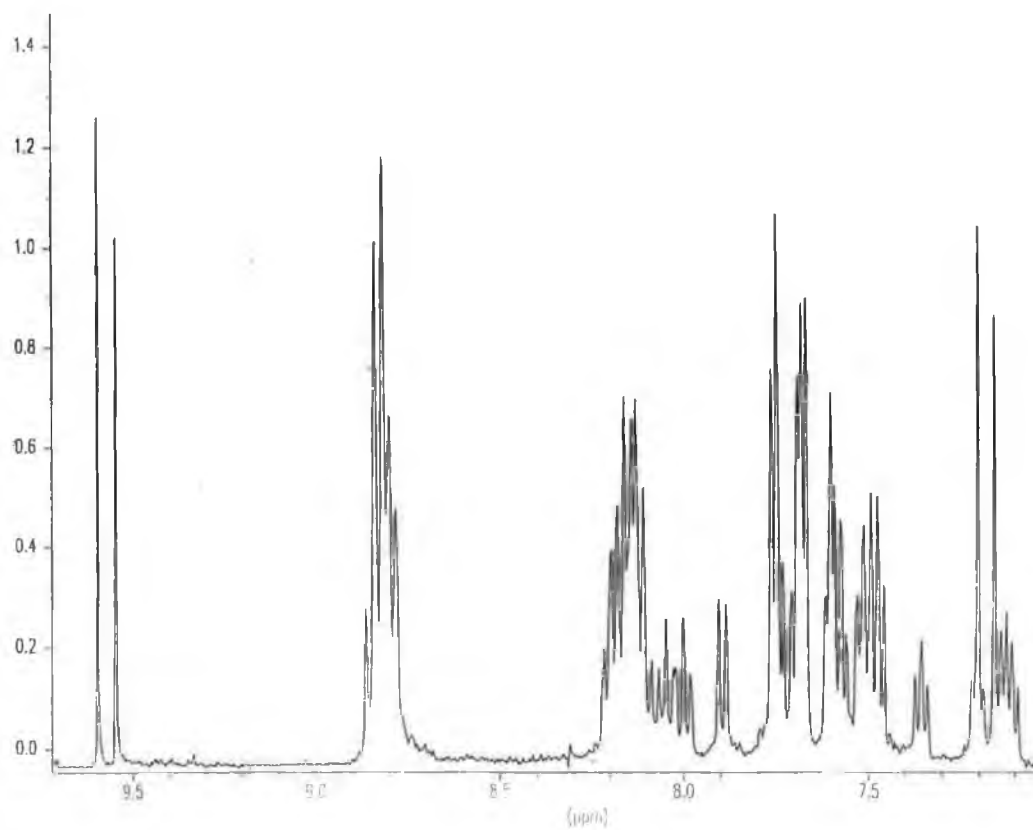


Figure 6.7.  $^1\text{H-NMR}$  spectrum of HQ-RuRu in  $d_6$ -dimethyl sulphoxide.

**Table 6.1**  $^1\text{H-NMR}$  data ( $\delta$  in ppm) for **HQ-Ru** and **HQ-RuRu**. Measurements in  $(\text{CD}_3)_2\text{SO}$  except otherwise stated. The values in parenthesis are the coordination induced shifts compared to the free ligand. *f* and *b* refer to free and bound pyridyltriazole rings, respectively.

| Compound                   | Pyridyl |         |         |         | Triazole          | Hydroquinone |          |
|----------------------------|---------|---------|---------|---------|-------------------|--------------|----------|
|                            | H3      | H4      | H5      | H6      |                   | H3/H6        | OH       |
| <b>H<sub>2</sub>L4</b>     | 7.82    | 7.79    | 7.35    | 8.55    | 8.76              | 7.17         | 10.15    |
| <b>HQ-Ru</b> ( <i>f</i> )  | 7.88    | 7.86    | 7.43    | 8.57    | 8.83              | 7.13-7.24    | 10.27    |
| ( <i>b</i> )               | 8.25    | 8.08    | 7.46    | 7.54    | 9.34              |              | 10.34    |
|                            | (+0.43) | (+0.29) | (+0.11) | (-1.01) | (+0.58)           |              |          |
| <b>HQ-RuRu</b>             | 8.12    | 8.00    | 7.50    | 7.61    | 9.55 (+0.79)      | 7.16-7.20    | 10.57    |
|                            | (+0.30) | (+0.21) | (+0.15) | (-0.94) | 9.60 (+0.84)      |              | 10.63    |
| <b>HQ-RuRu<sup>a</sup></b> | 7.93    | 8.02    | 7.42    | 7.59    | 8.63 ( <i>d</i> ) | 7.16-7.19    | <i>b</i> |
| <b>bpy rings</b>           | 8.60-   | 8.00-   | 7.10-   | 7.50-   |                   |              |          |
|                            | 8.80    | 8.20    | 7.40    | 7.70    |                   |              |          |

<sup>a</sup> measured in  $\text{d}_3$ -acetonitrile <sup>b</sup> not observed.

An examination of the  $^1\text{H-NMR}$  data for the complexes in Table 6.1 shows that for both **HQ-Ru** and **HQ-RuRu** an upfield shift of approximately 1 ppm is observed for the pyridine H6 proton compared to the spectrum of the free ligand. This shift to lower field is indicative of coordinated pyridines as a result of diamagnetic anisotropic interaction with the adjacent bipyridyl ring<sup>16</sup>. The observed shift upon binding of the metal units eliminates the possibility that the hydroquinone moiety is involved in coordination.

In order to ascertain which nitrogen of the triazole ring serves as the second coordination site the shift in resonances associated with the hydroquinone ring and H5 of the triazole ring were examined. It is anticipated that the resonances associated

with H5 of the triazole ring and the protons of the hydroquinone moiety will be strongly affected by a neighbouring bpy ring and are therefore expected to be diagnostic of the coordination mode of the complex. In the case of **HQ-Ru** a comparison of the resonance positions of the H3/H6 protons of the hydroquinone ring in the metal complexes with those in the free ligand reveals that the resonance positions of these protons do not change appreciably upon coordination. The splitting pattern observed is typical of asymmetric 2,5-disubstitution of a 1,4-disubstituted-phenyl ring, which supports formation of a mononuclear complex. The resonance of the H5 proton however experiences a downfield shift of +0.58 ppm upon coordination of the Ru(bpy)<sub>2</sub> unit. For **HQ-Ru** there are two coordination possibilities- via N2 or N4 of the triazole ring. From steric considerations it would be anticipated that binding via N4 would be the preferred mode of coordination, as binding via N2 would place the bipyridyl rings in close proximity to the hydroquinone ring. The N4 site, having only H5 on the neighbouring atom, appears less sterically hindered. It was seen in Chapter 5 for the ligand L3, in which the N2 and N4 coordination sites have as substituents on the neighbouring atom a methyl and phenyl moiety, respectively, that binding occurred preferentially at N2- the less sterically hindered site. On this basis coordination via N4 might be expected. If coordination occurred via N4, a shift in resonance of H5 would be anticipated on the basis of previous findings for substituents on the neighbouring atom to a coordination site<sup>17,18</sup>. Furthermore, it would be expected that the observed shift would be upfield because of the diamagnetic interaction of an adjacent bpy ligand, in a manner similar to that found for the pyridyl H6 proton. That this is not the case could also suggest that in **HQ-Ru** the Ru(bpy)<sub>2</sub>-units are coordinated via N2 of the triazole ring and the pyridyl nitrogen. From a

simplistic perspective, the ligand  $H_2L4$  may be regarded as being similar in structure to the ligands 1-methyl-3-(2-pyridyl)-1,2,4-triazole (1M3ptr) and 1-methyl-3-(2-pyrazinyl)-1,2,4-triazole (1M3pztr) (Fig. 6.8) with regards to triazole ring substitution.

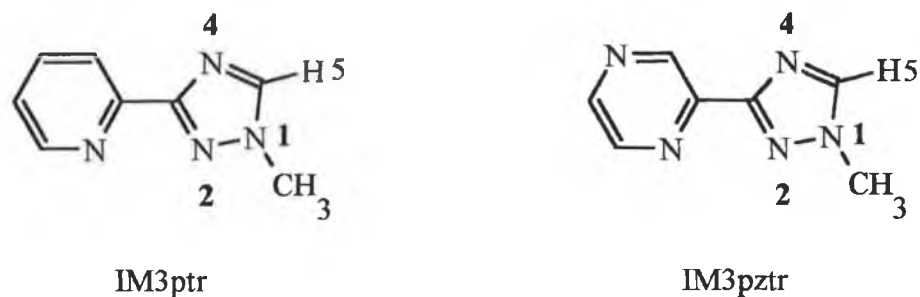


Figure 6.8 Structures of ligands 1M3ptr and 1M3pztr.

Using this analogy H5 of the triazole in  $H_2L4$  is equivalent to H5 of 1M3ptr and 1M3pztr. In 1M3ptr, H5 was observed to shift downfield by +0.12 ppm compared to the free ligand in the N4-coordinated isomer, whilst a greater downfield shift of +0.25 ppm was found for the N2-coordinated isomer. In the case of 1M3pztr, a downfield shift of +0.53 ppm was observed for H5 upon N4 coordination of  $Ru(bpy)_2$ . This value is comparable to that observed here for  $H_2L4$ . N4 coordination was also assigned in the case of the structurally similar ligand 1,3-bis(2-pyridyl)-1,2,4-triazole (bptn)<sup>19</sup> where the resonance associated with H5 was observed at 9.59 ppm (in acetone- $d_6$ ) (Fig. 6.9).

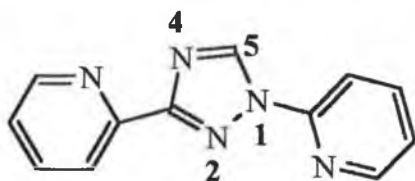


Figure 6.9 Structure of the ligand 1,3-bis(2-pyridyl)-1,2,4-triazole.

From the proton resonance data it is not possible to unambiguously assign the coordination mode of  $\text{Ru}(\text{bpy})_2$  to  $\text{H}_2\text{L}_4$  based purely on the observed shifts for this proton alone, particularly since only one product has been obtained and so a comparison between N2 and N4 sites cannot be made. However steric considerations and the previously observed downfield shifts for the N4-coordinated isomers of the ligands 1M3ptr, 1M3pztr and bptn would seem to favour coordination at the pyridyl nitrogen and N4 of the triazole ring.

In the case of **HQ-RuRu** however, two closely spaced resonances associated with the triazole H5 proton are observed. Furthermore a splitting of the hydroquinone ring protons, in a manner similar to that observed for the mononuclear complex, is also found and two OH resonances occur at approx. 10.5-10.6 ppm. These observations could be accounted for by the following: (i) The dinuclear complex is asymmetric whereby coordination occurs via N2 of one triazole ring and N4 of the other, (ii) the asymmetry arises as a result of different conformations in solution and (iii) a 1:1 mixture of N2/N2 and N4/N4 bound species is present. The latter case may be ruled out by the observation of only one sharp peak using HPLC analysis of the product and the overall simplicity of the NMR spectrum. It is also unlikely that both isomers would exist in exactly a 1:1 mixture. The observed shifts associated with H5 in **HQ-RuRu** correspond to that found for the H5 resonance of the bound pyridyltriazole ring in **HQ-Ru**. If the same arguments are applied in this case then it appears likely that coordination of the  $\text{Ru}(\text{bpy})_2$  units occurs either via N4/N2 or N4/N4. It is also interesting to note that the spectrum obtained in acetonitrile differs considerably with respect to the resonances associated with H5 and the hydroxyl groups. The latter are absent, whilst the former occur as a doublet at 8.63 ppm (Fig. 6.10).

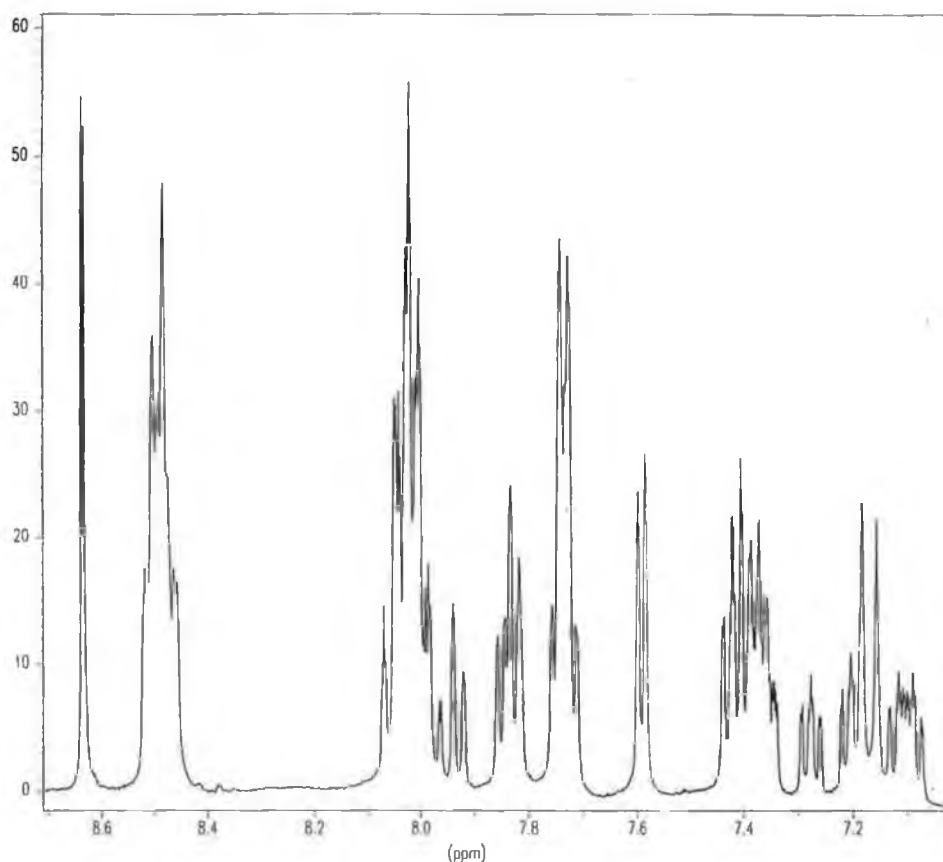


Figure 6.10  $^1\text{H-NMR}$  spectrum of **HQ-RuRu** in  $d_3$ -acetonitrile.

It is very difficult to unambiguously assign a coordination mode to these complexes. The data available is not sufficient to support one mode of coordination over the other and more detailed experiments such as NOE or NOESY may prove to be helpful in making a complete structural assignment. NOE has been previously used by Fennema *et al* in the elucidation of the structure of the  $\text{Ru}(\text{bpy})_2$  complex of the ligand 3,3'-dimethyl-5,5'-bis-1,2,4-triazole<sup>20</sup> and for other ruthenium polypyridyl complexes<sup>21</sup>. The preparation of deuterated complexes using  $\text{Ru}(d_8\text{-bpy})_2\text{Cl}_2$  would also greatly simplify the spectra and hence aid identification of resonances associated with  $\text{H}_2\text{L}4$ <sup>22</sup>.

### 6.3.3 Electronic Properties.

The electronic data for the complexes **HQ-Ru** and **HQ-RuRu** are presented in Table 6.2.

**Table 6.2** *Electronic data for the complexes HQ-Ru and HQ-RuRu. All measurements carried out in acetonitrile unless otherwise stated.*

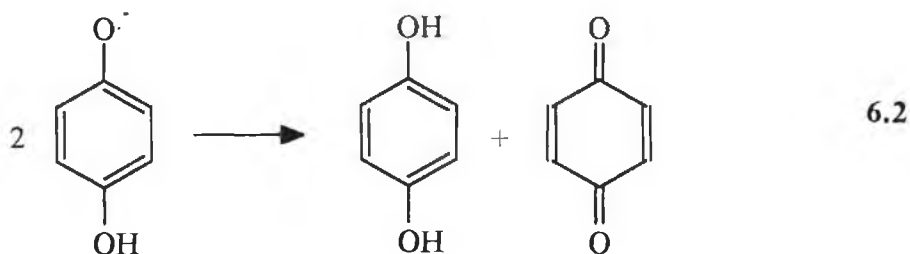
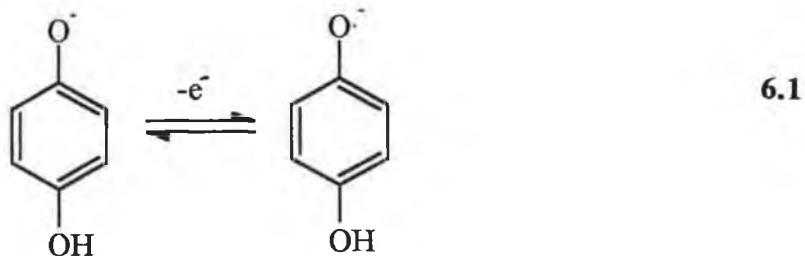
| Complex                                   | Absorption   | Emission $\lambda_{\max}/\text{nm}$ |                  | Lifetime          | $\Phi_{\text{em}}^c$ |
|---|--|-------------------------------------|------------------|-------------------|----------------------|
|   | $\lambda_{\max}/\text{nm}$<br>( $\epsilon/10^4 \text{ M}^{-1} \text{ cm}^{-1}$ ) | 300K                                | 77K <sup>a</sup> | (ns) <sup>b</sup> |                      |
| <b>HQ-Ru</b>                              | 447 (1.22)   | 610                                 | 582              | 92                | $2.2 \times 10^{-4}$ |
| <b>HQ-RuRu</b>                            | 447 (2.11), 426  | 613                                 | 583              | 210               | $1.3 \times 10^{-4}$ |
| <b>[Ru(bpy)<sub>3</sub>]<sup>2+</sup></b> | 452 (1.29)   | 608                                 | 582              | 170               |                      |

<sup>a</sup> measured in ethanol/methanol (4:1 v/v) <sup>b</sup> measured under deaerated conditions.

<sup>c</sup> measured in acetonitrile under aerated conditions.

As expected the complexes exhibit MLCT bands at around 450 nm and intense absorptions at wavelengths below 300 nm associated with  $\pi-\pi^*$  ligand-based transitions. The energies of the MLCT bands are comparable to  $[\text{Ru}(\text{bpy})_3]^{2+}$ . This suggests, as was found for the *N*-substituted ligand L3, that the  $\sigma$ -donor properties of the ligand H<sub>2</sub>L4 are considerably reduced compared to the normal unsubstituted triazolate bridges. It is clear that adding a substituent on the nitrogen of the triazole ring greatly affects the electronic  $\sigma$ -donor and  $\pi$ -acceptor properties of the bridging ligand. The ligand appears to become more like 2,2'-bipyridyl in terms of its  $\sigma$ -donor/ $\pi$ -acceptor properties. The shape of the MLCT band observed for both **HQ-Ru** and **HQ-RuRu** also deserves a mention. It shows the characteristic low energy shoulder at its  $\lambda_{\max}$ , characteristic of 1,2,4-triazole systems. This was observed for the

N4-bound isomers of 1M3ptr and L3 and would therefore seem to support an assignment of N4 coordination. Increasing the pH causes significant changes in the absorption spectra of both **HQ-Ru** and **HQ-RuRu** (Figs. 6.11,6.12). A slight shift in the absorption maximum to lower energy occurs which is accompanied by a broadening of the MLCT band with tailing in the region 600-700 nm. Significant changes also occur in the region 340-370 nm which are associated with the hydroquinone moiety (Sections 3.3.2 and 6.3.4). It is important to note that the changes are not fully reversible and are therefore probably associated with the formation of semiquinone and subsequently quinone species in solution. The spontaneous production of semiquinone radical species in basic solution has been previously reported (Equation 6.1). Furthermore, the semiquinone radical species thus formed can undergo disproportionation to form the corresponding hydroquinone and quinone species (Equation 6.2).



In order to verify this it would be necessary to prepare the quinone analogues of **HQ-Ru** and **HQ-RuRu** and/or to isolate the species formed from basic solution.

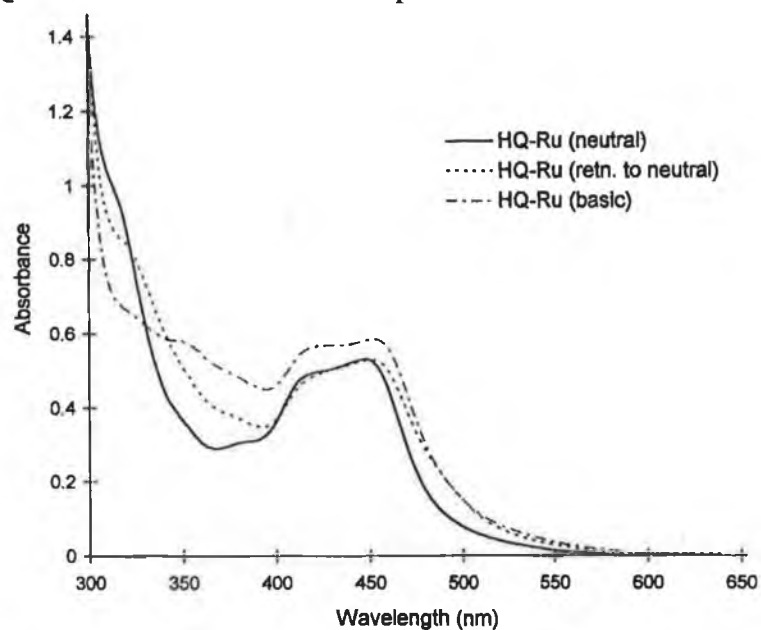


Figure 6.11 Absorption spectra of **HQ-Ru** in neutral and basic acetonitrile and of solution upon returning to neutral solution by adding acid to **HQ-Ru** (basic).

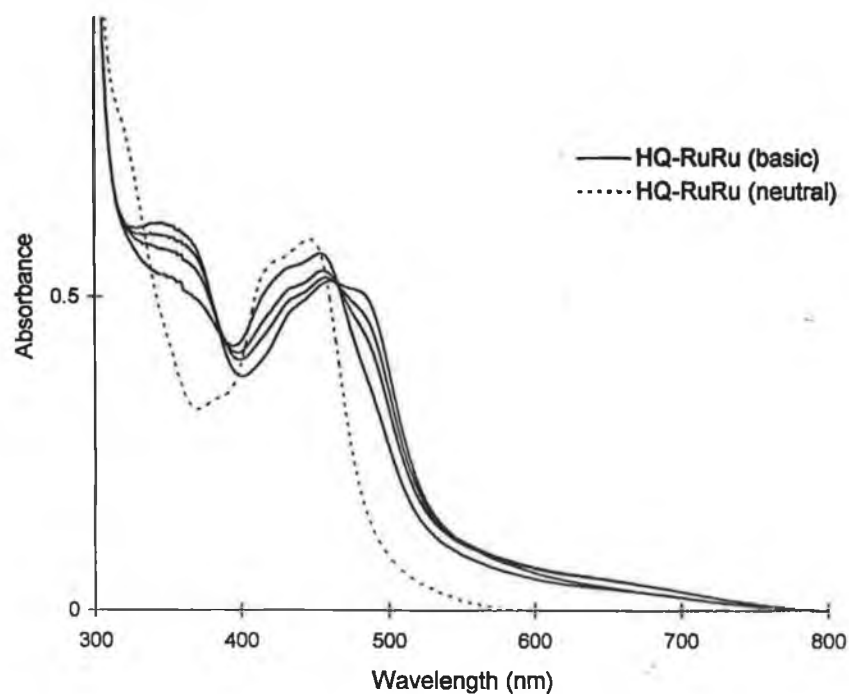
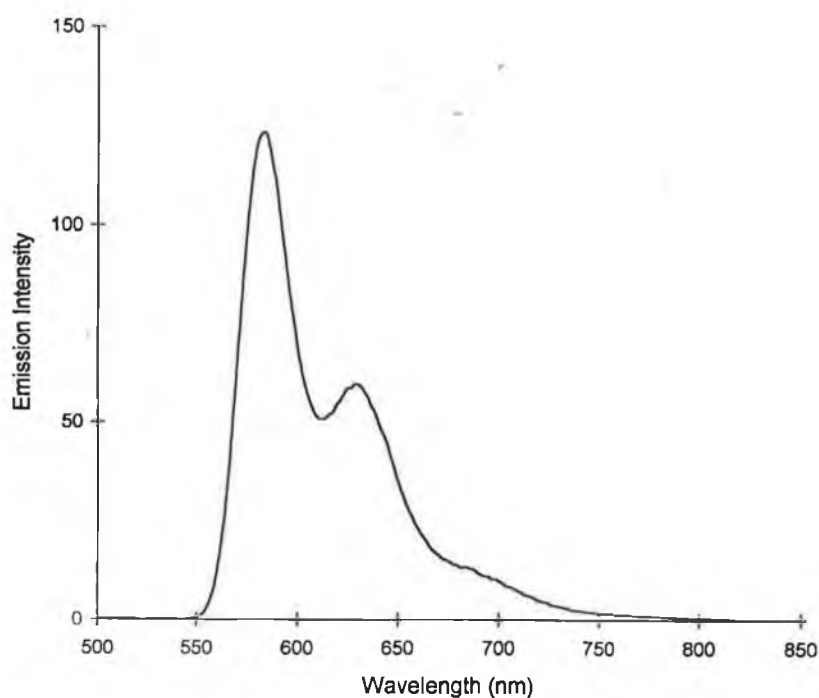


Figure 6.12 Spectral changes which occur for **HQ-RuRu** upon addition of base.

Both complexes exhibit room temperature emissions associated with decay from the  $^3\text{MLCT}$  state. At neutral pH the emission is observed at around the same energy as that found for  $[\text{Ru}(\text{bpy})_3]^{2+}$ . It would appear upon examination of the first reduction potentials for both **HQ-Ru** and **HQ-RuRu** that the emission is bpy-based (*vide infra*).

At 77 K the emissions are shifted to higher energy as a result of solvent-rigidochromic effects which have been previously discussed in Chapter 4. Vibrational fine structure is also evident as shown by the intense shoulder at 633 nm (Fig. 6.13). The intensity of the emission also increases. This is associated with the rigid nature of the complex and its environment and also with the fact that there is insufficient thermal energy to populate the strongly deactivating  $^3\text{MC}$  level at 77 K.



*Figure 6.13* Low Temperature emission spectrum of **HQ-RuRu** in ethanol/methanol (4:1)

The emission properties of **HQ-Ru** and **HQ-RuRu** in basic solution are complex. There is a significant red-shift to 673 nm in the emission maximum which is associated with an increase in intensity. This is unexpected as it would be anticipated that quenching of the excited state by the anionic  $\text{HQ}^-$ , semiquinone radical or quinone species formed upon deprotonation would result in a decrease in emission intensity. As was seen for the absorption spectra, the pH dependence behaviour of the emission of **HQ-Ru** and **HQ-RuRu** is not reversible. The reason for this is unclear and therefore warrants further investigation.

An examination of the room temperature lifetimes reveal that the mononuclear and dinuclear complexes have relatively long-lived excited states. Given that considerably shorter lifetimes are usually observed for complexes containing N-substituted triazoles ligands, this might suggest that the hydroquinone moiety plays a significant role in determining the excited state properties of **HQ-Ru** and **HQ-RuRu**.

#### **6.3.4 Acid-Base Properties.**

The changes in the absorption spectra of **HQ-RuRu** upon increasing the pH are shown in Fig. 6.14. As expected one ground-state pKa associated with protonation/deprotonation of the hydroquinone hydroxyl group is observed. This equilibrium is associated with a change in absorbance at around 350-370 nm. The absorbances in this region are associated with  $\pi-\pi^*$  transitions of the hydroquinone hydroxyl groups. At basic pH a slight increase in intensity of the high energy side of the MLCT band (430 nm) is observed. This may be associated with formation of semiquinone radical species which are known to absorb in the region 400-440 nm<sup>23</sup>.

Isobestic points are only maintained for 2-3 pH units. At high pH the situation becomes more complex. Since the titrations have been performed in aqueous solution it is likely that there are additional intermediates such as semiquinone radicals being formed<sup>24</sup>. The formation of intermediates such as semiquinone radicals and products from disproportionation reactions makes an analysis difficult and prone to errors. In addition, the acid-base chemistry of the complexes is not reversible as noted in Section 6.3.3. Nevertheless pKa values of 9.55 and 9.75 ( $\pm 0.10$ ) are calculated for **HQ-Ru** and **HQ-RuRu**, respectively. That these compare well within experimental error with the pKa of the free ligand ( $9.70 \pm 0.10$ ) suggests that coordination has little influence on the electronic distribution of the hydroquinone moiety.

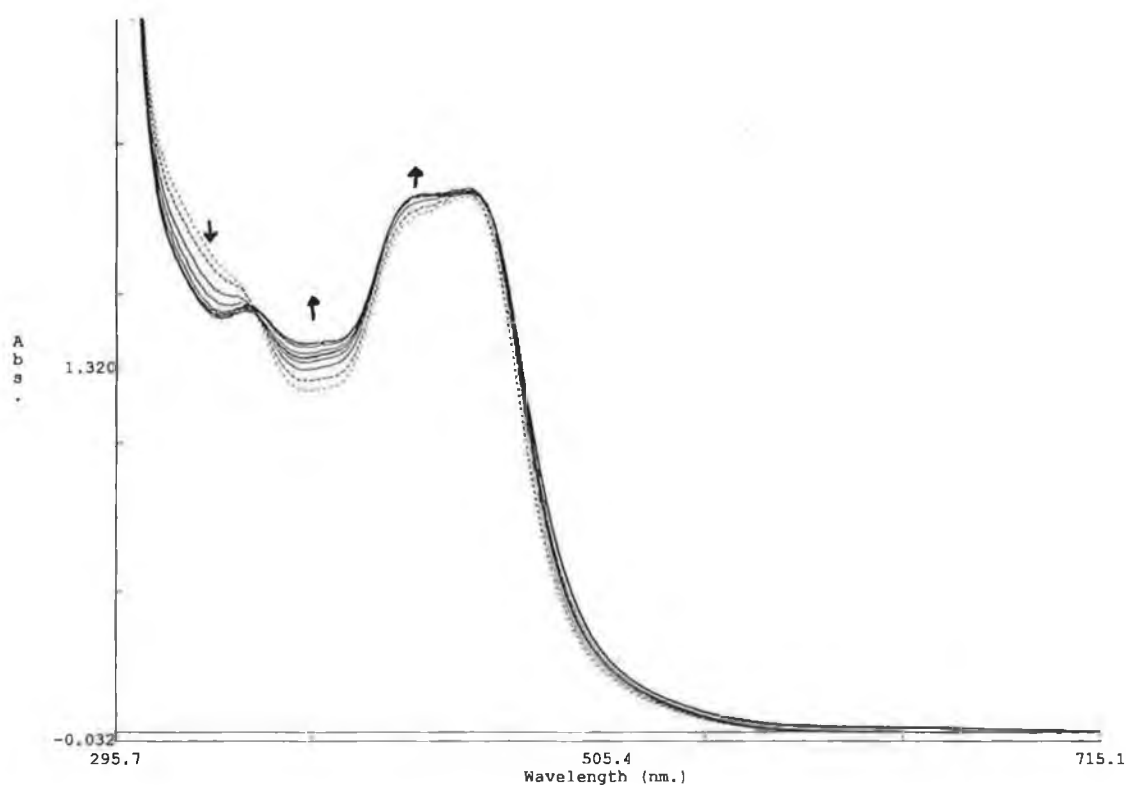
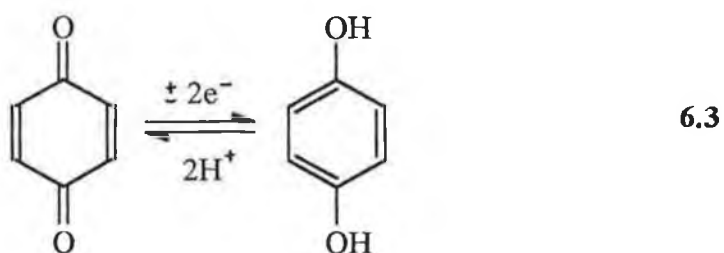


*Figure 6.14 Spectral changes which occur for HQ-RuRu during pKa titration (pH = 7-12)*

### 6.3.5 Electrochemistry and Spectroelectrochemistry.

The redox potentials of the ligand H<sub>2</sub>L4 and its mononuclear and dinuclear ruthenium bipyridyl complexes are presented in Table 6.3.

The electrochemistry of the ligand features oxidation of the hydroquinone moiety to form the corresponding quinone. The quinone/hydroquinone couple may be represented as shown by the half-reaction in Equation 6.3:



In aprotic solvents quinones are reduced in two successive electrochemically reversible steps involving the formation of a semiquinone radical intermediate as shown in Equation 6.4:

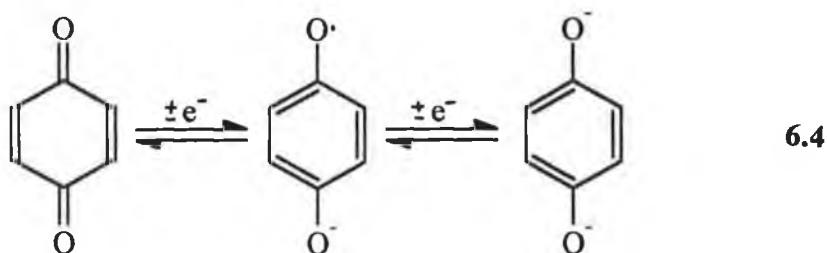


**Table 6.4** *Relevant redox parameters for the ligand H<sub>2</sub>L4 and its ruthenium mononuclear and dinuclear complexes. All measurements carried out in Acetonitrile containing 0.1 M TEAP. All potentials in V vs SCE.*

| Compound                    | Oxidation Potential                 |                      | Reduction Potential      |
|-----------------------------|-------------------------------------|----------------------|--------------------------|
|                             | E <sub>redox</sub> (ligand),(ΔE(V)) | Ru <sup>II/III</sup> |                          |
| H <sub>2</sub> L4 (neutral) | 0.65 (0.38)                         |                      |                          |
| H <sub>2</sub> L4 (basic)   | -0.03 (0.08)                        |                      |                          |
| H <sub>2</sub> L4 (acidic)  | 1.15 (0.94)                         |                      |                          |
| HQ-Ru (neutral)             | 1.18 (irr.)                         | 1.30                 | -1.50 (irr), -1.69 (irr) |
| HQ-Ru (basic)               | 0.35                                | 1.28                 |                          |
| HQ-Ru (acidic)              | 1.12 (irr.)                         | 1.30                 |                          |
| HQ-RuRu (neutral)           | 1.18 (irr.)                         | 1.28                 | -1.53 (irr), -1.72 (irr) |
| HQ-RuRu (basic)             | 0.22                                | 1.29                 |                          |
| HQ-RuRu (acidic)            | 1.15(irr.)                          | 1.30                 |                          |

The ligand H<sub>2</sub>L4 exhibits a two electron quasi-reversible redox wave at 0.65 V under neutral conditions associated with oxidation of the hydroquinone moiety to the corresponding quinone unit (Fig. 6.15). Protonation results in an increase in current and a decrease in reversibility. This effect has also been observed by T. Keyes for the ligand 3-(2,5-dihydroxyphenyl)-5-(2-pyridyl)-1,2,4-triazole<sup>13</sup> (Fig. 6.3). In addition upon performing multiple scans at low pH evidence for polymerisation onto the electrode surface is observed.

The addition of base results in a cathodic shift in the oxidation potential of the ligand and is accompanied by a change in colour of the solution from colourless to yellow. This is probably due to increased electron density on the ligand as a result of the negative charges on the oxygens upon deprotonation. The process also becomes more reversible at higher pH (Fig. 6.16).

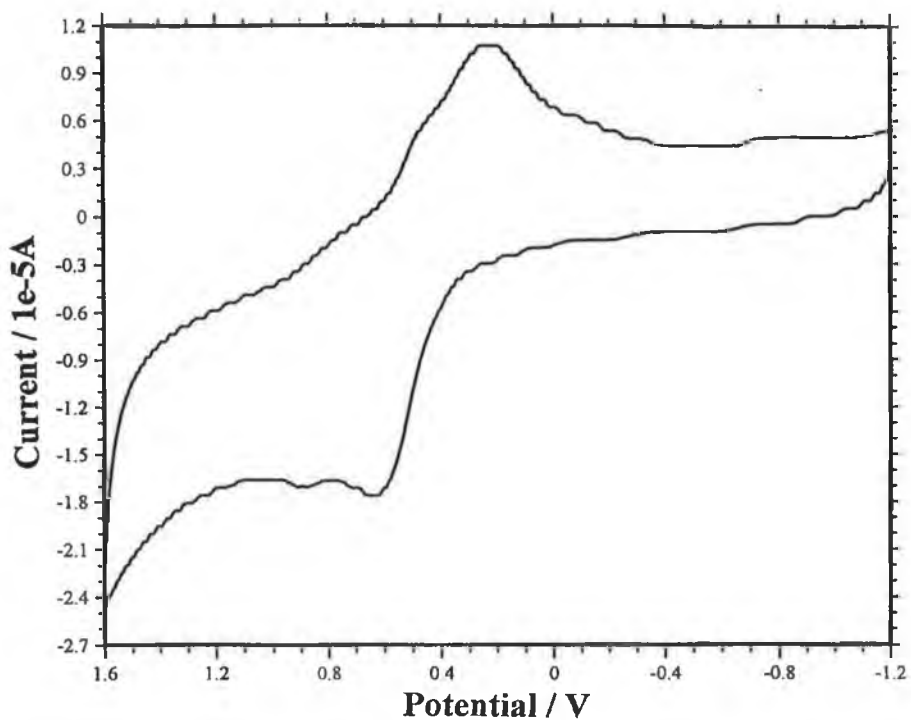


Figure 6.15 Cyclic voltammogram of  $H_2L4$  in neutral acetonitrile.

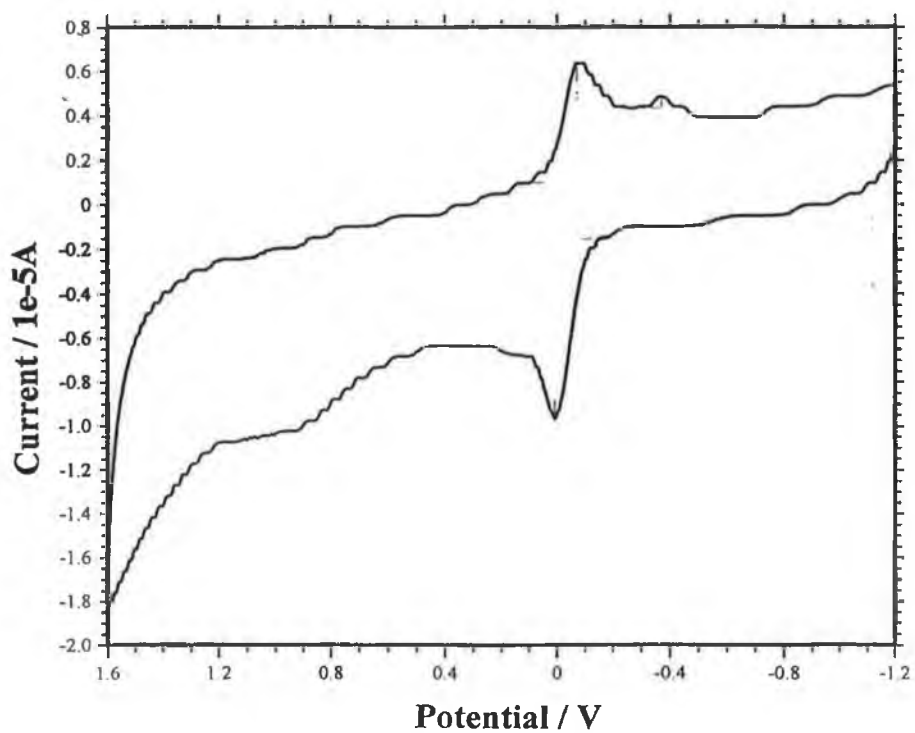


Figure 6.16 Cyclic voltammogram of  $H_2L4$  in basic acetonitrile solution.

For the metal complexes two oxidation processes are observed, associated with the oxidation of the hydroquinone moiety of H<sub>2</sub>L4 and the Ru<sup>II</sup>/Ru<sup>III</sup> couple, respectively (Fig. 6.17). Coulometry experiments need to be performed on the metal complexes to determine the exact nature of the redox processes observed. The Ru<sup>II</sup>/Ru<sup>III</sup> couples in both the mononuclear and dinuclear complexes occur at similar potentials to those observed for the *N*-substituted ligand L3. This perhaps suggests that the hydroquinone ring has little effect on the ground state properties of the complexes<sup>25</sup>.

However it should be noted that the true oxidation potential of the metal in **HQ-Ru** and **HQ-RuRu** cannot be determined as this redox couple is preceded by oxidation of the hydroquinone moiety. Therefore what is actually observed is the oxidation of the metal centre associated with the semiquinone or quinone species. As was found for L3 in Chapter 5, the absence of a negative charge on the triazole ring results in a decrease in electron density at the metal centre as the  $\sigma$ -donor capacity of the triazole is diminished.

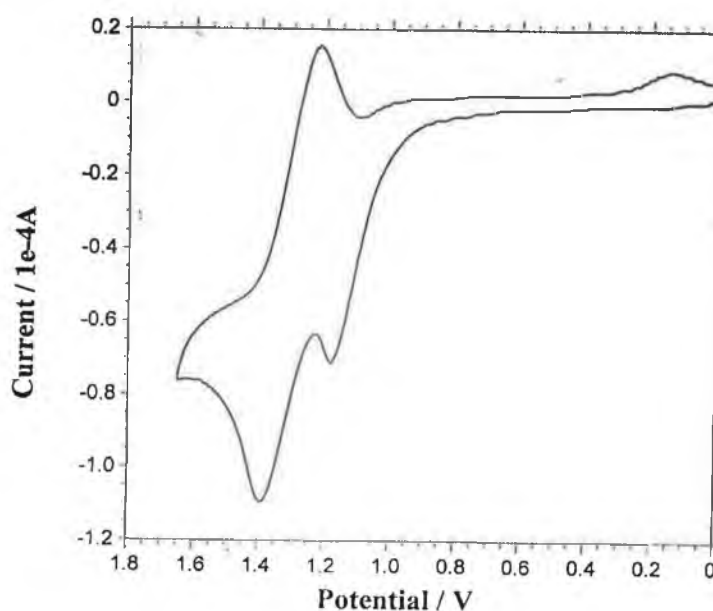


Figure 6.17 Cyclic voltammogram of **HQ-RuRu** in Acetonitrile.

The assignment of the order of the redox processes (ie. oxidation of hydroquinone followed by metal centre) in **HQ-Ru** and **HQ-RuRu** under neutral conditions was verified by spectroelectrochemical measurements (Figs. 6.18, 6.19). Upon oxidation at up to 1.1V the only discernable change in the spectrum is an increase in the intensity of the MLCT band on the high energy side at 422 nm and also in the region around 375 nm (this has already been assigned as being due to transitions associated with the hydroquinone moiety in Section 6.3.4). In addition, a weak, broad tail at lower energy around 600 nm appears. These are changes which were already associated with the hydroquinone ring from an examination of the acid-base behaviour. It suggests that the changes which occur are associated with generation of semiquinone and quinone species and correlates with the assignment of hydroquinone oxidation. Oxidation at around 1.2-1.6 V sees the gradual collapse of the MLCT band which provides evidence that the redox process observed in this potential window corresponds to the  $\text{Ru}^{\text{II/III}}$  redox couple. The concomitant growth of a very weak band at 650 nm and 850 nm for **HQ-Ru** and **HQ-RuRu**, respectively is also observed. In the case of the mononuclear complex this band is attributed to an LMCT transition. However for **HQ-RuRu**, the assignment is not so straightforward. It has been seen in the previous chapters that very weak intervalence transitions are observed for the ruthenium homodinuclear complexes of  $\text{H}_2\text{L}_2$  and  $\text{L}_3$ . Because the band is extremely weak in intensity, it is difficult to say in the case of **HQ-RuRu** whether or not the band observed is due solely to a LMCT transition or to both LMCT and IVCT bands. Further studies would need to be carried out. The generation of  $\text{Ru}(\text{III})$  species is also accompanied by a decrease in intensity and low energy shift of the ligand-based

transitions at  $\lambda < 300$  nm and the formation of the characteristic shoulder at 314 nm typical of Ru(III)-bpy species<sup>26</sup>.

The reduction potentials for the complexes are very similar to those observed in  $[\text{Ru}(\text{bpy})_3]^{2+}$  and are therefore assigned as being bpy-based. As has been seen before desorption spikes result in the irreversible nature of these redox couples<sup>27</sup>.

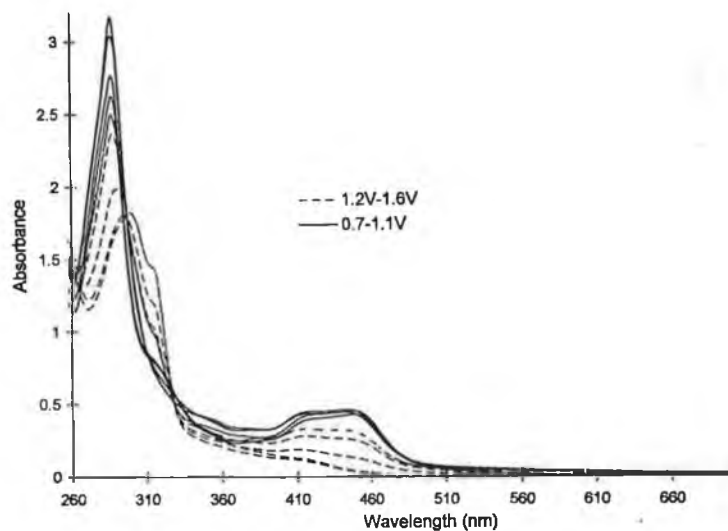


Figure 6.18 Spectral changes during oxidation of HQ-Ru.

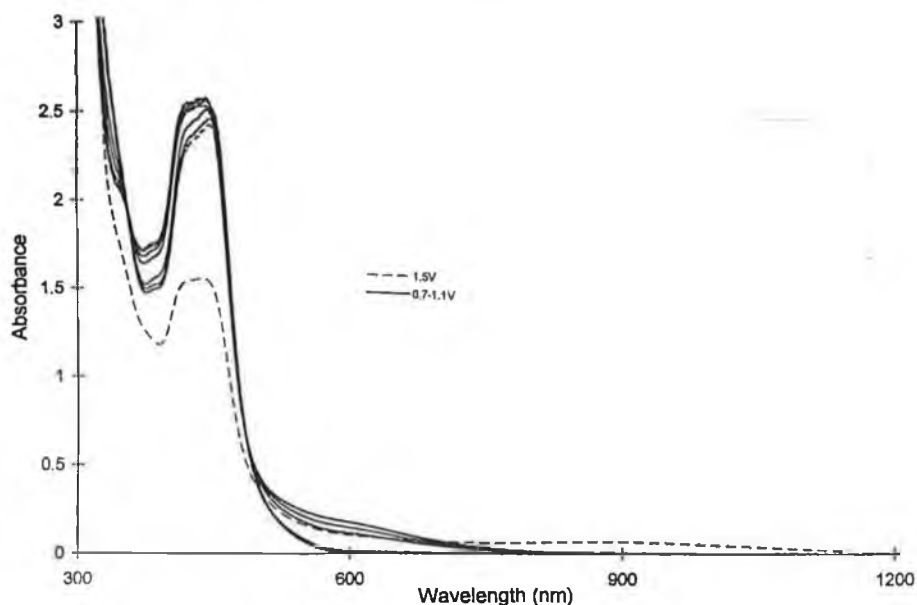


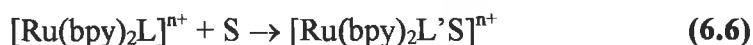
Figure 6.19 Spectral changes which occur during oxidation of HQ-RuRu.

### 6.3.6 Photolysis Studies.

Preliminary photolysis experiments were carried out on **HQ-Ru** and **HQ-RuRu** in neutral and basic acetonitrile solutions. The photolyses were monitored by both HPLC and UV/Vis spectroscopy.

The photoreactivity of ruthenium(II) polypyridyl complexes is known<sup>28</sup>. The photoreactions of complexes of the type  $[\text{Ru}(\text{bpy})_2\text{L}]^{2+}$  involve mainly two processes<sup>29</sup>:

- (i) loss of L and coordination of S **(6.5)**
- (ii) monodentate coordination of L and substitution by S (L' = monodentate bound ligand) **(6.6)**



In coordinating solvents such as acetonitrile, S will usually be the solvent molecule, while in poor coordinating solvents such as dichloromethane, S may be the counterion, added ions or residual water in the solvent.

The spectral changes which occur for **HQ-Ru** and **HQ-RuRu** in neutral acetonitrile upon photolysis are shown in Figs. 6.20 and 6.21, respectively. The similarities for both complexes is striking. Upon photolysis the intensity of the MLCT band, particularly at 447 nm, is seen to decrease. As the photolysis proceeds the MLCT band gradually shifts to 425 nm. The intensity in the region around 350 nm also decreases. Isobestic points at 396 nm and 305 nm are observed.

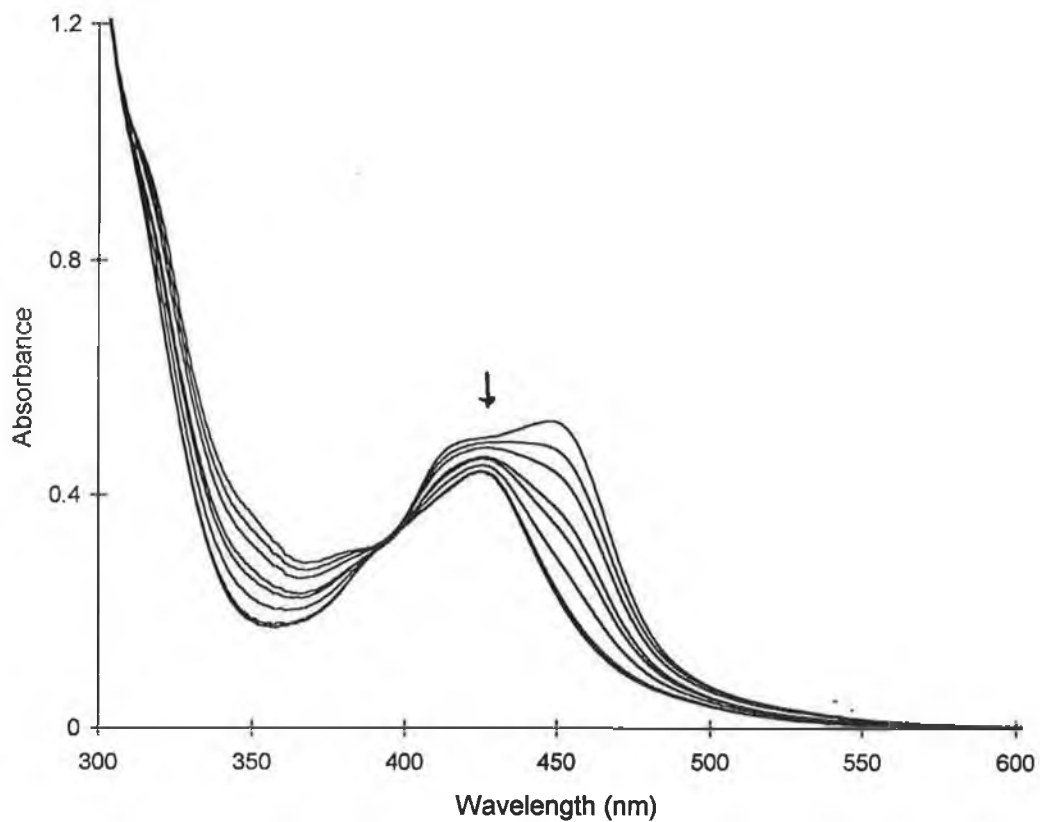


*Figure 6.20* Changes in absorption spectrum of **HQ-Ru** during photolysis in  $CH_3CN$ .

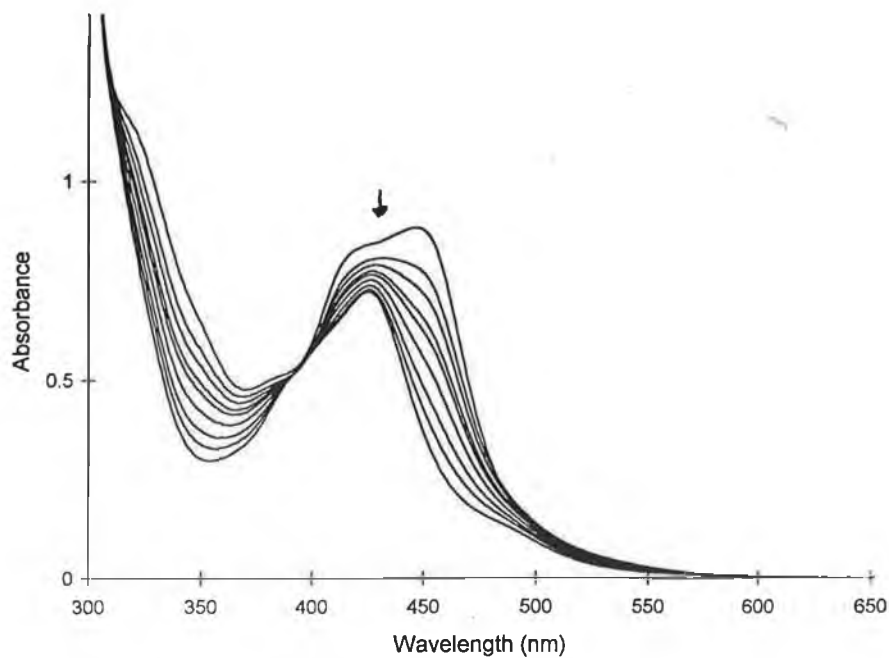


*Figure 6.21* Changes in absorption spectrum of **HQ-RuRu** during photolysis in  $CH_3CN$ .

HPLC analysis of the photolysis of **HQ-Ru** reveals the formation of a photoproduct at 2.2 min (Fig. 6.22). The UV/Vis spectrum of this peak has an absorption maximum of 425 nm and on this basis and the comparison of its retention time with an authentic sample is attributed to  $[\text{Ru}(\text{bpy})_2(\text{MeCN})_2]^{2+}$ . After two hours photolysis this is the only species present in solution.

In the case of the dinuclear complex **HQ-RuRu** HPLC analysis of the photolysis mixture reveals a decrease in the relative concentration of **HQ-RuRu** and the formation of two more species with retention times of 2.2 and 2.78 min. By comparison with **HQ-Ru**, these may be assigned as being due to the bis(acetonitrile) complex  $[\text{Ru}(\text{bpy})_2(\text{MeCN})_2]^{2+}$  and the mononuclear complex, respectively. After 45 min photolysis all the dinuclear complex has decomposed to give **HQ-Ru** and  $[\text{Ru}(\text{bpy})_2(\text{MeCN})_2]^{2+}$ . Further photolysis then sees the photodecomposition of the mononuclear complex to give  $[\text{Ru}(\text{bpy})_2(\text{MeCN})_2]^{2+}$ .

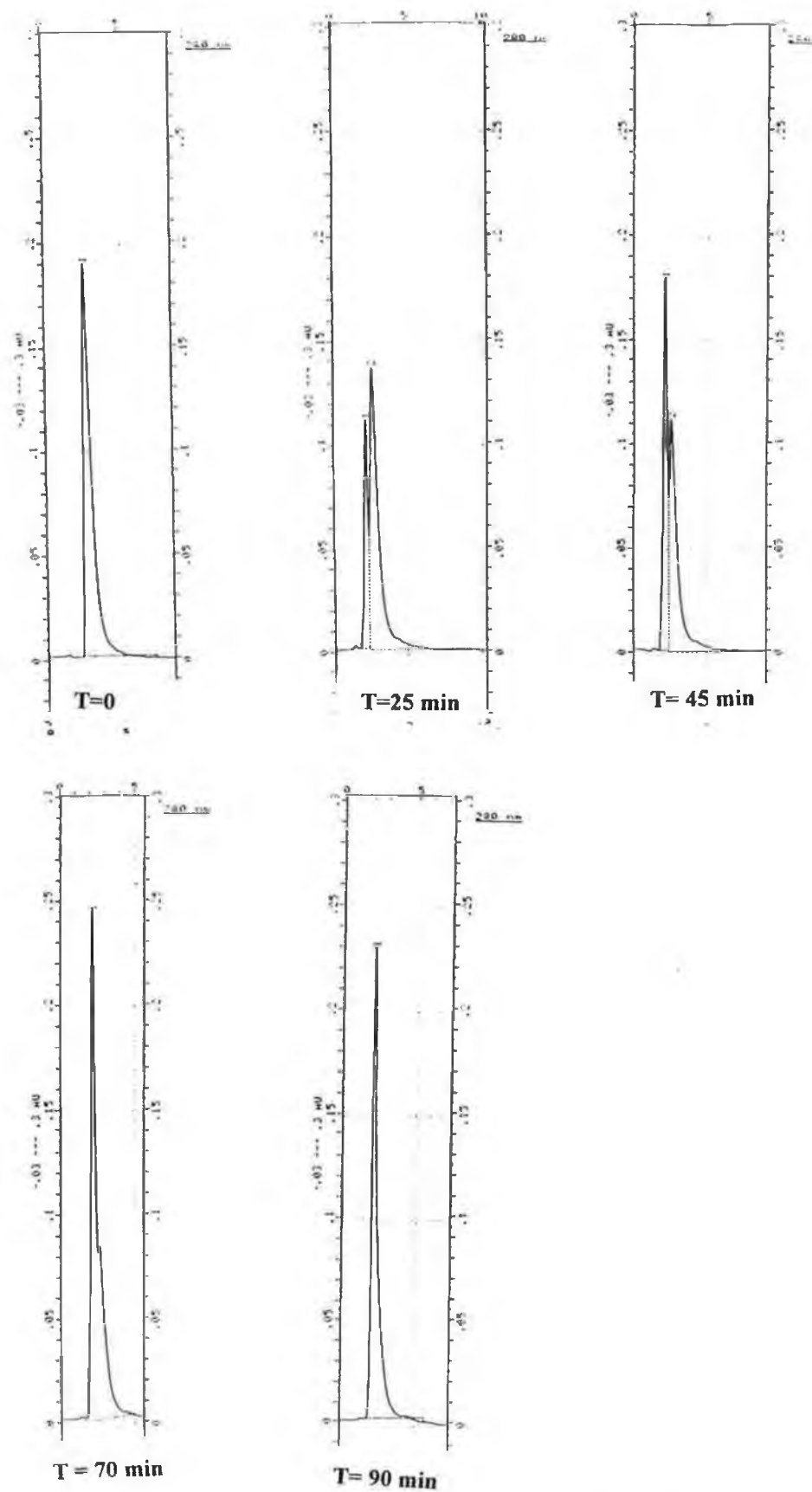
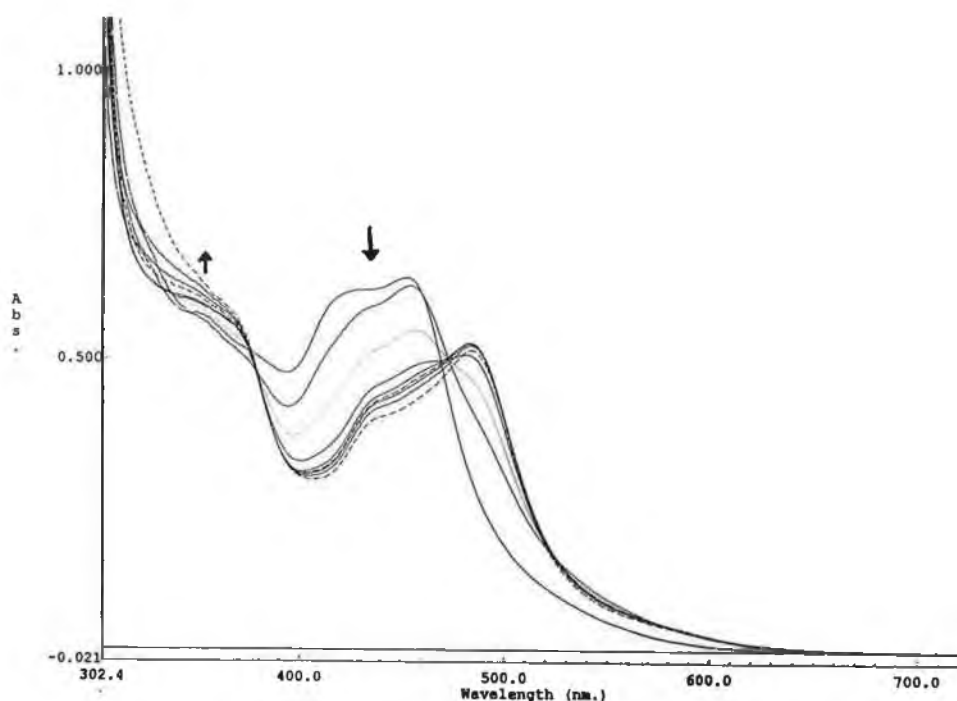


Figure 6.22 HPLC chromatograms obtained during photolysis of HQ-Ru in acetonitrile under neutral conditions).

When the photolysis are performed in basic acetonitrile solution the spectral changes which occur for both complexes **HQ-Ru** and **HQ-RuRu**, although similar, are more complex (Fig. 6.23). In contrast to the photolyses in neutral solution, isobestic points are not maintained. Initially the photolysis results in a decrease in the MLCT band at 447 nm and the formation of a shoulder at lower energy. As the photolysis progresses a spectrum with a broad MLCT band and  $\lambda_{\text{max}}$  at 484 nm is formed.



*Figure 6.23 Changes which occur in the Absorption Spectrum of **HQ-Ru** in basic acetonitrile solution.*

HPLC analysis of the photolysis of **HQ-Ru** in basic solution sees the immediate formation of a photoproduct at 2.89 min, the absorption spectrum of which closely resembles that of the original mononuclear complex. After 30 min photolysis only a

small amount of the deprotonated mononuclear complex is present in solution and an additional peak at 1.89 min appears- this corresponds to free ligand. Further photolysis for 1 hr 20 min sees little change in the ratio of the two photoproducts.

The photolysis of **HQ-RuRu** when deprotonated is also quite complex (Fig. 6.24). Deprotonation sees the immediate formation of three photoproducts at 1.41, 2.04 and 2.72 min in addition to the deprotonated dinuclear complex (4.23 min). After just 20 min, the chromatogram has been greatly simplified, showing predominantly one peak at 2.71 min and two minor peaks at 1.43 and 1.89 min. The main photoproduct appears to be the same as that formed during photolysis of the mononuclear complex by comparison of the retention times and UV/Vis absorption spectra. It appears itself to be photolabile, as suggested by the slight decrease in its abundance after 1.5 hr photolysis. It is difficult to state the nature of the photoproducts formed in basic solution- as has been seen from the absorption spectra, the changes which occur may be associated with a quinone species. More studies would need to be carried out, including the preparative photolysis of both complexes, whereby the photoproducts can be isolated and characterised.

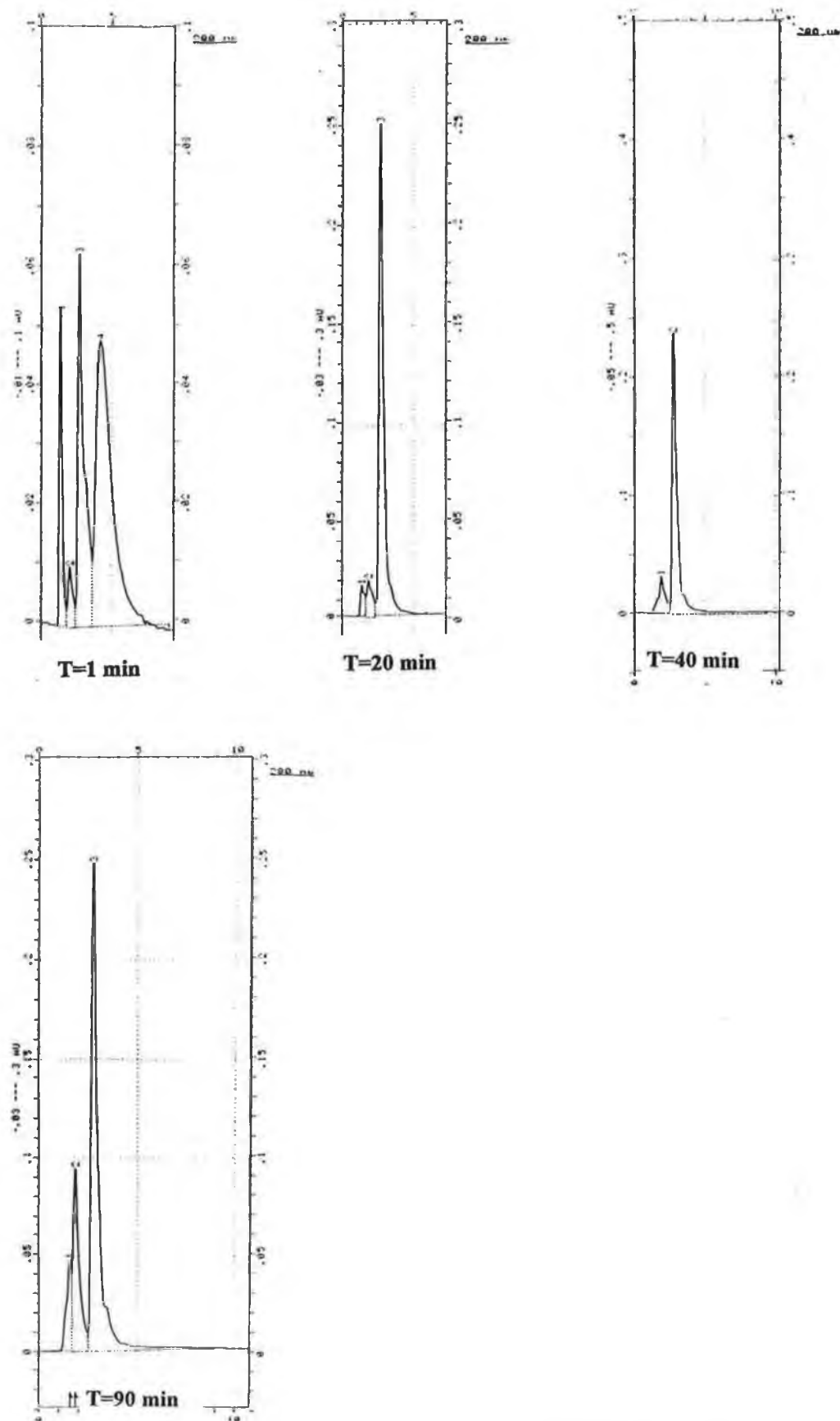


Figure 6.24 HPLC Chromatograms obtained during photolysis of HQ-RuRu in basic acetonitrile solution.

## 6.5 Concluding Comments.

The mononuclear and dinuclear ruthenium complexes of the ligand H<sub>2</sub>L4 have been prepared. Because of the availability of the N2 and N4 coordination sites, the possibility exists for a number of coordination modes. Whilst <sup>1</sup>H-NMR spectroscopy allowed a characterisation of the coordination isomers for the analogously substituted ligand L3, a similar assignment of coordination mode in these complexes has not been possible from NMR studies carried out to date. The application of other techniques, such as NOE and the deuteration of the complexes needs to be carried out.

The presence of the hydroquinone ring introduces a number of complexities in terms of the acid-base behaviour of these compounds. The changes observed do not appear to be completely reversible, and it is proposed that this is due to semiquinone/quinone formation at high pH. It will be necessary to prepare the corresponding quinone complexes in order to clarify the changes observed.

As was found for the other dinuclear complexes in the preceding chapters the similarity in redox couples and absorption and emission data for the mononuclear and dinuclear complexes suggests that the interaction between the metal centres is very weak.

## 6.5 References.

- 1 H. Kurreck and M. Huber, *Angew. Chem. Int. Ed. Engl.*, 1995, 34, 849.
- 2 The Chemistry of the Quinoid compounds; S. Patai, Ed., John Wiley & Sons, New York, 1974; Vol 1, Parts 1 and 2.
- 3 M.R. Wasielewsky, *Chem. Rev.*, 1992, 932, 435.
- 4 D.G. Johnson, M.P. Niemczyk, D.W. Minsek, G.P. Wiederrecht, W.A. Svec, G.L. Gaines III, M.R. Wasielewski, *J. Am. Chem. Soc.*, 1993, 115, 5692.
- 5 M. Haga, E.S. Dodsworth and A.B.P. Lever, *Inorg. Chem.*, 1986, 25, 447.
- 6 M.D. Ward, *Inorg. Chem.*, 1996, 35, 1712.
- 7 V.M. Gooden, H. Cai, T.P. Dasgupta, N.R. Gordon, L.J. Hughes, G.G. Sadler, *Inorg. Chim. Acta.*, 1997, 105.
- 8 H. Masui, A.B.P. Lever and E.S. Dodsworth, *Inorg. Chem.*, 1993, 32, 258.
- 9 H. Masui, A.B.P. Lever and P.R. Auburn, *Inorg. Chem.*, 1991, 30, 2402.
- 10 K.S. Schanze and K. Sauer, *J. Am. Chem. Soc.*, 1988, 110, 1180.
- 11 V. Goulle, A. Harriman, and J.-M. Lehn, *J. Chem. Soc., Chem. Commun.*, 1993, 1034.
- 12 K.A. Opperman, S.L. Mecklenburg and T.J. Meyer, *Inorg. Chem.*, 1994, 33, 5295.
- 13 T.E. Keyes, PhD. Thesis 1994, Dublin City University.
- 14 T.E. Keyes, R.J. Forster, C. Coates, P.M. Jayaweera, J. Mc Garvey and J.G. Vos, *Inorg. Chem.*, in press.
- 15 R. Wang, T.E. Keyes, R. Hage, R.H. Schmehl and J.G. Vos, *J. Chem. Soc. Chem. Commun.*, 1993, 1652.
- 16 P. Belser and A. von Zelewsky, *Helv. Chim. Acta*, 1980, 63, 1675.

- 
- 17 P.J. Steel, F. Lahousse, D. Lerner and C. Marzin, *Inorg. Chem.*, 1983, 22, 1488.
- 18 E.M. Ryan, R. Wang, J.G. Vos, R. Hage and J.G. Haasnoot, *Inorg. Chim. Acta.*, 1993, 208, 49.
- 19 B. Buchanan, Ph.D. Thesis 1989, Dublin City University,.
- 20 B.D.J.R. Fennema, R. Haga, J.G. Haasnoot, J. Reedijk and J.G. Vos, *Inorg. Chim. Acta.*, 1990, 171, 223.
- 21 J.A. Bolger, G. Ferguson, J.P. James, C. Long, P. Mc Ardle and J.G. Vos, *J. Chem. Soc., Dalton Trans.*, 1993, 1577.
- 22 T.E. Keyes, F. Weldon, E. Mueller, P. Pechy, M. Graetzel and J.G. Vos, *J. Chem. Soc., Dalton Trans.*, 1995, 2705.
- 23 N.K. Bridge and G. Porter, *Proc. Roy. Soc. A.*, 1958, 244, 259.
- 24 H.H. Thorp, J.E. Surneski, G.W. Brudvig and R.H. Crabtree, *J. Am. Chem. Soc.*, 1989, 111, 9249.
- 25 A.M.W. Cargill-Thompson, M.C.C. Smailes, J.G. Jeffery and M.D. Ward, *J. Chem. Soc., Dalton Trans.*, 1997, 737.
- 26 G.A. Heath, L.J. Yellowlees and P.S. Braterman, *J. Chem. Soc., Chem. Commun.*, 1981, 287.
- 27 N.E. Tokel-Takvoryan, R.E. Hemingway and A.J. Bard, *J. Am. Chem. Soc.*, 1973, 95, 6582.
- 28 B. Durham, J.V. Caspar, J.K. Nagle and T.J. Meyer, *J. Am. Chem. Soc.*, 1982, 104, 4803.
- 29 D.V. Pinnick and B. Durham, *Inorg. Chem.*, 1984, 23, 1440.

## **Chapter Seven**

### **Final Remarks and Future Work**

In this work, the synthesis and characterisation of a number of novel Ruthenium (II) and Osmium (II) bipyridyl mononuclear and dinuclear complexes containing aryl-substituted 1,2,4-triazole ligands is described. In studying the photophysical and electrochemical properties of these compounds, particular attention has been paid to the degree of metal-metal interaction between metal centres in the dinuclear complexes.

It appears from the results obtained that the phenyl moiety is a weak mediator of metal-metal interaction. The first oxidation potential, first reduction potential, and absorption and emission maxima are identical (within experimental error) for the mononuclear and dinuclear complexes studied. The homodinuclear complexes show only one redox wave, without any sign of splitting, associated with oxidation of the metal centre. Further confirmation of a very weak interaction comes from the fact that identical absorption spectra are exhibited by the heterodinuclear Ru/Os complexes and a 1:1 mixture of their homometallic "parent" dinuclear complexes. However, the observation of very weak intervalence band transitions in the region 1000-1500 nm for the RuRu and OsOs complexes of H<sub>2</sub>L2 and L3 indicates that an interaction, albeit very weak, does however exist to a certain extent.

From emission studies there is substantial evidence to suggest that intercomponent energy transfer occurs from the ruthenium bound unit to the osmium bound moiety in these systems. Luminescence associated with both metal centres is observed for the deprotonated RuOs complexes of the ligands H<sub>2</sub>L1 and H<sub>2</sub>L2. Upon protonation almost sole emission from the osmium bound unit is observed. This result is reflected in the emission studies of the RuOs complex of L3, the *N,N*-methylated analogue of H<sub>2</sub>L2, for which predominantly osmium-based luminescence is observed

at room temperature and 77 K. The possibility of energy transfer needs to be examined further in the mixed-metal dinuclear complexes of the ligands H<sub>2</sub>L1, H<sub>2</sub>L2 and L3. It is necessary to compile reliable lifetime data for these complexes using instrumentation capable of measuring lifetimes of the order of 20-30 ns.

The effect of methylation at the N1 site affords an opportunity to isolate coordination isomers of the mononuclear and dinuclear complexes. For the unsubstituted triazole systems of H<sub>2</sub>L1 and H<sub>2</sub>L2 only one coordination mode prevailed *i.e.* via the pyridyl nitrogen and N1 of the triazole ring. The steric effect caused by the phenyl group appeared to be the main reason for this. In the case of L3, however, there is an additional steric effect as the result of the methyl substituent on N1. Two coordination modes are found in the mononuclear complexes, corresponding to binding at N2 site of the triazole and at the pyridyl nitrogen and the N4 site of the triazole. On the basis of ratio of isomers obtained, the former appears to be the preferred mode of coordination, which on the basis of steric effects alone is not surprising. Analysis of the reaction mixtures for the dinuclear complexes revealed the presence of two isomers, the main fraction being the N2/N2 coordinated complex. The isolation and characterisation of the other fraction would be of interest. From the photophysical and electrochemical data obtained for L3 it may be concluded that methylation of the N1 position of the triazole ring results in a ligand with decreased  $\sigma$ -donor capacity and increased  $\pi$ -acceptor capability. This is reflected in the higher oxidation potentials and higher absorption and emission energies observed for the complexes of L3 compared to those of H<sub>2</sub>L2. The ligand appears to become very similar to 2,2'-bipyridyl in terms of its  $\sigma$ -donor/ $\pi$ -acceptor properties and this may have important implications for the photochemical properties of these compounds. The

difference in the photophysical and photochemical properties of the N2 and N4 isomers should be investigated further. Such a study should also involve complexes of the precursor ligand 1M3ptr.

In a similar manner, substitution of N1 of the triazole ring with a hydroquinone moiety introduced a number of coordination possibilities for the Ru(bpy)<sub>2</sub> unit as was seen in Chapter 6. Unfortunately it was not possible to unambiguously assign a coordination mode based purely on the chemical shifts observed. The work carried out in this chapter needs to be revisited and extended. If possible, crystal structures for the complexes should be obtained. The deuterated analogues should also be prepared using Ru(d<sub>8</sub>-bpy)<sub>2</sub>Cl<sub>2</sub> in an attempt to elucidate the coordination mode. In addition the application of other NMR techniques such as NOE experiments, <sup>99</sup>Ru or <sup>15</sup>N NMR may prove helpful in this regard. In order to clarify the spectral changes which occur upon deprotonation of the hydroquinone hydroxyls, the corresponding quinone complexes should be prepared and characterised. Furthermore, the isolation and characterisation of the species formed in basic solution could also be attempted. Much work is required regarding an investigation of photoinduced electron transfer and excited state quenching in these complexes and transient absorption studies need to be carried out. The photostability of the complexes in other solvents such as dichloromethane should also be investigated.

## **Appendix 1**

Table 1. Crystal data and structure refinement for 1.

|                                      |  |
|--------------------------------------|--|
| Identification code                  | frances1   |
| Empirical formula                    | $C_{40}H_{30}F_6N_{10}O_{0.40}PRu$   |
| Formula weight                       | 903.18   |
| Temperature                          | 293(2) K   |
| Wavelength                           | 0.71073 Å  |
| Crystal system                       | ?  |
| Space group                          | ?  |
| Unit cell dimensions                 | $a = 31.254(8)$ Å $\alpha = 90^\circ$<br>$b = 27.204(5)$ Å $\beta = 90^\circ$<br>$c = 11.075(3)$ Å $\gamma = 90^\circ$ |
| Volume, Z                            | $9416(4)$ Å <sup>3</sup> , 10  |
| Density (calculated)                 | $1.593$ Mg/m <sup>3</sup>  |
| Absorption coefficient               | $0.536$ mm <sup>-1</sup>   |
| F(000)                               | 4562   |
| Crystal size                         | ? x ? x ? mm   |
| $\theta$ range for data collection   | 2.09 to $20.17^\circ$  |
| Limiting indices                     | $-30 \leq h \leq 30$ , $-26 \leq k \leq 1$ , $-1 \leq l \leq 10$   |
| Reflections collected                | 10405  |
| Independent reflections              | 4449 ( $R_{int} = 0.1774$ )  |
| Refinement method                    | Full-matrix least-squares on $F^2$   |
| Data / restraints / parameters       | 4445 / 0 / 276   |
| Goodness-of-fit on $F^2$             | 1.940  |
| Final R indices [ $I > 2\sigma(I)$ ] | $R1 = 0.1645$ , $wR2 = 0.3864$   |
| R indices (all data)                 | $R1 = 0.2391$ , $wR2 = 0.4171$   |
| Largest diff. peak and hole          | $1.509$ and $-0.537$ eÅ <sup>-3</sup>  |

Table 2. Atomic coordinates [ $\times 10^4$ ] and equivalent isotropic displacement parameters [ $\text{\AA}^2 \times 10^3$ ] for 1.  $U(\text{eq})$  is defined as one third of the trace of the orthogonalized  $U_{ij}$  tensor.

|       | x       | y         | z         | $U(\text{eq})$ |
|-------|---------|-----------|-----------|----------------|
| Ru(1) | 6298(1) | 9772(1)   | 1988(2)   | 72(1)          |
| N(12) | 6682(5) | 10249(6)  | 2956(19)  | 63(5)          |
| N(10) | 6400(5) | 9199(6)   | 3177(18)  | 61(5)          |
| N(9)  | 6267(5) | 10382(5)  | 837(18)   | 52(5)          |
| N(8)  | 5827(5) | 9395(6)   | 1035(20)  | 59(5)          |
| N(7)  | 4588(6) | 6776(7)   | -7106(21) | 78(6)          |
| C(7)  | 4867(6) | 8185(7)   | -3072(21) | 48(5)          |
| C(8)  | 5174(8) | 6390(9)   | -8296(27) | 86(8)          |
| C(9)  | 5461(6) | 8619(8)   | -2230(25) | 65(6)          |
| N(6)  | 4312(5) | 7455(6)   | -5394(19) | 70(5)          |
| C(11) | 5205(6) | 8761(7)   | -1178(22) | 52(6)          |
| N(5)  | 5728(5) | 10046(6)  | 2734(19)  | 62(5)          |
| N(4)  | 4315(5) | 7785(6)   | -4503(19) | 66(5)          |
| N(3)  | 6817(6) | 9442(6)   | 1235(22)  | 74(6)          |
| N(2)  | 4995(4) | 7591(5)   | -4745(16) | 49(4)          |
| C(19) | 5317(6) | 6990(7)   | -6605(23) | 59(6)          |
| C(20) | 5288(7) | 8340(8)   | -3186(24) | 68(7)          |
| C(22) | 4729(6) | 7854(7)   | -4094(22) | 51(6)          |
| N(1)  | 5128(5) | 9354(5)   | 450(16)   | 45(4)          |
| C(26) | 4614(7) | 8328(8)   | -2143(24) | 65(6)          |
| C(27) | 5309(7) | 10489(8)  | 4109(27)  | 79(7)          |
| C(28) | 4780(6) | 8612(7)   | -1171(22) | 56(6)          |
| N(7)  | 5795(5) | 9075(6)   | 124(19)   | 58(5)          |
| C(30) | 4929(8) | 10370(9)  | 3577(28)  | 79(7)          |
| C(32) | 5364(6) | 9082(7)   | -220(23)  | 56(6)          |
| C(33) | 6140(6) | 8727(8)   | -219(26)  | 70(7)          |
| C(34) | 4888(7) | 7022(8)   | -6470(26) | 67(7)          |
| C(35) | 5351(6) | 9899(6)   | 2246(21)  | 48(6)          |
| C(36) | 5417(6) | 9524(7)   | 1160(22)  | 51(6)          |
| C(37) | 4976(6) | 10041(8)  | 2610(23)  | 60(6)          |
| C(41) | 4733(7) | 6471(8)   | -7998(25) | 77(7)          |
| C(42) | 5725(7) | 10369(8)  | 3657(27)  | 71(7)          |
| C(45) | 5462(8) | 6676(10)  | -7506(33) | 99(9)          |
| C(50) | 6991(7) | 9588(8)   | 168(28)   | 76(7)          |
| C(53) | 3918(7) | 8003(9)   | -4172(27) | 88(8)          |
| C(59) | 4739(6) | 7374(7)   | -5510(21) | 56(6)          |
| C(2)  | 6247(8) | 8784(9)   | 5142(30)  | 90(8)          |
| C(4)  | 6181(7) | 9151(8)   | 4167(27)  | 74(7)          |
| C(6)  | 7098(7) | 11007(8)  | 4138(26)  | 73(7)          |
| C(10) | 7268(8) | 8711(9)   | 1331(29)  | 87(8)          |
| C(9)  | 6893(7) | 10157(7)  | 3908(26)  | 64(7)          |
| C(8)  | 6941(6) | 8995(7)   | 1909(23)  | 59(6)          |
| C(12) | 6706(7) | 8912(8)   | 2925(26)  | 72(7)          |
| C(16) | 7357(8) | 9324(10)  | -389(31)  | 104(9)         |
| C(7)  | 6839(7) | 8530(9)   | 3704(29)  | 80(8)          |
| C(21) | 6676(6) | 10720(8)  | 2417(26)  | 63(6)          |
| C(4)  | 7099(7) | 10530(10) | 4530(28)  | 91(8)          |
| C(5)  | 6607(9) | 8472(11)  | 4665(33)  | 111(10)        |

|        |         |          |          |        |
|--------|---------|----------|----------|--------|
| C(16)  | 6452(7) | 10787(8) | 1338(25) | 64(6)  |
| C(15)  | 7463(8) | 8861(10) | 273(32)  | 102(9) |
| C(221) | 6902(7) | 11126(8) | 3084(25) | 73(7)  |
| C(222) | 6080(7) | 10403(8) | -92(28)  | 69(7)  |

|        |          |           |           |         |
|--------|----------|-----------|-----------|---------|
| C(233) | 6060(8)  | 10807(10) | -897(30)  | 90(8)   |
| C(225) | 6234(7)  | 11249(8)  | -403(26)  | 79(8)   |
| C(224) | 6443(7)  | 11241(9)  | 664(27)   | 78(8)   |
| O(10)  | 3725(11) | 7500      | -7500     | 65(11)  |
| O(9)   | 5906(6)  | 7531(8)   | -4599(22) | 34(6)   |
| O(8)   | 6527(8)  | 7257(9)   | 3792(29)  | 61(8)   |
| O(7)   | 6130(6)  | 10965(7)  | 5912(25)  | 38(6)   |
| O(6)   | 6963(11) | 12259(15) | 1791(44)  | 99(12)  |
| O(4)   | 3293(8)  | 8341(10)  | -6759(31) | 72(9)   |
| O(3)   | 6631(20) | 9912(21)  | 6915(59)  | 183(23) |
| O(2)   | 6071(13) | 9949(15)  | 6584(44)  | 117(13) |
| O(1)   | 6198(15) | 9501(19)  | 7654(54)  | 139(18) |
| O(21)  | 7201(13) | 7361(16)  | 5553(45)  | 153(17) |
| N(14)  | 6331(20) | 9729(22)  | 7195(60)  | 111(17) |
| O(111) | 7067(17) | 12672(26) | 2123(69)  | 198(26) |
| O(122) | 7172(16) | 9108(19)  | 6742(57)  | 184(21) |

---

Table 3. Bond lengths [ $\text{\AA}$ ] and angles [ $^\circ$ ] for 1.

|                   |          |                   |           |
|-------------------|----------|-------------------|-----------|
| Ru(1)-N(3)        | 2.03(2)  | Ru(1)-N(10)       | 2.06(2)   |
| Ru(1)-N(5)        | 2.10(2)  | Ru(1)-N(12)       | 2.07(2)   |
| Ru(1)-N(9)        | 2.10(2)  | Ru(1)-N(8)        | 2.08(2)   |
| N(12)-C(9)        | 1.27(3)  | N(12)-C(21)       | 1.41(3)   |
| N(10)-C(12)       | 1.27(2)  | N(10)-C(4)        | 1.30(3)   |
| N(9)-C(222)       | 1.19(3)  | N(9)-C(16)        | 1.36(2)   |
| N(8)-N(7)         | 1.34(2)  | N(8)-C(36)        | 1.34(2)   |
| N(7)-C(41)        | 1.37(3)  | N(7)-C(34)        | 1.35(3)   |
| C(7)-C(26)        | 1.35(3)  | C(7)-C(20)        | 1.39(3)   |
| C(7)-C(22)        | 1.51(3)  | C(8)-C(41)        | 1.44(3)   |
| C(8)-C(45)        | 1.48(3)  | C(9)-C(20)        | 1.41(3)   |
| C(9)-C(11)        | 1.47(3)  | N(6)-C(59)        | 1.36(2)   |
| N(6)-N(4)         | 1.33(2)  | C(11)-C(28)       | 1.39(2)   |
| C(11)-C(32)       | 1.46(3)  | N(5)-C(42)        | 1.35(3)   |
| N(5)-C(35)        | 1.35(2)  | N(4)-C(22)        | 1.38(2)   |
| N(4)-C(53)        | 1.42(3)  | N(3)-C(50)        | 1.36(3)   |
| N(3)-C(8)         | 1.48(3)  | N(2)-C(59)        | 1.31(2)   |
| N(2)-C(22)        | 1.31(2)  | C(19)-C(34)       | 1.35(3)   |
| C(19)-C(45)       | 1.39(3)  | N(1)-C(36)        | 1.28(2)   |
| N(1)-C(32)        | 1.28(2)  | C(26)-C(28)       | 1.42(3)   |
| C(27)-C(30)       | 1.36(3)  | C(27)-C(42)       | 1.43(3)   |
| N(7)-C(32)        | 1.40(2)  | N(7)-C(33)        | 1.48(2)   |
| C(30)-C(37)       | 1.40(3)  | C(32)-C(36)       | 1.95(3)   |
| C(34)-C(59)       | 1.50(3)  | C(35)-C(37)       | 1.30(2)   |
| C(35)-C(36)       | 1.59(3)  | C(50)-C(16)       | 1.48(3)   |
| C(2)-C(5)         | 1.51(3)  | C(2)-C(4)         | 1.49(4)   |
| C(6)-C(221)       | 1.36(3)  | C(6)-C(4)         | 1.37(3)   |
| C(10)-C(15)       | 1.38(4)  | C(10)-C(8)        | 1.43(3)   |
| C(9)-C(4)         | 1.39(3)  | C(8)-C(12)        | 1.36(3)   |
| C(12)-C(7)        | 1.41(3)  | C(16)-C(15)       | 1.49(4)   |
| C(7)-C(5)         | 1.30(4)  | C(21)-C(16)       | 1.40(3)   |
| C(21)-C(221)      | 1.50(3)  | C(16)-C(224)      | 1.44(3)   |
| C(222)-C(233)     | 1.42(3)  | C(233)-C(225)     | 1.43(3)   |
| C(225)-C(224)     | 1.35(3)  | O(6)-O(111)       | 1.23(7)   |
| O(6)-O(111)#1     | 1.26(7)  | O(3)-N(14)        | 1.11(6)   |
| O(2)-N(14)        | 1.21(6)  | O(2)-O(1)         | 1.74(7)   |
| O(1)-N(14)        | 0.90(7)  | O(111)-O(6)#1     | 1.26(7)   |
| O(111)-O(111)#1   | 1.25(12) |                   |           |
| N(3)-Ru(1)-N(10)  | 78.8(8)  | N(3)-Ru(1)-N(5)   | 174.2(7)  |
| N(10)-Ru(1)-N(5)  | 98.6(7)  | N(3)-Ru(1)-N(12)  | 91.5(7)   |
| N(10)-Ru(1)-N(12) | 93.1(7)  | N(5)-Ru(1)-N(12)  | 93.7(7)   |
| N(3)-Ru(1)-N(9)   | 97.8(7)  | N(10)-Ru(1)-N(9)  | 173.2(6)  |
| N(5)-Ru(1)-N(9)   | 85.3(7)  | N(12)-Ru(1)-N(9)  | 81.0(7)   |
| N(3)-Ru(1)-N(8)   | 98.0(7)  | N(10)-Ru(1)-N(8)  | 93.5(7)   |
| N(5)-Ru(1)-N(8)   | 77.0(7)  | N(12)-Ru(1)-N(8)  | 169.3(6)  |
| N(9)-Ru(1)-N(8)   | 92.8(7)  | C(9)-N(12)-C(21)  | 123(2)    |
| C(9)-N(12)-Ru(1)  | 127(2)   | C(21)-N(12)-Ru(1) | 110(2)    |
| C(12)-N(10)-C(4)  | 122(2)   | C(12)-N(10)-Ru(1) | 116(2)    |
| C(4)-N(10)-Ru(1)  | 122(2)   | C(222)-N(9)-C(16) | 122(2)    |
| C(222)-N(9)-Ru(1) | 126(2)   | C(16)-N(9)-Ru(1)  | 112(2)    |
| N(7)-N(8)-C(36)   | 100(2)   | N(7)-N(8)-Ru(1)   | 139.3(13) |
| C(36)-N(8)-Ru(1)  | 120(2)   | C(41)-N(7)-C(34)  | 117(2)    |
| C(26)-C(7)-C(20)  | 122(2)   | C(26)-C(7)-C(22)  | 125(2)    |
| C(20)-C(7)-C(22)  | 113(2)   | C(41)-C(8)-C(45)  | 112(2)    |

|                         |               |                          |               |
|-------------------------|---------------|--------------------------|---------------|
| <b>C(20)-C(9)-C(11)</b> | <b>122(2)</b> | <b>C(59)-N(6)-N(4)</b>   | <b>100(2)</b> |
| <b>C(28)-C(11)-C(9)</b> | <b>117(2)</b> | <b>C(28)-C(11)-C(32)</b> | <b>120(2)</b> |
| <b>C(9)-C(11)-C(32)</b> | <b>123(2)</b> | <b>C(42)-N(5)-C(35)</b>  | <b>119(2)</b> |
| <b>C(42)-N(5)-Ru(1)</b> | <b>122(2)</b> | <b>C(35)-N(5)-Ru(1)</b>  | <b>118(2)</b> |

|                      |          |                        |          |
|----------------------|----------|------------------------|----------|
| N(6)-N(4)-C(22)      | 110(2)   | N(6)-N(4)-C(53)        | 118(2)   |
| C(22)-N(4)-C(53)     | 133(2)   | C(50)-N(3)-C(8)        | 125(2)   |
| C(50)-N(3)-Ru(1)     | 123(2)   | C(8)-N(3)-Ru(1)        | 111(2)   |
| C(59)-N(2)-C(22)     | 102(2)   | C(34)-C(19)-C(45)      | 116(2)   |
| C(7)-C(20)-C(9)      | 117(2)   | N(2)-C(22)-N(4)        | 110(2)   |
| N(2)-C(22)-C(7)      | 124(2)   | N(4)-C(22)-C(7)        | 126(2)   |
| C(36)-N(1)-C(32)     | 99(2)    | C(7)-C(26)-C(28)       | 121(2)   |
| C(30)-C(27)-C(42)    | 126(3)   | C(11)-C(28)-C(26)      | 120(2)   |
| N(8)-N(7)-C(32)      | 106(2)   | N(8)-N(7)-C(33)        | 124(2)   |
| C(32)-N(7)-C(33)     | 130(2)   | C(37)-C(30)-C(27)      | 113(2)   |
| N(1)-C(32)-N(7)      | 114(2)   | N(1)-C(32)-C(11)       | 125(2)   |
| N(7)-C(32)-C(11)     | 121(2)   | N(1)-C(32)-C(36)       | 40.5(10) |
| N(7)-C(32)-C(36)     | 73.4(14) | C(11)-C(32)-C(36)      | 165(2)   |
| N(7)-C(34)-C(19)     | 127(2)   | N(7)-C(34)-C(59)       | 118(2)   |
| C(19)-C(34)-C(59)    | 115(2)   | C(37)-C(35)-N(5)       | 125(2)   |
| C(37)-C(35)-C(36)    | 123(2)   | N(5)-C(35)-C(36)       | 112(2)   |
| N(1)-C(36)-N(8)      | 121(2)   | N(1)-C(36)-C(35)       | 127(2)   |
| N(8)-C(36)-C(35)     | 112(2)   | N(1)-C(36)-C(32)       | 40.5(10) |
| N(8)-C(36)-C(32)     | 81(2)    | C(35)-C(36)-C(32)      | 168(2)   |
| C(35)-C(37)-C(30)    | 121(2)   | N(7)-C(41)-C(8)        | 125(2)   |
| N(5)-C(42)-C(27)     | 115(2)   | C(19)-C(45)-C(8)       | 123(2)   |
| N(3)-C(50)-C(16)     | 122(2)   | N(2)-C(59)-N(6)        | 118(2)   |
| N(2)-C(59)-C(34)     | 124(2)   | N(6)-C(59)-C(34)       | 118(2)   |
| C(5)-C(2)-C(4)       | 103(3)   | N(10)-C(4)-C(2)        | 127(2)   |
| C(221)-C(6)-C(4)     | 120(3)   | C(15)-C(10)-C(8)       | 122(3)   |
| N(12)-C(9)-C(4)      | 121(2)   | C(12)-C(8)-C(10)       | 132(2)   |
| C(12)-C(8)-N(3)      | 114(2)   | C(10)-C(8)-N(3)        | 114(2)   |
| N(10)-C(12)-C(8)     | 119(2)   | N(10)-C(12)-C(7)       | 123(3)   |
| C(8)-C(12)-C(7)      | 118(2)   | C(15)-C(16)-C(50)      | 112(3)   |
| C(5)-C(7)-C(12)      | 115(3)   | C(16)-C(21)-N(12)      | 119(2)   |
| C(16)-C(21)-C(221)   | 124(2)   | N(12)-C(21)-C(221)     | 117(2)   |
| C(9)-C(4)-C(6)       | 122(3)   | C(7)-C(5)-C(2)         | 130(3)   |
| N(9)-C(16)-C(21)     | 117(2)   | N(9)-C(16)-C(224)      | 118(2)   |
| C(21)-C(16)-C(224)   | 124(2)   | C(10)-C(15)-C(16)      | 125(3)   |
| C(6)-C(221)-C(21)    | 117(2)   | N(9)-C(222)-C(233)     | 127(2)   |
| C(225)-C(233)-C(222) | 113(3)   | C(224)-C(225)-C(233)   | 120(2)   |
| C(225)-C(224)-C(16)  | 118(2)   | O(111)-O(6)-O(111)#1   | 61(6)    |
| N(14)-O(2)-O(1)      | 29(4)    | N(14)-O(1)-O(2)        | 41(5)    |
| O(1)-N(14)-O(3)      | 149(9)   | O(1)-N(14)-O(2)        | 110(7)   |
| O(3)-N(14)-O(2)      | 101(7)   | O(6)-O(111)-O(6)#1     | 111(7)   |
| O(6)-O(111)-O(111)#1 | 61(5)    | O(6)#1-O(111)-O(111)#1 | 58(6)    |

---

Symmetry transformations used to generate equivalent atoms:

#1 x, -y+5/2, -z+1/2

## Appendix 2

### Posters:

1. **Electrochemical and Spectroscopic Properties of Ruthenium and Osmium Polypyridyl Complexes.**  
The Sixth International Conference on the Chemistry of the Platinum Group Metals University of York 1996.
2. **Spectroelectrochemistry of Ruthenium and Osmium Polypyridyl Complexes with Substituted Triazoles.**  
The Forty Ninth Irish Universities Chemistry Research Colloquium Dublin City University 1997.

### Publications:

1. H.E.B. Lempers, J.G. Haasnoot, J. Reedijk, R. Hage, F.M. Weldon, J.G. Vos;  
*Inorg. Chim. Acta.* 1994, 225, 67.
2. T.E. Keyes, F. Weldon, E. Mueller, P. Pechy, M. Graetzel, J.G. Vos;  
*J. Chem. Soc., Dalton Trans.*, 1995, 16, 2705.
3. R. Hage, H.E.B. Lempers, J.G. Haasnoot, J. Reedijk, F.M. Weldon, J.G. Vos;  
*Inorg. Chem.* 1997, 36 (14), 3139.



LSEVIER

# Electrochemical, photophysical and photochemical properties of a hexanuclear ruthenium(II) bis(2,2'-bipyridyl) complex containing a tris(pyrazyltriazole)benzene ligand

Hans E.B. Lempers<sup>a</sup>, Jaap G. Haasnoot<sup>a,\*</sup>, Jan Reedijk<sup>a</sup>, Ronald Hage<sup>b</sup>,  
Frances M. Weldon<sup>c</sup>, Johannes G. Vos<sup>c,\*</sup>

<sup>a</sup>Leiden Institute of Chemistry, Gorlaeus Laboratories, PO Box 9502, 2300 RA Leiden, Netherlands

<sup>b</sup>Unilever Research Laboratory, Olivier van Noortlaan 120, 3133 AT Vlaardingen, Netherlands

<sup>c</sup>School of Chemical Sciences, Dublin City University, Dublin 9, Ireland

Received 27 January 1994

## Abstract

The synthesis of a hexanuclear ruthenium(II) bis(2,2'-bipyridyl) complex with 1,3,5-tris(5-(pyrazine-2-yl)-1,2,4-triazol-3-yl)benzene ( $H_3tpzb$ ) is reported. Three  $Ru(bpy)_2$  groups are bound to the ligand in a bidentate mode (via N1 of the triazole ring and N2 of the pyrazine ring) and three  $Ru(bpy)_2Cl$  groups are bound in a monodentate fashion (via N4 of the pyrazine ring). The absorption spectrum of the deprotonated complex shows two intense MLCT bands in the visible region, one at 465 nm originating from the bidentate  $Ru(bpy)_2$  moieties and the other one at 515 nm from the  $Ru(bpy)_2Cl$  groups. Protonation leads to a shift to 445 nm of the MLCT band for the bidentate sites and to 530 nm for the monodentate sites. The oxidation potential of the bidentate  $Ru(bpy)_2$  groups is 220 mV higher than that of the monodentate bound  $Ru(bpy)_2Cl$  for the protonated complex. Protonation of the triazole rings leads to a further increase of the redox potential of only the  $Ru(bpy)_2$  sites. No differences in redox potentials for each of the three  $Ru(bpy)_2$  groups and each of the three  $Ru(bpy)_2Cl$  groups were observed, suggesting at best a very weak interaction between these metal centres. The electrochemical properties have been correlated with the electronic energies. Photolysis experiments have revealed that the monodentate ruthenium groups are associated when the complex is irradiated. This process is much faster for the deprotonated complex than the protonated compound. The analysis of the reaction products indicate the formation of  $[Ru(bpy)_2]_3(tpzb)]^{3+}$  and  $[Ru(bpy)_2]_3(H_3tpzb)]^{6+}$ , respectively.

**Keywords:** Electrochemistry; Photophysics; Photochemistry; Ruthenium complexes; Bidentate ligand complexes; Chelate complexes

## Introduction

The electrochemical and photophysical properties of  $[Ru(bpy)_3]^{2+}$  ( $bpy = 2,2'$ -bipyridine) and its analogues have been investigated in great detail during the last decades because of the application of these compounds in solar energy devices [1,2]. As a result an extensive chemistry has been developed around these compounds which is aimed at obtaining photostable coordination compounds with well-developed excited-state properties [3,4]. The synthetic control available for these compounds has subsequently led to their incorporation in polynuclear structures in search of well-defined supra-molecular structures [5-23]. As the photochemical and

photophysical of the mononuclear complexes are fairly well understood [4], the effect of the presence of more metal ions on the photochemical and photophysical properties of multinuclear compounds can now be studied in detail.

Recently, we reported the synthesis and characterisation of a number of mononuclear, dinuclear and trinuclear ruthenium and osmium complexes with various triazole ligands [9-20]. With the 3,5-bis(pyridin-2-yl)-1,2,4-triazolate anion, both mononuclear and dinuclear  $Ru(bpy)_2$  complexes have been isolated and studied [9-18]. Electrochemical and photophysical experiments showed that in the dinuclear compounds the interaction between the two metal centres is very efficient. It was furthermore found that the deprotonated mononuclear compound is photostable, whilst the pro-

\*Corresponding authors.

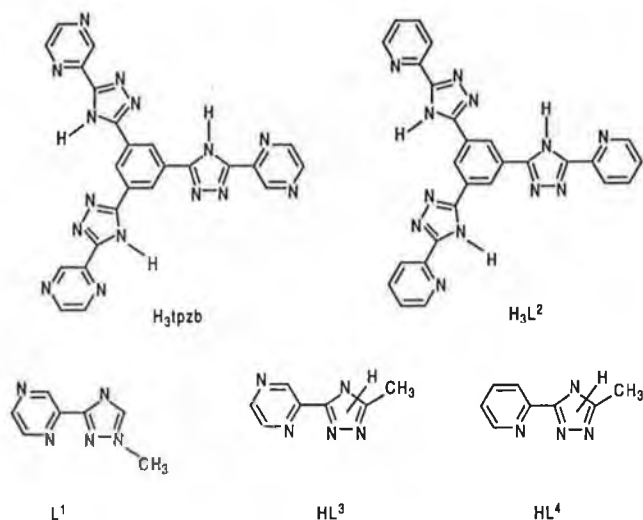


Fig. 1. Schematic representation of the ligands described in the text.

tonated mononuclear and the dinuclear ruthenium complexes are photolabile [18]. With the bridging ligand tris(5-(pyridin-2-yl)-1,2,4-triazol-3-yl)benzene ( $H_3L^2$ ; see Fig. 1) trinuclear ruthenium and osmium complexes were obtained. Interestingly in this case no interaction between the different metal sites was observed [19].

In this contribution we report a novel ligand system: 1,3,5-tris(pyrazin-2-yl-1,2,4-triazole)benzene ( $H_3tpzb$ ; see Fig. 1). The structure of this ligand allows for the coordination of three bidentate 'Ru(bpy)<sub>2</sub> groups' as well as three monodentate 'Ru(bpy)<sub>2</sub>Cl groups'. In this study the interaction between the 'short distance' ruthenium groups, i.e. the Ru(bpy)<sub>2</sub> and Ru(bpy)<sub>2</sub>Cl moieties at the same pyrazyltriazole ligand, and the 'long distance' Ru groups, i.e. the three Ru(bpy)<sub>2</sub> groups with each other or the Ru(bpy)<sub>2</sub>Cl groups with each other, is investigated. The effect of protonation of the triazole rings on the electrochemical, photophysical and photochemical properties of the hexanuclear compound is also studied. Finally, the photochemical preparation of a trinuclear complex from the hexanuclear compound is reported. The properties observed for these compounds are compared with those observed for other similar dinuclear structures based on various triazole [9–20] and pyrazine [21–23] bridging ligands.

## 2. Experimental

### 2.1. Materials

Hydrated ruthenium trichloride was obtained as a loan from Johnson Matthey and used without further purification. The starting material, *cis*-[Ru(bpy)<sub>2</sub>Cl<sub>2</sub>]·2H<sub>2</sub>O, was synthesised according to literature methods [24].

### 2.2. Synthesis of $H_3tpzb$

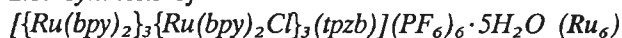
The bridging ligand 1,3,5-tris(5-(pyrazin-2-yl)-1,2,4-triazol-3-yl)benzene ( $H_3tpzb$ ) was synthesised in four steps. A suspension of 30 g (0.24 mol) of 2-pyrazinamide and 150 ml of phosphorylchloride was stirred for 4 h at room temperature. After the mixture had been heated at reflux for 20 min, the excess of phosphorylchloride was evaporated under reduced pressure. The remaining red oil was neutralised with a saturated sodium bicarbonate solution. The 2-cyanopyrazine was extracted with diethyl ether and evaporated until dryness. Yield 14.4 g [25].

In a beaker 14.1 g (0.137 mol) of 2-cyanopyrazin was heated and after melting 6.9 g (0.137 mol) of hydrazine monohydrate were added. Ethanol was added until a clear solution was obtained. The mixture was allowed to react for 16 h, after which the pale yellow 2-pyrazylamidrazone was isolated by filtration. Yield 11.3 g.

A solution of 7.3 g (27 mmol) of 1,3,5-benzenetri-carbonyl chloride in 20 ml of *N,N*-dimethylacetamide was added dropwise to a suspension of 11.3 g (82 mmol) of 2-pyrazylamidrazone and 8.7 g (82 mmol) of sodium carbonate in 80 ml of *N,N*-dimethylacetamide at 0 °C. The reaction mixture was stirred at room temperature for 3 h, after which it was poured into an ice/water mixture to precipitate a yellow solid. This material was isolated, washed with water and dried. Thermal cyclisation of the product was performed by heating the material at 200 °C for 1 h. The reaction was finished when no more water vapour escaped, yielding a grey–yellow product. Purification took place by boiling the product in ethylene glycol, in which impurities dissolved. After filtration a grey powder was isolated. Yield of  $H_3tpzb$ : 8.65 g (total yield 4%).

<sup>1</sup>H NMR data ((CD)<sub>3</sub>SO) (ppm): 9.45 (d; H3); 8.97 (s; Hbenzene); 8.82 (q; H5); 8.65 (d; H6). Mass spectroscopy: {*M* + H}<sup>+</sup>: 514 [26].

### 2.3. Synthesis of



This compound was synthesised by refluxing 50 mg (0.1 mmol) of  $H_3tpzb$  with 360 mg (0.7 mmol) of *cis*-[Ru(bpy)<sub>2</sub>Cl<sub>2</sub>]·2H<sub>2</sub>O in 50 ml ethanol/water (1/1 vol./vol.) for 48 h. The solution was filtered and the solvent was removed by rotary evaporation. The remaining solid was dissolved in water and precipitated by adding an excess of an aqueous NH<sub>4</sub>PF<sub>6</sub> solution. The precipitate was dissolved in acetone and purified by column chromatography (neutral alumina; acetone as eluent). The compound was further purified by crystallisation from water/acetone. Yield 310 mg (78%). *Anal.* Found: C, 43.0; H, 3.1; N, 13.2; P, 4.3. *Calc.*: C, 42.6; H, 3.0; N, 13.5; P, 4.6%. Addition of acid leads to protonation

of the triazole rings, yielding  $[\{\text{Ru}(\text{bpy})_2\}_3\{\text{Ru}(\text{bpy})_2\text{Cl}\}_3\text{-(H}_3\text{tpzb)}]^{9+}$  in situ (abbreviated as  $\text{H}_3\text{Ru}_6$ ).

## 2.4. Instrumentation and methods

$^1\text{H}$  NMR spectra were recorded on a Bruker WM 300 spectrometer. UV–Vis measurements were obtained on  $10^{-5}$ – $10^{-4}$  molar solutions on a Perkin-Elmer 330 spectrophotometer using 1 cm quartz cells. The absorption spectra of the photolysis experiments were recorded on a Shimadzu UV-240 spectrophotometer. Emission spectra were recorded on a Perkin-Elmer LS5 and on a Perkin-Elmer LS50 luminescence spectrometer with a variable slit width between 2.5 and 20 nm. The room temperature measurements were carried out in acetonitrile solutions, while the luminescence measurements at 77 K were carried out in methanol (approximately  $10^{-5}$  M solutions). The spectra were not corrected for photomultiplier response. Small-scale photolysis experiments were carried out at room temperature in acetone using 1 cm cells and a 400 W medium-pressure mercury lamp with a glass cut-off filter. Preparative photochemical experiments were carried out using a medium-pressure 400 W mercury lamp fitted in an immersion well. The differential pulse polarography (DPP) experiments and the cyclic voltammograms (CV) were carried out on a EG&G Par C model 303 instrument with an EG&G 384 B polarographic analyser. The scan rate was 4 mV/s for the DPP experiments with a pulse height of 20 mV. For the cyclic voltammograms the scan rate was 100 mV/s. A saturated calomel electrode (SCE) was used as a reference electrode. The electrolyte used was acetonitrile, containing 0.1 M tetrabutylammonium perchlorate (TBAP).

Laser desorption mass spectrometry experiments were carried out as reported elsewhere [19,26].

## 3. Results and discussion

### 3.1. Synthesis of the ruthenium complex

The synthesis of the hexanuclear ruthenium(II) complex proved to be straightforward based on the known chemistry of pyrazyltriazole and tris(pyridyltriazole)-benzene ligands [9–20]. Refluxing an excess of  $[\text{Ru}(\text{bpy})_2\text{Cl}_2] \cdot 2\text{H}_2\text{O}$  with the  $\text{H}_3\text{tpzb}$  ligand yielded the hexanuclear compound in high yield. This compound contains three bidentate  $\text{Ru}(\text{bpy})_2$  moieties and three monodentate  $\text{Ru}(\text{bpy})_2\text{Cl}$  groups. From our experience with other similar triazole ligands it is likely that the coordination mode of the bidentate coordination unit is via N1 of the triazole ring, rather than N4, and the pyrazine ring. Such a coordination mode would minimise steric hindrance in the molecule [9–20]. It is noted

that many geometrical isomers may exist, depending on the relative alignment of the bpy ligands [10]. We did not attempt to separate these isomers as it has already been shown that the electronic and electrochemical properties of the geometrical isomers are very similar [27]. In the compound isolated the three triazole rings are deprotonated. This compound can easily be protonated, yielding a species that exhibits different electronic and electrochemical properties (vide infra). Refluxing smaller quantities of  $\text{Ru}(\text{bpy})_2\text{Cl}_2$  with the ligand, yielded mixtures of mono-, di-, tri-, tetra- and pentanuclear species [28]. Unfortunately, we were not able to obtain these complexes in a pure form.

### 3.2. Redox properties

The redox potentials of  $\text{Ru}_6$  and  $\text{H}_3\text{Ru}_6$  are listed in Table 1. The deprotonated compound exhibits a first reduction potential at  $-1.14$  V versus SCE which is considerably less negative than in the analogous mononuclear complex with pyrazyltriazole,  $\text{RuL}^4$  (see Table 1). Also the analogous tris(pyridyltriazole)benzene complex shows a much more negative first bpy-based reduction. The much less negative reduction reported here is in agreement with the presence of an extra electron-withdrawing metal centre on the pyrazine ring [21–23]. The ligand-based reductions of these compounds are not very well defined. This is most likely due to adsorption processes and/or deprotonation of the ligands. Nevertheless the first reduction potential observed for  $\text{Ru}_6$  strongly suggests that the first reduction potential is based on the bridging ligand [4,9–20]. The further reductions observed for  $\text{Ru}_6$  are assigned to bpy-based reductions.

The first oxidation wave is assigned to a  $\text{Ru}(\text{bpy})_2\text{Cl}$  oxidation, as the presence of the chloride ion reduces the charge on the metal ion. The second oxidation wave is therefore located on the bidentate coordination unit. The metal-based oxidation potentials have some interesting features. First of all, the  $\text{Ru}(\text{bpy})_2\text{Cl}$  based oxidation wave is not effected very much by protonation of the triazole ring. Furthermore, if one compares the redox potential observed for the  $\text{Ru}(\text{bpy})_2\text{Cl}$  units in the hexanuclear complex (0.94 V) with that reported for  $[\text{Ru}(\text{bpy})_2(\text{pyrazine})\text{Cl}]^+$  (0.88 V) [21], it is clear that the value of this redox potential is also not changed very much by the formation of the dinuclear compound. The same observation has been made for other pyrazine-based dinuclear systems [21–23]. Clearly, the distance between the  $\text{Ru}(\text{bpy})_2\text{Cl}$  centre and the triazole ring is too large to result in an appreciable interaction and therefore no substantial shift of the redox potential upon formation of a dinuclear compound, or alternatively, protonation has been observed. The fact that the first metal-based redox potential is only slightly affected by protonation of the triazole ring confirms

Table 1

Electrochemical data of the ruthenium complexes discussed in the text. Relevant compounds reported before have also been included. The measurements were carried out in acetonitrile containing 0.1 M TBAP. The values were obtained by using differential pulse polarography. Potentials are listed in volt vs. SCE

| Compound                                      | Oxidation potential     |                      | Reduction potential (V) | Reference |
|---|-------------------------|----------------------|-------------------------|-----------|
|   | Ru(bpy) <sub>2</sub> Cl | Ru(bpy) <sub>2</sub> |                         |           |
| Ru <sub>6</sub>                               | 0.94                    | 1.16                 | -1.14 -1.50 -1.71       | this work |
| H <sub>3</sub> Ru <sub>6</sub>                | 0.97                    | 1.35                 | adsorption              | this work |
| Ru <sub>3</sub>                               |                         | 1.05                 | adsorption              | this work |
| RuL <sup>1</sup>                              |                         | 1.32                 | -1.27 -1.54 -1.81       | [20]      |
| Ru <sub>2</sub> L <sup>1</sup>                | 0.92                    | 1.41                 | -0.97 -1.51 -1.57 -1.76 | [20]      |
| Ru <sub>3</sub> L <sup>2</sup>                |                         | 0.86                 | -1.47 -1.66 -1.82       | [19]      |
| Ru <sub>3</sub> H <sub>3</sub> L <sup>2</sup> |                         | 1.18                 | not observed            | [19]      |
| RuHL <sup>3</sup>                             |                         | 1.20                 | -1.48 -1.74 -2.27       | [10]      |
| RuL <sup>3</sup>                              |                         | 0.80                 | -1.55 -1.88             | [10]      |
| RuHL <sup>4</sup>                             |                         | 1.29                 | -1.22 -1.52 -1.77       | [10]      |
| RuL <sup>4</sup>                              |                         | 0.92                 | -1.44 -1.66 -1.80       | [10]      |

L<sup>1</sup> = 1-methyl-3-(pyrazin-2-yl)-1,2,4-triazole.

H<sub>3</sub>L<sup>2</sup> = 1,3,5-(tris(5-(pyridin-2'-yl)-1,2,4-triazol-3-yl)benzene.

HL<sup>3</sup> = 3-methyl-5-(pyridin-2-yl)-1,2,4-triazole.

HL<sup>4</sup> = 3-methyl-5-(pyrazin-2-yl)-1,2,4-triazole.

the nature of the redox process as being based on the ruthenium–chloro site. An interesting comparison can also be made with the 2-pyrazinecarboxylate dimer reported by Goldsby and Meyer [23]. In this compound the coordination sites are also asymmetric and the second site contains a negative charge on the bridge as well. In this compound the redox potential of the Ru–chloro site is only 40 mV higher than that observed for the symmetrical pyrazine dimer which does not contain a negatively charged carboxylate group. So clearly there is very little interaction in this type of pyrazine-based dimer between the metal centres. The differential pulse polarograms of the hexanuclear Ru<sub>6</sub> and H<sub>3</sub>Ru<sub>6</sub> complexes each show two sharp oxidation peaks, indicating there is at best a very weak long range interaction between the three Ru(bpy)<sub>2</sub> and Ru(bpy)<sub>2</sub>Cl moieties coordinated to the bridging (H<sub>3</sub>)tpzb ligands [8,19]. The relative position of the redox potentials observed for the bidentate Ru(bpy)<sub>2</sub> dinuclear site and the RuCl site suggests that interaction over the pyrazine bridge is also weak.

There is, however, one interesting feature. The value observed for the second oxidation potential for the deprotonated complex (Ru<sub>6</sub>) is surprisingly high. This value is 300 mV higher than that of the analogous trinuclear Ru(bpy)<sub>2</sub> complex with tris(pyridyltriazole)-benzene [19] and 240 mV higher than observed in a mononuclear pyrazine analogue RuL<sup>4</sup> (see Table 1). Furthermore, the difference between the redox potential observed for the protonated and deprotonated complex is rather small (190 mV), when compared to the one observed for the mononuclear analogue Ru(H)L<sup>4</sup> where it is 370 mV. Since interaction via the pyrazine ring is weak, the increased redox potential cannot be ex-

plained by strong delocalisation or by electrostatic effects. In similar pyrazine dimers the shift observed for the second redox site is generally less than 150 mV [22,23]. This suggests one could expect a maximum value of about 1.07 V for the second oxidation potential. The reduction potential measured for Ru<sub>6</sub> suggested that the lowest π\* level is tpzb based. It is known that in general a strong π-accepting ligand yields a decrease in electron density on the metal centres and therefore a raise in oxidation potential is expected [4]. Therefore, it is likely that the relatively low π\* for the tpzb compound, yields an unexpected increase in redox potential. This conclusion is supported by the electronic spectra (vide infra). This shift in redox potential of the bidentate ruthenium moiety upon protonation of the triazole ring has been explained previously by the weaker σ-donor properties of the protonated triazole ring [8,19].

Spectroelectrochemical investigations were also carried out. However, using both electrochemical and chemical oxidation methods no evidence was obtained for the presence of an intervalence band in the near-IR region. An investigation of the visible part of the spectrum did show the expected spectroscopic changes. Also the appearance of the LMCT band at about 900 nm confirms that the complexes are indeed oxidised. This unexpected phenomenon is at present under further investigation.

### 3.3. Absorption spectra

The absorption spectra of [{Ru(bpy)<sub>2</sub>]<sub>3</sub>{Ru(bpy)<sub>2</sub>Cl}<sub>3</sub>-(H<sub>3</sub>tpzb)]<sup>9+</sup> and [{Ru(bpy)<sub>2</sub>]<sub>3</sub>{Ru(bpy)<sub>2</sub>Cl}<sub>3</sub>(tpzb)]<sup>6+</sup> are shown in Fig. 2. Both species exhibit two intense

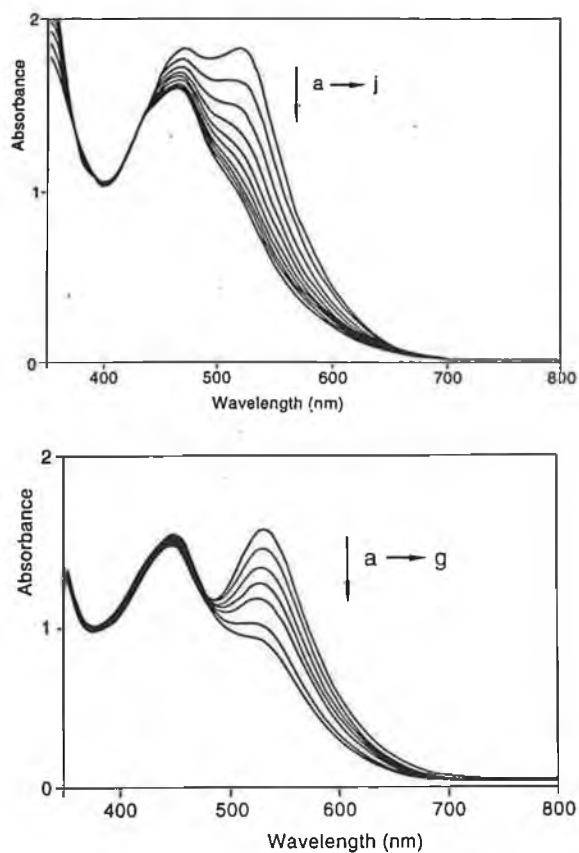


Fig. 2. Changes of the absorption spectra on irradiation of  $\text{Ru}_6$  (top) and  $\text{H}_3\text{Ru}_6$  (bottom) in acetone. For the  $\text{Ru}_6$  compound every 15 s a spectrum was taken (a  $\rightarrow$  j: from  $t=0$  to 150 s). For  $\text{H}_3\text{Ru}_6$ : a ( $t=0$ ); b ( $t=15$  min); c ( $t=30$  min); d ( $t=45$  min); e ( $t=60$  min); f ( $t=90$  min); g ( $t=120$  min).

absorption bands in the visible region. By comparison with other similar mononuclear and dinuclear compounds (see Table 2) the higher energy band around 450 nm has been assigned to a metal-to-ligand charge transfer (MLCT) transition located on the  $\text{Ru}(\text{bpy})_2$  moiety bound to the pyrazyltriazole ligand in a bidentate manner [20,34]. The low-energy absorption band has been assigned to an MLCT band located on the  $\text{Ru}(\text{bpy})_2\text{Cl}$  moiety [20]. In other dinuclear complexes which also contain the  $\text{RuCl}$ -pyrazine moiety an absorption band at similar energy is observed [21]. The electrochemical data strongly suggest that the lowest unoccupied molecular orbital (LUMO) is located on the bridging ( $\text{H}_3$ )tpzb ligand. The highest occupied molecular orbital (HOMO) is related to the oxidation potential of the metal centres [4]. As the oxidation potential of the  $\text{Ru}(\text{bpy})_2\text{Cl}$  moiety is much lower than that of the  $\text{Ru}(\text{bpy})_2$  group, the energy gap between the HOMO and LUMO is smaller for the monodentate  $\text{Ru}(\text{bpy})_2\text{Cl}$  group than for the bidentate  $\text{Ru}(\text{bpy})_2$  mode.

Protonation of the triazole rings leads to a blue shift of the high-energy MLCT band. This effect has been noted before (see also Table 2) and has been explained by a stabilisation of the HOMO level upon protonation

due to the weaker  $\sigma$ -donor properties of the protonated triazole rings [10]. A major difference with the tpzb-containing complexes and other mononuclear ruthenium-pyrazyltriazole complexes is that in the latter case a change of the LUMO from the auxiliary bpy ligands to the pyrazyltriazole ligand has been observed upon protonation [34]. For the tpzb system, the LUMO is always located on the bridging ligand system and therefore the shift in absorption energy is dominated by the change in HOMO levels rather than the switch-over of the LUMO levels.

Interestingly, the absorption energy of the  $\text{Ru}(\text{bpy})_2\text{Cl}$  group moves to a lower energy level when the triazole ring becomes protonated. As discussed before, the oxidation potential of the  $\text{Ru}(\text{bpy})_2\text{Cl}$  site is hardly affected by protonation of the triazole rings. As a result the energy of the HOMO level will not be affected to a large extent. On the other hand the protonation leads to a stabilization of the lowest  $\pi^*$  level [35] with the result that the energy gap between the LUMO and HOMO level becomes smaller and consequently a lowering of the MLCT band is observed.

### 3.4. Emission spectra

The luminescence bands of  $\text{Ru}_6$  and  $\text{H}_3\text{Ru}_6$  at room temperature and 77 K are listed in Table 2. The emission intensity for  $\text{H}_3\text{Ru}_6$  is much weaker than that for its deprotonated analogue. Comparison with the emission bands of the trinuclear  $\text{L}^2$  complex [19], reveals that the emission energy for  $\text{Ru}_6$  is at a much lower energy. This does not correlate with the fact that the absorption bands observed for the bidentate  $\text{Ru}(\text{bpy})_2$  groups attached to  $\text{L}^2$  and tpzb have similar energies. The emission energy observed for  $\text{Ru}_6$  is very similar to those observed for the pyrazine-bridged ruthenium dinuclear complexes ( $\text{L}^1$ ) as shown in Table 2. No change in the emission spectrum of  $\text{Ru}_6$  has been observed upon changing the excitation wavelength between 400 and 500 nm, suggesting efficient energy-transfer processes. We therefore conclude that the emission band observed originates from the monodentate  $\text{Ru}(\text{bpy})_2\text{Cl}$  groups and that energy-transfer processes take place from the high-energy  $^3\text{MLCT}$  states (originated from the bidentate  $\text{Ru}(\text{bpy})_2$  groups) to the low-energy  $^3\text{MLCT}$  states (monodentate  $\text{Ru}(\text{bpy})_2\text{Cl}$  sites). In Fig. 3, the various processes (absorption, emission and energy transfer) are schematically presented. This interpretation is in agreement with the observation that the emission energy, like the absorption obtained for the  $\text{Ru}(\text{bpy})_2\text{Cl}$  moiety, does not change upon protonation of the triazole ring.

### 3.5. Photochemistry

As mentioned before, many of the ruthenium(II) complexes studied show photoinstability. We have shown

Table 2  
Electronic data for the complexes

| Compound                          | Absorption max. $\lambda_{\max}$<br>(nm) | $(\epsilon (10^4 \text{ M}^{-1} \text{ cm}^{-1}))^a$ | Emission max. (nm) |                   | Reference |
|-----------------------------------|--|--|--------------------|-------------------|-----------|
|                                   |  |  | 300 K <sup>b</sup> | 77 K <sup>c</sup> |           |
| $\text{Ru}_6$                     | 465 (6.72)                               | 515 (6.72)   | 775                | 685               | this work |
| $\text{H}_3\text{Ru}_6$           | 445 (6.35)                               | 530 (6.50)   | 769                | 695               | this work |
| $\text{Ru}_3$                     | 460                                      |  | 677                | 650               | this work |
| $\text{H}_3\text{Ru}_3$           | 445                                      |  | 675                | 645               | this work |
| $\text{RuL}^1$                    | 437 (1.46)                               |  | 633                | 577               | [20]      |
| $\text{Ru}_2\text{L}^1$           | 440 (1.70)                               | 530 (1.90)   | not observed       | 705               | [20]      |
| $\text{Ru}_3\text{L}^2$           | 475 (2.71)                               |  | 683                | 632               | [19]      |
| $\text{Ru}_3\text{H}_3\text{L}^2$ | 441 (3.23)                               |  | 620                | 604               | [19]      |
| $\text{RuHL}^3$                   | 438 (1.07)                               |  | 612                | 587               | [10]      |
| $\text{RuL}^3$                    | 467 (0.85)                               |  | 660                | 610               | [10]      |
| $\text{RuHL}^4$                   | 441 (1.27)                               |  | 665                | 620               | [10]      |
| $\text{RuL}^4$                    | 458 (1.21)                               |  | 670                | 627               | [10]      |

<sup>a</sup>Measured in ethanol.

<sup>b</sup>Measured in acetonitrile.

<sup>c</sup>Measured in methanol.

$\text{L}^1$  = 1-methyl-3-(pyrazin-2-yl)-1,2,4-triazole.

$\text{H}_3\text{L}^2$  = 1,3,5-(tris(5-pyridin-2'-yl)-1,2,4-triazol-3-yl)benzene.

$\text{HL}^3$  = 3-methyl-5-(pyridin-2-yl)-1,2,4-triazole.

$\text{HL}^4$  = 3-methyl-5-(pyrazin-2-yl)-1,2,4-triazole.

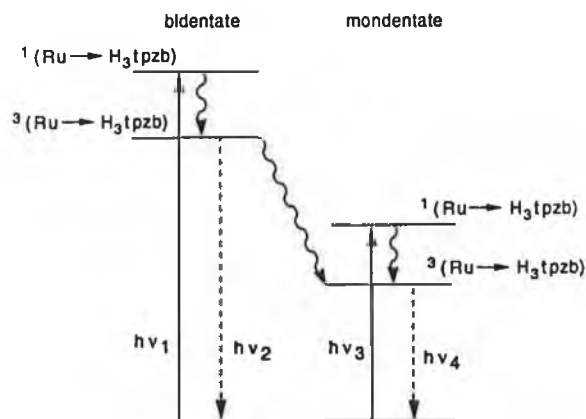


Fig. 3. Schematic energy-level diagram for  $\text{H}_3\text{Ru}_6$ . The excited states are indicated by the electronic transitions needed to obtain them starting from the ground states.

before that  $\text{Ru}(\text{bpy})_2$  complexes containing deprotonated triazole ligands yield complexes that do not decompose upon irradiation [10,13]. This has been explained by the strong donating properties of the triazolone ring, yielding a large ligand-field splitting. As a consequence population of metal-centred excited states, that cause photo-decomposition, is not feasible. As already mentioned above we were not successful in preparing compounds of the type  $\text{Ru}_3$ , where only bidentate coordination ruthenium groupings are present. Based on our expectation that the bidentate coordination  $\text{Ru}(\text{bpy})_2$  unit would be photostable it was decided to try and prepare the trinuclear  $\text{Ru}_3$  compound

by photochemical means, since the photo-instability of the  $\text{Ru}(\text{bpy})_2\text{Cl}$  groupings is well documented [36]. No detailed photochemical experiments have been carried out on dinuclear pyrazine compounds, although the decomposition of such a species upon photolysis in acetonitrile has been noted [21].

Fig. 2 shows the absorption spectra taken during the photolysis of  $\text{H}_3\text{Ru}_6$  and  $\text{Ru}_6$  in acetone. The deprotonated complex is very photo-instable; in 2 min nearly all of the complex has decomposed. An isosbestic point at 430 nm was observed, suggesting a clean photochemical reaction. The  $\text{H}_3\text{Ru}_6$  compound shows a much slower decomposition, as a reaction time of approximately 2 h is needed to fully decompose the compound (isosbestic point at 478 nm). Fig. 4 shows the changes in the emission spectrum of  $\text{Ru}_6$  upon irradiation.

The increased photostability upon protonation of the triazole ring is surprising since it is contrary to the results obtained for other pyrazyl- and pyridyltriazole complexes [9–20]. As the luminescence measurements have revealed similar emission energies and thus <sup>3</sup>MLCT energies for both the protonated and deprotonated species, the difference in photostability is likely to be caused by different <sup>3</sup>MC levels. This very unusual feature is at present under further investigation.

After preparative photolysis (see Section 2 for details) crystallisation from water/acetone yields products that exhibit absorption and emission maxima as shown in Table 2 ( $\text{Ru}_3$  and  $\text{H}_3\text{Ru}_3$ , respectively). It is interesting to note that the absorption and emission bands do not shift to a large extent upon protonation/deprotonation

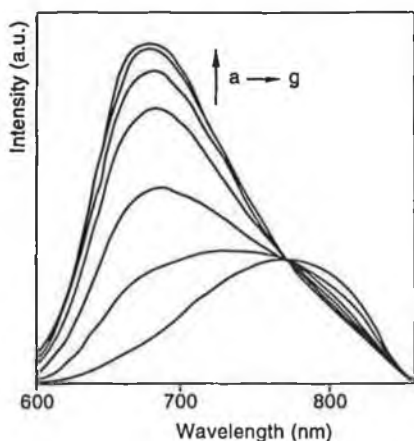


Fig. 4. Changes of the emission spectra (r.t.) upon irradiation of  $\text{Ru}_6$  in acetone (430 nm). Every 25 s a spectrum was taken (a  $\rightarrow$  g:  $t=0$  to 150 s).

of the triazole rings. Such behaviour has already been observed for the analogous mononuclear  $\text{Ru}(\text{bpy})_2$  complexes containing  $\text{L}^4$  ligand (Table 2). Based on these results it is very likely that, upon irradiation, the three  $\text{Ru}(\text{bpy})_2\text{Cl}$  groups are dissociated from the pyrazine ring, yielding the trinuclear  $\text{tpzb}$  complex. This is the case for both the protonated and the deprotonated complexes. Further indications for such a structure have been obtained by measuring the oxidation potential for  $\text{Ru}_3$  (Table 1). The oxidation potential is very similar to those found for other bidentate pyrazyltriazole  $\text{Ru}(\text{bpy})_2$  complexes [10–34].

#### 4. Conclusions

The hexanuclear ruthenium compounds with  $\text{tpzb}$  and  $\text{H}_3\text{tpzb}$  exhibit very interesting and unusual properties. Although the electrochemical measurements point to at best a very weak interaction between the metal centres, the luminescence experiments revealed an efficient energy-transfer process from the bidentate  $\text{Ru}(\text{bpy})_2$  groups to the monodentate  $\text{Ru}(\text{bpy})_2\text{Cl}$  moieties. Also the photolysis experiments suggest very efficient energy processes, as only the monodentate groups are dissociated upon irradiation. A very interesting observation is the different photostability for the protonated and deprotonated species. Although the emission experiments have clearly revealed that the  $^3\text{MLCT}$  states for both the protonated and the deprotonated species are roughly equal in energy, the stability for the protonated species seems to be approximately 60 times higher. Currently we are carrying out temperature-dependent lifetime measurements to gain information about the  $^3\text{MLCT}$ – $^3\text{MC}$  gap for both species.

#### Acknowledgements

The authors thank EOLAS, the Irish Science and Technology Agency for financial assistance. Johnson Matthey is acknowledged for their generous loan of ruthenium chloride.

#### References

- [1] T.J. Meyer, *Acc. Chem. Res.*, **11** (1978) 94.
- [2] T.J. Meyer, *Pure Appl. Chem.*, **58** (1986) 1193.
- [3] J.v. Houten and R.J. Watts, *Inorg. Chem.*, **17** (1978) 3381.
- [4] A. Juris, V. Balzani, F. Barigelletti, S. Campagna, P. Belser and A. von Zelewsky, *Coord. Chem. Rev.*, **84** (1988) 85.
- [5] V. Balzani and F. Scandola, *Supramolecular Photochemistry*, Ellis Horwood, Chichester, UK, 1991.
- [6] F. Scandola, M.T. Indelli, C. Chiorboli and C.A. Bignozzi, *Top. Curr. Chem.*, **158** (1990) 73.
- [7] N.E. Katz, C. Creutz and N. Sutin, *Inorg. Chem.*, **27** (1988) 1687.
- [8] L. De Cola, V. Balzani, F. Barigelletti, L. Flamigni, P. Belser, A. von Zelewsky, M. Frank and F. Vögtle, *Inorg. Chem.*, **32** (1993) 5228.
- [9] R. Hage, J.G. Haasnoot, J. Reedijk and J.G. Vos, *Chemtracts*, (1992) 75.
- [10] R. Hage, *Ph.D. Thesis*, Leiden University, Netherlands, 1991.
- [11] R. Hage, A.H.J. Dijkhuis, J.G. Haasnoot, R. Prins, J. Reedijk, B.E. Buchanan and J.G. Vos, *Inorg. Chem.*, **27** (1988) 2185.
- [12] R. Hage, J.G. Haasnoot, D.J. Stufkens, T.L. Snoeck, J. Reedijk and J.G. Vos, *Inorg. Chem.*, **28** (1989) 1413.
- [13] F. Barigelletti, L. De Cola, V. Balzani, R. Hage, J.G. Haasnoot, J. Reedijk and J.G. Vos, *Inorg. Chem.*, **28** (1989) 4344.
- [14] R. Hage, J.G. Haasnoot, H.A. Nieuwenhuis, J. Reedijk, D.J.A. de Ridder and J.G. Vos, *J. Am. Chem. Soc.*, **112** (1990) 9245.
- [15] F. Barigelletti, L. De Cola, V. Balzani, R. Hage, J.G. Haasnoot, J. Reedijk and J.G. Vos, *Inorg. Chem.*, **30** (1991) 641.
- [16] F. Barigelletti, L. De Cola, V. Balzani, R. Hage, J.G. Haasnoot, J. Reedijk and J.G. Vos, *J. Phys. Lett.*, **178** (1991) 491.
- [17] R. Hage, J.G. Haasnoot, J. Reedijk, R. Wang and J.G. Vos, *Inorg. Chem.*, **30** (1991) 3263.
- [18] R. Hage, *Coord. Chem. Rev.*, **111** (1991) 161.
- [19] J.M. de Wolf, R. Hage, J.G. Haasnoot, J. Reedijk and J.G. Vos, *Nouv. J. Chim.*, **15** (1991) 501.
- [20] H.E.B. Lempers, J.G. Haasnoot, Jan Reedijk, R. Hage and J.G. Vos, to be submitted.
- [21] R.W. Callahan, G.M. Brown and T.J. Meyer, *Inorg. Chem.*, **14** (1975) 1443.
- [22] M.J. Powers and T.J. Meyer, *J. Am. Chem. Soc.*, **102** (1980) 1289.
- [23] K.A. Goldsby and T.J. Meyer, *Inorg. Chem.*, **23** (1984) 3002.
- [24] B.P. Sullivan, D.J. Salmon and T.J. Meyer, *Inorg. Chem.*, **17** (1978) 3334.
- [25] R. Delaby, R. Damiens and M. Robba, *C.R. Acad. Sci., Ser. C*, **247** (1968) 822.
- [26] P.A. van Veelen, U.R. Tjaden, J. van der Greef and R. Hage, *Org. Mass. Spectrom.*, **26** (1991) 74.
- [27] S. Serroni and G. Denti, *Inorg. Chem.*, **31** (1992) 4251.
- [28] H.E.B. Lempers, unpublished results.
- [29] R. Hage, R. Prins, J.G. Haasnoot, J. Reedijk and J.G. Vos, *J. Chem. Soc., Dalton Trans.*, (1987) 1389.

- [30] B.P. Sullivan, D. Conrad and T.J. Meyer, *Inorg. Chem.*, **24** (1985) 3640.
- [31] A.M. Bond and M. Haga, *Inorg. Chem.*, **25** (1986) 4507.
- [32] M. Haga, T. Matsumura-Inoue and S. Yamabe, *Inorg. Chem.*, **26** (1987) 4148.
- [33] T. Ohni, N. Nokazi and M. Haga, *Inorg. Chem.*, **31** (1992) 4256.
- [34] H.A. Nieuwenhuis, R. Hage, J.G. Haasnoot, D.J. Stufkens, T.L. Snoeck, J. Reedijk and J.G. Vos, *Inorg. Chem.*, **30** (1991) 48.
- [35] O. Haas, M. Kriens and J.G. Vos, *J. Am. Chem. Soc.*, **103** (1981) 1318.
- [36] R.J. Crutchley, N. Kress and A.B.P. Lever, *J. Am. Chem. Soc.*, **105** (1983) 1170.

## Dalton Communication

Application of Deuteriation to Determine the Location of the Emitting State in Mixed-ligand Ru<sup>II</sup> Polypyridyl ComplexesTia E. Keyes,<sup>a</sup> Frances Weldon,<sup>a</sup> Edgar Müller,<sup>b</sup> Peter Pechy,<sup>b</sup> Michael Grätzel<sup>b</sup> and Johannes G. Vos<sup>\*,a</sup><sup>a</sup> School of Chemical Sciences, Dublin City University, Dublin 9, Ireland<sup>b</sup> Institute de Chimie Physique II, Ecole Polytechnique Federale de Lausanne, Ecublens, CH-1015 Lausanne, Switzerland

The location of the emitting triplet state in heteroleptic Ru<sup>II</sup> polypyridyl complexes has been determined by a new method using deuteriated ligands and emission-lifetime measurements, and a new single-step, high yield synthesis of perdeuteriated 2,2'-bipyridyl has been developed.

With the increasing interest in supramolecular chemistry, and in particular in the design of photonic devices,<sup>1</sup> simple methods to determine the location of excited states in mixed-ligand metal complexes are needed. A number of methods are available which achieve this objective, amongst them time-resolved resonance Raman spectroscopy.<sup>2</sup> Here we report a new simple method to determine the emitting ligand in heteroleptic Ru<sup>II</sup> complexes, based on the effect of deuteriation of one of the ligands on the emission lifetime of the Ru<sup>II</sup> complex.

Although it has long been noted that upon deuteriation of the ligands in homoleptic Ru<sup>II</sup> polypyridyl complexes the excited-state lifetimes of the metal complexes increase,<sup>3,4</sup> a systematic investigation of this phenomenon in mixed-ligand Ru<sup>II</sup> complexes has not been carried out. There are a small number of reports in the literature, where deuteriation of polypyridyl ligands has been employed either to simplify <sup>1</sup>H NMR spectra,<sup>5</sup> or to obtain information about the excited-state behaviour of the complexes, using either time-resolved resonance Raman spectroscopy<sup>2</sup> or by investigating the detailed fine structure of emission spectra at low temperatures.<sup>4</sup>

Ligand deuteriation as a tool for the study of excited states is a relatively under-exploited method, mainly due to the synthetic difficulties in obtaining deuteriated compounds. At present the most convenient preparation of perdeuteriated 2,2'-bipyridyl reported in the literature involves several steps. As proposed by Cook *et al.*,<sup>6</sup> 2,2'-bipyridyl 1,1'-dioxide can be deuteriated with D<sub>2</sub>O–NaOD and then reduced with PCl<sub>3</sub>. However, this synthesis is arduous, particularly because of the low overall yield. Furthermore, the bis(*N*-oxide) must be prepared from 2,2'-bipyridyl.

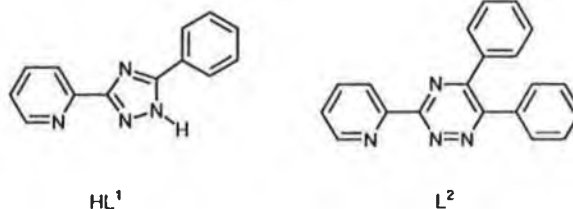
The improved synthesis reported here employs mild conditions and allows for a single-step, direct deuteriation of 2,2'-bipyridyl. Although the reaction times are long, the synthesis is simple and the yields are high. In a typical run, 2,2'-bipyridyl (bipy) (3 g, 0.19 mol) was added to 30 cm<sup>3</sup> of D<sub>2</sub>O (deuteriation 99.9%) and the reaction mixture allowed to react in the presence of the H–D exchange catalyst Pd/C (Aldrich, 10% Pd) (0.5 g) in a Teflon-coated steel high pressure reactor at 200 °C for 8 d. The contents of the reactor were then collected and filtered hot to remove the Pd catalyst and D<sub>2</sub>O was removed under vacuum to obtain the product. The Pd/C catalyst was washed with acetone to remove any product

present on its surface and the material obtained in this manner was recrystallised from hot water. The <sup>1</sup>H NMR spectrum of the product obtained revealed four singlets, indicating >80% deuteriation. To achieve complete deuteriation, the same procedure was repeated with fresh D<sub>2</sub>O for another week and the reaction mixture worked up as described above. The overall yield of the fully deuteriated product [<sup>2</sup>H<sub>8</sub>]bipy was >80%, and the material obtained was <sup>1</sup>H-NMR silent. Infrared spectroscopy showed bands at 2250–2295 cm<sup>-1</sup>, attributed to ν<sub>C–D</sub> vibrations.

Our method to determine the emitting and spectator ligands in mixed-ligand complexes is best illustrated by considering two different Ru<sup>II</sup> complexes [Ru(bipy)L<sup>1</sup>]<sup>+</sup> **1** and [Ru(bipy)L<sup>2</sup>]<sup>2+</sup> **2** [HL<sup>1</sup> = 3-phenyl-5-(pyridin-2-yl)-1,2,4-triazole, L<sup>2</sup> = 5,6-diphenyl-3-(pyridin-2-yl)-1,2,4-triazine]. (Similar results were obtained for a range of other Ru<sup>II</sup> polypyridyl compounds.<sup>7</sup>) These complexes were isolated as their PF<sub>6</sub> salts using literature methods,<sup>8,9</sup> yielding the undeuteriated [Ru(bipy)<sub>2</sub>L][PF<sub>6</sub>]<sub>n</sub> compounds **1h** (L = L<sup>1</sup>, n = 1) and **2h** (L = L<sup>2</sup>, n = 2) and the deuteriated [Ru-(<sup>2</sup>H<sub>8</sub>]bipy)<sub>2</sub>L][PF<sub>6</sub>]<sub>n</sub> compounds **1d** and **2d**.

For the undeuteriated complexes **1h** and **2h**, emission lifetimes (room temperature, acetonitrile, deaerated) of 225 and 740 ns were obtained respectively. Their deuteriated counterparts, **1d** and **2d**, yielded values of 410 and 780 ns under the same conditions (all values ± 15 ns). No significant differences were observed in the absorption and emission energies for the bipy and [<sup>2</sup>H<sub>8</sub>]bipy species. The absorption and emission maxima are found at respectively 482 nm and 690 nm for **1h** and **1d** and at 480 nm and 714 nm for **2h** and **2d** (all values ± 5 nm).

According to Siebrand's theory of the non-radiative transition,<sup>10</sup> high energy, anharmonic C–H stretching vibrations



are important promotional modes in non-radiative decay. This implies that excited-state lifetimes should increase upon deuteration. For compound **1**, the expected increase of the emission lifetime upon deuteration of bipy is indeed observed. However, for compound **2** no significant change in the emission lifetime is observed upon deuteration of bipy. We propose that this behaviour is associated with the location of the excited state, *i.e.* whether the excited state is bipy or L based. In compound **1**, which contains an electron-rich triazolone donor, the emitting state is firmly bipy based.<sup>8</sup> In the triazine-containing complex **2**, however, the emitting state is based on the electron-poor triazine ligand<sup>9</sup> and as a result the vibrational modes affected by the deuteration are *not available* for a deactivation of the excited state.

Our results therefore suggest strongly that in heteroleptic compounds the emission lifetimes will only increase upon deuteration of a particular ligand when the excited state is located on this ligand. This result is on reflection not unexpected. However, there is to the best of our knowledge no prior mention of this phenomenon in the literature, which may be of considerable importance in the field of supramolecular chemistry. By a systematic deuteration of the different components in a supramolecular system information about the relative excited-state energies of these components in the supramolecular system can be obtained in a very direct manner. Importantly, we expect that our method can be adapted to other polypyridyl-type ligands. Experiments have already shown that perdeuterated 1,10-phenanthroline can be prepared by the same method. In particular, we see application of our method in the study of mixed-ligand ruthenium dyes used in solar-energy conversion systems<sup>11</sup> and in the investigation of large multinuclear ruthenium and osmium clusters such as those reported by Balzani and co-workers.<sup>12</sup>

#### Acknowledgements

We thank Forbairt and the EC JOULE Programme for financial assistance. J. G. V. also thanks CIBA for a Senior Fellowship and the EPFL for a visiting Professorship.

#### References

- 1 V. Balzani and F. Scandola, *Supramolecular Photochemistry*, Ellis Horwood, Chichester, 1991.
- 2 P. K. Mallick, G. D. Danzer, D. P. Strommen and J. R. Kincaid, *J. Phys. Chem.*, 1988, **92**, 5628; G. D. Danzer, J. A. Golus, D. P. Strommen and J. R. Kincaid, *J. Raman Spectrosc.*, 1990, **1**, 21; P. G. Bradley, N. Kress, B. A. Hornberger, R. F. Dallinger and W. H. Woodruff, *J. Am. Chem. Soc.*, 1981, **103**, 7441; H. P. Hughes, D. Martin, S. Bell, J. J. McGarvey and J. G. Vos, *Inorg. Chem.*, 1993, **32**, 4402.
- 3 J. van Houten and R. J. Watts, *J. Am. Chem. Soc.*, 1975, **97**, 3843; J. van Houten and R. J. Watts, *J. Am. Chem. Soc.*, 1976, **98**, 4853.
- 4 H. Yersin and D. Braun, *Chem. Phys. Lett.*, 1991, **179**, 85; P. Huber and H. Yersin, *J. Phys. Chem.*, 1993, **97**, 12705; D. Braun, P. Huber, J. Wudy, J. Schmidt and H. Yersin, *J. Phys. Chem.*, 1994, **98**, 8044.
- 5 S. Chirayil and R. P. Thummel, *Inorg. Chem.*, 1989, **28**, 813.
- 6 M. J. Cook, A. P. Lewis, G. S. G. McAuliffe, V. Skarda, A. J. Thompson, J. L. Glasper and D. J. Robbins, *J. Chem. Soc., Perkin Trans. 2*, 1984, 1293.
- 7 T. E. Keyes, Ph.D. Thesis, Dublin City University, 1994.
- 8 R. Hage, J. G. Haasnoot, J. Reedijk and J. G. Vos, *Chemtracts-Inorg. Chem.*, 1992, **4**, 75.
- 9 R. Hage, J. H. van Dieman, G. Ehrlich, J. G. Haasnoot, D. J. Stufkens, T. L. Snoeck, J. G. Vos and J. Reedijk, *Inorg. Chem.*, 1990, **29**, 988.
- 10 W. Siebrand, *J. Chem. Phys.*, 1967, **46**, 440; W. Siebrand, *J. Chem. Phys.*, 1971, **55**, 5843.
- 11 B. O'Regan and M. Grätzel, *Nature (London)*, 1991, **353**, 737; M. K. Nazeeruddin, A. Kay, I. Rodicio, R. Humphry-Baker, E. Müller, P. Liska, N. Vlachopoulos and M. Grätzel, *J. Am. Chem. Soc.*, 1993, **115**, 6382; P. Pechy, F. P. Rotzinger, M. K. Nazeeruddin, O. Kohle, S. M. Zakeeruddin, R. Humphry-Baker and M. Grätzel, *J. Chem. Soc., Chem. Commun.*, in the press.
- 12 G. Denti, S. Campagna, S. Serroni, M. Ciano and V. Balzani, *J. Am. Chem. Soc.*, 1992, **114**, 2944; A. Juris, V. Balzani, S. Campagna, G. Denti, S. Serroni, G. Frei and H. U. Gudel, *Inorg. Chem.*, 1994, **33**, 1491.

Received 22nd June 1995; Communication 5/04038H

# Homo- and Heteronuclear Ruthenium and Osmium Complexes Containing an Asymmetric Pyrazine-Based Bridging Ligand

Ronald Hage,<sup>†</sup> Hans E. B. Lempers,<sup>‡</sup> Jaap G. Haasnoot, and Jan Reedijk

Leiden Institute of Chemistry, Gorlaeus Laboratories, P.O. Box 9502, 2300 RA Leiden, The Netherlands

Frances M. Weldon and Johannes G. Vos\*

School of Chemical Sciences, Dublin City University, Dublin 9, Ireland

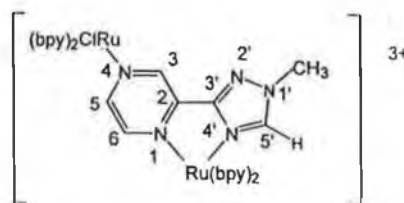
Received October 22, 1996<sup>⊗</sup>

The synthesis, characterization, and electrochemical, photophysical, and photochemical properties of the compounds  $[\text{Ru}(\text{bpy})_2(\text{L})]^{2+}$  (**Ru**),  $[\text{Os}(\text{bpy})_2(\text{L})]^{2+}$  (**Os**),  $[(\text{L})\text{Os}(\text{bpy})_2\text{Cl}]^+$  (**OsCl**),  $[\text{Ru}(\text{bpy})_2(\text{L})\text{Ru}(\text{bpy})_2\text{Cl}]^{3+}$  (**RuRuCl**),  $[\text{Os}(\text{bpy})_2(\text{L})\text{Os}(\text{bpy})_2\text{Cl}]^{3+}$  (**OsOsCl**),  $[\text{Ru}(\text{bpy})_2(\text{L})\text{Os}(\text{bpy})_2\text{Cl}]^{3+}$  (**RuOsCl**), and  $[\text{Os}(\text{bpy})_2(\text{L})\text{Ru}(\text{bpy})_2\text{Cl}]^{3+}$  (**OsRuCl**) are reported (bpy = 2,2'-bipyridine, L = 1-methyl-3-(pyrazin-2-yl)-1,2,4-triazole). The  $\text{Os}(\text{bpy})_2$  and the  $\text{Ru}(\text{bpy})_2$  moieties are coordinated to the pyrazyltriazole ligand in two different ways, *i.e.* in a bidentate fashion *via* the triazole ring and N1 of the pyrazine ring and in a monodentate fashion only *via* N4 of the pyrazine ring. In the homonuclear dimers the monodentate bound metal has an oxidation potential that is approximately 400 mV lower than that of the bidentate bound metal. Spectroelectrochemical investigations suggest the presence of a weak interaction between the metal centers in the dinuclear species. The emission properties of the compounds are indicative of efficient energy transfer in the excited state, leading to emission from only one metal unit. In acetone both **RuRuCl** and the **OsRuCl** show photodissociation of the monodentate ruthenium moiety; however, **RuOsCl** and **OsOsCl** were found to be photostable.

## Introduction

Extensive investigations have revealed that mononuclear and polynuclear ruthenium compounds exhibit interesting electrochemical, photophysical, and photochemical properties.<sup>1–7</sup> The polynuclear compounds exhibit in many cases photoinduced energy- and electron-transfer processes that are strongly related to the properties of the bridging ligand employed. We have undertaken a systematic study of mononuclear and dinuclear ruthenium–bpy complexes containing various triazole ligands. An interesting feature of triazole ligands is that the position of substituents on the triazole ring determines which coordination mode prevails, *i.e.* N1' vs N4' coordination.<sup>8</sup> In addition, triazole-based ligands, being strong  $\sigma$ -donors, have been shown to promote electronic interaction between metal centers.<sup>9</sup> In a previous paper the synthesis and physical properties of a series of ruthenium complexes containing pyrazyltriazoles were presented. We have shown that for 3-(pyrazin-2-yl)-1,2,4-

triazole the lowest unoccupied molecular orbital (LUMO) in these complexes can be located on the pyrazinyltriazole ligand or on the bpy ligands, depending on whether the triazole ring is protonated or not.<sup>10</sup> Pyrazines can also act as bidentate ligands. Protons or metal ions may coordinate to the uncoordinated N4 atom of pyrazine-based ligands for example as in  $[\text{Ru}(\text{bpz})_3]^{2+}$  (bpz = 2,2'-bipyrazine),<sup>11,12</sup> and pyrazine-based dinuclear compounds have been studied in great detail.<sup>13</sup> In this contribution we report the properties of a series of homo- and heteronuclear ruthenium- and osmium-based dinuclear compounds with the pyrazyltriazole ligand 1-methyl-3-(pyrazin-2-yl)-1,2,4-triazole (L), where one metal center is bound in a bidentate fashion and a second *via* N4 of the pyrazine ring shown as follows:



The effect of the asymmetric coordination geometry on the electrochemical, electronic, and photochemical properties will be discussed. The electronic properties of the intervalence compounds are investigated. Emission and electrochemical

<sup>†</sup> Current address: Unilever Research Laboratory, Olivier van Noortlaan 120, 3133 AT Vlaardingen, The Netherlands.

<sup>‡</sup> Current address: Department of Organic Chemistry and Catalysis, Technical University Delft, Julianalaan 136, 2628 BL, Delft, The Netherlands.

<sup>⊗</sup> Abstract published in *Advance ACS Abstracts*, June 1, 1997.

- (1) Seddon, E. A.; Seddon, K. R. *The Chemistry of Ruthenium*; Elsevier: Amsterdam, 1984.
- (2) Krause, R. A. *Struct. Bonding* 1987, 67, 1.
- (3) Kalyanasundaram, K. *Coord. Chem. Rev.* 1982, 46, 159.
- (4) Kalyanasundaram, K.; Grätzel, M.; Perlizzetti, E. *Coord. Chem. Rev.* 1986, 69, 57.
- (5) Dürr, H.; Dörr G.; Zengerle, K.; Mayer, E.; Curchod, J. H.; Braun, A. M. *Nouv. J. Chim.* 1985, 9, 717.
- (6) Crutchley, R. J.; Lever, A. B. P. *J. Am. Chem. Soc.* 1980, 102, 7129.
- (7) Juris, A.; Balzani, V.; Barigelli, F.; Campagna, S.; Belsler, P.; von Zelewsky, A. *Coord. Chem. Rev.* 1988, 84, 85.
- (8) Forster, R. J.; Boyle, A.; Vos, J. G.; Hage, R.; Dijkhuis, A. H. J.; Graaf, R. A. G.; Haasnoot, J. G.; Reedijk, J. *J. Chem. Soc., Dalton Trans.* 1990, 121.
- (9) Hage, R.; Prins, R.; de Graaff, R. A. G.; Haasnoot, J. G.; Reedijk, J.; Vos, J. G. *Acta Crystallogr., Sect. C* 1988, C44, 56.

- (10) Nieuwenhuis, H. A.; Haasnoot, J. G.; Hage, R.; Reedijk, J.; Snoeck, T. L.; Stufkens, D. J.; Vos, J. G. *Inorg. Chem.* 1991, 30, 48.
- (11) (a) Toma, H. E.; Lever, A. B. P. *Inorg. Chem.* 1986, 25, 176. (b) *Ibid.* *Inorg. Chem.* 1987, 26, 4257. (c) Toma, H. E.; Santos, P. S.; Lever, A. B. P. *Inorg. Chem.* 1988, 27, 3850.
- (12) Crutchley, R. J.; Kress, N.; Lever, A. B. P. *J. Am. Chem. Soc.* 1983, 105, 1170.
- (13) Balzani, V.; Juris, J.; Venturi, M.; Campagna, S.; Serroni, S. *Chem. Rev.* 1996, 96, 759.

experiments suggest that in these compounds interaction exists between the two metal centers *via* the pyrazine bridge.

## Experimental Section

**Synthesis and Materials.** 1-Methyl-3-(pyrazin-2-yl)-1,2,4-triazole (L) was obtained as reported elsewhere.<sup>10</sup> *cis*-[Ru(bpy)<sub>2</sub>Cl<sub>2</sub>]<sub>2</sub>·2H<sub>2</sub>O and *cis*-[Os(bpy)<sub>2</sub>Cl<sub>2</sub>] were prepared according to literature methods.<sup>14,15</sup>

**[Ru(bpy)<sub>2</sub>(L)](PF<sub>6</sub>)<sub>2</sub>·H<sub>2</sub>O (Ru).** L (0.5 mmol, 80 mg) was dissolved in 400 mL of hot ethanol/water (1/1 v/v). *cis*-[Ru(bpy)<sub>2</sub>Cl<sub>2</sub>]<sub>2</sub>·2H<sub>2</sub>O (0.5 mmol, 240 mg) was added in small portions to the dissolved ligand, and the mixture was heated at reflux for 24 h. The solution was filtered, evaporated to dryness, and dissolved in 20 mL of water. The complex was purified using a Sephadex SP-25 cation exchange column. Elution took place with a 0.6 M NaCl solution. The complex was isolated as the PF<sub>6</sub><sup>-</sup> salt, further purified using neutral alumina as column material and acetone as eluent, and finally recrystallized from an acetone/water mixture (1/1 v/v) Yield: 240 mg (55%). Anal. Found: C, 36.41; H, 2.51; N, 14.03. Calcd for C<sub>27</sub>H<sub>25</sub>F<sub>12</sub>N<sub>9</sub>P<sub>2</sub>O<sub>2</sub>Ru: C, 36.75; H, 2.86; N, 14.28.

<sup>1</sup>H NMR [(CD)<sub>3</sub>CO] for L: 9.46 (d; H<sub>3</sub> L), 8.06 (q; H<sub>6</sub> L), 8.59 (d; H<sub>5</sub> L), 8.71 (s; H<sub>5'</sub>), 4.09 ppm (s; CH<sub>3</sub>). The chemical shifts of the bpy ligands are in the range found for other Ru(bpy)<sub>2</sub> compounds.<sup>10</sup>

**[Os(bpy)<sub>2</sub>(L)](PF<sub>6</sub>)<sub>2</sub> (Os) and [(L)Os(bpy)<sub>2</sub>Cl]PF<sub>6</sub>·H<sub>2</sub>O (OsCl).** These compounds were prepared as Ru except that the monocationic charged OsCl complex was collected after elution with a 0.08 M NaCl solution and Os was collected after elution with a 0.6 M NaCl solution. Yield for Os: 180 mg (38%). Anal. Found: C, 33.93; H, 2.40; N, 13.43. Calcd for C<sub>27</sub>H<sub>23</sub>F<sub>12</sub>N<sub>9</sub>P<sub>2</sub>O<sub>2</sub>Os: C, 34.01; H, 2.43; N, 13.22. Yield for OsCl: 30 mg (6%). Anal. Found: C, 38.16; H, 2.91; N, 14.05. Calcd for C<sub>27</sub>H<sub>25</sub>ClF<sub>6</sub>N<sub>9</sub>OPOs: C, 37.61; H, 2.92; N 14.62.

<sup>1</sup>H NMR for L in Os [(CD)<sub>3</sub>CO]: 9.41 (d; H<sub>3</sub> L), 8.06 (q; H<sub>6</sub> L), 8.38 (d; H<sub>5</sub> L), 8.71 (s; H<sub>5'</sub>), 4.08 ppm (s; CH<sub>3</sub>). <sup>1</sup>H NMR for L in OsCl [(CD)<sub>3</sub>CO, 298 K]: 9.73 (d; H<sub>6</sub> bpy), 8.42 (s; H<sub>5'</sub> L), 8.32 (br H<sub>6</sub> L), 4.05 ppm (s; CH<sub>3</sub>). The chemical shifts of the protons of the bpy ligands are in the range as found for the analogous ruthenium complex.

**[Ru(bpy)<sub>2</sub>(L)Ru(bpy)<sub>2</sub>Cl](PF<sub>6</sub>)<sub>3</sub>·4H<sub>2</sub>O (RuRuCl).** L (0.25 mmol, 40 mg) and an excess of *cis*-[Ru(bpy)<sub>2</sub>Cl<sub>2</sub>]<sub>2</sub>·2H<sub>2</sub>O were heated at reflux in 50 mL of ethanol/water (1/1 v/v) for 24 h. The compound was purified and isolated as described for Ru, except that elution took place with a 3 M NaCl solution. Yield: 300 mg (82%). Anal. Found: C, 37.12; H, 2.59; N, 11.90. Calcd for C<sub>47</sub>H<sub>47</sub>ClF<sub>18</sub>N<sub>13</sub>O<sub>4</sub>P<sub>3</sub>Ru<sub>2</sub>: C, 36.89; H, 3.10; N, 11.90. MS (*m/e*): [(M - PF<sub>6</sub><sup>-</sup>)]<sup>+</sup>, 1313 (calcd, 1312.5).

**[Os(bpy)<sub>2</sub>(L)Os(bpy)<sub>2</sub>Cl](PF<sub>6</sub>)<sub>3</sub>·H<sub>2</sub>O (OsOsCl).** This complex was prepared as for RuRuCl, except that the solution containing *cis*-[Os(bpy)<sub>2</sub>Cl<sub>2</sub>] and ligand was refluxed for 3 days. Yield: 180 mg (44%). Anal. Found: C, 34.20; H, 2.53; N, 10.80. Calcd for C<sub>47</sub>H<sub>41</sub>ClF<sub>18</sub>N<sub>13</sub>O<sub>3</sub>Os<sub>2</sub>: C, 34.12; H, 2.50; N, 11.00. MS (*m/e*): [(M - PF<sub>6</sub><sup>-</sup>)]<sup>+</sup>, 1491 (calcd, 1490.5).

**[Ru(bpy)<sub>2</sub>(L)Os(bpy)<sub>2</sub>Cl](PF<sub>6</sub>)<sub>3</sub>·4H<sub>2</sub>O (RuOsCl).** A 0.125 mmol amount of [Ru(bpy)<sub>2</sub>(L)]<sup>2+</sup> and 0.125 mmol of *cis*-[Os(bpy)<sub>2</sub>Cl<sub>2</sub>] were heated at reflux in 50 mL of ethanol/water (1/1 v/v) for 3 days. The complex was purified as described for RuRuCl. Yield: 125 mg (64%). Anal. Found: C, 34.96; H, 2.32; N, 11.15. Calcd for C<sub>47</sub>H<sub>47</sub>ClF<sub>18</sub>N<sub>13</sub>O<sub>4</sub>P<sub>3</sub>OsRu: C, 34.86; H, 2.93; N, 11.24. MS (*m/e*): [(M - PF<sub>6</sub><sup>-</sup>)]<sup>+</sup>, 1402 (calcd, 1401.5).

**[Os(bpy)<sub>2</sub>(L)Ru(bpy)<sub>2</sub>Cl](PF<sub>6</sub>)<sub>3</sub>·HPF<sub>6</sub>·2H<sub>2</sub>O (OsRuCl).** A 0.125 mmol amount of [Os(bpy)<sub>2</sub>(L)]<sup>2+</sup> and 0.125 mmol of *cis*-[Ru(bpy)<sub>2</sub>Cl<sub>2</sub>]<sub>2</sub>·2H<sub>2</sub>O were heated at reflux in 50 mL of ethanol/water (1/1 v/v) for 24 h. The complex was purified as described for RuRuCl. Yield: 100 mg (51%). Anal. Found: C, 32.98; H, 2.43; N, 10.19. Calcd for C<sub>47</sub>H<sub>44</sub>ClF<sub>24</sub>N<sub>13</sub>O<sub>2</sub>P<sub>4</sub>OsRu: C, 32.64; H, 2.56; N, 10.53.

**Physical Measurements.** <sup>1</sup>H-NMR and COSY <sup>1</sup>H-NMR were recorded on a Bruker WM 300 spectrometer. UV-vis measurements were obtained on 10<sup>-5</sup>–10<sup>-4</sup> M solutions on a Perkin-Elmer 330 or a Shimadzu UV-240 spectrophotometer by using 1 cm quartz cells. Emission spectra were recorded on a Perkin-Elmer LS5 and on a Perkin-

## Scheme 1

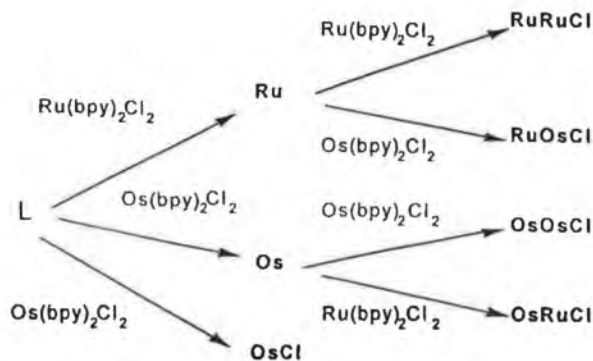


**Table 1.** Electrochemical Data for Mononuclear and Dinuclear Pyrazyltriazole Complexes

| compd  | metal-based oxidn potential |      | ligand-based redn potential <sup>a</sup> |       |                    |                    |
|--------|-----------------------------|------|--|-------|--------------------|--------------------|
|        |                             |      |  |       |                    |                    |
| OsCl   | 0.45                        |      | -1.44                                    | -1.68 | -1.90 <sup>b</sup> |                    |
| Os     | 0.86                        |      | -1.20                                    | -1.48 | -1.60 <sup>b</sup> |                    |
| Ru     | 1.32                        |      | -1.27                                    | -1.54 | -1.81              |                    |
| RuRuCl | 0.92                        | 1.41 | -0.97                                    | -1.51 | -1.57              | -1.76 <sup>b</sup> |
| OsOsCl | 0.50                        | 1.00 | -0.80                                    | -1.53 | -1.74 <sup>b</sup> | -1.89 <sup>b</sup> |
| RuOsCl | 0.53                        | 1.41 | -0.95                                    | -1.51 | -1.75 <sup>b</sup> | -1.89 <sup>b</sup> |
| OsRuCl | 0.86                        | 1.04 | -0.87                                    | -1.49 | -1.70 <sup>b</sup> | -1.87 <sup>b</sup> |

<sup>a</sup> Measurements were carried out in acetonitrile containing 0.1 M TBAP using differential pulse polarography. Potentials are listed in volt *versus* SCE. <sup>b</sup> Irreversible wave.

Elmer LS50 luminescence spectrometer. Room-temperature measurements were carried out in acetonitrile, while measurements at 77 K were carried out in methanol (approximately 10<sup>-5</sup> M solutions). Spectra were not corrected for photomultiplier response. Photolysis experiments were carried out at room temperature in acetone using visible light with a 400 W light source.

The differential pulse voltammetry (DPV) experiments (4 mV/s, pulse height 20 mV) and the cyclic voltammograms (CV) (100 mV/s) were carried out on a EG & G Par C Model 303 instrument with an EG & G 384 B polarographic analyzer. A saturated calomel electrode (SCE) was used as a reference electrode. The electrolyte used for all electrochemical experiments was acetonitrile, containing 0.1 M tetrabutylammonium perchlorate (TBAP). Spectroelectrochemical experiments were carried out using a Shimadzu UV-3100 UV-vis-NIR spectrophotometer and an EG & G Princeton Applied Research (PAR) Mode 362 scanning potentiostat. Platinum-mesh working, platinum-wire counter, and anodized silver-wire quasi-reference electrodes were used for the electrolysis experiments. Experiments in the UV-vis and near-infrared regions were performed on solutions of approximately 2.0 × 10<sup>-5</sup> and 2.0 × 10<sup>-3</sup> M, respectively. Spectra were recorded at regular intervals until the solution had equilibrated at a given potential. The plasma-desorption mass spectra were obtained as described before.<sup>16</sup>

The purity of the complexes was checked using analytical high performance liquid chromatography (HPLC). A Waters 990 photodiode array HPLC system with a NEC PAC 3 computer, a Waters Model 6000A pump, a 20 μL injector loop, and a μ Particil SCX radial PAK cartridge have been used for the measurements. The detection wavelength was 280 nm. Chromatography was performed by using acetonitrile/water (4/1 v/v) containing 0.08 M LiClO<sub>4</sub> with a flow rate of 3.5 mL/min.

## Results

An outline for the synthesis of the mononuclear, homo- and heterodinuclear ruthenium and osmium complexes with 1-methyl-3-(pyrazin-2-yl)-1,2,4-triazole (L) is presented in Scheme 1. By this controlled reaction of Os(bpy)<sub>2</sub> and Ru(bpy)<sub>2</sub> moieties

(14) Sullivan, B. P.; Salmon, D. J.; Meyer, T. J. *Inorg. Chem.* 1978, 17, 3334.

(15) Lay, P. A.; Sargeson, A. M.; Taube, H.; Chou, M. H.; Creutz, C. *Inorg. Synth.* 1986, 24, 291.

(16) Van Veelen, P. A.; Hage, R.; Tjaden, U. R.; van der Greef, J. *Org. Mass. Spectrosc.* 1991, 26, 74.

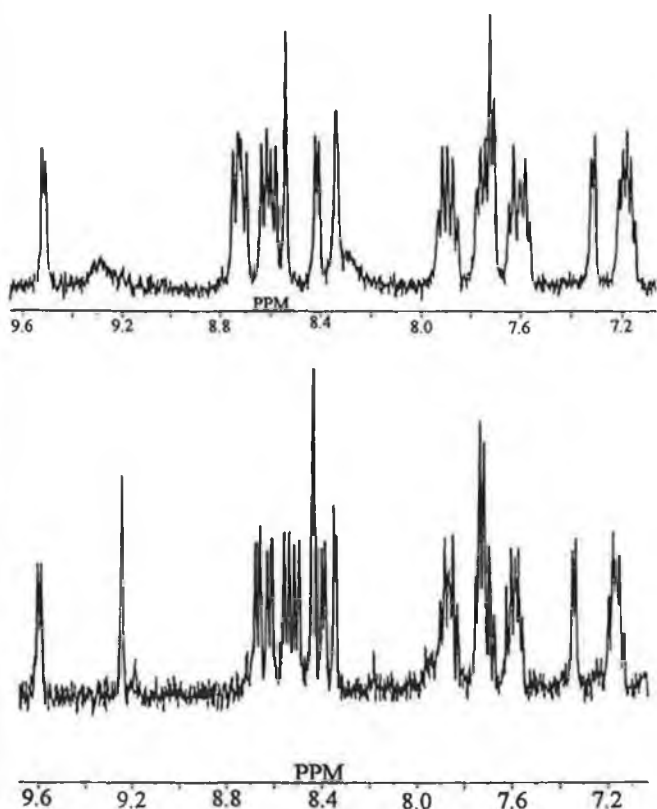


Figure 1.  $^1\text{H}$  NMR spectra obtained for  $\text{OsCl}$  in  $(\text{CD}_3)_2\text{SO}$  at (a) 323 and (b) 403 K.

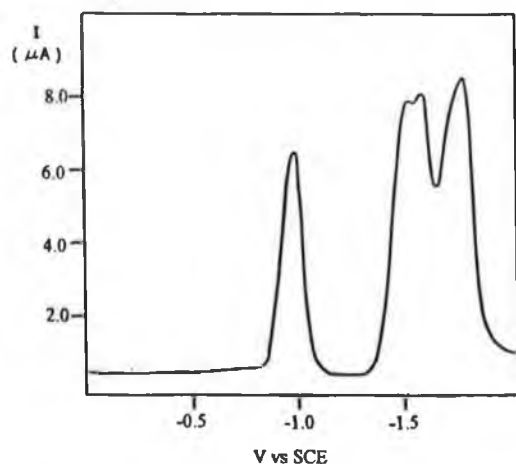


Figure 2. Differential pulse voltammogram for  $\text{RuRuCl}$  in acetonitrile containing 0.1 M TBAP.

with the two coordination sites of the pyrazyltriazole ligand seven complexes have been synthesized. The compounds have been fully characterized by elemental analysis and  $^1\text{H}$  NMR spectroscopy. The  $^1\text{H}$  NMR spectra obtained for  $\text{OsCl}$  are temperature dependent. Spectra obtained for this compound at 323 and 403 K are shown in Figure 1.

The electrochemical data of the compounds are listed in Table 1. Most redox processes are reversible with peak-to-peak separations of about 90 mV. A typical differential pulse voltammogram obtained for the reduction of  $\text{RuRuCl}$  is presented in Figure 2. The absorption maxima in the visible part of the spectrum and the emission data are listed in Table 2. Some typical spectra are shown in Figures 3 and 4.

Spectroelectrochemical experiments have also been carried out. Upon one-electron oxidation of the dinuclear compounds  $\text{MM}'\text{Cl}$  stable mixed-valence species  $\text{MM}'\text{Cl}^+$  were obtained. The UV-vis spectral features observed for these singly oxidized

Table 2. UV/Vis Absorption and Emission Data for Compounds Prepared and Their Singly Oxidized Analogues<sup>a</sup>

| compd             | absorption <sup>b</sup> [ $\lambda_{\text{max}}/\text{nm}$ ( $\epsilon/10^4 \text{ M}^{-1} \text{ cm}^{-1}$ )] |            |            |            | emission <sup>c</sup> ( $\lambda_{\text{max}}/\text{nm}$ ) |       |
|-------------------|--|------------|------------|------------|--|-------|
|                   |  |            |            |            | 77 K   | 300 K |
| $\text{OsCl}$     | 412 (1.21)   | 490 (1.33) | 620 (0.40) | 740 (sh)   | n.o.   | n.o.  |
| $\text{Os}$       | 425 (1.20)   | 465 (1.38) | 570 (0.39) | 620 (sh)   | 708  | 755   |
| $\text{Os}^+$     | 460 (0.4)  | 551 (0.35) |            |            |  |       |
| $\text{Ru}$       | 437 (1.46)   |            |            |            | 577  | 633   |
| $\text{Ru}^+$     | 415 (0.16)   |            |            |            |  |       |
| $\text{RuRuCl}$   | 440 (1.70)   | 530 (1.90) |            |            | 705  | 730   |
| $\text{RuRuCl}^+$ | 423 (0.95)   | 504 (1.9)  |            |            |  |       |
| $\text{OsOsCl}$   | 445 (1.76)   | 563 (2.55) | 687 (1.08) | 775 (1.87) | n.o.   | n.o.  |
| $\text{OsOsCl}^+$ | 423 (1.15)   | 522 (1.90) | 749 (0.40) |            |  |       |
| $\text{RuOsCl}$   | 443 (1.87)   | 560 (2.61) | 745 (0.95) |            | n.o.   | n.o.  |
| $\text{RuOsCl}^+$ | 418 (1.26)   | 509 (1.96) |            |            |  |       |
| $\text{OsRuCl}$   | 455 (1.92)   | 545 (2.17) | 680 (0.94) |            | 786  | n.o.  |
| $\text{OsRuCl}^+$ | 425 (1.40)   | 520 (1.36) |            |            |  |       |

<sup>a</sup> n.o.: not observed. <sup>b</sup> In ethanol. <sup>c</sup> In  $\text{CH}_3\text{CN}$  at room temperature and methanol at 77 K.

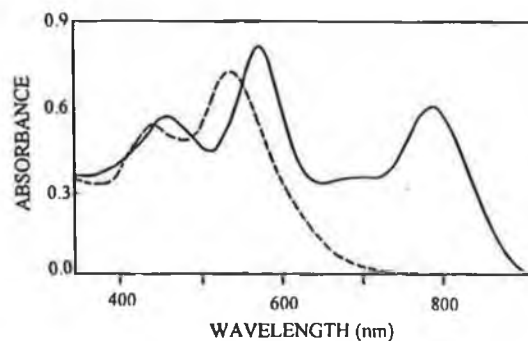


Figure 3. Absorption spectra of  $\text{RuRuCl}$  (a) and  $\text{OsOsCl}$  (b) in ethanol.

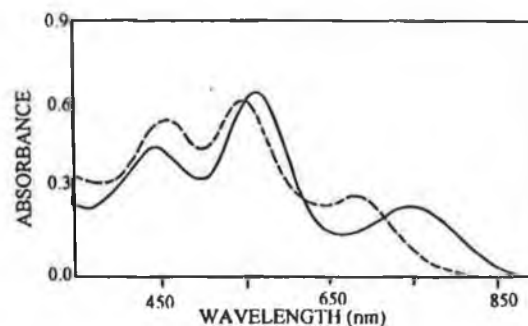
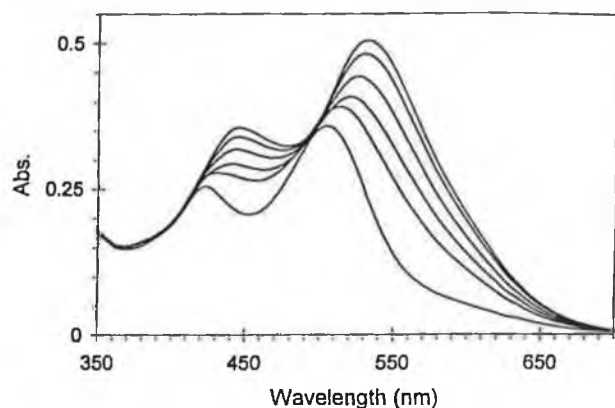


Figure 4. Absorption spectra of  $\text{RuOsCl}$  (a) and  $\text{OsRuCl}$  (b) in ethanol.

compounds are listed in Table 2. A typical set of results obtained in the UV/vis region for  $\text{RuRuCl}$  is shown in Figure 5. Further oxidation of the compounds leads to a complete bleaching of the absorption features in the visible part of the spectrum. Intervalence charge transfer bands obtained upon the formation of the  $\text{MM}'\text{Cl}^+$  species are listed in Table 3. Since a slow decomposition of the fully oxidized species was observed, these spectra were not analyzed in detail. Near-infrared spectra for  $\text{OsOsCl}^+$  and the totally oxidized  $\text{Os(III)}$  compound are available as Supporting Information (Figure S1).

Irradiation of  $\text{OsRuCl}$  and  $\text{RuRuCl}$  in acetone leads to photochemically induced ligand labilization as shown in Figure 6 for  $\text{RuRuCl}$ . The spectroscopic changes observed upon irradiation of  $\text{OsRuCl}$  are available as Supporting Information (Figure S2). HPLC analysis of the reaction shows the formation of  $\text{Os}$  and  $\text{Ru}$ , respectively.  $\text{Ru}$ ,  $\text{Os}$ ,  $\text{OsCl}$ ,  $\text{OsOsCl}$ , and  $\text{RuOsCl}$  were all photostable under the conditions used for at least 4 h.



**Figure 5.** Spectroelectrochemistry for **RuRuCl** in the UV/vis region. Potentials applied from top to bottom: 0, 0.90, 0.93, 0.95, 0.97, and 1 V vs SCE. Solvent: acetonitrile.

**Table 3.** Intervalence Transition Parameters for Mixed-Valence Species

|                           | $E_{\text{obs}}$<br>( $\text{cm}^{-1}$ ) | $E_{\text{calc}}^a$<br>( $\text{cm}^{-1}$ ) | $\epsilon$<br>( $\text{M}^{-1} \text{cm}^{-1}$ ) | $\Delta\nu_{1/2}^{\text{obs}}$<br>( $\text{cm}^{-1}$ ) | $\Delta\nu_{1/2}^{\text{calc } b}$<br>( $\text{cm}^{-1}$ ) | $\alpha^2$           |
|---------------------------|--|---|--|--|--|----------------------|
| <b>RuRuCl<sup>+</sup></b> | 10400                                    |   | 480  | 4300   | 4000   | $1.8 \times 10^{-3}$ |
| <b>OsOsCl<sup>+</sup></b> | 7812                                     | 10500                                       | 360  | 2900   | 3200   | $1.2 \times 10^{-3}$ |
|                           | 5470                                     |   | 1200   | 1240   | 2250   | $1.7 \times 10^{-3}$ |
|                           | 4000                                     |   | 1050   | 460  | 1300   | $1.1 \times 10^{-3}$ |
| <b>RuOsCl<sup>+</sup></b> | 6000                                     | 13600                                       | 720  | 1070   | 2550   | $1.2 \times 10^{-3}$ |
| <b>OsRuCl<sup>+</sup></b> | 7690                                     | 7900  | 850  | 3100   | 3200   | $3.0 \times 10^{-3}$ |

<sup>a</sup> Values calculated with respect to **RuRuCl**; see text. <sup>b</sup> Values calculated according to: Hush, N. S. *Prog. Inorg. Chem.* **1967**, *8*, 391.

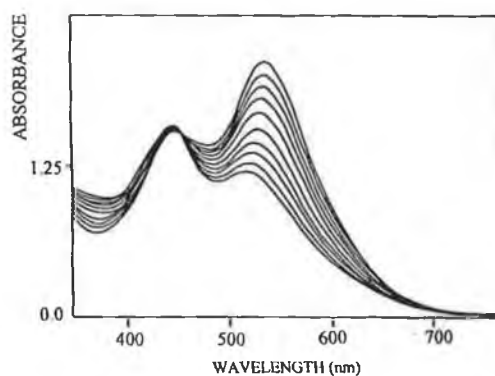


**Figure 6.** UV-vis absorption spectra of **RuRuCl** upon irradiation in acetone. The time between scans is 30 min.

## Discussion

**Synthesis and Characterization.** By a systematic variation of the reaction components and the use of chromatographic techniques, all compounds reported in this study could be prepared without much difficulty. We were however unable to isolate **RuCl**. Even in the absence of water, a reaction condition that normally favors the formation of species with a **[Ru(N<sub>5</sub>)Cl]** coordination mode,<sup>17</sup> only **Ru** was obtained. The osmium analog **OsCl** was obtained in small yield. Taking into account the decreased reactivity of osmium polypyridyl complexes, this is not unexpected. The homonuclear dimers were synthesized by reacting the ligand with an excess of *cis*-**[M(bpy)<sub>2</sub>Cl<sub>2</sub>]**. **RuOsCl** was prepared from the mononuclear ruthenium complex with an equimolar amount of *cis*-**[Os-**

**(bpy)<sub>2</sub>Cl<sub>2</sub>]**. **OsRuCl** was obtained in the same way but starting with mononuclear osmium complex and *cis*-**[Ru(bpy)<sub>2</sub>Cl<sub>2</sub>]**·2H<sub>2</sub>O.

We have shown before<sup>8-10,17,18</sup> that <sup>1</sup>H NMR can be helpful in the elucidation of the coordination modes of triazole-based ligands. The <sup>1</sup>H NMR spectra and in particular the resonances observed for the ligand **L** were therefore carefully analyzed. Resonances observed for the **bpy** ligands are as expected and do not yield any additional information.

The proton NMR spectra of **Ru** and **Os** are very similar (see Experimental Section), indicating similar structures for both compounds. Comparison with NMR and X-ray structural analyses on related compounds<sup>8-10</sup> suggests binding of **L** *via* N4' of the triazole group and N1 of the pyrazine ring. With this in mind, coordination of the second metal center in the mixed-metal dinuclear compounds has to be *via* either N2' of the triazole ring or N4 of the pyrazine moiety. This issue can be addressed by considering the <sup>1</sup>H NMR spectra obtained for **OsCl**. For this compound evidence for the presence of the coordinated chloride anion is obtained from the H6-**bpy** proton resonance at 9.73 ppm. A resonance at such low field is indicative of the presence of nonaromatic ligands and is caused by the absence of through-space interaction of this H6 proton with an adjacent aromatic ring.<sup>17</sup> The spectra obtained for this compound were shown to be temperature dependent (see Figure 1), and spectra were therefore recorded between 203 and 403 K. At 323 K the H3 and H5 pyrazine-based resonances are broadened considerably and are ill-defined. However, upon heating, sharp resonances at 9.24, 8.45, and 8.34 ppm are observed that can be assigned to the pyrazine protons H3, H5, and H6, respectively. The doublet observed for the H5 proton at 8.45 ppm overlaps with the signal obtained for H6 of a bipyridyl ring. Upon lowering of the temperature, sharpening of the resonances is again observed at about 250 K. The triazole- and **bpy**-based resonances in the spectrum are hardly affected by a change in temperature. The observed broadening of the pyrazine protons, in particular H3, suggests the presence of hindered rotation around the **Os**-pyrazine bond and therefore coordination of the monodentate bound metal center *via* the N4 atom of the pyrazine ring. The NMR spectra observed for the dimers are complex but show similar features. Most importantly we can rule out a coordination of the N2' triazole atom since in this case we would expect a significant shift of the neighboring methyl group to higher field because changes in electron density but most importantly because of interaction of the methyl group with the **bpy** ligands. In ruthenium complexes containing similar triazole ligands upfield shifts of between 0.5 and 1.0 ppm were observed as a result of these combined effects.<sup>18</sup> We therefore conclude that the coordination in all dinuclear compounds is the same and consistent with that observed for **OsCl**. This assumption is furthermore substantiated by the electrochemical properties of the compounds (*vide infra*).

**Electrochemistry.** The metal-based redox potentials for the **RuCl** and **OsCl** units are indicative of the coordination mode of the pyrazyltriazole ligand. The value observed for the **OsCl** complex of 0.45 V is similar to that reported by Meyer and co-workers for **[(bpy)<sub>2</sub>Os(pyr)Cl]<sup>+</sup>** (0.51 V) (pyr = pyrazine).<sup>19</sup> The coordination of an azole type ligand rather than pyrazine would lead to a lower redox potential. For example, the value obtained for the **[(bpy)<sub>2</sub>Os(imidazole)Cl]<sup>+</sup>** of 0.23 V<sup>20</sup> is substantially lower than that observed for **OsCl**. In addition, the redox potential reported by Meyer and co-workers of 0.88

(17) Buchanan, B. E.; Degn, P.; Pavon Velasco, J. M.; Hughes, H.; Creaven, B. S.; Long, C.; Vos, J. G.; Howie, R. A.; Hage, R.; van Diemen, J. H.; Haasnoot, J. G.; Reedijk, J. *J. Chem. Soc., Dalton Trans.* **1992**, 1177.

(18) Ryan, E. M.; Wang, R.; Vos, J. G.; Hage, R.; Haasnoot, J. G. *Inorg. Chim. Acta* **1993**, *208*, 49.

(19) Callahan, R. W.; Brown, G. M.; Meyer, T. J. *Inorg. Chem.* **1975**, *7*, 1443.

(20) Forster, R. J.; Vos, J. G. *Macromolecules* **1990**, *23*, 4372.

V for the  $[\text{Ru}(\text{bpy})_2(\text{pyz})\text{Cl}]^+$  moiety and of 0.89 V in the corresponding dinuclear compound<sup>21</sup> is in line with the value observed for the  $(\text{bpy})_2\text{RuCl}$  center in this investigation. The only value reported in the literature for a  $[(\text{bpy})_2\text{Ru}(\text{triazole})\text{Cl}]^+$  moiety is substantially lower at 0.66 V.<sup>17</sup> This again indicates that the monodentate unit is coordinated through the pyrazine rather than the triazole ring. In general, comparison of analogous osmium and ruthenium complexes shows a difference in the metal-based redox potential of 400 mV. This is explained by the higher energy of the 5d orbitals compared to the 4d orbitals of ruthenium leading to a lower redox potential for the osmium centers.<sup>22</sup> The dinuclear complexes reported exhibit two metal-based oxidation potentials. The difference in potentials varies from 180 mV for **OsRuCl** and 500 mV for **RuRuCl** and **OsOsCl** to 880 mV for **RuOsCl** (Table 1). These potential differences may be caused by a number of effects.<sup>23–29</sup> First, the different chemical environment of the two metal centers due to the different coordination modes will greatly influence the oxidation potential. In particular, the presence of the chloride group yields a significant lowering in oxidation potential. Also electrostatic effects play a role; oxidation of the first metal unit will cause an increase in charge of the complex, and this will result in a higher oxidation potential for the second metal unit. Finally, delocalization of charge of the mixed-valence species will shift the second oxidation potential to higher values than for localized systems. By comparison of the difference between the first and second oxidation potential of **OsOsCl** ( $\Delta E = 500$  mV) with that observed between **Os** and **OsCl** (410 mV), the combined influence of electrostatic and delocalization effects of 90 mV in the dimer has been inferred. Similarly, the second, ruthenium-based oxidation potential in **RuOsCl** and **RuRuCl** is 90 mV higher than observed for **Ru**.

While in **RuOsCl** the low oxidation potential has been assigned to the  $\text{OsCl}(\text{bpy})_2$  site and the higher oxidation potential to the bidentate-bound  $\text{Ru}(\text{bpy})_2$  group, an unambiguous assignment of the first oxidation potential for **OsRuCl** cannot be given, since both redox couples are expected at around 0.9 V.

The first reduction potential of **Ru** is observed at  $-1.27$  V and has been assigned to a reduction of the pyrazyltriazole ligand.<sup>10,26</sup> The second and third reductions are assigned to bpy-based reductions. The currents measured for all redox processes are indicative of one-electron redox reactions. The first reduction of **RuRuCl** at  $-0.97$  V is at considerably less negative potential than the first reduction of **Ru**. This is explained by a decrease in the electron density on the bridging ligand because of the presence of a second electron accepting ruthenium moiety. As expected, the pyrazine-based reduction is still a one-electron reduction, but the bpy-based reductions are now two-electron reductions (see Figure 2). Similarly, we propose that in the **Os**, **OsRuCl**, **RuOsCl**, and **OsOsCl** complexes the first reduction is pyrazine-based. The first reduction of **OsCl** is observed at considerably more negative potentials ( $-1.44$  V) and has been tentatively assigned as a bpy reduction.

**Electronic Spectroscopy.** The spectra obtained for the mononuclear compounds show the expected features. A series of bands in the UV can be assigned to bpy-based  $\pi \rightarrow \pi^*$  transitions. L-based transitions of this type could not be identified. For **Ru** <sup>1</sup>MLCT bands are observed in the visible part of the spectrum at about 440 nm. For **Os** and **OsCl** such bands are observed at 465 and 490 nm, respectively. The lower energy of these transitions is explained by a destabilization of the metal-based ground state in the **Os** complexes. The osmium complexes show additional bands in the 500–800 nm region. These are assigned to formally spin forbidden <sup>3</sup>MLCT transitions, which in osmium-based systems become partially allowed because of the large spin-orbit coupling observed for this second-row metal ion.<sup>22</sup>

The absorption observed for **RuRuCl** at 530 nm is in agreement with values observed for systems such as  $[\text{Ru}(\text{bpy})_2\text{Cl}(\text{pyz})\text{Ru}(\text{bpy})_2\text{Cl}]^{2+}$  and can be assigned to the monodentate coordinated **RuCl** unit. Work by Meyer and co-workers has shown that, upon assembly of the  $[\text{Ru}(\text{bpy})_2(\text{pyz})\text{Cl}]^+$  unit in the dinuclear complex  $[\text{Ru}(\text{bpy})_2\text{Cl}(\text{pyz})\text{Ru}(\text{bpy})_2\text{Cl}]^{2+}$ , a shift to lower energy is observed for the lowest MLCT transition from 478 to 513 nm.<sup>19,21</sup> For  $[\text{Ru}(\text{NH}_3)_5(\text{pyz})\text{Ru}(\text{bpy})_2\text{Cl}]^{3+}$  a similar shift from 455 to around 500 nm was observed for the  $\text{Ru}(\text{NH}_3)_5$  moiety upon incorporation into the dinuclear compound.<sup>19</sup> With this in mind it is unlikely that the band observed at 440 nm in **RuRuCl** can be assigned to the  $\text{Ru} \rightarrow \text{L}$  transition in the **Ru** moiety in this complex. We therefore propose that in **RuRuCl** the lowest energy MLCT band for the bidentate coordinated **Ru** center is hidden under the strong band at 530 nm. This analysis is confirmed by the spectra observed for the mixed-valence compounds discussed below. Because of their complexity the osmium spectra were not analyzed in detail. However, it is noted that the absorption spectrum of **OsOsCl** is not simply the sum of the spectra **Os** and **OsCl**. The interaction between the metal centers, as inferred from the electrochemical experiments, also affects the energies of the excited-state energy levels. It is worth noting that in the 400–500 nm region the osmium and ruthenium compounds show quite similar features (Figures 3 and 4). All dinuclear complexes show a band between 440 and 455 nm and a second one between 530 and 563 nm. This complicates a complete assignment of the absorption spectra of the compounds.

**Mixed-Valence Compounds.** In this section the spectral features of the  $\text{MM}'\text{Cl}^+$  mixed-valence compounds in the UV/vis region are discussed. In the UV part of the spectra oxidation of the first metal center leads in all compounds to the formation of a new double peak between 300 and 320 nm. The appearance of this peak is typical for the formation of trivalent **Ru** and **Os** species.<sup>30</sup> The disappearance of the band at 437 nm of the mononuclear **Ru** upon oxidation of the complex is in agreement with its assignment as a MLCT band. A new weak band at 680 nm has been assigned to a LMCT (ligand-to-metal charge transfer) band originating from the **Ru(III)** species.<sup>7,31</sup> In a similar way the visible absorptions observed for **Os** disappear upon oxidation.

The electrochemical data suggest that, upon formation of the mixed-valence species **RuRuCl**<sup>+</sup>, the **RuCl** moiety is oxidized first and therefore any features associated with this center should be absent in the spectrum obtained for the singly oxidized species (Figure 5). The remaining band at 504 nm (Table 2) has consequently been assigned as a <sup>1</sup>MLCT transition located

(21) Goldsby, K. A.; Meyer, T. J. *Inorg. Chem.* 1984, 23, 3002.  
 (22) (a) Kalyanasundaram, K.; Nazeeruddin, Md. K. *Chem. Phys. Lett.* 1989, 158, 45. (b) Kalyanasundaram, K.; Nazeeruddin, Md. K. *Inorg. Chim. Acta.* 1990, 171, 213.  
 (23) Ernst, S. D.; Kaim, W. *Inorg. Chem.* 1989, 28, 1520.  
 (24) Haga, M.; Matsumura-Inoue, T.; Yamabe, S. *Inorg. Chem.* 1987, 26, 4148.  
 (25) Rillema, D. P.; Mack, K. B. *Inorg. Chem.* 1982, 21, 3849.  
 (26) Braunstein, C. H.; Baker, A. D.; Streckas, T. C.; Gafney, H. D. *Inorg. Chem.* 1984, 23, 857.  
 (27) Sahai, R.; Baucom, D. A.; Rillema, D. P. *Inorg. Chem.* 1986, 25, 3843.  
 (28) Sahai, R.; Morgan, L.; Rillema, D. P. *Inorg. Chem.* 1988, 27, 3495.  
 (29) Haga, M. *Inorg. Chim. Acta* 1980, 45, L183.

(30) Heath, G. A.; Yellowlees, L. J.; Braterman, P. S. *J. Chem. Soc., Chem. Commun.* 1981, 287.  
 (31) Nazeeruddin, Md. K.; Zakeeruddin, S. M.; Kalyanasundaram, K. *J. Phys. Chem.* 1993, 97, 9607.

on the Ru center remaining. It has been shown before that upon oxidation of one of the metal centers in pyrazine dimers only a relatively small change is observed in the absorption spectrum of the remaining Ru(II) moiety even if interaction between the centers is present.<sup>19</sup> The values observed in the mixed-valence compound for the bidentate bound Ru center, therefore, support our earlier assumption that in **RuRuCl** species the lowest <sup>1</sup>MLCT absorption of this Ru unit is located under the 530 nm band.

Using similar arguments the bands at 563, 455, 687, and 775 nm that disappear upon the formation of the mixed-valence **OsOsCl**<sup>+</sup> species have been assigned to <sup>1</sup>MLCT and <sup>3</sup>MLCT bands from the monodentate bound OsCl site. The remaining absorptions at 526 and 428 nm are assigned to transitions originating from the bidentate bound metal center.

A single electron oxidation of **RuOsCl** leads to the disappearance of the absorptions at 745, 560, and 443 nm, which on the basis of the electrochemical data are assigned to the OsCl moiety. The new features at 504 and 423 nm are assigned to the ruthenium site. The energy of these absorptions is very similar to those observed for **RuRuCl**<sup>+</sup>, suggesting that the bidentate coordinated Ru moieties in both compounds have very similar properties.

As already stated above the location of the first oxidation in **OsRuCl** is difficult to establish since both sites have similar redox potentials. Upon formation of **OsRuCl**<sup>+</sup> bands at 683, 545, and 459 nm disappear while new bands are observed at 523 and 425 nm. The band at 680 nm is most likely associated with the osmium center, while the new band at 523 nm is similar to that observed for the RuCl center in **RuRuCl**. We therefore propose that the first redox process is osmium-based.

**Intervalence Transitions.** In this section the spectroscopic features of the singly oxidized compounds in the near infrared region are investigated. **RuRuCl**<sup>+</sup> shows a weak absorption band at 10 400 cm<sup>-1</sup> that disappears upon further oxidation. By comparison with other similar compounds<sup>19,21</sup> and since the band disappears upon further oxidation, this absorption has been assigned to an intervalence transition (IT). Information about the electron delocalization between the metal centers ( $\alpha^2$ ) can be obtained from the spectral features observed for the IT band using eq 1,<sup>22,32,33</sup> where  $\epsilon$  is the extinction coefficient of the IT

$$\alpha^2 = \frac{(4.2 \times 10^{-4})\epsilon(\Delta\nu_{1/2}^{\text{obs}})}{d^2 E_{\text{obs}}} \quad (1)$$

band (M<sup>-1</sup> cm<sup>-1</sup>),  $\Delta\nu_{1/2}^{\text{obs}}$  is observed bandwidth (cm<sup>-1</sup>),  $d$  is the distance estimated between the metal centers (6.8 Å), and  $E_{\text{obs}}$  is energy of the IT band. The values obtained from this equation for the various compounds are given in Table 3 and are similar to those reported for other pyrazine-bridged dimers.<sup>21</sup>

For the compounds containing osmium centers the analysis in the near-infrared region is complicated by the overlap of solvents peaks, Os(III)-based  $d\pi-d\pi$  transitions, and intervalence bands. **Os<sup>II</sup>Os<sup>III</sup>Cl**<sup>+</sup> exhibits bands at 7812, 5470, and 4000 cm<sup>-1</sup>. Upon further oxidation of the species bands at 6290, 5305, and 4274 cm<sup>-1</sup> are observed, while the three bands observed for the mixed-valence species have disappeared. We assign the bands observed for the totally oxidized species to transitions between different spin-orbit states localized at the Os(III) centers.<sup>21</sup> The bands observed for the mixed-valence species are tentatively assigned to the three IT bands expected

for a dinuclear osmium compound. The parameters obtained for these transitions are given in Table 3.

A band observed at 6000 cm<sup>-1</sup> in the spectrum of **RuOsCl**<sup>+</sup> has been assigned to an intervalence transition since the band disappears upon formation of the fully oxidized species. In the totally oxidized species a band at 6349 cm<sup>-1</sup> has been assigned to a transition between different spin-orbit states located on the osmium(III) center. **OsRuCl**<sup>+</sup> shows an IT band at 7690 cm<sup>-1</sup>. For this compound bands at 5947 and 4814 cm<sup>-1</sup> also appear in the spectrum upon initial oxidation, which are assigned as Os(III) spin-orbit state transitions. This also indicates that the first redox process is osmium-based.

Some additional remarks can be made about the intervalence bands. As shown previously, the location of the IT bands is partly dependent on the coordination environment of the two metal centers.<sup>21,34</sup> By comparing the differences in the metal-based redox potentials for the various compounds, we can make some predictions about the location of intervalence transitions. The difference in these redox potentials ( $\Delta E_{1/2}$ ) for **RuRuCl** is 490 mV and for **OsRuCl** is 180 mV. The difference in  $\Delta E_{1/2}$  for the compounds ( $\Delta\Delta E_{1/2} = 310$  mV or 2500 cm<sup>-1</sup>) suggests by comparison with **RuRuCl**<sup>+</sup> (10 400 cm<sup>-1</sup>) an energy of 7900 cm<sup>-1</sup> for the intervalence transition in **OsRuCl**<sup>+</sup>, close to the observed one at 7690 cm<sup>-1</sup> (Table 3).

Applying the same approach to **RuOsCl**, we calculate an energy of 13 600 cm<sup>-1</sup> for the IT transition for **RuOsCl**<sup>+</sup>. This is at quite high energy, and this band is therefore most likely buried under the other bands in the visible region. The band observed at 6000 cm<sup>-1</sup> is therefore most likely one of the other two IT bands expected. The calculated IT band energy of 10 500 cm<sup>-1</sup> for the **OsOsCl**<sup>+</sup> species is higher than the value observed (Table 3). This suggests that the transition observed at 7812 cm<sup>-1</sup> is not the highest energy IT transition. If that is the case, one of the two bands observed at lower energy is not related to IT transitions. The spectroelectrochemical data observed for the mixed-valence compounds are clearly indicative of a weak interaction via the pyrazine ring. In comparison with other compounds this most likely occurs *via* a superexchange mechanism<sup>35</sup> involving pyrazine-based excited-state levels.

**Emission Spectroscopy.** The complexes **OsCl**, **OsOsCl**, and **RuOsCl** do not exhibit emission at room temperature or at 77 K. This is in line with the observed low oxidation potential of the OsCl unit, yielding a small energy gap between excited and ground state. Consequently the emission is expected to be weak<sup>36,37</sup> and in addition most likely outside the range of our equipment (limit of 900 nm). Emission is, however, observed for **RuRuCl** and **OsRuCl**. **RuRuCl** exhibits a weak emission at 705 nm at 77 K and 730 nm at room temperature (Table 2) in agreement with the energy expected for the emission of a RuN<sub>5</sub>Cl moiety.<sup>20</sup>

While the emission in **RuRuCl** is based on the RuCl center, for **OsRuCl** the situation is less clear. The spectroelectrochemical data suggest that, in **OsRuCl**, the Os(bpy)<sub>2</sub> moiety has a lower oxidation potential than the Ru(bpy)<sub>2</sub>Cl moiety (*vide supra*), and one would consequently infer the emission to be Os(bpy)<sub>2</sub>-based. Furthermore the emission energy observed is much lower than found for **RuRuCl**. This makes a RuCl-based emission unlikely. The fact that the emission band of **OsRuCl**

(32) Hush, N. S. *Prog. Inorg. Chem.* 1967, 8, 391.

(33) Kober, E. M.; Goldsby, K. A.; Narayana, D. N. S.; Meyer, T. J. *J. Am. Chem. Soc.* 1983, 105, 4303.

(34) Hage, R.; Haasnoot, J. G.; Nieuwenhuis, H. A.; Reedijk, J.; de Ridder, J. A.; Vos, J. G. *J. Am. Chem. Soc.* 1990, 112, 9245.

(35) Balzani, V.; Scandola, F. *Supramolecular Chemistry*; Ellis Horwood: Chichester, U.K., 1991; p 96 and references therein.

(36) Lumpkin, R. S.; Kober, E. M.; Worl, L. A.; Murtara, Z.; Meyer, T. J. *J. Phys. Chem.* 1990, 94, 239.

(37) Kober, E. M.; Casper, J. V.; Lumpkin, R. S.; Meyer, T. J. *J. Phys. Chem.* 1986, 90, 3722.

is at considerably lower energy than observed for the mononuclear Os compound is explained by a stabilization of the emitting  $\pi^*$  level in the dinuclear compound.<sup>7,38,39</sup>

All dinuclear compounds could in principle show a dual emission. This is however not observed, and this reflects effective quenching of the higher energy emitting state. For example, excitation of RuRuCl at various wavelengths between 550 and 400 nm at 77 K showed only a RuCl-based emission at 705 nm, indicating that the emission occurs only from the low energy RuCl unit. Quenching of the higher energy emission can occur either by an energy-transfer or a electron-transfer mechanism.<sup>40-42</sup> Support from the presence of an energy-transfer mechanism is obtained from the fact that the excitation spectrum of RuRuCl attained at 705 nm is quite similar ( $\lambda_{\text{max}}$  at 511 and 446 nm) to the absorption bands assigned to the RuRuCl complex (530 and 440 nm). Similar arguments are also valid for OsOsCl and RuOsCl.

**Photochemical Properties.** As expected Os, OsCl, and OsOsCl are stable upon irradiation in acetone for at least 4 h. This photostability can be explained by the large ligand-field splitting of the Os(II) ion, which prevents population of the photoreactive  $^3\text{MC}$  state.<sup>37</sup> Also Ru and RuOsCl are photostable upon irradiation in the same solvent. The stability of the mononuclear Ru complex is most likely caused by the relatively low-lying  $\pi^*$  orbitals of pyrazyltriazole ligand, yielding a relatively large  $^3\text{MLCT}$ - $^3\text{MC}$  gap. Such an effect has been noted previously for other  $[\text{Ru}(\text{bpy})_2(\text{LL})]^{2+}$  complexes (LL = 2,2'-bipyrazine, 2,2'-bipyrimidine).<sup>43</sup> In addition, for

RuOsCl efficient energy-transfer processes take place from the ruthenium center to the OsCl moiety, which further prevent population of the  $^3\text{MC}$  state located on the ruthenium(II). Irradiation of RuRuCl and OsRuCl in acetone leads to a well-defined clean photochemically induced ligand exchange reaction (Figure 6). The spectral changes observed, together with an HPLC analysis of the reaction, indicate the formation of the mononuclear Ru and Os compound, respectively. The photolability of the ruthenium site in OsRuCl is interesting since, on the basis of the electrochemical and emission results, we concluded that in this compound the emitting site is most likely osmium-based. In this case we would not expect a photolability of the ruthenium site. An explanation for the behavior observed may be that the energies of the Os- and Ru-based  $^3\text{MLCT}$  states are comparable. In that case equilibrium between the Ru- and Os-based  $^3\text{MLCT}$  states can be established<sup>44</sup> and the  $^3\text{MC}$  state of the Ru site can be thermally populated leading to the observed photolability.

## Conclusions

The results obtained here suggest that pyrazyltriazoles have several attractive features as bridging ligands, and in view of the continuing interest in the pyrazine-based bridging systems this new ligand offers a valuable alternative approach. In the ligand a strong  $\pi$ -acceptor, pyrazine, is bound to a strong  $\sigma$ -donor, the triazole ring. This yields compounds that are substantially different from those reported by Brewer,<sup>45</sup> Balzani,<sup>46</sup> and others,<sup>7</sup> where pyrazine groupings are bound to pyridine type moieties. In addition the presence of the triazole ring might lead to solvent-dependent behavior as recently observed by Meyer and co-workers.<sup>47</sup> In view of this we are at present investigating pyrazine-triazole-based ligands with triazole rings containing an N-H bond rather than N-CH<sub>3</sub>. This will allow the study of the interaction between the two units in the dimer as a function of the protonation of the triazole ring and introduce a strong  $\sigma$ -donor in the bridge.

**Acknowledgment.** F.M.W. and J.G.V. thank Forbairt for financial assistance. Johnson-Matthey is thanked for a generous loan of RuCl<sub>3</sub>·xH<sub>2</sub>O and K<sub>2</sub>OsCl<sub>6</sub>.

**Supporting Information Available:** Figures showing spectroelectrochemical data for the compound OsOsCl (Figure S1) and UV-vis absorption spectra of OsRuCl obtained upon radiation in acetone (Figure S2) (2 pages). Ordering information is given on any current masthead page.

IC961277W

- (38) Barigelletti, F.; Juris, A.; Balzani, V.; Belser, P.; von Zelewsky, A. *Inorg. Chem.* **1987**, *28*, 4115.
- (39) (a) Dodsworth, E. S.; Lever, A. B. P. *Chem. Phys. Lett.* **1986**, *124*, 152. (b) Dodsworth, E. S.; Lever, A. B. P. *Chem. Phys. Lett.* **1985**, *119*, 61.
- (40) De Cola, L.; Balzani, V.; Barigelletti, F.; Flamingi, L.; Belser, P.; Bernhard, S. *Recl. Trav. Chim. Pays-Bas* **1995**, *114*, 534.
- (41) Balzani, V.; Bolletta, F.; Gandolfi, M. T.; Maestri, M. *Top. Curr. Chem.* **1978**, *75*, 1.
- (42) Indelli, M. T.; Scandola, F.; Collin, J.-P.; Sauvage, J.-P.; Sour, A. *Inorg. Chem.* **1996**, *35*, 303.
- (43) Allen, G. H.; White, R. P.; Rillema, D. P.; Meyer, T. J. *J. Am. Chem. Soc.* **1984**, *216*, 2613.
- (44) Barigelletti, F.; Juris, A.; Balzani, V.; Belser, P.; von Zelewsky, A. *J. Phys. Chem.* **1987**, *91*, 1095.
- (45) Vogler, L. M.; Brewer, K. J. *Inorg. Chem.* **1996**, *35*, 818.
- (46) Serroni, S.; Dentí, G.; Campagna, S.; Juris, A.; Ciano, M.; Balzani, V. *Angew. Chem., Int. Ed. Engl.* **1992**, *31*, 1493.
- (47) Neyhart, G. A.; Timpson, C. J.; Bates, W. D.; Meyer, T. J. *J. Am. Chem. Soc.* **1996**, *118*, 3730.